Thesis

Ship-Monopile Interaction in combination with Lashings and Friction contacts

Jumbo Maritime

Davey Mikail

Delft University of Technology

TU Delft

Thesis

Ship-Monopile Interaction in combination with Lashings and Friction contacts

by

Davey Mikail

To obtain the degree of Master of Science
at the Delft University of Technology,
to be defended publicly on Juli 22th, 2022

Student number: 4737377

Project duration: July 1, 2021 - Juli 22, 2022

Thesis committee:

Dr. C.L. Walters	TU Delft, Chair
Dr. A. Grammatikopoulos	TU Delft, Committee member & Daily supervisor
Dr. J. Jovanova	TU Delft, Committee member
Ing. M. Teunis	Jumbo Maritime, Industrial supervisor

Faculty of 3mE, Department of Ship and Offshore Structures, Delft

An electronic version of this thesis is available at: repository.tudelft.nl

Cover: Jumbo Maritime's Fairpartner shipping monopiles (Yunlin project)

TU Delft

Preface

The thesis presented has been the result of my research in the section Ship & Offshore Structures of TU Delft, made in collaboration with Jumbo Maritime's structural department. This thesis is written as part of, and the finalization of my MSc degree in Offshore & Dredging Engineering.

Firstly, I would like to express my gratitude to Dr. A. Grammatikopoulos for being my daily supervisor, spending a lot of time and effort into the guidance of this thesis, and delivering great feedback. Dr. A. Grammatikopoulos also honored me by presenting the opportunity to publish my work in the *'9th International Conference on HYDROELASTICITY IN MARINE TECHNOLOGY'*. During this process he helped me tremendously in the writing, communications and the feedback process.

Secondly, I would like to also express my gratitude to Dr. C.L. Walters for supervising me in the literature review stages of the research, basically providing a beacon of light in the darkness, as it often felt like walking in the dark in that stage.

Thirdly, I would like to thank Ing. M. Teunis and all structural engineers of Jumbo Maritime that assisted in my modelling quest in ANSYS workbench, as I had zero experience in the software and often had to use their expertise.

Fourthly, I would like to thank my family for supporting me throughout my entire journey of acquiring my BSc degree in Mechanical Engineering, and MSc degree in Offshore & Dredging Engineering. A special thanks goes to my father A. Mikail for allowing me to finish my study without any financial stress, and my girlfriend J.P.M.M. Schiedon for having the patience and support I needed.

Finally, I would like to thank God, the holy trinity. He made me realize I had to chance my life and couldn't continue with the path I was walking on. Walking up the ladder from working with my hands as Ironworker at a shipyard, to my MSc degree has been a major challenge in all possible ways. His help and guidance throughout this process was, and still is, essential.

Davey Mikail
Gouda, July 2022

Abstract

The increasing demand for renewable energy sources, to achieve ‘green goals’ such as the Paris agreement, and their related projects, are becoming increasingly challenging to accomplish. Nowadays, offshore wind farm projects move into deeper waters and require larger individual Offshore Wind Turbines (OWT’s), which results in larger monopiles. As a result, heavy lift vessels shipping and installing the monopiles can transport fewer monopiles at a time, as they have outgrown the cargo hold and can only be shipped on the top deck. Considering the stiff nature of the monopile and that it spans almost the entire length of a ship nowadays, companies involved in such projects, such as Jumbo Maritime, have concerns this might heavily affect the ships dynamic behaviour. Therefore, the research presented in this thesis is focused on investigating what effects a lashed monopile on the deck of a heavy lift vessel causes and if friction contact between ship and monopile plays a role. To answer these questions the ship and monopiles are modelled as a coupled system with appropriate boundary conditions. The research is focused on finding lashing & friction contact effects, but also what effects of the number of monopiles introduces onto the system.

Contents

List of Figures

List of Tables

Nomenclature

Abbreviations

Abbreviation	Definition
OWT	Offshore Wind Turbine
1P	First excitation frequency of an OWT
3P	Second excitation frequency, the rotorblade passing frequency of a 3-bladed rotor of an OWT
EB-beam	Euler-Beroulli beam
T-Beam	Timoshenko beam
K-M	Stiffness over mass (factor)
DOF	Degree Of Freedom

Symbols

Symbol	Definition
ω_n	Natural frequency
ω	frequency
k_l	lashing stiffness
F_{fr}	friction force
L	Length
T	Draft
B	Beam
A	Cross-sectional area
I	Area- / Second moment of inertia
D_l	Lashing grommet diameter
t	Thickness
B	Beam
l_0	initial length
E	Young's Modulus
ρ_s	Density (steel)
h_{min}	Smallest mesh/element dimension in the model
f	Safety factor
T	Total timespan
n	Amount of cycles
c	Wave speed
t	(Travel) time
TF	Time-Frequency coefficient

1

Introduction

As countries progressively look into renewable energy sources to achieve sustainable goals such as discussed, for example, in the Paris agreement, the renewable energy market's demand grows with the projects becoming increasingly challenging to accomplish. From all renewable energy markets offshore wind is in particular subject to more difficult challenges, namely because it is offshore [14], but also because of its adoption rate [1]. Offshore wind's adoption rate increases over time as it has already surpassed all development stages and is basically considered a proven concept, while most other (offshore) renewable energy sources are still very much in development [17]. As a result, offshore wind farms become increasingly complicated in their requirements as their individual Offshore Wind Turbine's (OWT's) need to generate more energy [11, 14]. A direct result of these requirements is that OWT's become larger and thus heavier over time [14]. The most popular foundation for OWT's is the 'monopile' [14], which is a long, straight and wide pipe, the dimensions of which are constantly growing. This is a result not only of the increased size of the turbines themselves, but also of the fact that offshore wind farms need to be installed into deeper waters [8, 11, 14]. Because of those two reasons the largest monopile sets the record at 10m in diameter in 2016 and over 100m of length [8, 14]. This makes heavy lift vessels from companies such as Jumbo Maritime no longer able to transport them in dedicated cargo holds and thus forces them to be transported on the top deck, as displayed in Figure 1.1.

Figure 1.1: Jumbo Maritime's J-type vessel the "Fairpartner" carrying large monopiles for the Yunlin project

1.1. The problem statement

Heavy lift vessels such as Jumbo Maritime's 'Fairpartner' is by default designed to have a suitable bending stiffness to sail both empty and loaded with heavy cargo that in general doesn't influence the ship longitudinal bending stiffness by much. When considering large monopiles this story becomes more complicated and the fear exists that the influence of the cargo's longitudinal bending stiffness on the ship can no longer be ignored, and as a result heavy lift vessels carry fewer monopiles for safety reasons. Large OWT are by default designed to have their first natural frequencies in between the 1P and 3P regions, also better known as the "soft-stiff region" [14, 18] (see Figure 1.2). As a result, this means the monopiles, by default, are designed very stiff and thus have higher first natural frequencies compared to the ship (see Table 3.1). This raises concerns at companies such as Jumbo Maritime that when lashed to their deck the ships natural frequencies shift by an unwanted amount and as a result vessels become far stiffer than anticipated.

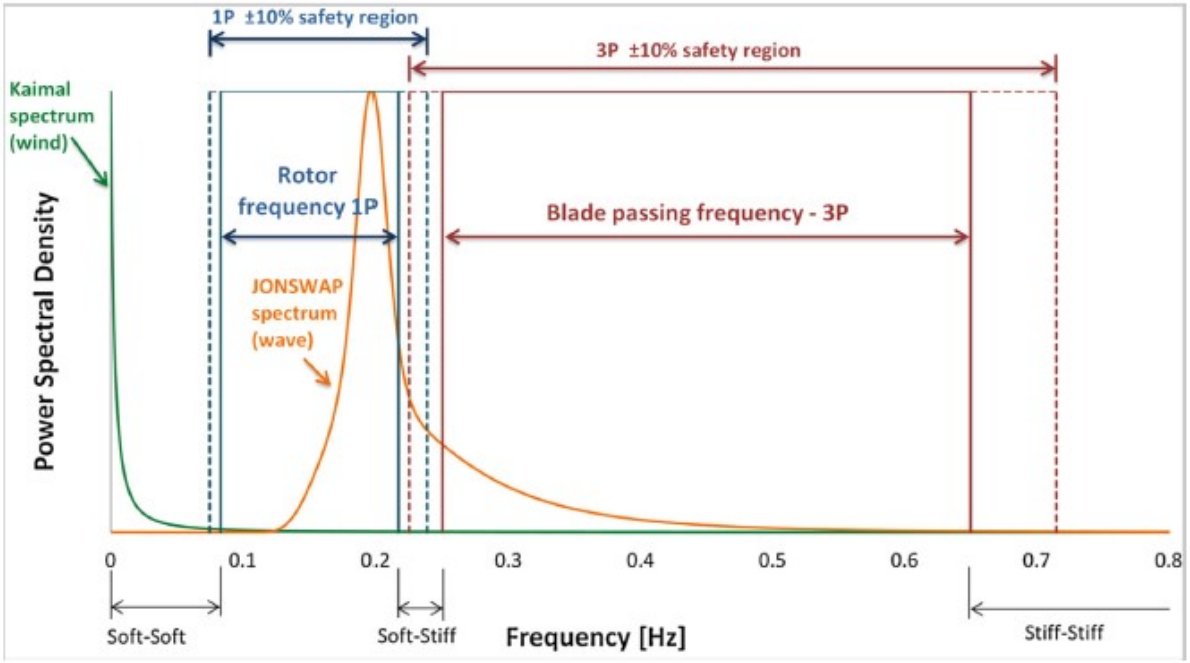

Figure 1.2: OWT design frequency ranges. with the x-axis depicting the frequency in Hz and the y-axis as the power spectral density in W/Hz [14]

1.2. Existing research

This section consists of a brief recap of the Literature Review [7] that has been documented separately in an earlier stage of this project, so for more detailed information refer to the corresponding document.

Since the pioneers Bishop and Price first published their work in the field of ship hydroelasticity an extensive number of cases for a wide range of vessel types have been analysed [2], with the most popular types being container ships, large bulk carriers and tankers. For all those vessel types many researchers developed models to predict warping, bending and or torsional loads in a sea state, often including coupling of their antisymmetric vibrations [12, 13]. Some models also include cargo, for example a container ship carrying containers or a bulk carrier carrying grain. In general, such models [16] are setup as pure mass contributions while stiffness contributions are ignored, all the while the size of the cargo is also not comparable to that of the ship. These models are in the basis either fully 2D/3D hydroelastic or semi 2D hydroelastic (Table 1.1)

		Structural	
		Beam theory	Shell theory
Hydrodynamics	Strip theory	Full 2D Hydroelasticity	Not used
	CFD	Semi 3D Hydroelasticity	Full 3D Hydroelasticity

Table 1.1: Modeling approaches

When comparing existing research with the problem statement one clear aspect stands out, namely that the vessel types are typically very long and have open cross-sections. An open cross-sections, when compared to a closed cross-section, has a very low shear-center which means that a coupling behaviour between horizontal bending and torsion is present [12]. When compared to heavy lift vessels, it is clear such vessels can have open-sections but do not reach such extreme lengths, but rather stick around 150m in length. Jumbo Maritime also possesses heavy lift vessels with open cross-sections when the hatch covers are not installed. However since monopiles, as mentioned in the problem statement, cannot be transported in dedicated cargo holds they have to be transported on the top deck, which means the cargo holds have to be covered with hatch covers. These hatch covers, when installed, do contain some play but are considered in this thesis, once closed, to be acting as a rigid cross section and thus operate as a closed cross-section.

The second aspect that stands out is the hydroelastic models that include cargo. Bulk carriers, tankers and container ships carry heavy cargo, which is also very small, in terms of dimensions, in comparison with the ship it self. As a result, these models are focused on mass contributions rather than mass- & stiffness contributions [16], while in the case of this thesis this is exactly what needs to be analyzed. So therefore such models are unfortunately not applicable in the scope of this project.

1.3. The research questions

From the problem statement the following main research question arises:

How do long and stiff objects lashed to the deck of a heavy lift vessel affect the dynamic behaviour?

To answer the main research question the following sub-question came to life:

How does friction of a lashed (framework of) monopile(s) influence the dynamic behaviour of a heavy lift vessel?

1.4. Project overview

The research- & sub question from the previous chapter are defined, the objective of this project is to perform the necessary research to answer them within the timeframe of this project. Therefore, the following question needs answering:

How does friction of a lashed (framework of) monopile(s) influence the dynamic behaviour of a heavy lift vessel?

Since no research exists in the field of ship hydroelasticity in regards of frictional and stiffness effects of cargo, both aspects can be considered a novelty on its own. For the scope of this project the cross-section of the ship has been assumed to be a rigid closed cross section rather than a semi-rigid closed cross section.

1.4.1. Scope

The scope of this project is to answer the above-mentioned sub-question by modelling multiple Timoshenko beams on top of each other (as in one as the ship and one as the monopile) and then identify changes in the dynamic responses of the considered system, such as natural frequencies and frequency responses functions, and finally perform time domain simulations to witness the frictional damping effects. To gain a realistic result the ship is considered as a non-uniform Timoshenko beam (T-beam) based on available data from Jumbo Maritime's heavy lift vessel the "Fairpartner". The model itself also is validated to make sure every aspect of it works as anticipated. Once the validation process of the model is completed the effects of the amount of monopiles, the saddle friction, and the lashing stiffness is analysed.

2

The Model

The fastest and cheapest method of answering the research question, which can be found in chapter 1, is by means of constructing and evaluating a model. This gives access to the analysis of the situation and the start of a discussion. In this chapter a substantiated description of the complete construction proces of the model can be found, including applied boundary conditions, constraints and assumptions.

2.1. Monopile configuration

Before any sort of modelling can be considered it is important to have an idea how monopiles are in fact shipped on the top deck, before they eventually are installed offshore[1].

To ship monopiles onto heavy lift vessels, so called 'saddles' are constructed and welded to the top deck. These saddles hold the monopile in place while also preventing the monopile from collapsing due to its own weight. Such saddles are mostly a one time use and are specifically designed for the frame of the ship upon which they are installed and the dimensions of the monopile itself. In addition, saddles are also equipped with a rubber padding to prevent sliding as much as possible. A few examples of how such a saddle could look like are given at Figure 2.1, these are just 3 out of many variations of saddles.

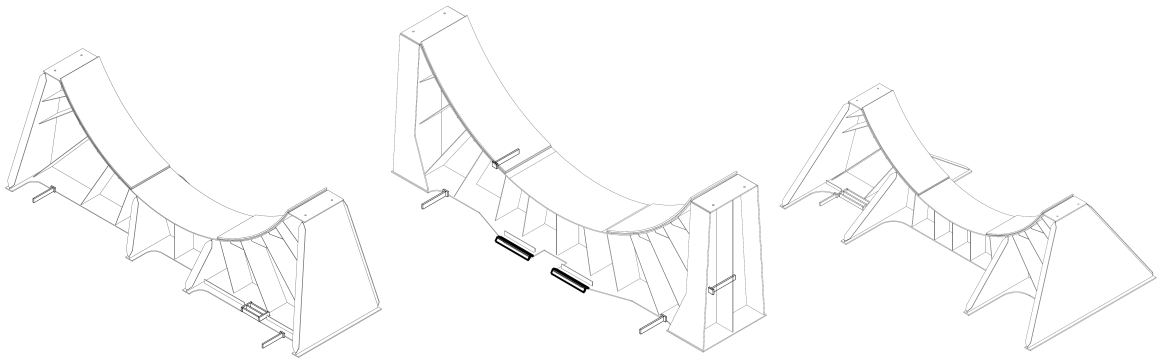

Figure 2.1: Jumbo Maritime's saddle variations

The saddles are then oriented on the top deck as in Figures 2.2 & 2.3. Once the monopiles are installed on the saddles, Jumbo Maritime uses lashing wires to tighten the monopiles with a pre-tension of approximately 50kN per monopile per side. In Figure 2.3 the lashings are illustrated at the beginning and the end of the monopile as springs.However, in reality the lashings are attached to deck, very close to the saddles (see Figure 2.4), but to simplify the model they are assumed to be lashed to the bottom of

[1] Disclaimer: the shipping method described in this section is a derivative of the data and drawings provided by Jumbo Maritime, so this topic is purly based on how Jumbo Maritime ships monopiles. Other companies might have different approaches to shipping monopiles.

the saddle itself so that the model has already a reduction of 2 interfaces. Overall, this should prevent unnecessary small meshing's, which can increase the computational time by a significant amount for the time domain analysis (Explicit Dynamics). In addition, it is expected that having the lashing attached in the described manner will still result in similar numerical results. More details regarding the Explicit Dynamics computational time topic can be found in Section 2.3.3.

Figure 2.2: General saddle orientation on the top deck

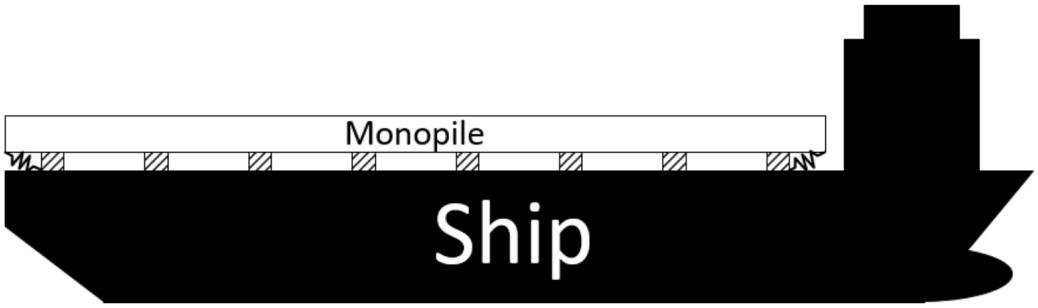

Figure 2.3: Saddle length orientation on the top deck

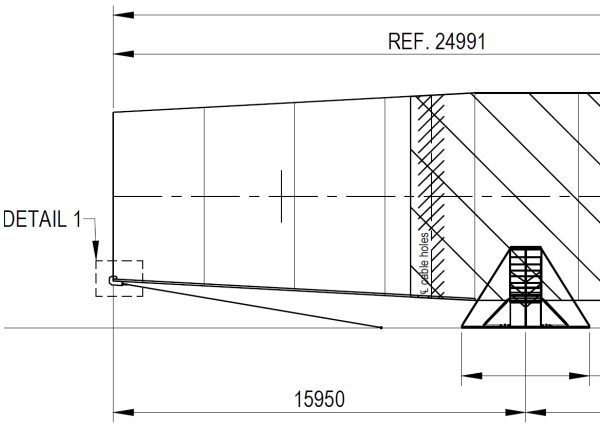

Figure 2.4: Actual lashing location on the ship

Furthermore, the tip of the monopile depicted in Figure 2.4 is in reality tapered in most cases, the reason behind this is because it increases the lifespan of the concrete that has to be moulded onto it after installation of the monopile is completed [4]. In terms of modelling, the tapered piece has been assumed straight and the same diameter as the rest of the monopile, which allows the monopile to be modelled as a uniform beam rather than a non-uniform beam.

2.2. Selecting the modelling approach

In Section 1.4.1 it is already discussed that the modelling configuration should be based of the T-beam theory. However, in doing so a few options arise and the selection process of a suitable candidate begins. First and foremost all considered options need to be capable of modelling a T-beam, (Coulomb) friction and the lashings as springs. The selection procedure involves several topics of interest, namely: simplicity, practicality, usage experience of author, usage experience of company, usage experience of TU Delft supervisor, presence of licensing and available material on the internet. The reason these topics are considered of interest is because Jumbo Maritime values practicality, cost-efficiency and simplicity [6]. Furthermore, the learning curve of a method becomes steeper when a source of support is lacking or even absent, which in turn can cause major delays. A few candidates for these topics have selected beforehand, namely: Matlab, Python, Maple, ANSYS workbench, ANSYS APDL and FEMAP.

Table 2.1: Overview of selection procedure with '—' being the absolute minimum and '+++' being the absolute maximum

	Matlab	Python	Maple	ANSYS workbench	ANSYS APDL	Femap
Simplicity	++	+++	+	+++	+	-
Practicality	+	++	-	++	+	++
Usage experience of author	Present	Little	Present	None	None	Little
Usage experience of company	Little	Present, used by (some) structural engineers	None	Used by all structural engineers	Very little, although ANSYS workbench is a derivative of ANSYS APDL	None
Usage experience of TU Delft supervisor	Little	Present	None	Little, but knows what happends in the background due to extensive experience in ANSYS APDL	Present	None
License TU Delft	Present	Free	Present	Present	Present	Present
License Jumbo Maritime	Absent	Free	Absent	Present	Present	Absent
Internet support	Very high	Very high	High	Very high	High	Medium

When considering Table 2.1 one can clearly witness that modelling with ANSYS workbench will be most advantageous for both the author, the company and TU Delft. As an extra advantage the model could be used afterwards by the company to predict change of ship responses for new projects as well as they own licenses of the chosen software package.

2.3. Constructing the model

In the construction phase of a model, it is important to have a plan in which one can be certain every step and detail works as intended and know exactly what impact certain properties have on the model. In this chapter a brief explanation of the construction process of the model can be found with choices of details that have a clear impact on how the model behaves.

2.3.1. Construction steps

During the literature review a study has been found that investigates the natural frequencies of a simple thin strip both experimentally, numerically and analytically and compared data with each other [15]. In order to begin the modelling process with a solid foundation the model first consisted of the same strip with identical geometry, properties and boundary conditions, namely (see Tables 2.2 & 2.3):

Table 2.2: Parameters used in study [15] and for the initial modeling steps

Material parameter	Geometric parameter [m]
$E = 2.05 \cdot 10^{11} N/m^2$	$L = 1.044$
$\rho = 7830 kg/m^3$	$B = 0.023$
$\nu = 0.3$	$t = 0.005$

Table 2.3: Comparison of natural frequencies of a free-free T-beam, numerical frequencies are based of T-beam theory, the theoretical/analytical frequencies are based of Euler-Bernoulli's beam (EB-beam) theory [15]

Boundary Condition	Mode	Numerical frequency [Hz]	Theoretical frequency [Hz]	Experimental frequency [Hz]
Free-free	1	24.12	24.07	25.63
	2	66.505	66.353	77.51
	3	130.37	130.07	128.8

In the study the numerical natural frequencies are calculated using ANSYS workbench 14.5 [15], in which beam elements are, by default, based on T-beam theory, while the analytical calculations were based on EB-beam theory [15]. The setup for the experiment to determine the natural frequencies exists of an impact hammer, which is used to excite the beam, and a vibrometer which registers the displacement with respect to time [15]. In case of this thesis the numerical frequencies are most important as they can give a clear indication if the constructed model (as in Figure 2.5) is similar to the model of the study.

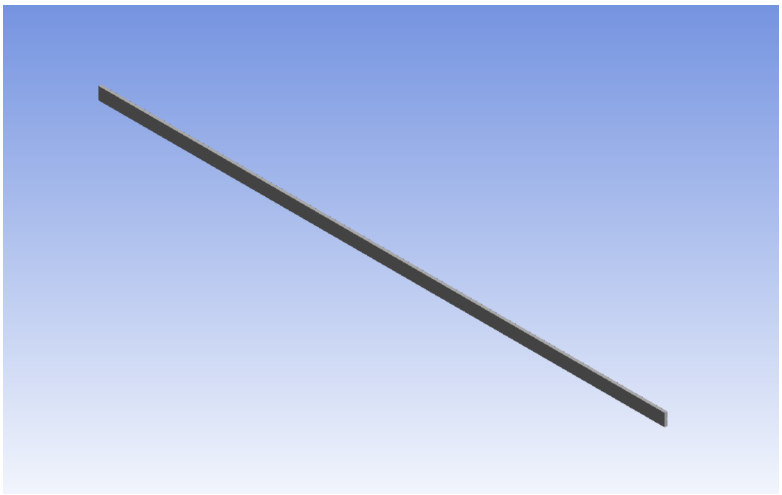

Figure 2.5: Modelling step 0a: simple strip, identical to considered study

The model has been found to have matching (numerical) natural frequencies with that of the study with an error far below 1%, which is within the margin of error (compare Tables 2.3 & 2.5. The next step considered the same strip but then with its considered axis at an offset at the top of the strip rather than its center (see Figure 2.6). This step is crucial, because in later steps the ship and monopile has been modelled also with their axis at the top deck and the bottom[2] of the monopile respectively.

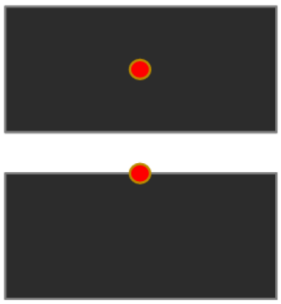

Figure 2.6: Modelling step 0b: same as step 0a, but now with the considered axis at an offset

The next step contained expanding the model to two individual beams without any sort of connection in between them as in Figure 2.7.

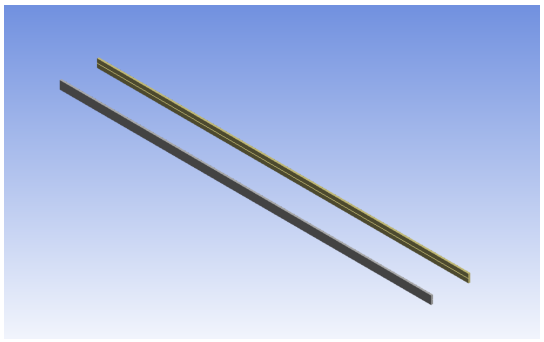

Figure 2.7: Modelling step 1: two individual strips, without saddle connections

Once completed the beams were connected with rigid beams in between them, acting as saddles between the ship and monopile, but instead of friction contacts bonded[3] contacts (see Figure 2.8).

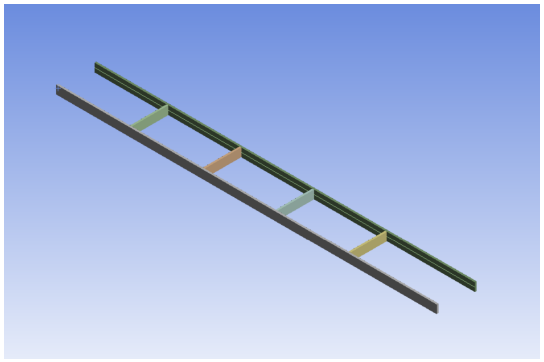

Figure 2.8: Modelling step 2: two individual strips, with saddle connections

[2] bottom, as in the lowest contact height/location of the monopile and saddle
[3] bonded contacts are equivalent to welded joints

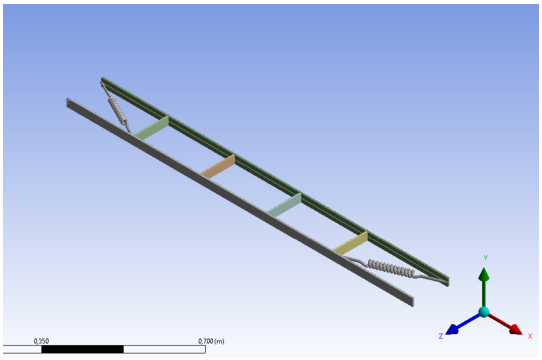

Figure 2.9: Modelling step 3 & 4: two individual strips, including friction contacts and lashings on both ends

The final piece that is missing from the last-mentioned step are the lashings, these are implemented, excluding pre-tension. Motivation about why pre-tension has been excluded can be found in Section 2.3.3).

Up to this step all parts are in the model, however, the implementation of the most important property isn't considered yet, namely friction contacts. The next step therefore consists of removing the fixed properties of the saddle's end connected to the strip, representing the monopile, and adding friction contacts (see Figure 2.9).

The next and last step in the process of constructing the model is the replacement of data, namely the bottom strip with a non-uniform ship beam, the top strip with an uniform monopile beam. The saddles also increased from 4 locations to 8 and represented the same height and locations as data of the Yunlin project indicated. For the monopile two cross sections were considered, namely the cross section of a single monopile, and the cross section of triple monopiles sitting next to each other with 1m spacing in between them. All other properties, and option remained the same in the process except for the offsets, these needed some adjustments to match deck height and the monopiles diameter.

Once done the model is copied and evaluated for 19 cases (see Table 2.4), for each case a slight tweaking of numbers has been performed to match the specifications of the case. These cases were strategically selected to be able to perform a comparison between the different contact types[4] to see if significant changes can be witnessed. These cases also needed to indicate if the lashing stiffness plays any role for both the system's dynamics and the behavior and/or moment friction may play a role[5]. Finally, the cases were also optimized to witness the effects of the number of shipped monopiles for both the systems dynamic behaviour and to witness if it effects of contact behaviour of the system. For each case then the following data has been collected:

1. The modal analysis
    - Natural frequencies
    - Modeshapes 1-8
2. The harmonic analysis
    - Ship frequency response function at 0.25L, 0.375L, 0.5L, 0.675L and 0.75L
    - Monopile frequency response function at 0.25L, 0.375L, 0.5L, 0.675L and 0.75L
3. Time domain analysis (Explicit Dynamics)
    - Ship directional deformation w.r.t. time at 0.25L, 0.375L, 0.5L, 0.675L and 0.75L
    - Monopile directional deformation w.r.t. time at 0.25L, 0.375L, 0.5L, 0.675L and 0.75L

[4] Frictionless, frictional, and very high friction

[5] no specific reason exists why 100%, 66% and 33% were selected

Table 2.4: Evaluated setups with their case numbers.

Property	Case number																		
	1	2	3	4	5	6	7	8	9	10	11	12	13	14	15	16	17	18	19
No monopiles	•																		
1 monopile		•	•	•	•	•	•	•	•	•									
3 monopiles											•	•	•	•	•	•	•	•	•
100% lashing stiffness		•	•	•							•	•	•						
66% lashing stiffness					•	•	•							•	•	•			
33% lashing stiffness								•	•	•							•	•	•
Frictionless contact		•			•			•			•			•			•		
Frictional contact			•			•			•			•			•			•	
Very high frictional contact ($\mu = 10^{11}$)				•			•			•			•			•			•

2.3.2. Validation steps

In order to guarantee each step transitioned to the next without the transfer of any mistake made in the process it is important to perform validation steps while doing so. To give a general overview of how this process was considered see Figure 2.10. What this basically means it that before the next step can be considered the current step should be validated by using the previous step, by for example switching off certain properties.

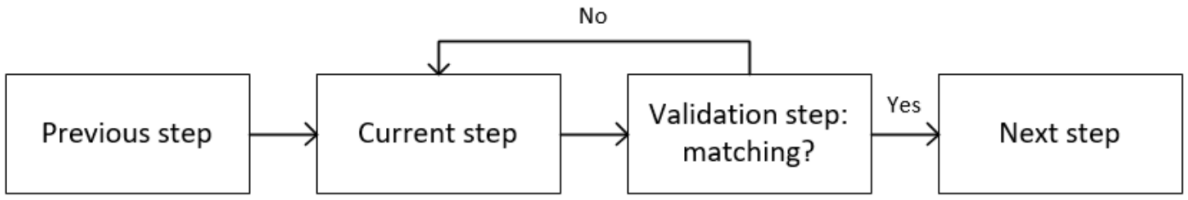

Figure 2.10: Validation process

The very first steps (step 0a, 0b & 1) obviously has no previous step to compare results with. Therefore, results were compared with the aforementioned study, performed by Sharma et al. [15], in which (numerical-) natural frequencies were presented of a thin strip. As a result, an exact match was found between this step and the study's reported (numerical-) natural frequencies (see Table 2.3 & 2.5).

Table 2.5: Concluded natural frequencies [Hz] from steps 0a (single beam, with its evaluated axis in the center of the strip), 0b (single beam, with its evaluated axis at an offset towards the surface of the strip, as described in Section....) and 1 (two free-free beams without any type of connection in between)

Mode	Step 0a: Single beam, centered	Step 0b: Single beam, offset	Step 1: Duo beams, unconnected
1	24.126	48.233	48.233
2	66.494	132.82	48.233
3	130.33	259.99	132.82
4	-	-	132.82
5	-	-	259.99
6	-	-	259.99

The second step (step 2) followed the pattern depicted Figure 2.10, where the saddle connections were temporarily given a very flexible property, as in that the connection had a Youngs Modulus of 10^{-11}. Results again matched with the previous step (see Table 2.6).

Table 2.6: Concluded natural frequencies [Hz] from steps 1 and 2 (two free-free beams connected with saddles, setup as "stiff beam", this option increases the Young's modulus by 10^4)

Mode	Step 1: Duo beams, unconnected	Val. Step 1: Duo beams, connected (super flexible)	Step 2: Duo beams, connected (fixed-rigid)
1	48.233	48.233	107.57
2	48.233	48.233	140
3	132.82	132.82	169.53
4	132.82	132.82	207.16
5	259.99	259.99	239.27
6	259.99	259.99	324.91

To validate the third step the lashings were given temporary a stiffness constant $k = 0$ and results did match with that of the previous step (see Table 2.7).

Table 2.7: Concluded natural frequencies [Hz] from steps 2 and 3

nr	Step 2: Duo beams, connected (fixed-rigid)	Val. Step 3: Lashed $k = 0$	Step 3: Lashed $k \neq 0$
1	107.57	107.57	108.64
2	140	140	145.82
3	169.53	169.53	177.16
4	207.16	207.16	214.1
5	239.27	239.27	247.82
6	324.91	324.91	329.94

The final validation step that can be performed is from step 3 to the friction type of contacts. But before heading straight for the details it is important to highlight how ANSYS performs any kind of linearized dynamic analysis when any kind of contact is present in the model. The modal- and Harmonic analysis are purely linear solvers and thus ignore non-linear effect, one of them being (Coulomb-) friction. Therefore when such features are used ANSYS makes one of the following assumptions (see Table 2.8):

Table 2.8: ANSYS contact assumptions

Contact Type	Static Analysis	Linear Dynamic Analysis		
		Initially Touching	Inside Pinball Region	Outside Pinball Region
Bonded	Bonded	Bonded	Bonded	Free
No Separation	No Separation	No Separation	No Separation	Free
Rough ($\mu = \infty$)	Rough ($\mu = \infty$)	Bonded	Free	Free
Frictionless	Frictionless	No Separation	Free	Free
Frictional	Frictional	$\mu = 0$, No Separation $\mu > 0$, Bonded	Free	Free

Since the Explicit Dynamics solver doesn't allow any presence of rough contacts in the model, these were substituted with high friction contacts of $\mu = 10^6$. Furthermore, when observing Table 2.8 one can notice that such contacts[6] should behave the same for all linear solvers. What this effectively means is that the responses should be identical with any kind of non-zero frictional contact. The same accounts for frictionless and a frictional contact of $\mu = 0$.

Table 2.9: Concluded natural frequencies [Hz] from steps 3 and beyond

nr	Step 3: Lashed $k \neq 0$	Step 4: Bonded contact x-movement constrained	Step 4: Bonded contact x-movement unconstrained	Step 4: Frictionless contact ($\mu = 0$) x-movement unconstrained	Friction contact ($\mu = 0.8$)	Friction contact ($\mu = 10^6$)	No-Seperation contact
1	108.64	108.64	74.507	12.098	71.078	71.078	12.098
2	145.82	145.82	99.886	38.754	72.762	72.762	38.754
3	177.16	177.16	113.95	56.9	100.25	100.25	56.9
4	214.1	214.1	138.01	78.358	108.21	108.21	78.358
5	247.82	247.82	174.8	89.287	151.11	151.11	89.287
6	329.94	329.94	215.05	114.13	206.69	206.69	114.13

In Table 2.9 one can witness what effects x-direction movements have on the systems natural frequencies and what friction contact does, for that particular system. From Table 2.8 the expectation is that the No-Separation- and the frictionless contact have an identical set of natural frequencies, just like a frictional contact of $\mu = 0.8$ and $\mu = 10^6$ should have identical sets of natural frequencies. When reviewing the resulting natural frequencies, it seems evident that the results match the expectations. However, when comparing the bonded contacts with the friction contacts one might question the result, for good reasons. The reason there is a mismatch between both results is because of the different inside pinball region differences. The bonded contacts use a 'bonded' assumption once inside the pinball region while all friction(less) contacts are 'free'. Before heading deeper into what this means it is important to also note the difference between the frictionless and frictional contact results, presented in Table 2.9. The reduced natural frequencies indicates that frictionless contacts might have a major impact on the systems natural frequencies, this observation will be part of this thesis discussion in the following chapter (see Chapter 3).

The region in which elements are checked if target- and contact nodes are, in fact, touching, is called in ANSYS the 'Pinball region' (see Figure 2.11). The real difference between the operation of 'bonded' & 'no separation' and 'rough', 'frictional' & 'frictionless' contacts inside the pinball region, is that it already activates their condition once inside. When 'bonded' or 'no-separation' is selected the approach is that it assumes all target & contact elements are, in fact, bonded in space, relative to each other. So, a touch is not necessarily the case for 'bonded' & 'no-separation' contacts. In addition, an unrealistic large pinball region can result in a large gap being present in between de saddle and monopile, for example. This can also cause a larger than usual area of the monopile(s) being bonded

[6] Rough contact versus high frictional contact

to the saddles. However, for rough, frictionless and frictional contacts, the operation can be considered a check, so: “are the target- & contact nodes touching?” is the check ANSYS performs. This check is performed for all elements inside the mentioned region.

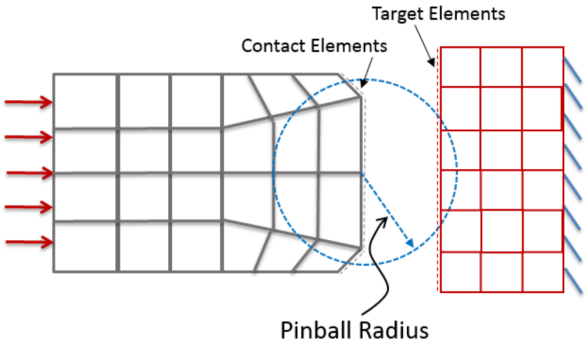

Figure 2.11: Pinball region visualisation [9]

2.3.3. Finalising the model

An important factor in the modelling process is data- acquisition, interpretation and implementation. In this chapter all these topics will be discussed.

Ship data

A very important data set is that of the ship, which is as mentioned in Section 1.4.1 modelled as a non-uniform T-beam from data of Jumbo Maritime’s ‘Fairpartner’. The data is acquired from Jumbo Maritime’s structural department, which consists of mass, draft and area moment of inertia data. All data has been compiled together and divided into blocks of 5m length, except for first block at the aft end of the ship, which started at $x = -3m$ and ended at $x = 2.5m$. This results in a total of 28 blocks. For each block the total mass, averaged cross-sectional area, which is a derivative of the light ship mass calculation, and area moment of inertia has been calculated. Motivation about this approach and the expected maximum error can be found a few paragraphs further. The cross-sectional area has been calculated using:

$$A_{block} = M_{block}/\rho_s \tag{2.1}$$

With ρ_s being the density of steel and M_{block} the total mass of the block.

The lightship mass distribution is represented as in Figure 2.12 and the cross-sectional area distribution, which is as in Equation 2.1 a function of the lightship mass and is represented in Figure 2.12.

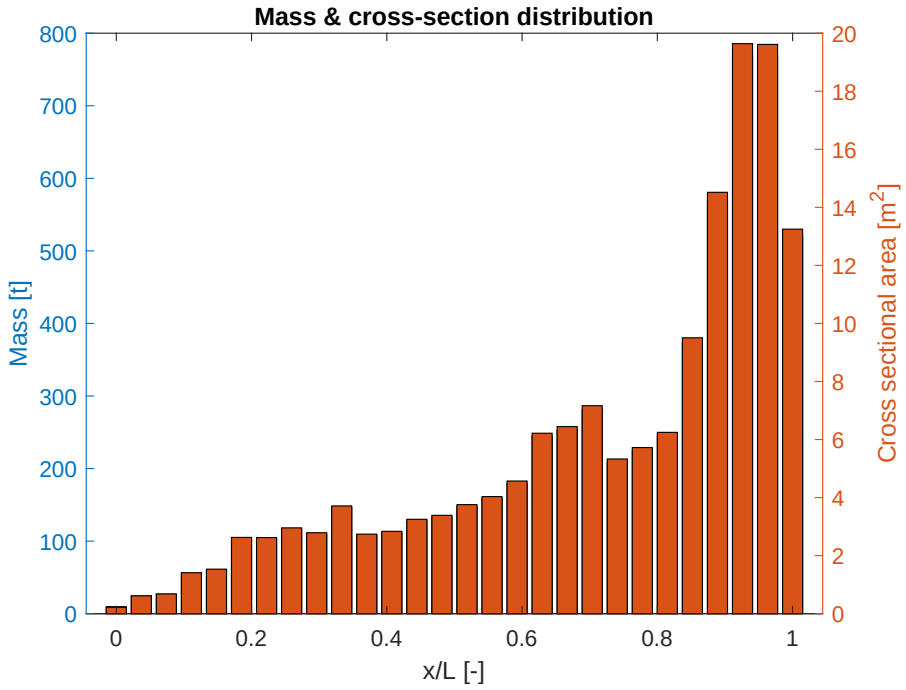

Figure 2.12: Light ship mass & cross-sectional area distribution Jumbo Maritime's 'Fairpartner'

Dividing the non-uniform beam into uniform blocks is a necessity in ANSYS, that is, unless shell elements are used instead of T-beam elements (BEAM188). ANSYS doesn't allow the use of fully non-uniform beam elements, instead it must be chopped into uniform pieces to approximate the non-uniformity of the beam. Therefore, using shell elements instead of T-beam elements could be considered a better, more accurate option, which is true. A downside of using shell elements is that computational time will drastically increase and overall, a lot more local (penetrating) modes will occur. As a result, a lot more filtering of the local modes is required for each case to collect the global modes. Since, as mentioned before, it is desired that the model aims for simplicity and practicality while maintaining a reliable accuracy, it is therefore important to highlight what kind of accuracy one could expect.

Huang et al. [3] formulated a similar (analytical) method of dividing the non-uniform beam into multiple uniform sets/blocks. Proving what the degree of accuracy of the method is, Huang et al. [3] also presented multiple sets of axially dimensionless natural frequencies for a uniform & non-uniform T-beam, up until the 5th mode. One aspect that stands out is that the number of blocks used, referred to as 'N' in Huang et al. [3], have more influence on higher modes. When dividing into 6 blocks the 3rd and 5th axial mode has a dimensionless natural frequency of 34.27 and 72.03 respectively, while 12 blocks results in a 3rd and 5th mode of 31.5 & 62.35 respectively. Therefore, based on the provided numbers of Huang et al. [3] a maximum error of 1% is expected. This percentage is based on comparing results of 12 blocks to results of Leung et al. [5]. Since the expected error is low and the reasons of previous paragraph it is therefore founded to be sufficiently reasonable to follow the T-beam route with the addition of dividing it into multiple blocks.

Ship draft data

When considering the shipment of one or more monopiles on the 'Fairpartner' the draft of the lightship has to increase, Jumbo Maritime's structural department has handed out criteria at which none, one or three monopiles can safely be shipped without stability issues, which is (see Table 2.10):

Table 2.10: Weight table per shipping situation, issued by Jumbo Maritime's structural department

Case nr's	# Monopiles	Draft [m]	Displacement ship (including monopile weight) [t]	Total weight monopile(s) [t]	Displacement ship (excluding monopile weight) [t]
1	0	5.5	13921.49	0	13921.49
2 - 10	1	6.5	17008.87	2268.1	14740.77
11 - 19	3	7.5	20223.24	6804.3	13418.94

What can be noticed from Table 2.10 is the fact that the displacement is given per draft situation, the delivered mass data however only consists of lightship mass data. The difference between the two types of mass is that the lightship mass is the total empty mass of the ship while the displacement is basically the lightship mass plus cargo such as fuel, crew, freshwater, food etc. This means the displacement also includes the total mass of the shipped monopiles. What this effectively means is that in order to have a more accurate weight representation of the ship in each case (see Table 2.4, the systems density has to be increased to match the displacement data, this also allows for the same mass distribution as displayed in Figure 2.12. The newly calculated system density's used for all cases are (see Table 2.11):

Table 2.11: New (structural) density's per case

	Case 1	Cases 2-10	Cases 11-19
Ship weight [t]	13921.49	14740.77	13418.94
Ship structural volume [m^3]	787.17	787.17	787.17
New (structural) density [kg/m^3]	17685.51	18726.31	17047.09

The delivered data set considering the area moment of inertia of the ship is considered around the neutral axis of the ship, unfortunately no information regarding the exact location of the neutral with respect to the ship's length coordinate exists. Therefore, since the ship is considered a closed cross section the neutral axis is assumed to be in the middle of the cross section. Since the mid-ship's cross-sectional height has been concluded to be 16m, the distance from top deck to the neutral axis (CGz) in the mid-ship has been assumed to be 8m in negative z-direction. Since the area moment of inertia has a linear decline at both the front and end of the ship the neutral axis location has been assumed to follow the same trend. In ANSYS the same procedure has been used as explained in Section 2.3, which is assigning an area moment of inertia per block, then enter the z-axis offset per block.

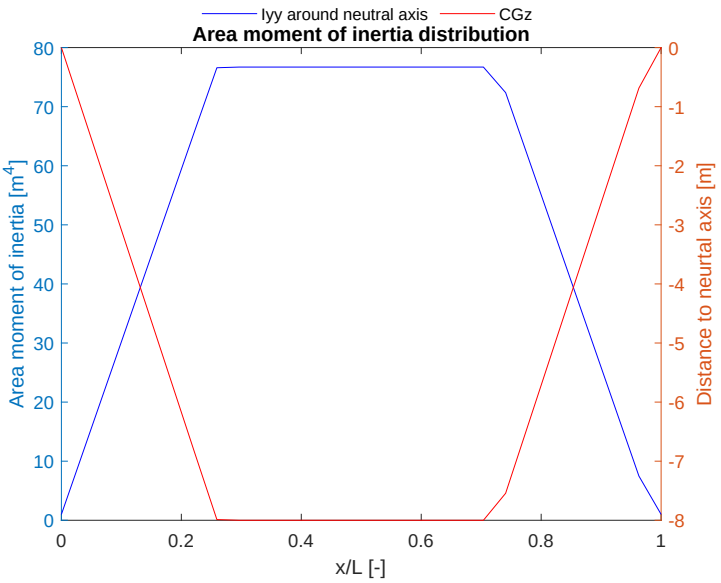

Figure 2.13: Area moment of inertia distribution Jumbo Maritime's 'Fairpartner'

Monopile data

As mentioned in the introduction, monopiles are becoming increasingly larger over time, with the current record set at 10m diameter and over 100m in length [8, 14]. For the purposes of this thesis data from Jumbo Maritime's Yunlin project has been used, which means monopiles of 8m in outer diameter, a thickness of 0.104m and a total length of 112m have been used in the model. For cases 11-19, which means 3 monopiles, the cross-section of the beam model representing the monopile(s) have been adjusted to properties of 3x the same monopile with a spacing of 1m in between the monopiles, which can be visualized as Figure 2.14:

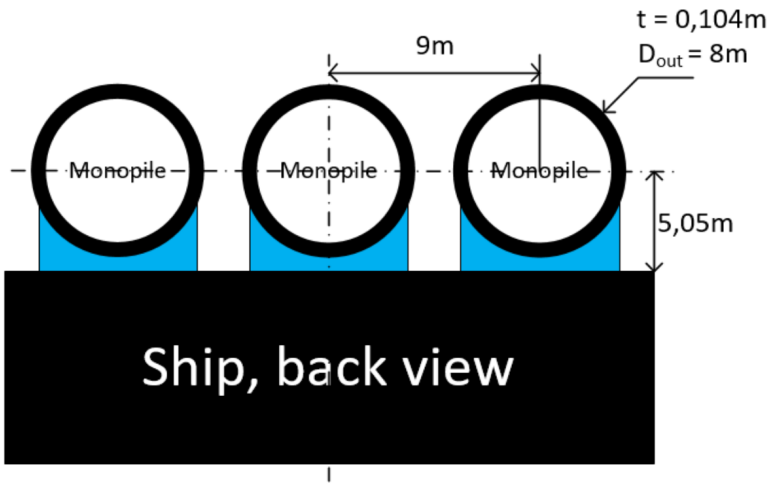

Figure 2.14: Monopile setup, rear view of system

The saddles, on top of which the monopiles rest, are necessary to hold the monopiles in position and prevent them from collapsing under their own weight. Under normal circumstances the saddles for each monopile are not necessarily aligned with the saddles of another, but for this thesis they are assumed to be aligned, which simplistically means all saddles are assumed to be located at the same x-coordinates on the top deck of the ship. This allows for a single (monopile) beam to be used for cases 2-19 rather than three for cases 11-19. The saddles are located at 8 interfaces, which have been setup as closely related to the Yunlin project as possible but forced at the beginning or end of a block to

minimize any occurrence of very small mesh sizes. The reasoning behind that will be further discussed in the subsection “Explicit dynamics solver”. Furthermore, the saddles introduces 1.05m elevation from the top deck, which is also depicted in Figure 2.14, the 8 saddle interfaces can be found in Figure 2.15:

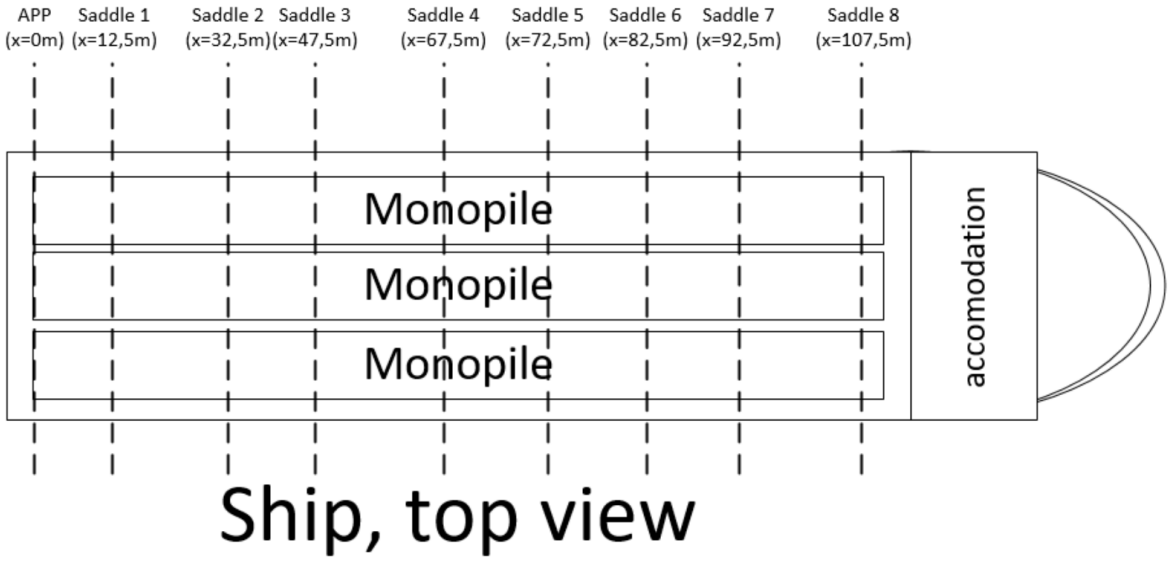

Figure 2.15: Saddle locations, top view

Lashing data

When shipping monopiles Jumbo Maritime also secures the monopiles at each end with ‘lashings’, which basically responds within the system as a spring. In normal circumstances the lashings are also pre-tensioned with approximately 50kN, but unfortunately the ANSYS explicit dynamics solver, which is a time-domain solver, doesn’t allow pre-tensions in springs. During the meshing optimalization study, which is covered in later paragraphs, it was found pre-tension wasn’t affecting natural frequencies at all (see Table 2.14 & 2.15), with that in mind and in concern of time planning a workaround has not been investigated.

Jumbo Maritime has lashed its monopiles on to the top deck by attaching them with L-brackets on the ends of each monopile to almost their nearest saddle. So, this means the cases considering 3 monopiles have also triple lashings, thus triple lashing stiffness, when comparing to the single monopile cases. As already mentioned in Section 2.1 the lashings are assumed to be attached to the bottom of the saddles for simplicity reasons while results should not differ by much. Such a lashing can be illustrated as in Figure 2.16:

Figure 2.16: Lashing illustration

The lashing properties are (see Table 2.12):

Table 2.12: Lashing properties

	l_0 $[m]$	E $[N/mm^2]$	D_l $[mm]$
Front-end	5.6976	1770	22
Aft-end	14.678	1770	22

Which means that when rewriting Hooke's law (Equation 2.2) a stiffness coefficient k_l can be defined as (Equations 2.3):

$$\begin{aligned} F &= k_l \cdot \delta x = k_l \cdot \delta L \\ \sigma &= \frac{F}{A} = E \cdot \varepsilon = E \cdot \frac{\delta L}{l_0} \end{aligned} \tag{2.2}$$

$$\begin{aligned} F &= E \cdot A \cdot \frac{\delta L}{l_0} = E \cdot \frac{\pi \cdot D_l^2}{4} \cdot \frac{\delta L}{l_0} = k_l \cdot \delta L \\ k_l &= E \cdot \frac{\pi \cdot D_l^2}{4 \cdot l_0} \end{aligned} \tag{2.3}$$

Applying Equation 2.3 to all cases, we find the following values (see Table 2.13):

Table 2.13: Lashing values

Lashing stiffness $[kN/m]$	Cases 2-4	Cases 5-7	Cases 8-10	Cases 11-13	Cases 14-16	Cases 17-19
Front-end	118.09	78.73	39.36	354.27	236.18	118.09
Aft-end	45.84	30.56	15.28	137.52	91.68	45.84

Mesh optimization

Meshing in ANSYS can be done using default settings, but can also by optimizing it manually. The goal of mesh optimization is to find a fine enough mesh for an accurate computation, but also coarse enough to reduce the computational time, this is especially true for the Explicit Dynamics solver. The Explicit Dynamics solver determines its maximum allowable time step using Courant-Friedrichs-Lewy CFL criterion. This criterion states that one element cannot enter and surpass another in space in a single time step, which means a rougher mesh can significantly decrease the computational time for the Explicit Dynamics solver. ANSYS calculates the maximum allowable timestep as following (Equation 2.4):

$$\delta t \leq f \cdot [\frac{h_{min}}{c}] \tag{2.4}$$

With h_{min} being the smallest element dimension present in the model, f as safety factor, which is by default 0.9 and c the longitudinal wave speed. ANSYS uses the longitudinal wave speed as that is the governing wave speed for the CFL criterion when one must choose between the longitudinal and transverse wave speed.

The minimum amount of cycles needed for the Explicit Dynamics solver then becomes (Equation 2.5):

$$n = \frac{T}{\delta t} \geq \frac{T}{f \cdot h_{min}} \cdot \sqrt{\frac{E}{\rho}} \tag{2.5}$$

with T the total amount of time in seconds, E the Young's modulus of the element(s) and ρ the density of the element(s).

So, in short it is essential to maintain as coarse a mesh as possible for the Explicit Dynamics solver, while still having a fine enough mesh to have reliable output. The optimization has been performed executing the modal analysis for case 2 & 11 as this analysis requires the least amount of computational time out of all solvers that were used during this project. The modal analysis ran several meshes for 8 modes and the coarsest mesh with an acceptable deviation for both cases from the finest mesh was selected. In Table 2.14 & 2.15 the results are shown for different sizes of meshes with their resulting natural frequencies, the selected mesh size became the 2m mesh.

Table 2.14: Mesh size comparison, case 2 natural frequencies in Hz with the mesh sizes represented in the top row in m

Case 2 Mode	0.85m	1m	2m (without lashing pre-load)	2m (with lashing pre-load)	2.5m	3m	5m
1	2.5277	2.5277	2.5277	2.5277	2.5277	2.5277	2.5278
2	5.9151	5.9151	5.9151	5.9151	5.9152	5.9152	5.917
3	9.7327	9.7327	9.7328	9.7328	9.7333	9.7333	9.7428
4	12.782	12.782	12.782	12.782	12.782	12.782	12.787
5	15.11	15.11	15.11	15.11	15.112	15.112	15.14
6	19.619	19.619	19.62	19.62	19.624	19.624	19.706
7	25.45	25.45	25.452	25.452	25.457	25.457	23.144
8	26.042	26.042	26.043	26.043	26.045	26.045	23.144

Table 2.15: Mesh size comparison, case 11 natural frequencies [Hz]

Case 11 Mode	0.85m	1m	2m (without lashing pre-load)	2m (with lashing pre-load)	2.5m	3m	5m
1	2.5705	2.5705	2.5705	2.5705	2.5706	2.5706	2.5706
2	5.8636	5.8636	5.8636	5.8636	5.8637	5.8637	5.8652
3	10.061	10.061	10.061	10.061	10.061	10.061	10.071
4	13.921	13.921	13.921	13.921	13.922	13.922	12.363
5	15.768	15.768	15.768	15.768	15.77	15.77	13.161
6	20.596	20.596	20.597	20.597	20.602	20.602	13.161
7	26.886	26.886	26.887	26.887	26.895	21.473	13.161
8	28.023	28.023	28.024	28.024	27.199	21.474	13.6

Explicit dynamics solver

For the Harmonic and Explicit Dynamics solver a forcing at the front of the ship has been applied to witness the systems responses, in both cases the amplitude of this force is set to 100kN. The Harmonic analysis solver is a linear, frequency-domain solver which have been set to analyze the system in between 0.1Hz and 30Hz, which should cover the most important natural frequencies of the system. However, the Explicit Dynamics solver is a non-linear, time-domain solver, which means the forcing frequencies need to be manually configured for each simulation. In concern of time-planning the simulations were ran three times for cases 2-19, with the first representing a forcing frequency the same as

the system's first natural frequency, the second corresponding to the second natural frequency and the final simulation corresponding the third natural frequency. The force is applied in all simulations for 10 periods of time to make sure the duration of the simulation is adequate long. Once a force is applied it takes time for the transverse wave, introduced by the force, to travel to the other end of the beam. To prove that all observation locations, such as 'Ship 0.25L' & 'Monopile 0.25L', actually 'feel' the effects of the applied force a quick wave calculation is performed. In the wave calculations the travel time is presented for the slowest wave (1st natural frequency) reaching the other end of the ship (see Tables 2.16 & 2.17). The required travel time is also a function of the forcing frequency ($t(\omega)$) and since multiple frequencies could be analyzed it is easiest to formulate a coefficient in which the frequency term has been isolated. This allows rapid calculations for an arbitrary set of frequencies as the coefficient has been made frequency independent. This coefficient is referred to as the 'time-frequency' (TF) coefficient and has been determined as (Equations 2.6):

$$\begin{aligned} c &= \sqrt[4]{\frac{EI}{\rho A} \cdot \omega^2} \\ \frac{c}{\sqrt{\omega}} &= \frac{\sqrt[4]{\frac{EI}{\rho A} \cdot \omega^2}}{\sqrt{\omega}} = \sqrt[4]{\frac{EI}{\rho A}} \\ t &= \frac{L_{ship}}{c} = \frac{TF}{\sqrt{\omega}} \\ TF &= t \cdot \sqrt{\omega} = \frac{L_{ship}}{c}\sqrt{\omega} = L_{ship} \cdot \sqrt[4]{\frac{\rho A}{EI}} \end{aligned} \tag{2.6}$$

With TF the time-frequency coefficient, c representing the (transverse) wavespeed, t representing the total time frame, ω the wave frequency and L_{ship} the ship's total length.

In the table below (Table 2.16 & 2.17) an overview of the calculated time that is needed for one transverse wave reaching the aft end of the ship is displayed, using Equations 2.6. For simplicity reasons the area moment of inertia and cross-sectional values are chosen at mid ship location.

Table 2.16: Wave speed and required time calculations cases 2-10

	Case 2	Case 3	Case 4	Case 5	Case 6	Case 7	Case 8	Case 9	Case 10
$E[Pa]$	2E+11	2E+11	2E+11	2E+11	2E+11	2E+11	2E+11	2E+11	2E+11
$I_{mid}[m^4]$	76.70	76.70	76.70	76.70	76.70	76.70	76.70	76.70	76.70
$\rho[kg/m^3]$	18726.31	18726.31	18726.31	18726.31	18726.31	18726.31	18726.31	18726.31	18726.31
$A_{mid}[m^2]$	3.76	3.76	3.76	3.76	3.76	3.76	3.76	3.76	3.76
$L_{ship}[m]$	140	140	140	140	140	140	140	140	140
$c/\sqrt{\omega}[m/\sqrt{s}]$	121.511	121.511	121.511	121.511	121.511	121.511	121.511	121.511	121.511
$TF[m/\sqrt{s}]$	1.152159	1.152159	1.152159	1.152159	1.152159	1.152159	1.152159	1.152159	1.152159
$\omega_{n1}[Hz]$	2.5277	2.5277	2.5277	2.5277	2.5277	2.5277	2.5277	2.5277	2.5277
$t_1[s]$	0.72	0.72	0.72	0.72	0.72	0.72	0.72	0.72	0.72

Table 2.17: Wave speed and required time calculations cases 11-19

	Case 11	Case 12	Case 13	Case 14	Case 15	Case 16	Case 17	Case 18	Case 19
$E[Pa]$	2E+11	2E+11	2E+11	2E+11	2E+11	2E+11	2E+11	2E+11	2E+11
$I_{mid}[m^4]$	76.70	76.70	76.70	76.70	76.70	76.70	76.70	76.70	76.70
$\rho[kg/m^3]$	17047.09	17047.09	17047.09	17047.09	17047.09	17047.09	17047.09	17047.09	17047.09
$A_{mid}[m^2]$	3.76	3.76	3.76	3.76	3.76	3.76	3.76	3.76	3.76
$L_{ship}[m]$	140	140	140	140	140	140	140	140	140
$c/\sqrt{\omega}[m/\sqrt{s}]$	124.3988	124.3988	124.3988	124.3988	124.3988	124.3988	124.3988	124.3988	124.3988
$TF[m/\sqrt{s}]$	1.125413	1.125413	1.125413	1.125413	1.125413	1.125413	1.125413	1.125413	1.,125413
$\omega_{n1}[Hz]$	2.5705	2.5705	2.5705	2.5705	2.5705	2.5705	2.5705	2.5705	2.5705
$t_1[s]$	0.7	0.7	0.7	0.7	0.7	0.7	0.7	0.7	0.7

With ω_{n1} being the first natural frequency, which governs, out of all natural frequencies, the required time for a transverse wave to reach the other end of the ship.

As mentioned earlier the Explicit dynamics solver is a non-linear time-domain solver, the reason this type of analysis is performed is because of the highly non-linear nature of Coulomb friction. In ANSYS Explicit Dynamics, the default type of friction is Coulomb friction, thus static and dynamic coefficients had to be defined. Since insufficient data is available about the rubber padding Jumbo Maritime applies on the saddles a steel-steel contact has been assumed, using a dynamic (sliding) coefficient of $\mu_d = 0.42$ and a static coefficient of $\mu_s = 0.8$ for all cases using frictional contacts. As mentioned before the explicit dynamics solver doesnt allow 'rough' contacts, therefore the high friction cases were given a dynamic- and static friction coefficient of $\mu = 10^6$.

2.4. Boundary conditions, constraints and assumptions

Now that the complete construction and finalization process of the model has been explained it is important to explain what the boundary conditions and constraints are of the model. Most information in this section has been explained in previous sections, but nonetheless it is still valuable to have all the relevant information regarding this subject in one spot. At first the real boundary conditions and constraints will be explained how they occur in practical application, then how the linearized model deals with them and then finally what this means for the non-linear model.

2.4.1. Practical application

As mentioned in Section 2.3.3 Jumbo Maritime lashes its monopiles to the top deck, close to its first saddle location. The lashing contains approximately 50kN pre-tension and since the monopile and ship are much larger in mass compared to the lashings the lashings can be considered as springs. Illustrating the application of such a boundary condition results in Figure 2.17 with the white beam representing the monopile and the black as the deck of the ship. The ship it self obviously is considered a free-free T-beam which in normal circumstances is exposed to wave forces and the addition of added mass. This still results in a free-free T-beam but with the support of a distributed spring/damper system along its length, as illustrated in Figure 2.18

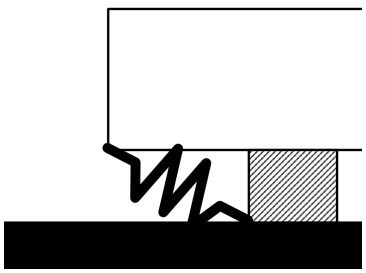

Figure 2.17: Illustration of the boundary conditions of the monopile (white beam)

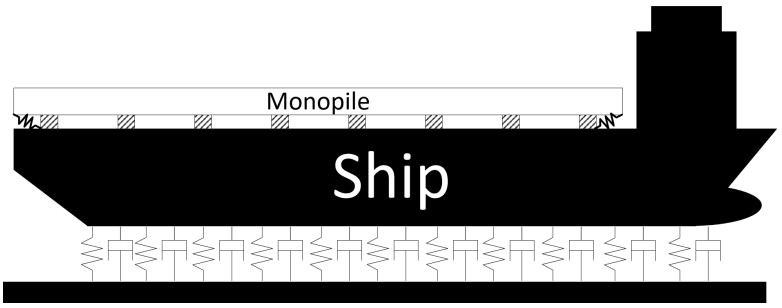

Figure 2.18: Illustration of the boundary conditions of the ship in practice

The monopiles rest on the saddles, at which they can experience upward forces when in contact, specifically at the saddle location, but moments are not transferred. Furthermore, the monopiles are exposed to a rubber-steel type of friction contact, specifically Coulomb friction.

2.4.2. Modelling application

During the modeling process some simplifications have been implemented, namely:

- No consideration of any kind of wave forces, which results in the removal of the distributed spring-damper system illustrated in Figure 2.18 and also means grafitational pull is left out of the equation.
- No consideration of added mass effects due time restrictions
- Since only the longitudinal bending is analyzed throughout this project all DOF are constrained except for:
    1. Z-axis displacement to allow heaving of the system
    2. X-axis displacement to allow sliding between monopile and saddles
    3. Y-axis rotation to allow pitching of the system
- No pre-tension of the lashings, because of limitations in ANSYS Explicit Dynamics.
- Instead of rubber-steel frictional contacts a steel-steel frictional contact has been assumed since insufficient data was available in regard of the rubber padding.

Linearised model specifics

Up until this point the non-linear modelling part is covered, except for the linear part. As mentioned in Section 2.3.2 in the linearized model ANSYS is forced to implement linearization simplifications / assumptions to be able to perform the analysis at all. In Table 2.8 a compressed version of these assumptions can be found, which in the basis means the following:

- All contacts remain in contact, which results in the monopile not only able to experience upward (pressing) forces when in contact, but also downward (pulling) forces. A clear example can be found in Figure 2.19 which illustrates the reality of sagging vs the effects of the assumptions.
- For frictionless contacts $\mu = 0$ sliding is allowed, which results in no transfer of horizontal forces between the monopile and ship.
- For frictional contacts $\mu > 0$ no sliding is allowed, which does result in the transfer of horizontal forces between the monopile and ship.

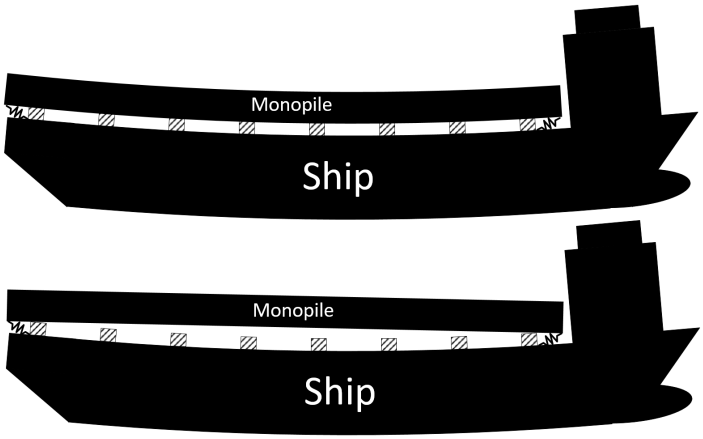

Figure 2.19: Ship sagging in reality (lower illustration) vs the effect of ANSYS linearisation assumption (upper illustration)

3

Results & discussion

In the previous chapter the topic discussed was concerning the process of constructing the model, in which for example the construction steps, boundary conditions and constraints are explained. In this chapter results from the constructed model will be evaluated and discussed for both the linear and non-linear set. This is an essential step towards answering the research question.

3.1. Linear, frequency domain analysis

The frequency domain analysis is a very useful modelling tool to observe system properties and behaviour. For example, this allows the evaluation of the natural frequencies, which can be used in the setup of the non-linear time domain analysis (see Figure 3.1). Although not as accurate[1] as the time-domain analysis, the linear, frequency analysis still allows one to develop an expectation of how a system responds to a certain forcing or excitation frequency. As this section will concentrate on the frequency domain analysis the goal of the discussion in this section is mainly to develop an expectation.

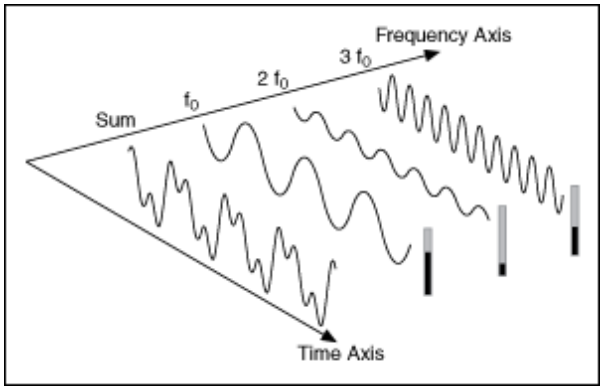

Figure 3.1: Frequency domain vs time domain [10]

3.1.1. Modal analysis

One set of data that can be reviewed in terms of frequency-domain analysis is regarding the natural frequencies (see Tables 3.1 & 3.2). When viewing the individual natural frequencies of the ship (case 1), a single monopile (case 1-2) and three monopiles (case 1-3) one can witness the monopiles indeed have higher natural frequencies, thus also having a higher bending stiffness over mass ratio than the ship. This could indicate that stiffness contributions are more pronounced than mass contributions for the monopile, that is until cases 2-19[2] are considered. When carefully examining Figure 3.2 it is evident

[1] because non-linearities are ignored
[2] when the monopile(s) are installed on the saddles on the deck of the ship

that for the shipping of a single monopiles (cases 2-10) 75% of the considered modes are lower than they initially were for a ship without any monopile (case 1), which means the mass contribution is more significant than its stiffness contribution. When shipping three monopiles (cases 11-19) the stiffness contribution becomes more pronounced, here only 37.5% of the considered natural frequencies are lower compared to shipping no monopiles (case 1). This makes sense as in Table 2.11 it has been shown that the structural density when the draft of the ship is changed throughout the cases is changed for each monopile setup. The single monopile cases (2-10) have the highest structural density for the ship out of all cases while the triple monopiles cases (11-19) have the lowest (see Section 2.3.3, subsection 'ship draft data' for a detailed explanation). Since the monopile's weight is only 13% out of the total displacement of the single monopile cases (2-10) and 34% for the triple monopiles cases (11-19), this means the system's responses are mostly dependent on the ship. In addition, as the triple monopiles cases (11-19) have less structural density for the ship, and the shipped monopiles become more significant in the total displacement, this means the total stiffness introduced by the monopiles are also more significant. As a result, such changes in structural density for the ship is most likely the explanation why the single monopile cases (2-10) differ so much with the triple monopiles cases (11-19), in terms of natural frequencies.

The other observation that can be made is in terms of lashing stiffness and type of friction contact. Changing lashing stiffness from 100% to 66% or 33% doesn't seem to change the systems natural frequencies (see Tables 3.1 & 3.2), which could mean that the systems (longitudinal bending) stiffness is far greater than that of the lashings. As a result, the system doesn't respond to the lashing stiffness at all. When considering the validation process of this research (see Section 2.3.2) this makes sense, as the differences in natural frequencies were already very low. This time the system has considerable more mass and stiffness and thus it makes perfect sense, with an unchanged lashing stiffness, that the effects of the lashing became redundant.

The same observation can be made for the types of friction contacts, no matter what type of friction contact is applied the linearized system doesn't respond to it in terms of natural frequencies. Since friction[3] isn't introducing any stiffness into the system, and is rather a damping term, this does make sense. However, since the validation process did show significant differences in natural frequencies amongst the contact types one would expect with a ship-monopile system the same kind of differences, especially when considering a frictionless setup. If any effect of friction can be witnessed this should be throughout the harmonic analysis, in which dampened peak amplitude(s) should show up, or the non-linear time domain analysis. However, since the validation process in Section 2.3.2 has showed that, even in the modal analysis, friction can play a role in terms of the system's natural frequencies it does indicate the following. Since the natural frequencies haven't changed in all cases, when changing the type of friction contact, it could indicate the monopile(s) do not slide. These results are questionable, as one would expect at least some degree of sliding happening between the ship and monopile(s) for the frictionless setup. Nevertheless, if this is truly the case, then that should be also shown throughout the non-linear time domain analysis.

Table 3.1: Case natural frequencies [Hz], Ship (no monopiles), 1x monopile and 3x monopiles (no ship) and cases 2-10

Mode	Ship	1-mono	3-mono	Case 2	Case 3	Case 4	Case 5	Case 6	Case 7	Case 8	Case 9	Case 10
1	2.5818	3.8659	3.8767	2.5277	2.5277	2.5277	2.5277	2.5277	2.5277	2.5277	2.5277	2.5277
2	6.2883	10.017	10.267	5.9151	5.9151	5.9151	5.9151	5.9151	5.9151	5.9151	5.9151	5.9151
3	10.132	18.16	19.112	9.7328	9.7328	9.7328	9.7328	9.7328	9.7328	9.7328	9.7328	9.7328
4	12.386	22.534	22.534	12.782	12.782	12.782	12.782	12.782	12.782	12.782	12.782	12.782
5	15.64	27.513	29.762	15.11	15.11	15.11	15.11	15.11	15.11	15.11	15.11	15.11
6	20.333	37.563	41.709	19.62	19.62	19.62	19.62	19.62	19.62	19.62	19.62	19.62
7	25.118	45.067	45.067	25.452	25.452	25.452	25.452	25.452	25.452	25.452	25.452	25.452
8	26.197	47.978	54.561	26.043	26.043	26.043	26.043	26.043	26.043	26.043	26.043	26.043

[3] in the case of simple, linear friction, or Coulomb friction

Table 3.2: Case natural frequencies [Hz], cases 11-19

Mode	Case 11	Case 12	Case 13	Case 14	Case 15	Case 16	Case 17	Case 18	Case 19
1	2.5705	2.5705	2.5705	2.5705	2.5705	2.5705	2.5705	2.5705	2.5705
2	5.8636	5.8636	5.8636	5.8636	5.8636	5.8636	5.8636	5.8636	5.8636
3	10.061	10.061	10.061	10.061	10.061	10.061	10.061	10.061	10.061
4	13.921	13.921	13.921	13.921	13.921	13.921	13.921	13.921	13.921
5	15.768	15.768	15.768	15.768	15.768	15.768	15.768	15.768	15.768
6	20.597	20.597	20.597	20.597	20.597	20.597	20.597	20.597	20.597
7	26.887	26.887	26.887	26.887	26.887	26.887	26.887	26.887	26.887
8	28.024	28.024	28.024	28.024	28.024	28.024	28.024	28.024	28.024

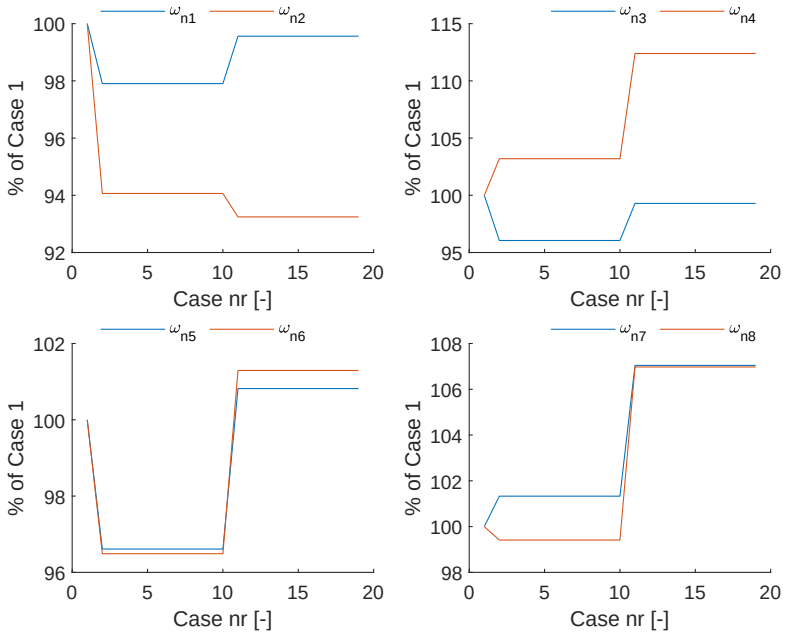

Figure 3.2: Change of natural frequencies compared to case 1

In order to have a better, substantiated answer regarding to what degree monopile(s) truly affect the system's natural frequencies, without also changing the structural density of the ship, cases 2 & 11 have been analyzed to a larger extent. In these cases the effects of pure mass[4], pure stiffness and suppressed monopile(s) are analyzed, these cases are further referred to the 'Xc'[5] cases (see Table 3.3). Without the addition of the aforementioned cases it becomes difficult to answer how monopile(s) truly effect the system's behaviour as multiple parameters are changed from cases 1 to 2, 1 to 11 or vice versa. Therefore, the addition of these case studies are essential as only a single parameter has changed, which is the investigated parameter.

[4] of monopile(s)
[5] The 'X' can be replaced by a 2 or 11, so for example 11c, 2c1 or 2c2

Table 3.3: Extra case study tweaks

Monopile setting	Case 2c	Case 2c1	Case 2c2	Case 11c	Case 11c1	Case 11c2
No stiffness	•			•		
No mass		•			•	
Suppressed			•			•

To further elaborate on Table 3.3, cases Xc has the goal to witness the pure mass effects of the monopile(s), with negligible stiffness effects. For these cases the monopile(s) have been given an area moment of inertia of $I_{yy} = I_{zz} = 2m^4$. Cases Xc1 creates the possibility to witness the pure stiffness effects of the monopile(s) on the ship, for which the monopile have been given a material density of $\rho = 10^{-11}$. For cases Xc2 the monopiles are suppressed entirely, creating the opportunity to witness basically a no shipped monopile conditions, such as case 1, with a structural density for the ship as the single (case 2) and triple monopile cases (case 11).

Table 3.4: 'Xc' series natural frequency data, all natural frequencies correspond to the same mode shape for each mode nr.

Mode	Case 2c (Pure stiffness effects of monopile)	Case 2c1 (Pure mass effects of monopile)	Case 2c2 (suppressed monopile)	Case 11c (Pure stiffness effects of monopiles)	Case 11c1 (Pure mass effects of monopiles)	Case 11c2 (suppressed monopiles)
1	2.3379	2.919	2.5077	2.0982	3.5258	2,6281
2	5.5683	6.6889	6.1083	4.8768	7.6803	6.4018
3	9.0498	10.982	9.8429	7.8887	13.102	10.316
4	12.435	14.511	12.03	10.922	17.919	12.608
5	13.949	17.073	15.193	13.642	20.585	15.923
6	17.277	21.424	19.754	15.259	25.233	20.704
7	20.414	27.746	24.398	18.08	32.32	25.57
8	24.709	29.297	25.449	21.908	36.569	26.673

The comparison of pure stiffness effects with pure mass effects and the suppressed effects of the monopile(s) results in a logical and expected deviation in natural frequencies from each other (see Tables 3.1, 3.2 & 3.4). So, as expected, the single, pure stiffness monopile case (2c1) has the highest natural frequency, while the single, pure mass monopile case (2c) has the lowest, with the suppressed monopile case (2c2) in between. When comparing the single, normal monopile case (2) with the single, suppressed monopile case (2c2) it becomes evident that, when shipping a single monopile, the mass-contribution is more pronounced than its stiffness contribution for 4 out of 8 modes (see Figure 3.3). The expectation was, just like the single monopile case (2), that the triple monopile case (11) would have higher natural frequencies than the triple, pure mass monopiles case (11c) and possible the triple, suppressed monopiles case (11c2). This has to do with the pure monopile(s) cases[6] (case 1-2 & 1-3) having the highest natural frequencies out of all cases. However, when comparing the triple monopiles case (11) with the triple, suppressed monopiles case (11c2) the story becomes slightly different as 5 out of 8 modes have higher natural frequencies. In this comparison the first mode this time has a slightly higher natural frequency instead of slightly lower, indicating that the stiffness contribution becomes slightly less important as the amount of monopiles shipped increases. Between the triple, pure mass monopiles case (11c) and the triple, suppressed monopiles case (11c2) the relations remain logical, just as for the single monopile cases. Although stiffer, the monopile(s) are not fixed over its entire length on the ship, which is the most probable reason why the monopile(s) are rather a mass than a stiffness contribution. Because of the aforementioned reasoning only a portion of the stiffness is transferred. Therefore, when comparing the triple, suppressed monopiles case (11c2) to the triple monopiles case (11) slightly more modes have higher natural frequencies than when comparing the single, suppressed monopile case (2c2) with the single monopile case (2) (see Figures 3.3 & 3.4).

[6] so without a ship

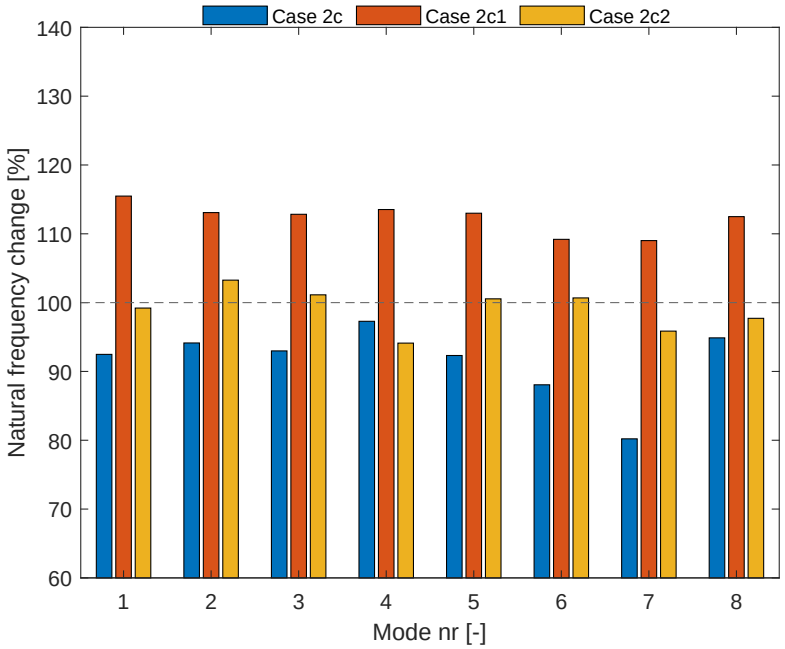

Figure 3.3: Change of natural frequencies compared to case 2, effects such as a shipped monopile with negligable stiffness (2c), negligable mass (2c1) or suppressed entirely (2c2)

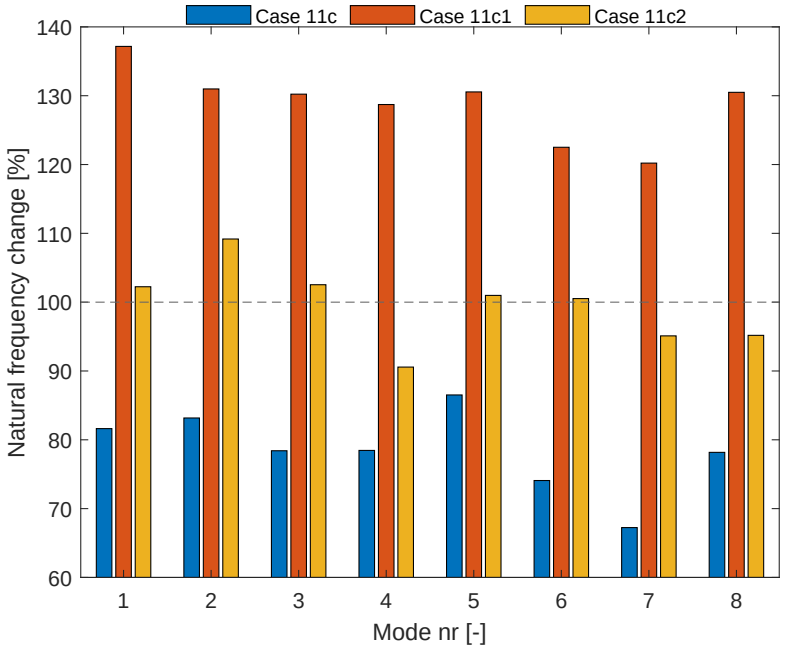

Figure 3.4: Change of natural frequencies compared to case 11, effects such as a shipped monopile with negligable stiffness (11c), negligable mass (11c1) or suppressed entirely (11c2)

Another tool in the linear frequency-domain analysis are the mode shapes. Examining Figure 3.2 the most interesting mode shapes to analyse would be the 2nd, 4th, 6th and 8th mode shapes for the case that has no monopile (1), a single monopile (2) and triple monopiles (11) so all form of changes can be witnessed, while having the same contact and lashing setup. All mode shapes below are plotted by dividing by its local maximum in z-direction, which means that at 1 the mode shapes most extreme deformation occurs while at 0 no deformation occurs at all. But before heading any further in the comparison it is very important to highlight that when shipping no monopiles (case 1) the first mode shape that dominates in axial direction is corresponding with its fourth natural frequency, this also

accounts for the single (cases 2-10) and triple monopile cases (cases 11-19). However, the second axial dominant mode shape occurring at case 1 (no monopiles shipped), which is corresponding with the 7th natural frequency, has shifted to the 8th natural frequency when monopile(s) are shipped (cases 2-19).

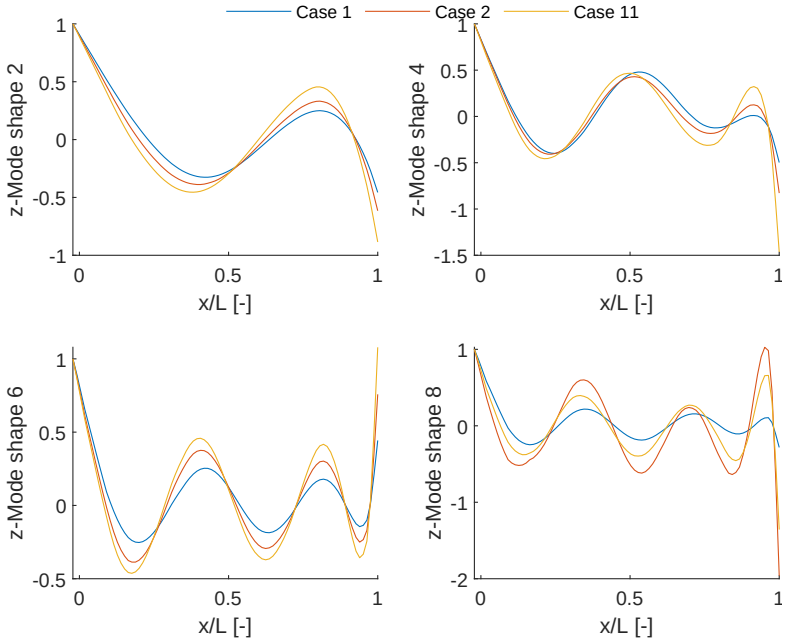

Figure 3.5: Ship mode shapes 2, 4, 6 & 8 for cases 1,2 & 11, pure Z-directional deformation devided by the occuring max deformation.

When comparing Figure 3.2 & 3.5 it is evident that there is no straightforward explanation for the correlation between all changing natural frequencies over the cases and their changing mode shapes. What can be said however is that for all modes the maximum amplitude seems to be shifting towards the front of the ship, when comparing case 1 to 2 & 11. This could indicate that the ship's dynamic behaviour is definitely influenced by carrying monopile(s). Also, the midship is definitely affected by the shipping of 1 or more monopiles when reviewing the mode shapes in Figure 3.5. For all observed modes the amplitude at midship increases from no shipped monopile(s) (case 1) to a single shipped monopile (case 2) to three shipped monopiles (case 11), which could be the effect of the linearized assumptions of ANSYS (see Table 2.8). Since the unrealistic nature of the linearization assumption of ANSYS these results doesn't make sense at all. As mentioned before, ANSYS assumes, for all forms of contacts in the linearized system, that separation is not possible, which means when sagging or hogging occurs the monopile(s) also must bend accordingly, while this is not necessarily the case in reality (see Figure 2.19). As a result, ANSYS assumes a less stiff bow compared to the rest of the ship since the monopile(s) do not reach the bow. The only part that doesn't seem to show the same response is for the aft half of the ship at the second mode, this could be due to the transfer of the maximum amplitude from the aft to the front of the vessel.

Coming back to the system detecting no or insignificant sliding of the monopile(s), reviewing Figures 3.6 & 3.7 it is evident that the monopile follows all ship mode shapes in z-direction at all contact nodes perfectly. However, as mentioned before this seems unrealistic, especially when considering that the frictionless setup should at least slide a little bit in the axial dominant modes such as the 4th and 8th mode. If one would believe these results then this indicates that at the saddle locations the monopile wants to follow the x-mode shape of the ship at all times. As a result this means that, even for the frictionless contacts, no-slippage is detected by the modal analysis. Although unrealistic, for the frictional contact cases ($\mu > 0$) this makes perfect sense as it is in line with the numerical linearization assumptions of ANSYS. These assumptions are performed during the computation of any linearized analysis, such as the modal- and harmonic analysis (see Table 2.8). For the frictionless contact cases this means, as mentioned before, no slippage is detected. And finally, witnessing matching bending

mode shapes over the cases between the ship and monopiles also matches the expectations from Table 2.8. This is because the linearization assumptions of ANSYS, always makes sure the contact interfaces remain in contact, being it of the type no-separation contact for the frictionless contacts or a bonded contact for frictional contacts. In Figure 2.19 an illustrative comparison can be found of how the contacts work in reality when a ship is sagging versus what the effects are when ANSYS applies its linearization assumptions. To further elaborate on what the effects of these assumptions are, the harmonic analysis has been expanded with a maximum bending moment analysis for all 8 modes. The effects of these linearization assumptions are clearly present in the maximum bending moment analysis, which will be further discussed in Section 3.1.3.

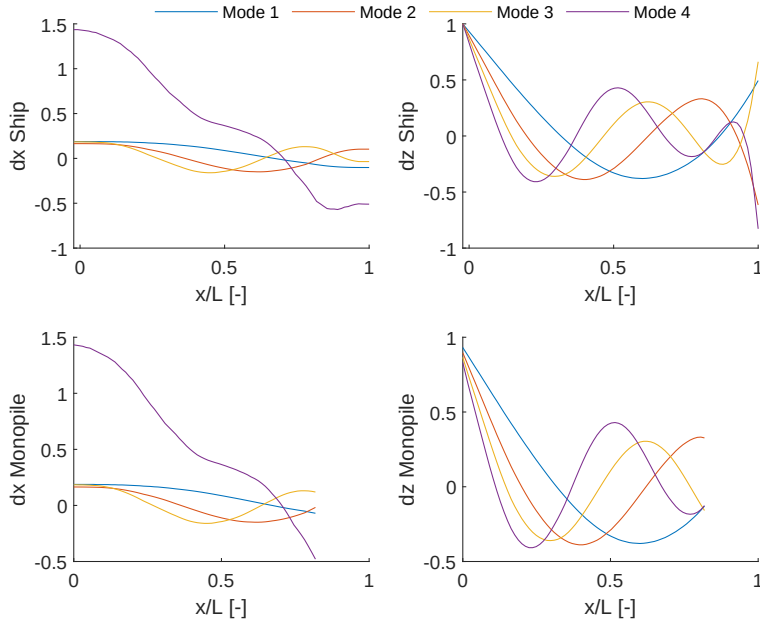

Figure 3.6: Monopile & ship x- & z- modeshapes 1 to 4 for 1 monopile (case 2,3,4), normalized by the ship's absolute maximum z-deformation

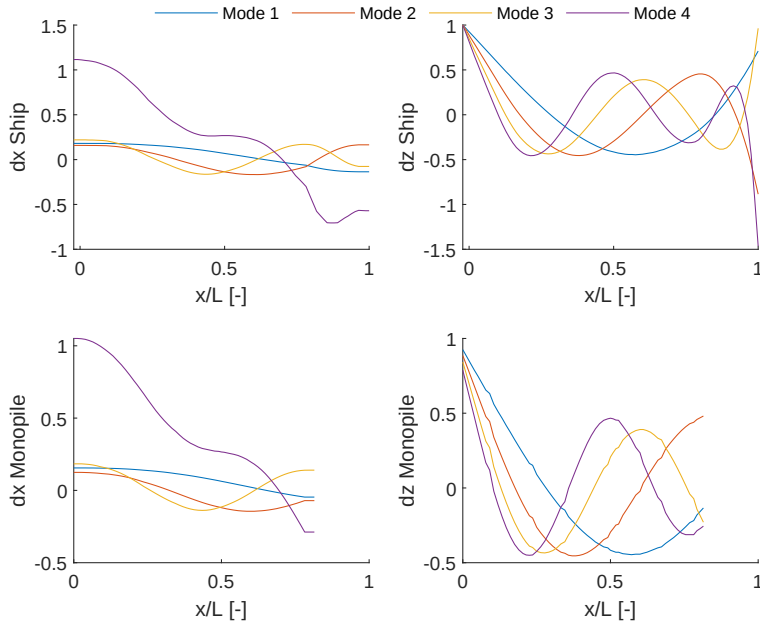

Figure 3.7: Monopile & ship x- & z- modeshapes 1 to 4 for 3 monopiles (case 11), normalized by the ship's absolute maximum z-deformation

3.1.2. Frequency responses

The harmonic analysis allows for forcing to be applied on the ship in which the frequency responses can be read from. Both the modal analysis and harmonic analysis are linear, with the major difference between the two being the possible visibility of linear damping in the harmonic analysis. Since the contacts are highly non-linear (Coulomb friction) the only type of damping that would be visible is the structural damping. According to Wu et al. a realistic coefficient for the structural damping would be 0.01 [19], which has been used throughout the harmonic analysis. As mentioned earlier this is also a linearized analysis, which means that the linearization assumptions of ANSYS in Table 2.8 are yet again applicable.

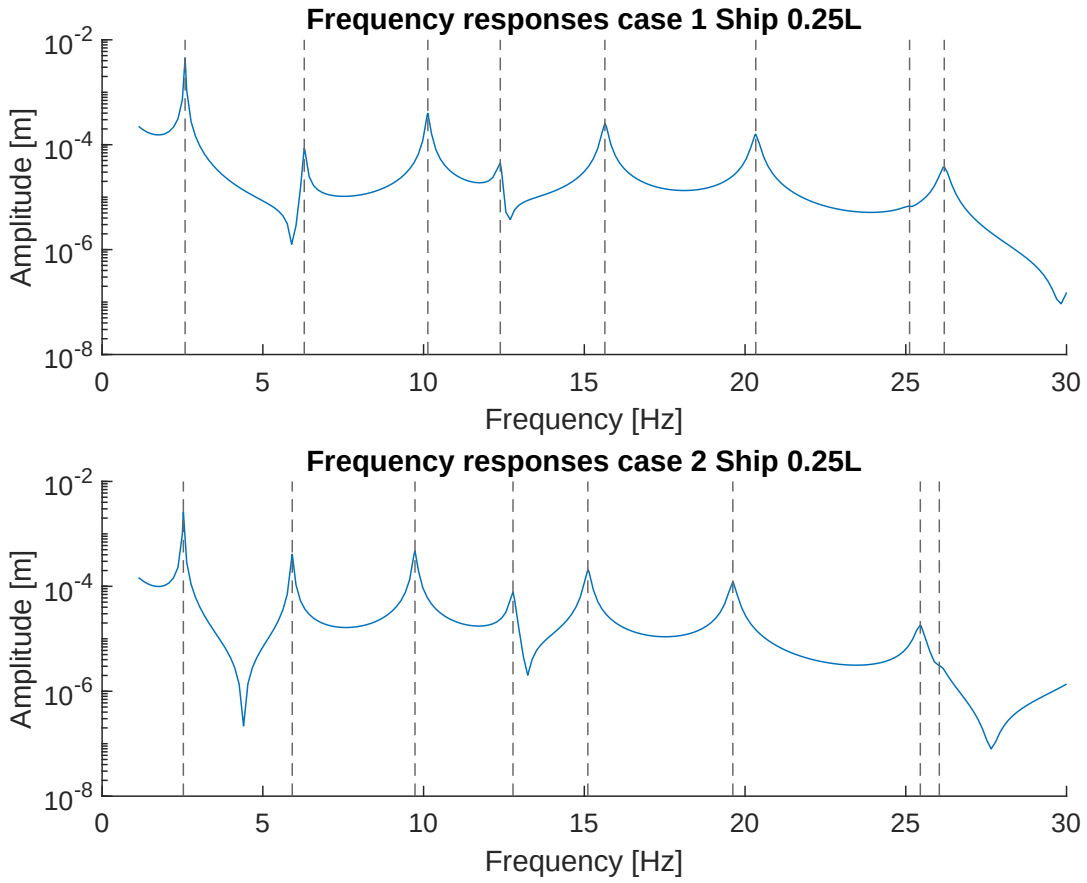

Figure 3.8: Ship 0,25L case 1 responses compared to case 2, with the vertical lines '- -' respresenting the natural frequency locations

As mentioned in Section 3.1.1 the 7th mode in case 1 (ship without monopile) is an axial dominant one and shifts to the 8th mode when one or more monopiles are installed (cases 2-19), Figure 3.8 is another indication of that. For the case without monopile(s) (case 1) no peak can be seen at all at the 7th mode, the same can be witnessed for the 8th mode for the single monopile case (2). Since these frequency amplitude plots are aimed at the z direction and the aforementioned modes are for the most part axial, this also indicates the axial mode shifted from the 7th to the 8th mode. For more ship locations and their frequency responses than the ones depicted here, please refer to Appendix A.1.

In terms of friction contacts, from Figure 3.9 it seems evident that the type of contact has no effect on the frequency reponses of the system on each ship & monopile location, when shipping a single monopile. The frictional type of contacts from case 3 compared with that of case 4 has a clear match in terms of frequency responses, which is exactly in line with the expectations highlighted in Table 2.8 and Section 2.4 but unrealistic as mentioned in the modal analysis. Figure 3.9 only considers the ship & monopile location at 0.25L, in Appendix A.2 all other locations can be found, which have the exact same result.

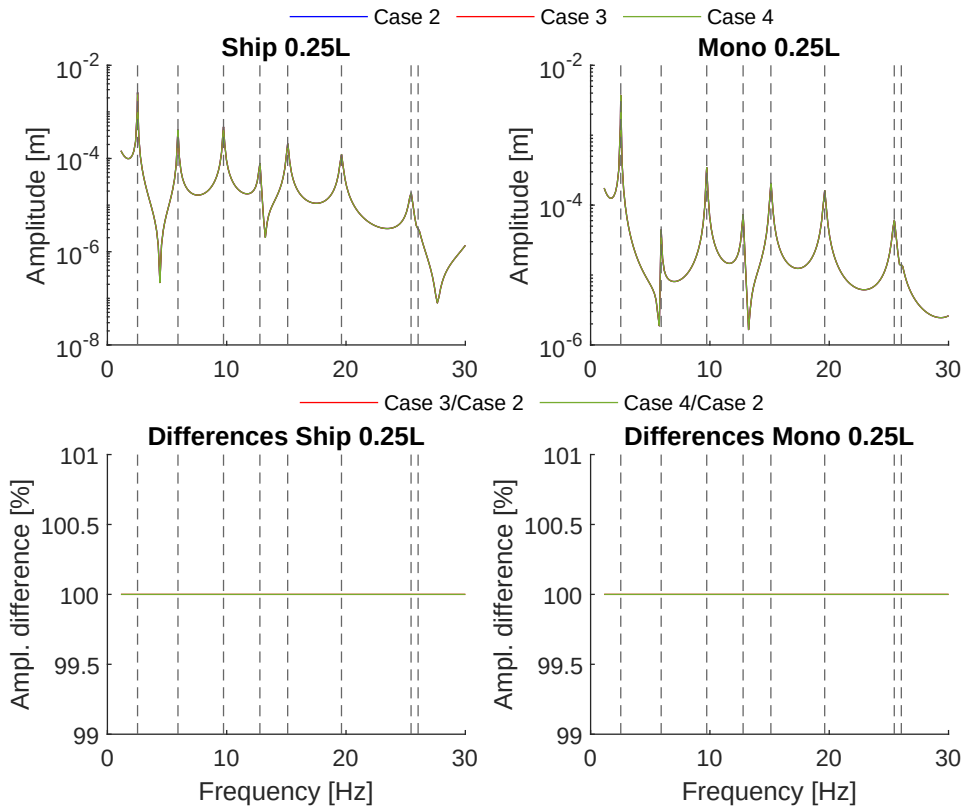

Figure 3.9: Ship & Mono 0,25L case 2 responses compared to case 3 & 4, with the vertical l lines '- -' respresenting the natural frequency locations

Constructing the same set of results, but this time for the purpose of analyzing the effects of lashing stiffness for the single monopile cases, which means comparing case 5(66%) & 8(33%) over case 2(100%) results in the same conclusion. In Figure 3.10 one can witness there are spikes this time around in the differences, when diving deeper into the represented numbers it seems clear that these are very small peaks, far below the 1% difference and can also not be seen on the frequency responses plot. Since these peaks are negligibly small and within the margin of error the same conclusion can be made in terms of lashings as for the type of friction contact. This means that lashing stiffness has no effect on both the ship and the monopile. Although pre-tension has not been included into the model, the expectation is that it has no effect on the ship and monopile as well. For all other locations please refer to Appendix A.3.

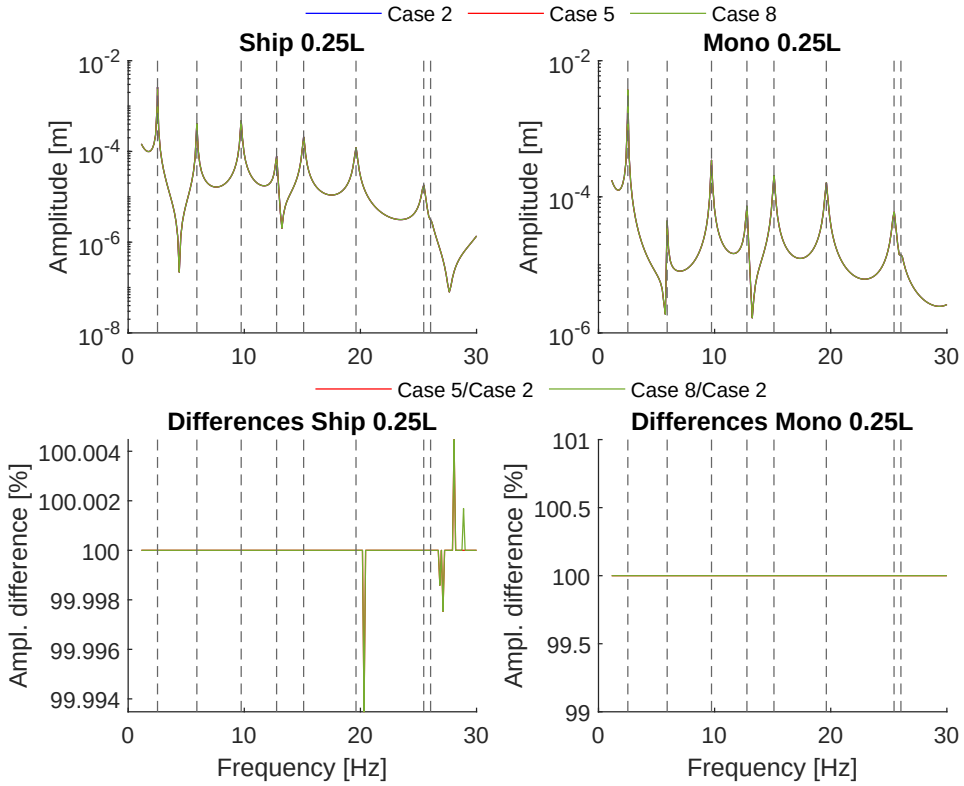

Figure 3.10: Ship & Mono 0,25L case 2 responses compared to case 5 & 8, with the vertical lines '- -' respresenting the natural frequency locations

When considering shipping three monopiles instead of one and witnessing the effects of friction type and lashing stiffness the same conclusion can be made. When comparing the frictionless (case 11), frictional (case 12) and very high friction (case 13) setup with each other and the 100% (case 11),66% (case 14) and 33% lashing stiffness (case 17) setups with each other, the same set of results are generated (Figures 3.11 & 3.12). So the amount of monopiles seems to not matter for both the lashing stiffness to take effect, but also the type of friction. Just like in Sections 3.1.1 the conclusion can be made, although unrealistic, that no sliding occurs between the saddles and monopile(s), as no differences can be witnessed in any case study comparing contact types in the harmonic analysis. For more information regarding the other ship & monopile locations please refer to Appendix A.4 & A.5.

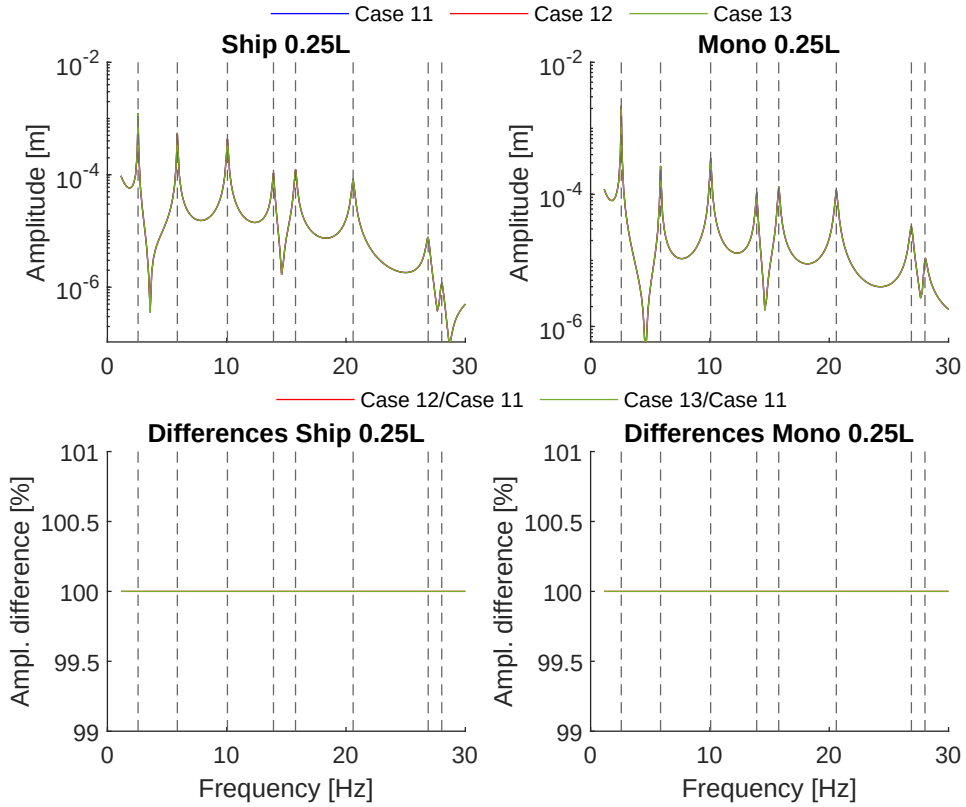

Figure 3.11: Ship & Mono 0,25L case 11 responses compared to case 12 & 13, with the vertical lines '- -' respresenting the natural frequency locations

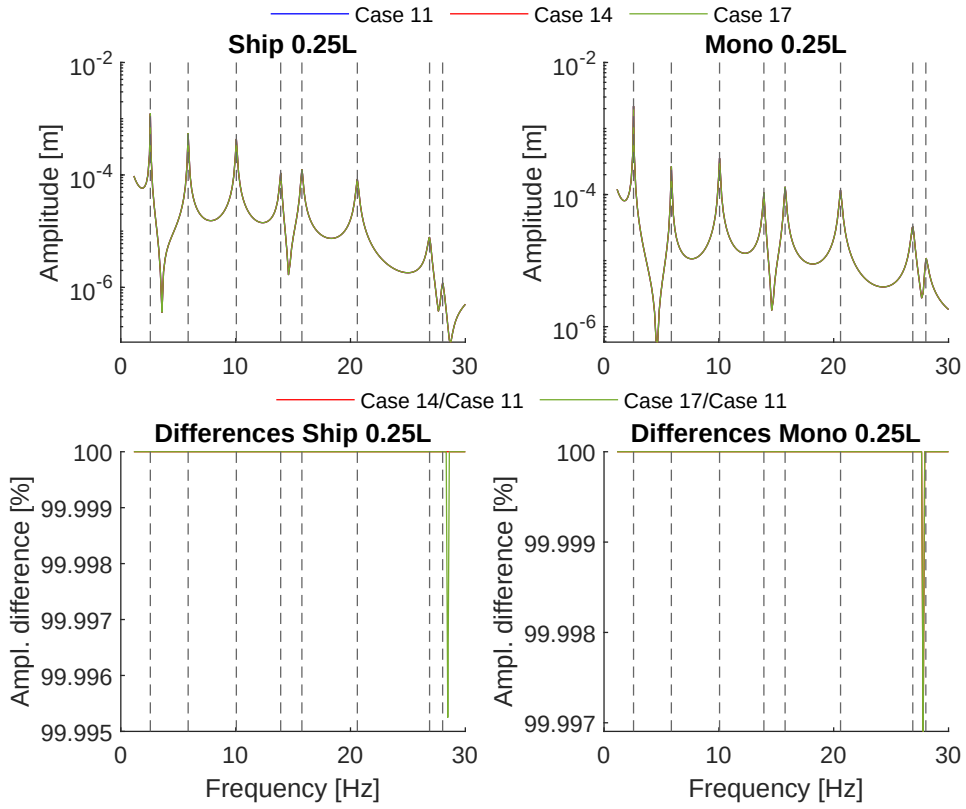

Figure 3.12: Ship & Mono 0,25L case 11 responses compared to case 14 & 17, with the vertical lines '- -' respresenting the natural frequency locations

To study the effects of the monopile on the ship, without influencing the draft of the ship for example, the 'Xc' cases were created. These cases allow one to address the specific mass- and stiffness effects of the monipile(s) (see Section 3.1.1 for more information). When carefully studying Figures 3.13 & 3.14 and comparing the initial state of the ship without any monopile on deck yet (cases Xc2) with the final state of the ship in which the monopiles are loaded (cases X) some observations can be made. First of all, the amplitudes for the ship for several natural frequencies remain more or less the same for the unloaded and loaded state, which modes are matching is for each considered ship location different. For all other natural frequencies mostly an increase in amplitude can be witnessed, which means that shipping a single monopile reduce the structural damping effects at least to some extent. In case three monopiles are shipped (case 11) the story becomes no different, other than that the 8th mode gained a peak when carrying monopiles. This indicates more pronounces z-displacements are occurring when resonating in the 8th mode, which in this case is an axial dominant mode.

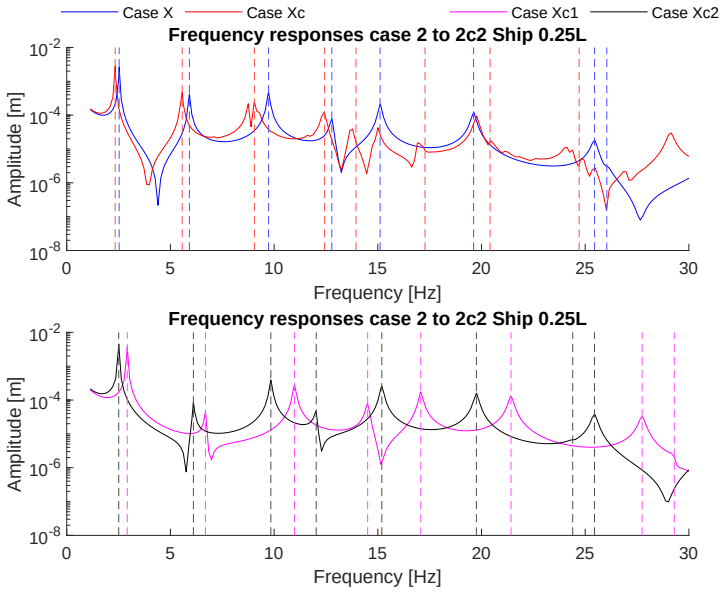

Figure 3.13: Ship 0,25L responses due to monopile (1x) parameter tweaks, with the horizontal lines '- -' respresenting the natural frequency locations

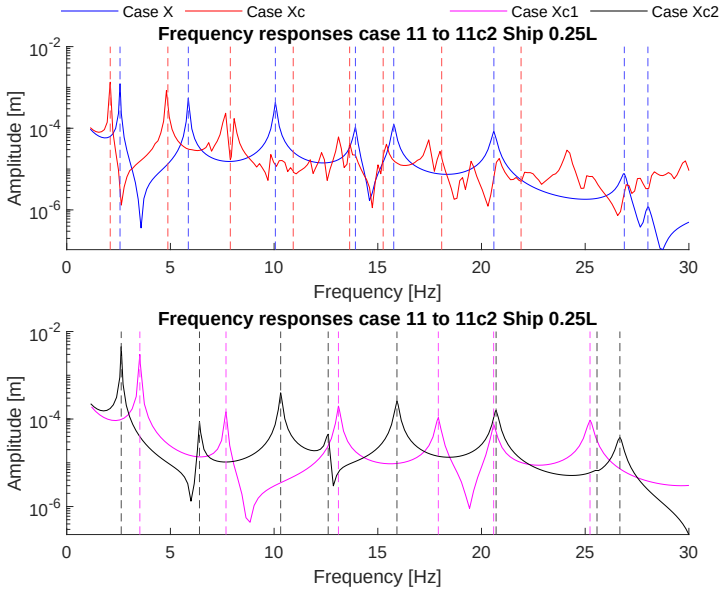

Figure 3.14: Ship 0,25L responses due to monopile (3x) parameter tweaks, with the horizontal lines '- -' respresenting the natural frequency locations

3.1.3. Bending moments

In the harmonic analysis not only the frequency responses have been collected but also the bending moment data of the ship and monopile(s). To follow-up from Section 3.1.1 the linearization assumptions performed by ANSYS (see Section 2.4) is expected to be causing bending moments into the monopile. This is due to the fact vertical forces for the frictionless contacts and also horizontal forces for the frictional contacts are transferred between ship & monopile (see Section 2.4). This logically results in a reduced (internal) bending moment in the ship as some of it is transferred to the monopile, because of the corresponding constraints. In practice the monopile(s) are not forced to follow the shape of the ship as its only lashed at the ends of the monopile to the deck (see Figure 2.19), which results practically in far less transferred bending moment to the monopiles.

When observing the bending moment for a particular (natural) frequency one will notice it will vary over time. This is because the bending moment follows the shape of its mode shape and thus varies during the period of the oscillation. Therefore, in order to find the maximum bending moments one has to make sure the presented oscillation moment is either at its maximum or minimum in its phase. To some this is known as a 'phase shift' and to others and ANSYS this is known as the 'sweeping phase', for the purpose of this project this has been set to 270 degrees. There is no specific reasoning why 270 degrees have been picked over 90 degrees, they should be the exact same with only their bending moment in opposite directions and since all presented values are absolute values this should not make any difference.

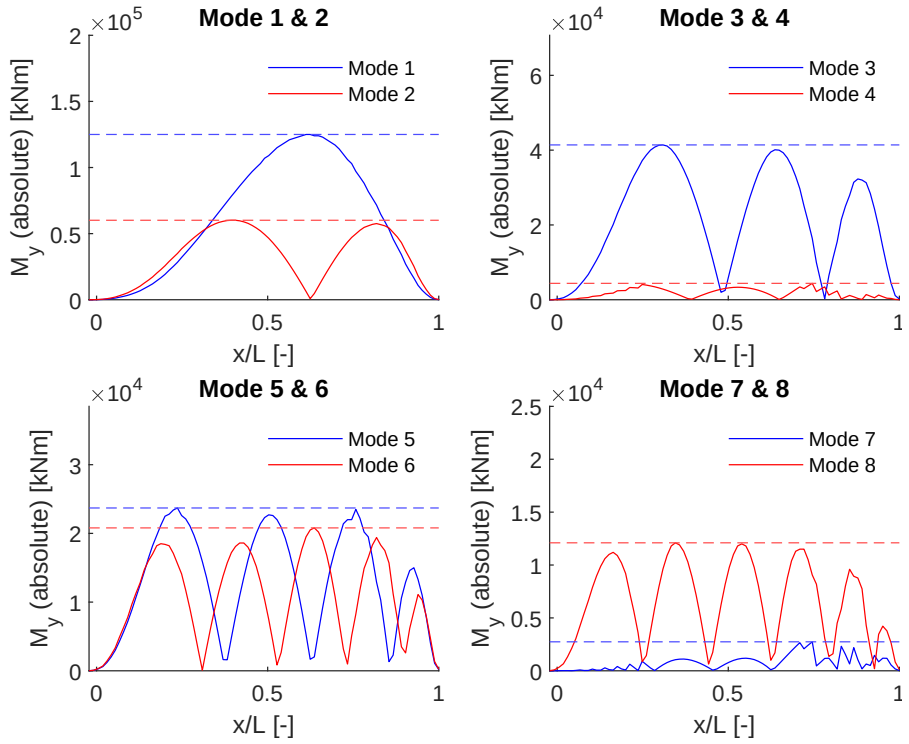

Figure 3.15: Case 1 absolute longitudinal bending moments for modes 1 to 8, with the horizontal lines '- -' respresenting the absolute maximums

As depicted in Figure 3.15 the 1st mode corresponds to the highest absolute bending moment. The higher the frequency and the more bending nodes the lower the maximum absolute bending moment becomes, which makes sense. Therefore, it seems logical to purely focus on bending moments in the 1st and 4th mode. This is because the 1st mode introduces the highest bending moments while the 4th has a high axial mode contribution. Furthermore, as mentioned before the 4th & 7th mode is an axial dominant mode, therefore these modes show lower bending moments than all other mode. For the bending moments regarding all 8 modes for all cases please refer to Appendix A.7.

When comparing bending moment data from Appendix A.7 one can state it is evident that type of friction contact and lashing stiffness doesn't influence the ship. This falls in line with Section 3.1.1 as

the same has been concluded for the contacts and lashings. Obviously, this isn't a realistic result as one would expect the frictionless setup to not transfer bending moments because of the no-separation condition. On the otherhand, although unrealistic the results of the frictional setups do make sense as ANSYS assumes a bonded contact, which effectively means bending moments are, in fact, transferred between ship and monopile(s). Therefore, since throughout the linear model the same conclusions follow from each analysis it seems safe to expect that the contact results needs further investigation and so far only the amount of monopiles influence the ships behaviour.

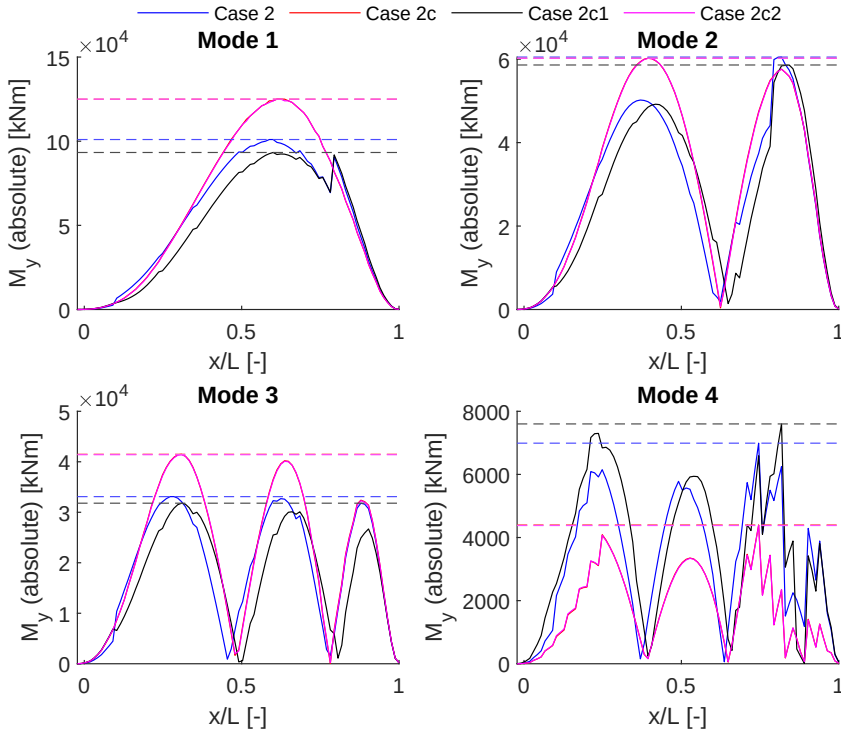

Figure 3.16: Cases 2 to 2c2 absolute longitudinal bending moments for modes 1 to 4, with the horizontal lines '- -' respresenting the absolute maximums. Side note: red & purple line overlap each other!

When specifically focusing on what effect the monopile(s) have on the ship the comparison between cases 2 to 2c2 and 11 to 11c2 can yet again be made. When Figure 3.16 is studied one can notice cases 2c and 2c2[7] have almost or exactly the same absolute bending moments across the length of the ship, for all 4 modes. As a result, this means that when comparing a setup with a suppressed monopile versus a setup with a pure mass contributing monopile, the ship will undertake a negligible amount of extra bending moment. When zooming into the actual effects of the monopile's stiffness (case 2 versus case 2c and 2c1) it seems that the stiffness of the monopile decreases the bending moment of the ship. This falls in line with the expectations mentioned in the first paragraph of this section. For mode 4, which is the first axial significant mode, the conclusion is almost the exact opposite of the others. Here it seems that the absolute bending moment is not affected by the monopiles mass but is affected by its stiffness, in the opposite direction from modes 1 to 3. If this is truly because of the axiality of the mode itself remains an unanswered and fairly difficult question.

[7] monopile without stiffness vs supressed monopile

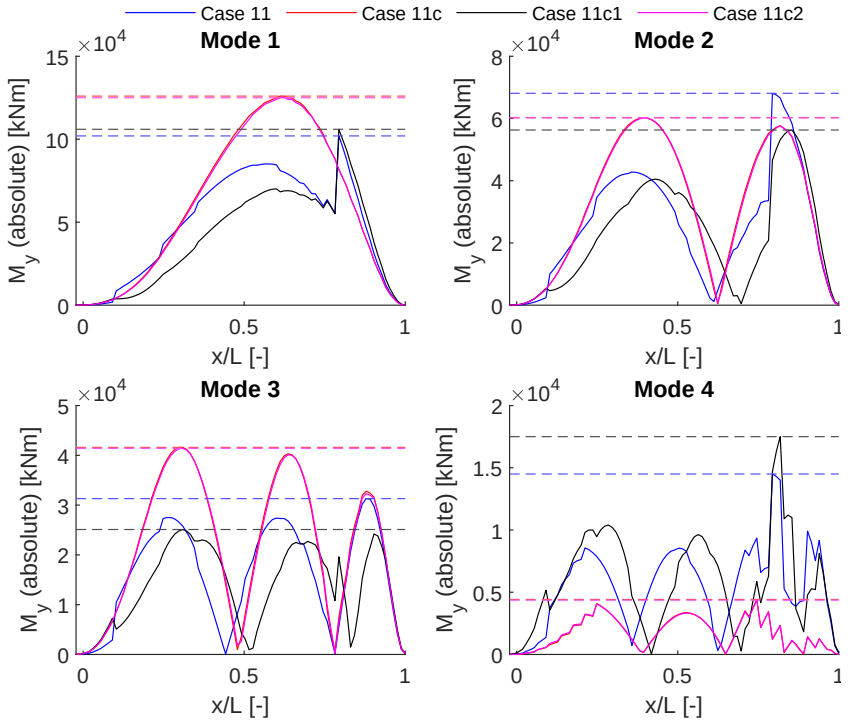

Figure 3.17: Cases 11 to 11c2 absolute longitudinal bending moments for modes 1 to 4, with the horizontal lines '- -' respresenting the absolute maximums. Side note: red & purple line overlap each other!

Doing the same review for case 11 this time around the exact same conclusions can be made. When observing Figure 3.17 the additional observation that can be made is that the amount of monopiles shipped will decrease the overall bending moment throughout the ship. This falls also inline with the expectation mentioned in the first paragraph of this section, but nonetheless is not logical as mentioned before and therefore is not expected to happen in practice.

When observing Figures 3.17 & 3.16 a sudden upward spike can be witnessed around 8th and last saddle location (see Figure 2.15). This spike is caused by the sudden decrease in combined structural stiffness, this is shown throughout cases 1, 2c, 2c2, 11c & 11c2[8] as they don't show such behaviour. Because of the absence of monopile(s) in the aforementioned cases the absolute bending moment has a smooth curvature while the other cases don't, in which, ANSYS applies its linearization assumptions.

Finally, the most interesting conclusion that can be made from Figures 3.16 & 3.17 is most likely hidden in the comparison of the pure mass contributing monopile (cases Xc) versus the suppressed monopile(s) (cases Xc2). What can be witnessed in these figures is that the mass of the monopile(s)s very slightly increase the bending moment across the ship, which means that the draft of the ship for the most part dictates what the max bending moment will become. Also, since it makes sense that only a very limited amount of bending moment is transferred between ship and monopile it is expected that the actual bending moment curve will be looking almost identical to the pure mass curves (cases Xc).

[8] cases in which the monopile(s) have no stiffness or are suppressed.

3.2. Non-linear, time domain analysis

During the linear frequency analysis an expectation has been formed, which will be reflected to the non-linear time domain analysis. During the review of this part of the analysis it should become clear whether the expectations match with the outcome of the more accurate, yet time consuming, time-domain analysis. A single simulation can require a significant amount of computational time, especially when considering this must be done for case studies 2 to 19. Therefore, the amount of time simulations per case has been limited to 3 each, which corresponds to, as mentioned before, the first three natural frequencies.

To recap the expectations from the previous section, the linear (frequency-domain) analysis indicated:

- No sliding occurs, thus the type of friction contact has no effect on the system's behaviour.
- Lashing stiffness has no effect on system.
- An increased amount of monopiles on deck results in a more pronounced mass contribution

3.2.1. Contact & lashing influences

When observing Figures 3.18 & 3.19 it seems evident that the type contacts has no influence on the x- or z-directional deformations, being it for the first, second or third applied natural forcing frequency. The same results were found throughout all other locations and cases, including the monopile's locations. This observation matches the expectations from the linear frequency analysis, as no differences could be spotted in that analysis either. However, as mentioned Section 3.1 it doesn't make sense that also the frictionless setup shows no sliding. Although the x-deformation are very limited it should be causing at least some sliding for the frictionless setup, being it only a very small amount. If the lashings would be the cause of this phenomena, then this would have shown for the frictionless setup at least some form of oscillation between the x-movements of the monopile and ship. Since this seems to be not case in both the linear and non-linear analysis it is expected that a flaw in the contact modelling exists, although the thorough validation process. From the responses the possibility exists that ANSYS overwritted all contacts, maybe because of certain settings, to bonded contacts although setup as friction(less) contacts.

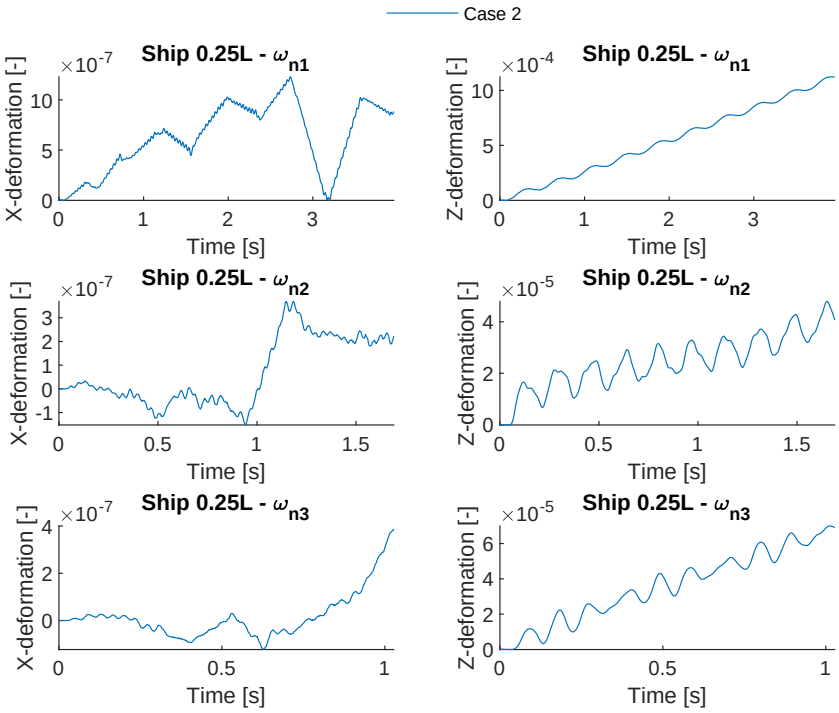

Figure 3.18: Deformations case 2 - Ship 0.25L X- & Z-direction

When the effects of lashing stiffness is considered, at some instances a major impact can be witnessed when comparing Figures 3.18 & 3.20. Here the effects are compared between a 100%, 66% and 33% lashing stiffness instances with identical contact types and ship-monopile configurations. In Figure 3.20 one can witness the lashing stiffness has little effect when the forcing frequency is in its first or third natural frequency, but does have a noticeable difference in the second natural frequency. For the first and third forcing frequencies the difference is approximately 6% or lower, while for the second, in X-direction, has a difference of 40000% percent (peak) difference. In Z-direction the difference seems more obvious for the second frequency, as the difference isn't displayed as a spike but rather an overall increasing difference, in which the maximum difference is approximately 60%. However, this difference looks mostly like a trendline or drift difference, since in reality[9] no upward drift exists this indicates these results are for the most part unrealistic and differences should be lower. Similar plots regarding all other observation locations can be found in Appendix B.2 & B.4.

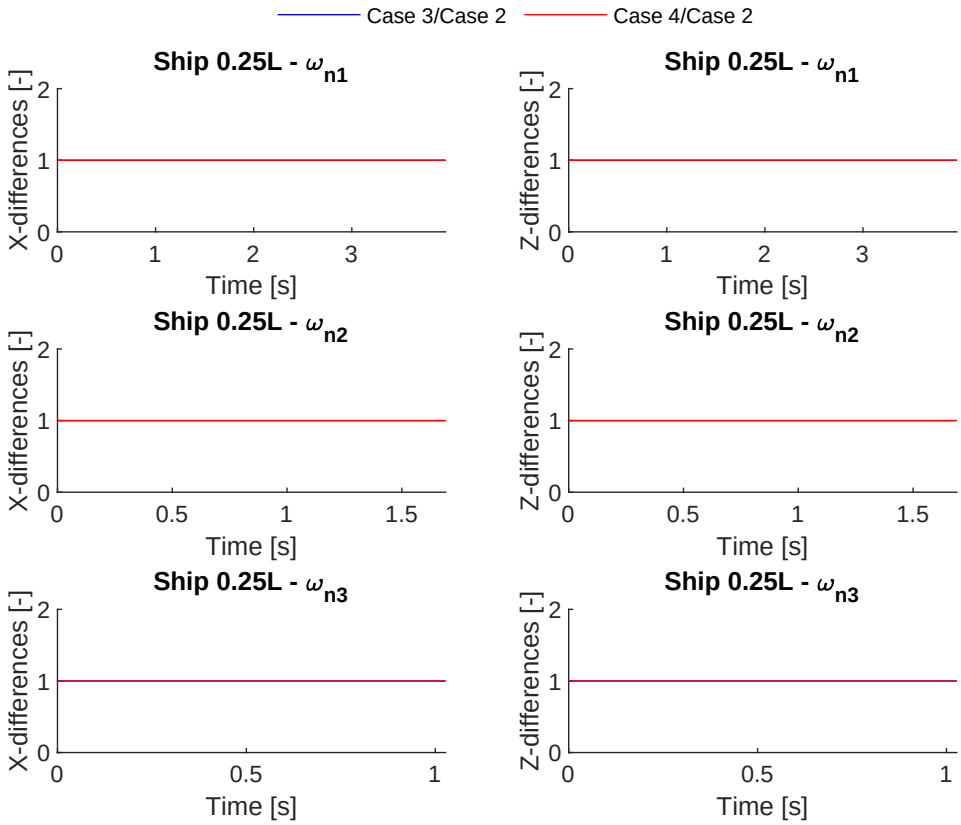

Figure 3.19: Differences between cases 2,3 & 4 - Ship 0.25L X- & Z-direction

[9]because the ship floats on water and is effected by gravity and doesn't float in space, which is the case in the model since it doesn't include FSI

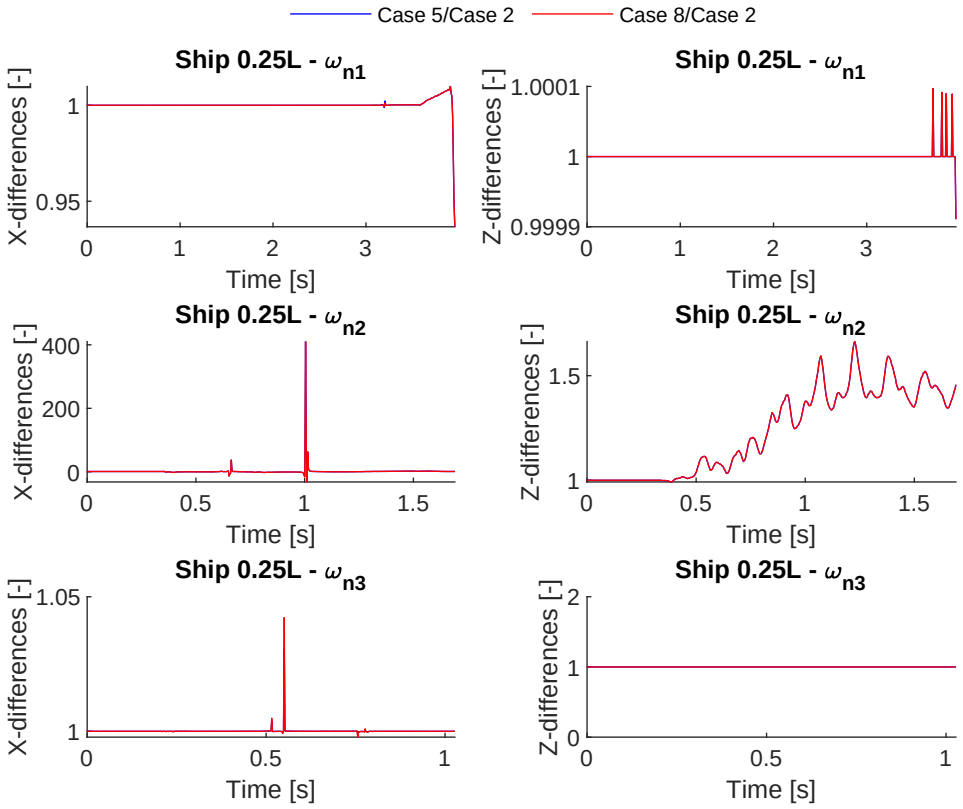

Figure 3.20: Differences between cases 2,5 & 8 - Ship 0.25L X- & Z-direction

When observing the effects of lashing stiffness for three monopiles the results become even more interesting. By observing Figures 3.21 & 3.22 it is shown that a lashing stiffness of 100% has almost identical deformations with 66% lashing stiffness for all forcing frequencies. However, decreasing the lashing stiffness further to 33% shows quite some difference at the second forcing frequency. So according to Figures 3.20 & 3.22 & Appendix B.2 & B.4 it seems to be evident that, depending on the amount of monopiles shipped, lashing stiffness does influence the ship & monopile responses. There seems to be no difference between the ship & monopile responses per case, but lashing stiffness definitely can alter the system's responses, depending on the applied frequency. Although it is expected, as mentioned in the previous paragraph, that these differences in reality as a lot smaller because of the absence of the trendline, representing an upward drift.

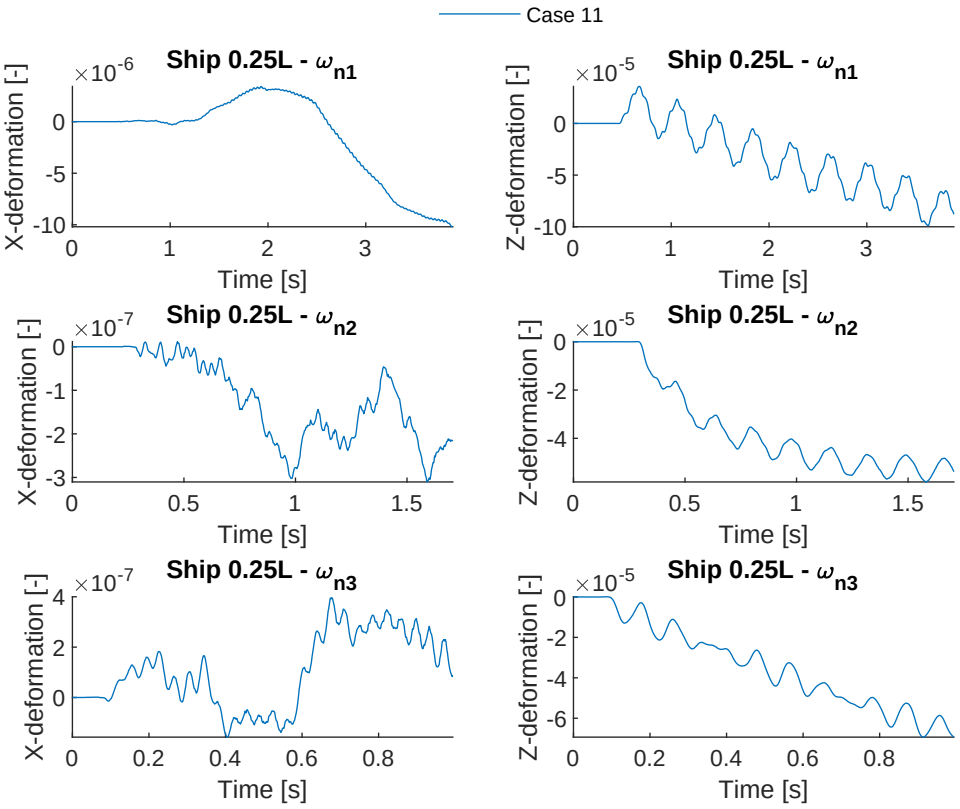

Figure 3.21: Deformations case 11 - Ship 0.25L X- & Z-direction

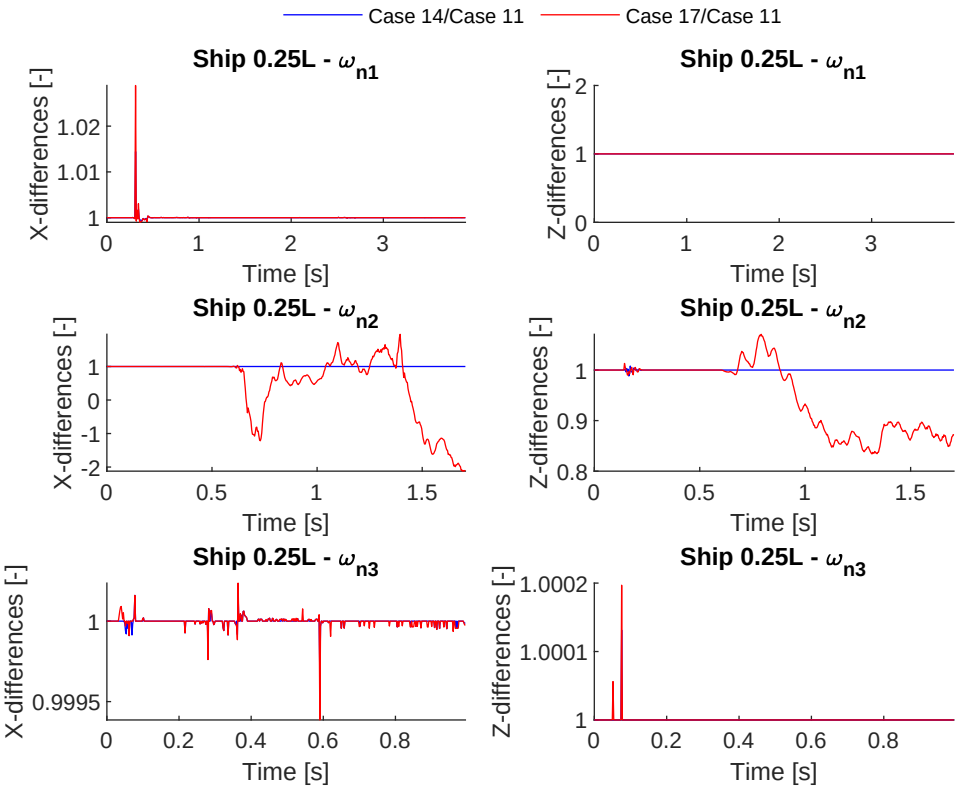

Figure 3.22: Differences between cases 11,14 & 17 - Ship 0.25L X- & Z-direction

In the linear frequency domain analysis, the expectation of lashing stiffness having no influence on the system's responses, seems to be not matching the non-linear time-domain analysis. During the time domain analysis, it became clear that, depending on the applied frequency, lashing stiffness can influence the system's responses. Althought it is expected that in reality these differences will be much smaller than indicated in the figures, lashing stiffness can alter the system's responses.

3.2.2. Monopile influences

In the linear, frequency domain analysis, it became clear that the amount of monopile shipped, influences the system's responses far beyond all other observed aspects, such as the type of friction contact & lashing stiffness. Therefore, the expectation is that the time domain simulations will show that the amount monopile shipped will influence the system's responses as well and also to the highest degree compared to the other observed aspects.

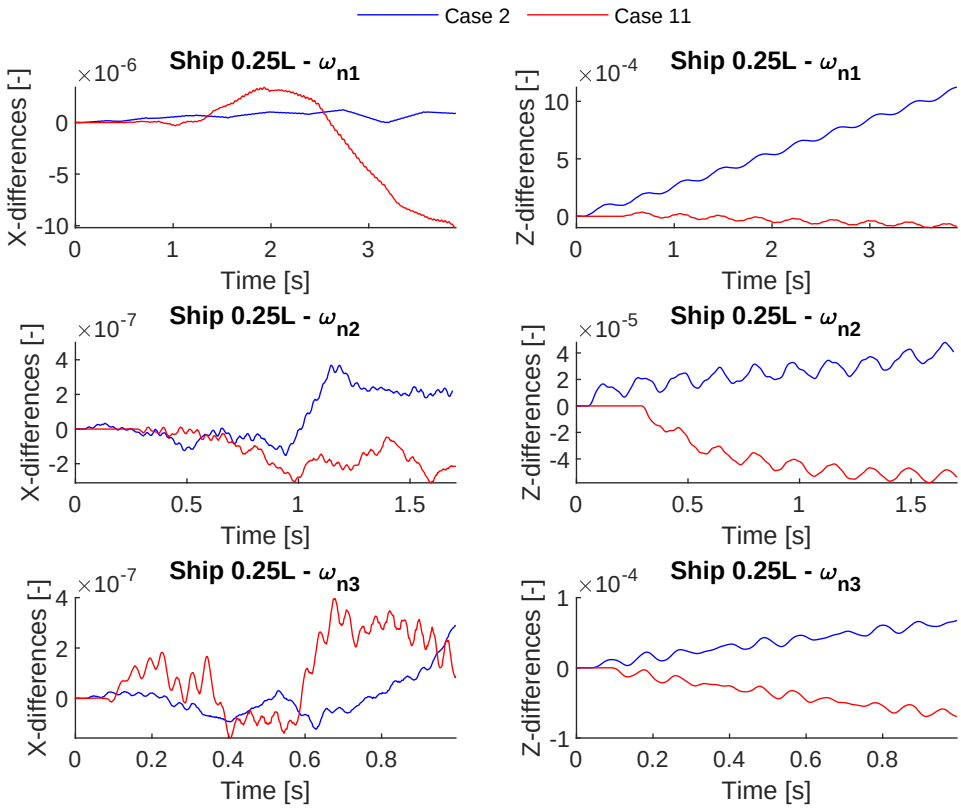

Figure 3.23: Deformations cases 2 & 11 - Ship 0.25L X- & Z-direction

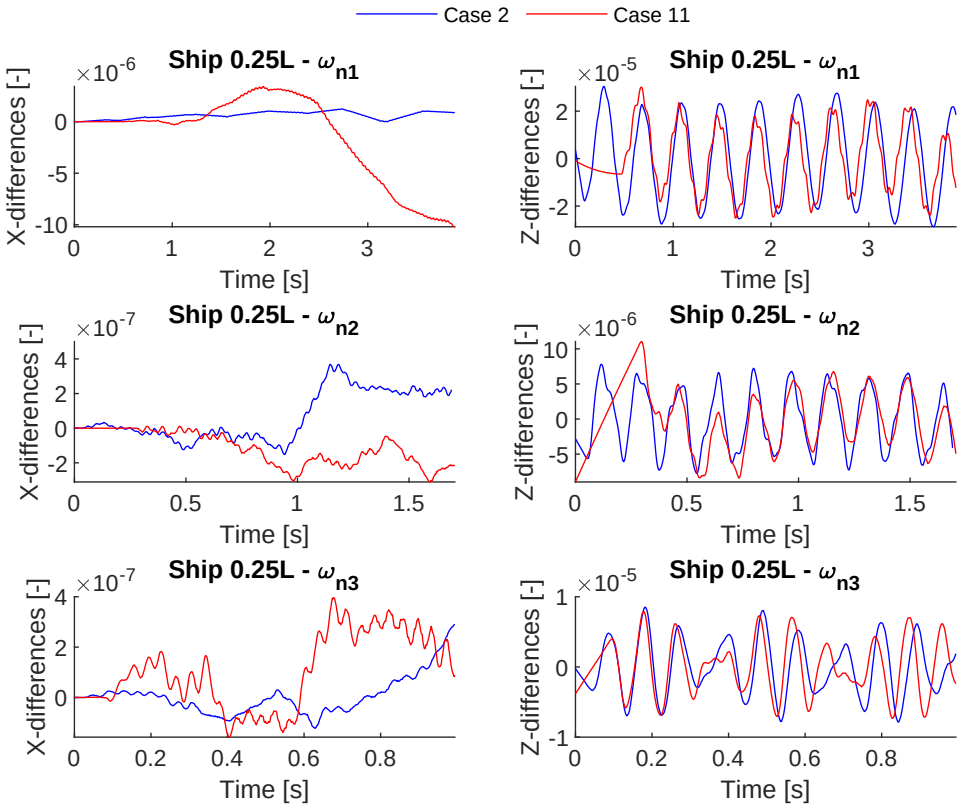

Figure 3.24: Deformations cases 2 & 11 - Ship 0.25L X- & Z-direction, detrended in Z-direction

Observing Figure 3.23 it seems clear that the ship responds differently in both directions for any given frequency, this has been the result for all observation locations. However, in the Z-direction a clear trendline, representing a drift, can be witnessed, when this trend is removed to observe the pure alternating responses both cases seem to respond closely to each other (see Figure 3.24). This indicated that the amount of monopiles will most likely not dictate the amplitude of the alternating deformations. However, observing the trends in Figure 3.23, one could state the direction and or shape of the trendlines are dictated by the moment the first forcing frequency is started to be felt by the system. So, the amount of monopiles shipped has lesser effect than expected as it only seems to dictate the direction of the trendline and the time until the system starts to be affected by the forcing frequency. This makes sense as both cases have different drafts, and thus a ship with different displacements. For the single monopile cases (2-10) the monopile's mass is approximately 13% of the total displacement, while the mass of the triple monopiles cases (11-19) 34%. Although the mass of the monopile is more pronounced in the total mass, the mass of the ship remains almost identical across the cases, with the single monopile cases (2-10) having a vessel mass of 91% compared to that of the triple monopiles cases (11-19). As a result, most experienced deformations will be dictated by the ship's properties rather than the monopile(s).

4

Conclusion

4.1. Answering the research question

When constructing & validating the model in early stages a clear difference in natural frequencies between the type of friction contacts could be witnessed (Table 2.9). However, when the strip data was replaced with ship & monopile data the same linear modal analysis showed no differences between the type of contacts. Performing the harmonic analysis and non-linear time domain analysis also showed no effects were caused by the type of friction contacts. The most likely reason this is the case is because in all cases no detection of slippage between the monopile and ship were found.

The lashings on the other hand showed mixed results throughout the different analysis performed. Initially, the lashings showed negligible increases in natural frequencies when constructing and validating the model ((Table 2.7). Advancing to ship and monopile data later showed in the modal and harmonic analysis no differences, indicating lashing stiffness having no effect on the system's responses, both in z- & x-direction. However, when running the time-domain analysis the lashing stiffness did seem to have effect on the systems responses after all. Here it became clear when decreasing the lashing stiffness to 66% or 33% for the second frequency the system's responses could deviate up to 60%, for the single monopile cases. When considering three monopiles[1] this time, the 100% and 66% cases looked almost identical, with the 33% differing in system responses. It became clear from the non-linear analysis that lashing stiffness, depending on the applied forcing frequency, can have a significant effect on the system's responses in z-direction. In the observed data this could mean differences of up to 60%. The x-direction differences could even grow up to 4000%, but were of microscopic short durations and were in axial direction while the considered mode had very little axial contributions in its overall mode shape. As a result, the severity of the 4000% growth can be questioned.

When considering all cases, the most profound property affecting the system's responses were the amount of monopiles shipped. During the modal analysis it became clear that the monopiles have higher natural frequencies than the ship, indicating that, indeed, the monopile having a high stiffness on its own, with larger natural frequencies than the ship. However, since monopile(s) are not fixed on its entire length on deck this means probably only a portion of its stiffness being transferred to the system. It has been found that increasing the amount of monopiles that are shipped decreases the significance of the stiffness contribution and increases the mass contribution significance. Overall, for both the single and three monopile cases it heavily depended on the considered mode as some showed a decrease in natural frequency and others an increase. The harmonic analysis showed unrealistic results in terms of absolute bending moment due to the linearization assumptions used by ANSYS. Overall, it showed a decrease in bending moment within the ship if more monopiles were carried, which is caused by the 'no-separation' condition of ANSYS. Because of the above reasoning the absolute bending moment results are not reliable. During the non-linear time domain analysis, it was found that the amount of monopiles do not dictate the systems alternating z-direction behaviour over time. In detrended plots it showed similar results between cases 2 and 11, indicating that the amount of monopiles dictate the direction and shape of the trend in z-direction.

[1] three monopiles results in triple lashing stiffness, when compared to the single monopile cases

4.2. Recommendations

In practice lashings are mounted on the monopiles and the deck with a pre-tension, Jumbo Maritime applies roughly 50kN but this could vary per company. Because the non-linear time domain solver of ANSYS, called 'Explicit Dynamics', did not allow pre-tension and no work around has been found, this could change results slightly in the non-linear time domain. Especially when considering this analysis has already shown lashing stiffness could change system responses in z-direction by a considerable amount, depending on the forcing frequency.

During this project it has also been assumed for cases 11 to 19 that the saddles are aligned over the width of the ship, so standing perfectly next to each other, in practice this is most likely not the case. Combined with the property that a single beam has been used for three monopiles, this could indicate a coupling between (longitudinal) bending and torsion exists in the ship, in a practical setup. Furthermore, having a single beam for three monopiles limits the number of axial modes the system can detect as all three monopile always have to move in a similar fashion. Therefore, investigating both a setup with unaligned saddles and independently moving monopiles can show interesting results.

Jumbo Maritimes provided ship data such as the area moment of inertia and mass data. However, the data that was available was questionable as manual manipulation had to be performed on some occasions in order to proceed with the project. First of all, the delivered area moment of inertia looked very linear and seems to have the same area moment of inertia at the aft end as the front end, which in practice is almost never the case, unless a very simple structure such as a barge is considered. Furthermore, it was unclear if the provided area moment of inertia was around the neutral axis, the company couldn't provide a clear and substantiated answer regarding this topic. Also, no data seems to exist regarding where the neutral axis is located over the length, this was assumed to be in the middle of the cross section and 'follow' the same area moment of inertia curve. Because of the above reasoning the doubt exists the delivered and manipulated data is not an accurate enough representation of a heavy lift vessel.

As a final recommendation, Due to time restrictions the FSI coupling has not been investigated. FSI coupling will change the systems overall dynamic behaviour and such an investigation could lead to a different conclusion. As mentioned in the introduction, the concern was that shipping monopiles will result in cargo that has more stiffness as mass contribution, during this research the answer to that question was leaning towards a no. When FSI coupling is introduced and thus added mass is considered the expectation is that it will indicate an even less stiff ship than initially what the model in this thesis indicated. As a result, when combined with monopile(s) this could lead to a different conclusion that indeed monopiles have more stiffness than mass contribution and will make the system overall stiffer. The reason this could be the case is that the natural frequencies of the monopile(s) and the ship will deviate even more as what this research has showed. Furthermore, the non-linear analysis showed a trend in z-direction, having FSI implemented into the model will most likely automatically detrend the plots in which oscillation can be better observed. The reason the trends occurred in this research is most likely due to the system being able to freely float through space, while FSI should restrict that.

References

[1] Rohan Best and Paul J. Burke. “Adoption of solar and wind energy: The roles of carbon pricing and aggregate policy support”. In: *Energy Policy* 118 (2018), pp. 404–417. ISSN: 0301-4215. DOI: https://doi.org/10.1016/j.enpol.2018.03.050. URL: https://www.sciencedirect.com/science/article/pii/S0301421518301848.

[2] Richard ED Bishop and WG Price. *Hydroelasticity of ships*. Cambridge University Press, 1979.

[3] Yong Huang, Ling-E Yang, and Qi-Zhi Luo. “Free vibration of axially functionally graded Timoshenko beams with non-uniform cross-section”. In: *Composites Part B: Engineering* 45.1 (2013), pp. 1493–1498.

[4] Yeon-Seung Lee et al. “Reliability-based design optimization of monopile transition piece for offshore wind turbine system”. In: *Renewable Energy* 71 (2014), pp. 729–741.

[5] Andrew Yee Tak Leung et al. “Dynamic stiffness for piecewise non-uniform Timoshenko column by power series—part I: Conservative axial force”. In: *International Journal for Numerical Methods in Engineering* 51.5 (2001), pp. 505–529.

[6] Jumbo Maritime. “Brochure”. In: 2009.

[7] D Mikail. “Literature review - D. Mikail”. In: *Structural and dynamic monopile-deck interaction*. 2021.

[8] AT Myers et al. “Strength, stiffness, resonance and the design of offshore wind turbine monopiles”. In: *Engineering structures* 100 (2015), pp. 332–341.

[9] padtinc. “padtinc.com/2015/11/09/be-a-pinball-wizard-with-contact-regions-in-ansys-mechanical/”. In: 2015.

[10] physik. “physik.uzh.ch/local/teaching/SPI301/LV-2015-Help/lvanlsconcepts.chm/”. In: 2015.

[11] Sergio Sánchez et al. “Foundations in offshore wind farms: Evolution, characteristics and range of use. Analysis of main dimensional parameters in monopile foundations”. In: *Journal of Marine Science and Engineering* 7.12 (2019), p. 441.

[12] Ivo Senjanović, Šime Malenica, and Stipe Tomašević. “Hydroelasticity of large container ships”. In: *Marine Structures* 22.2 (2009), pp. 287–314.

[13] Ivo Senjanović, Marko Tomić, and Stipe Tomašević. “An explicit formulation for restoring stiffness and its performance in ship hydroelasticity”. In: *Ocean Engineering* 35.13 (2008), pp. 1322–1338.

[14] Masoud Shadlou and Subhamoy Bhattacharya. “Dynamic stiffness of monopiles supporting offshore wind turbine generators”. In: *Soil Dynamics and Earthquake Engineering* 88 (2016), pp. 15–32.

[15] Jai Kumar Sharma. “Theoretical and experimental modal analysis of beam”. In: *Engineering Vibration, Communication and Information Processing*. Springer, 2019, pp. 177–186.

[16] Christos C Spandonidis and Kostas J Spyrou. “Micro-scale modeling of excited granular ship cargos: A numerical approach”. In: *Ocean Engineering* 74 (2013), pp. 22–36.

[17] Wim C Turkenburg, A Faaij, et al. *Renewable energy technologies*. Tech. rep. UNDP/UNDESA/WEC: Energy and the Challenge of Sustainability. World Energy …, 2000.

[18] J Van der Tempel and DP Molenaar. “Soft-soft, not hard enough?” In: *Proceedings of the World Wind Energy Conference, Berlin*. 2002.

[19] MingKang Wu and Torgeir Moan. “Sensitivity of extreme hydroelastic load effects to changes in ship hull stiffness and structural damping”. In: *Ocean engineering* 34.11-12 (2007), pp. 1745–1756.

A Appendix: Linear modelling data

A.1. Ship responses, case 1 vs 2

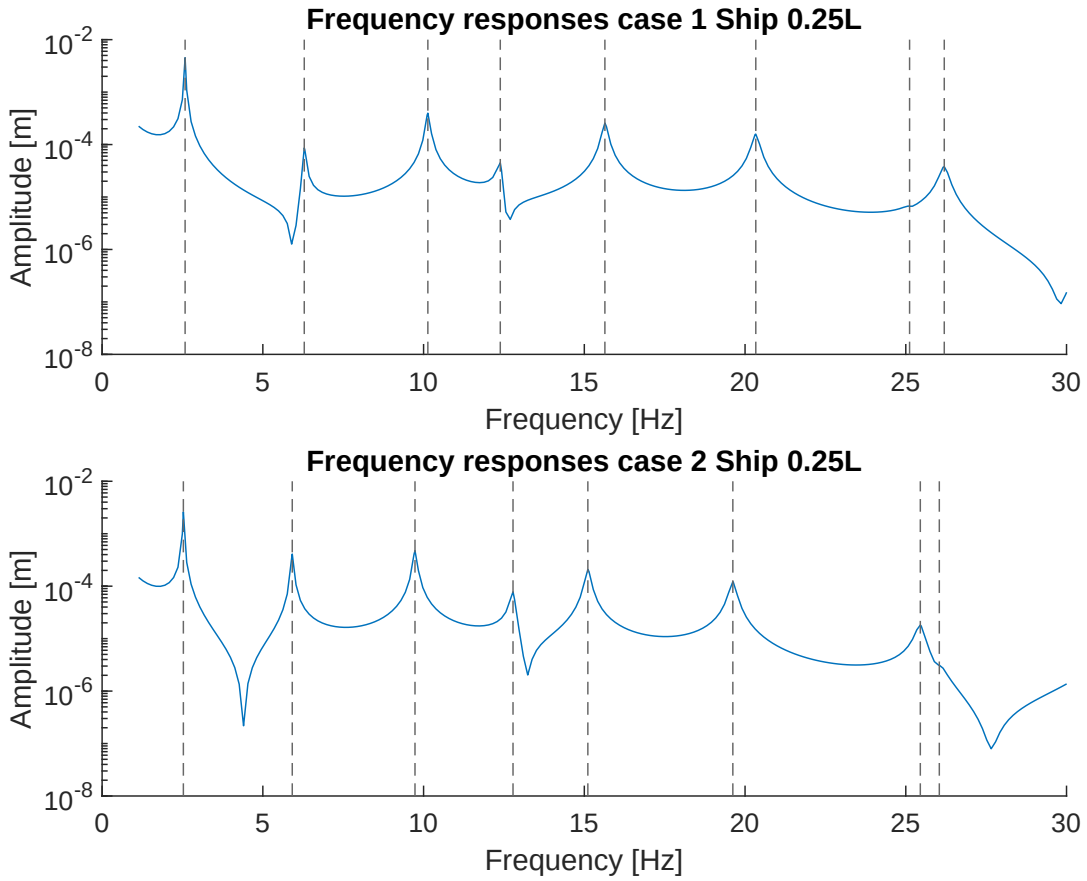

Figure A.1: Ship 0,25L case 1 responses compared to case 2, with the vertical lines '- -' respresenting the natural frequency locations

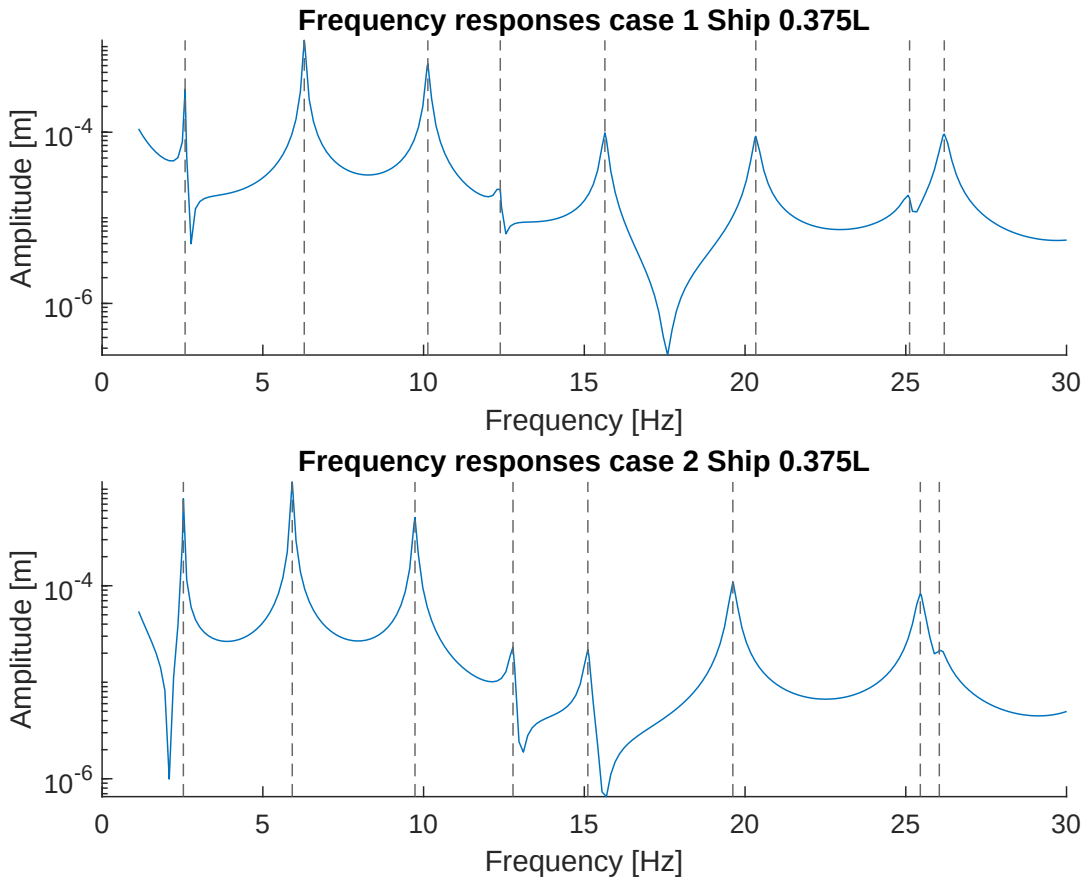

Figure A.2: Ship 0,375L case 1 responses compared to case 2, with the vertical lines '- -' respresenting the natural frequency locations

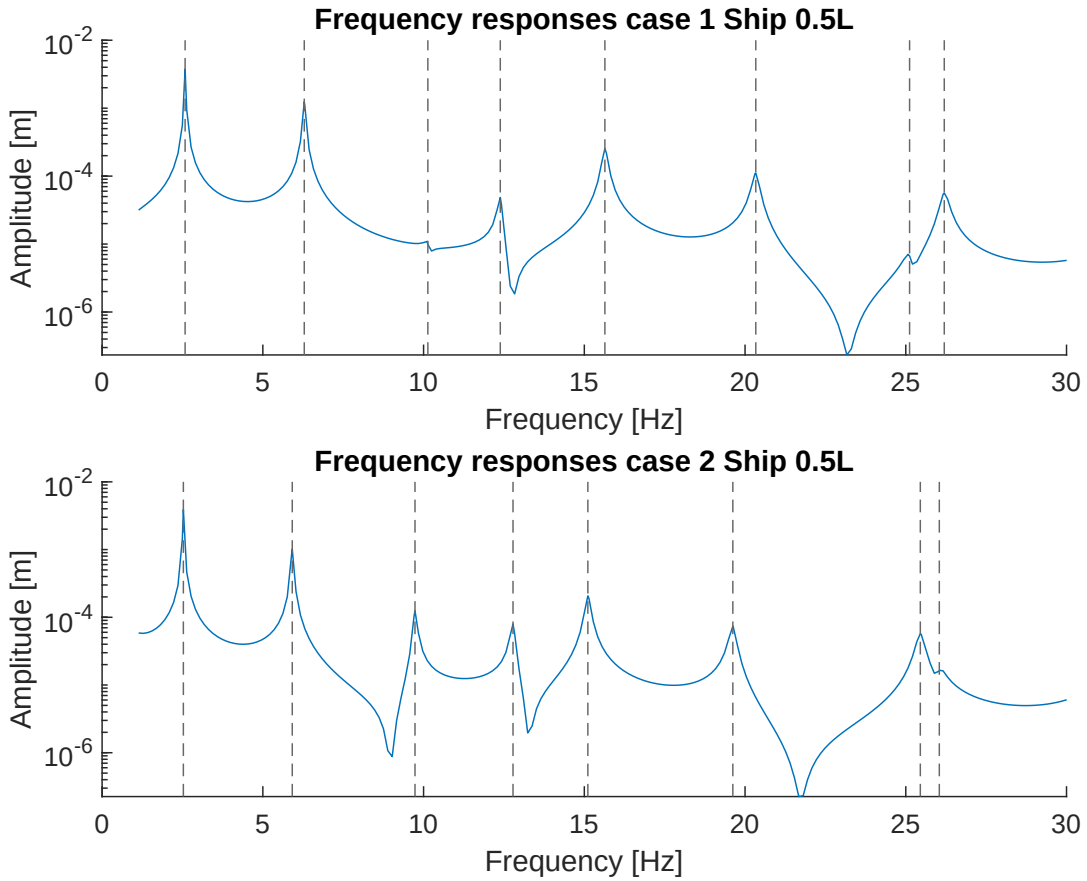

Figure A.3: Ship 0,5L case 1 responses compared to case 2, with the vertical '- -' respresenting the natural frequency locations

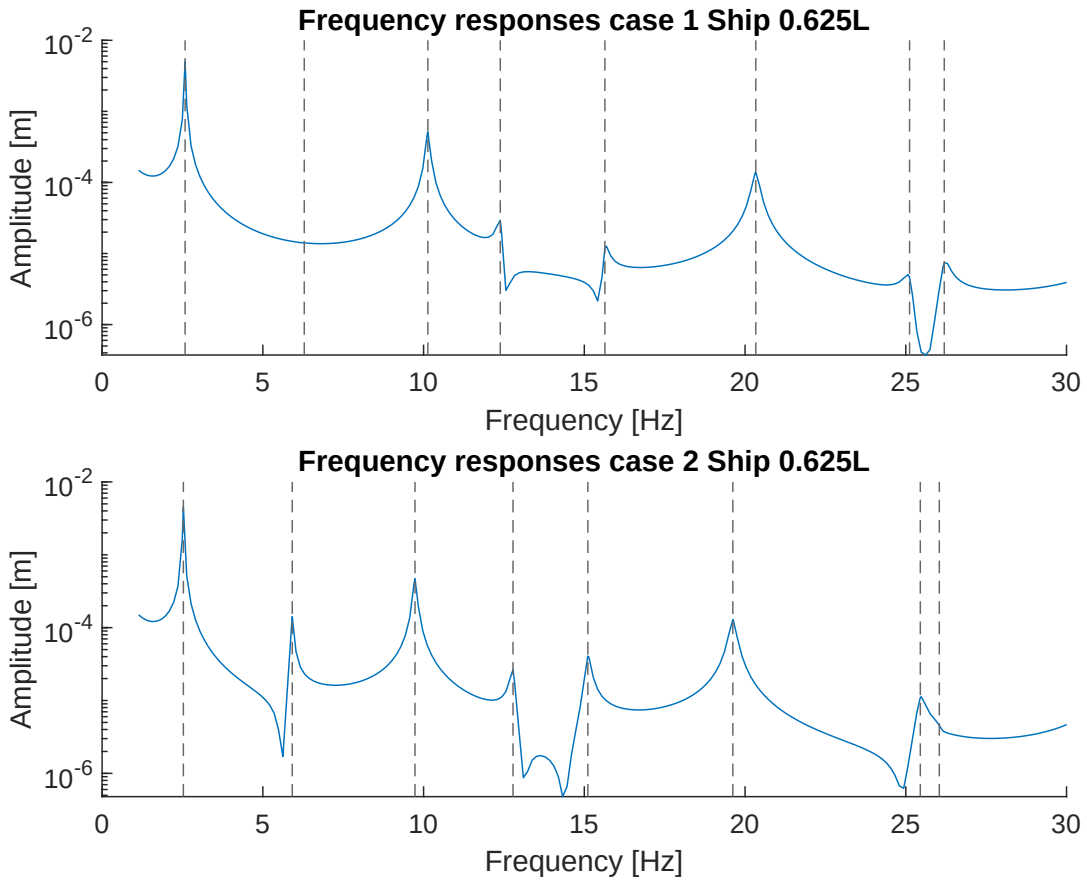

Figure A.4: Ship 0,625L case 1 responses compared to case 2, with the vertical lines '- -' respresenting the natural frequency locations

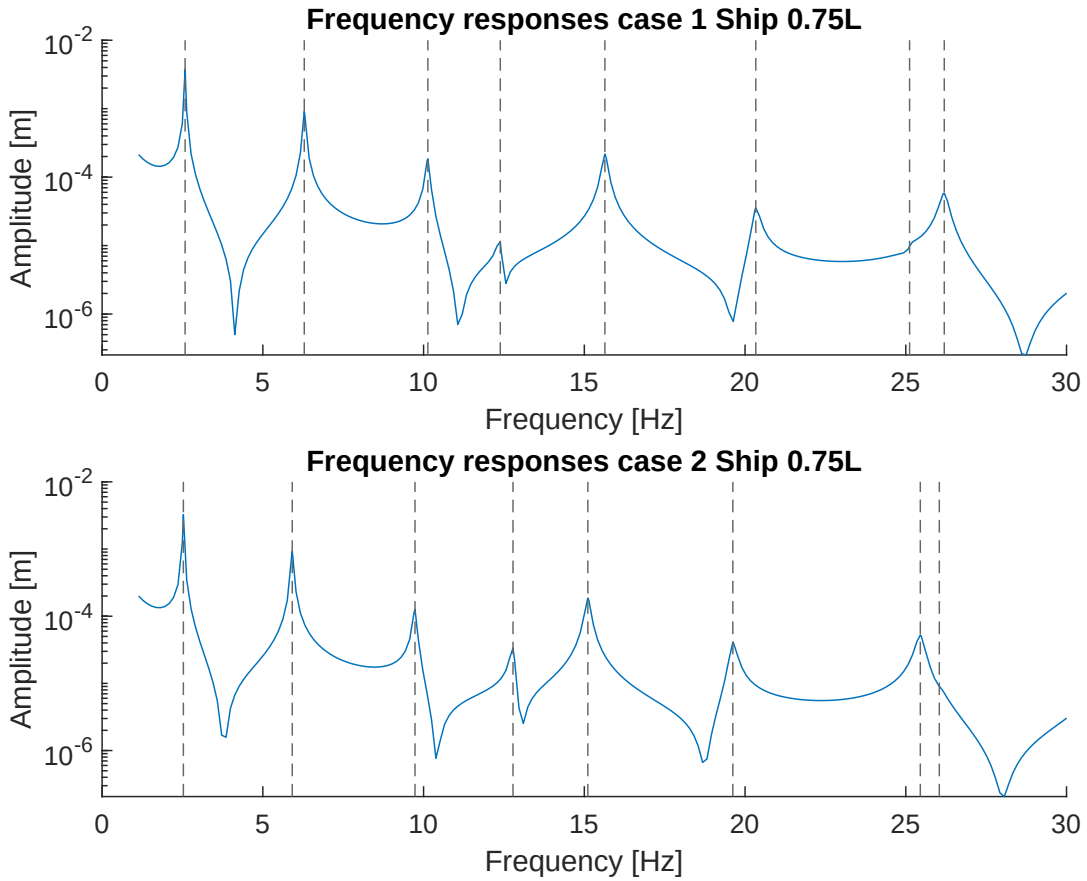

Figure A.5: Ship 0,75L case 1 responses compared to case 2, with the vertical lines '- -' respresenting the natural frequency locations

A.2. Ship & monopile (1x) responses factor, friction contact influence

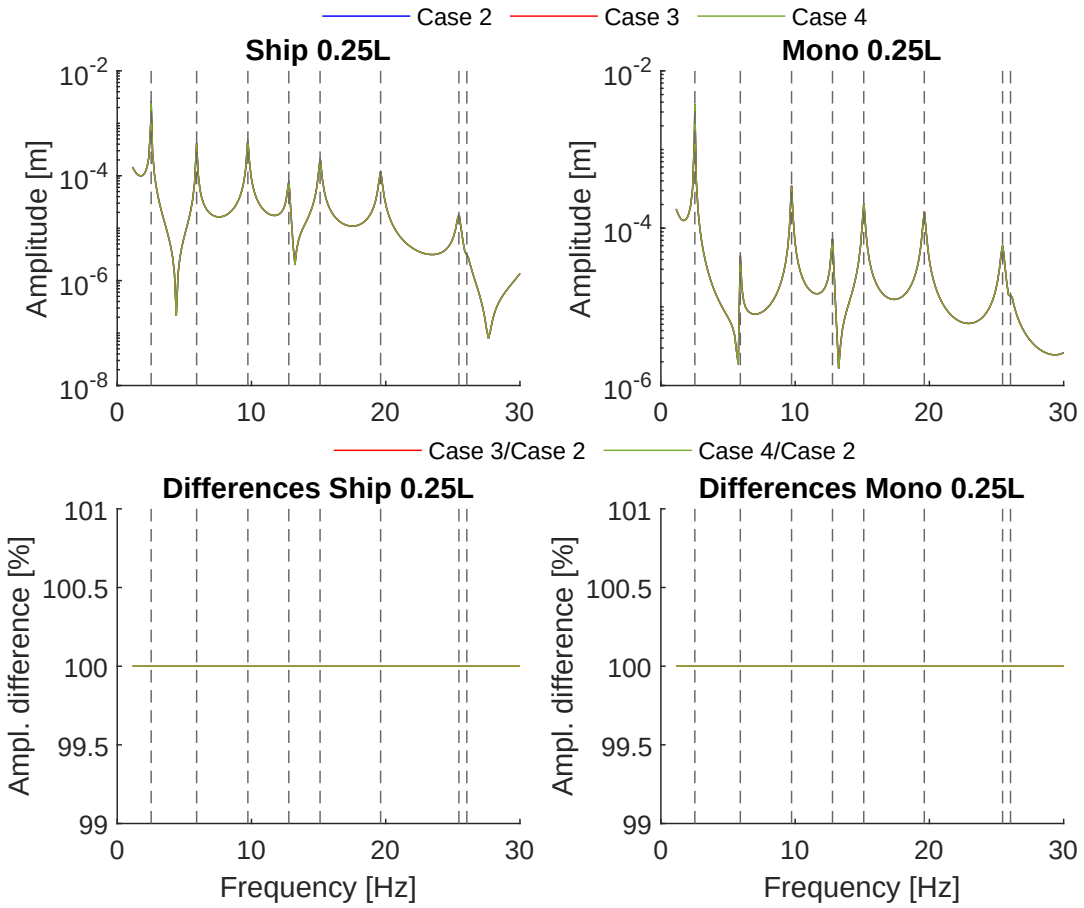

Figure A.6: Ship & Mono 0,25L case 2 responses compared to case 3 & 4, with the vertical lines '- -' respresenting the natural frequency locations

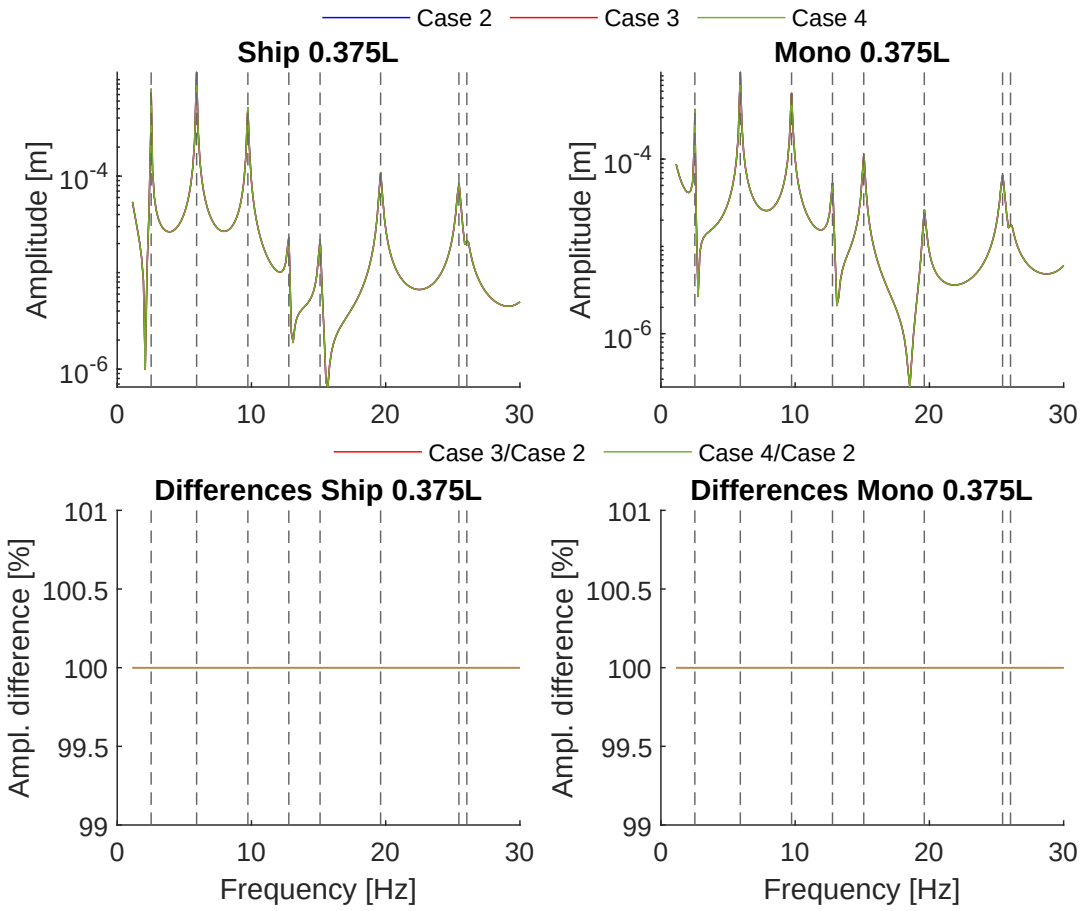

Figure A.7: Ship & Mono 0,375L case 2 responses compared to case 3 & 4, with the vertical lines '- -' respresenting the natural frequency locations

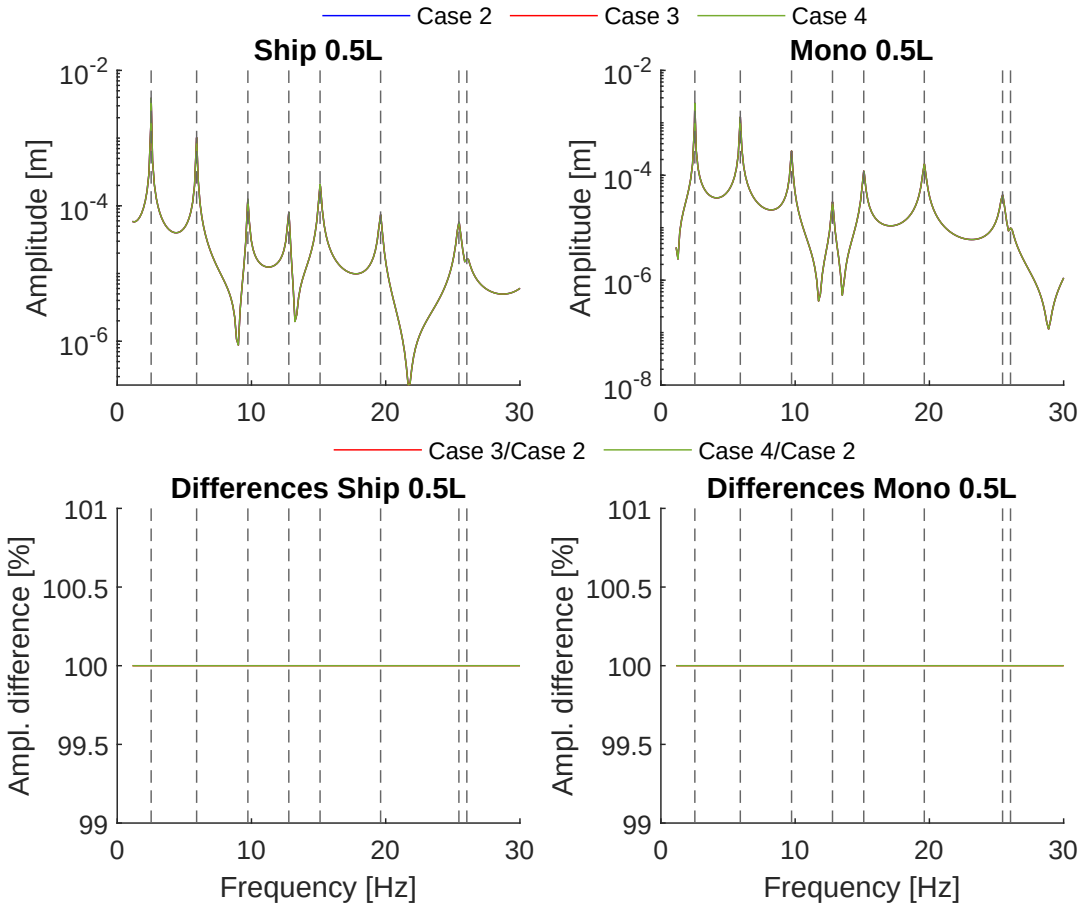

Figure A.8: Ship & Mono 0,5L case 2 responses compared to case 3 & 4, with the vertical lines '- -' respresenting the natural frequency locations

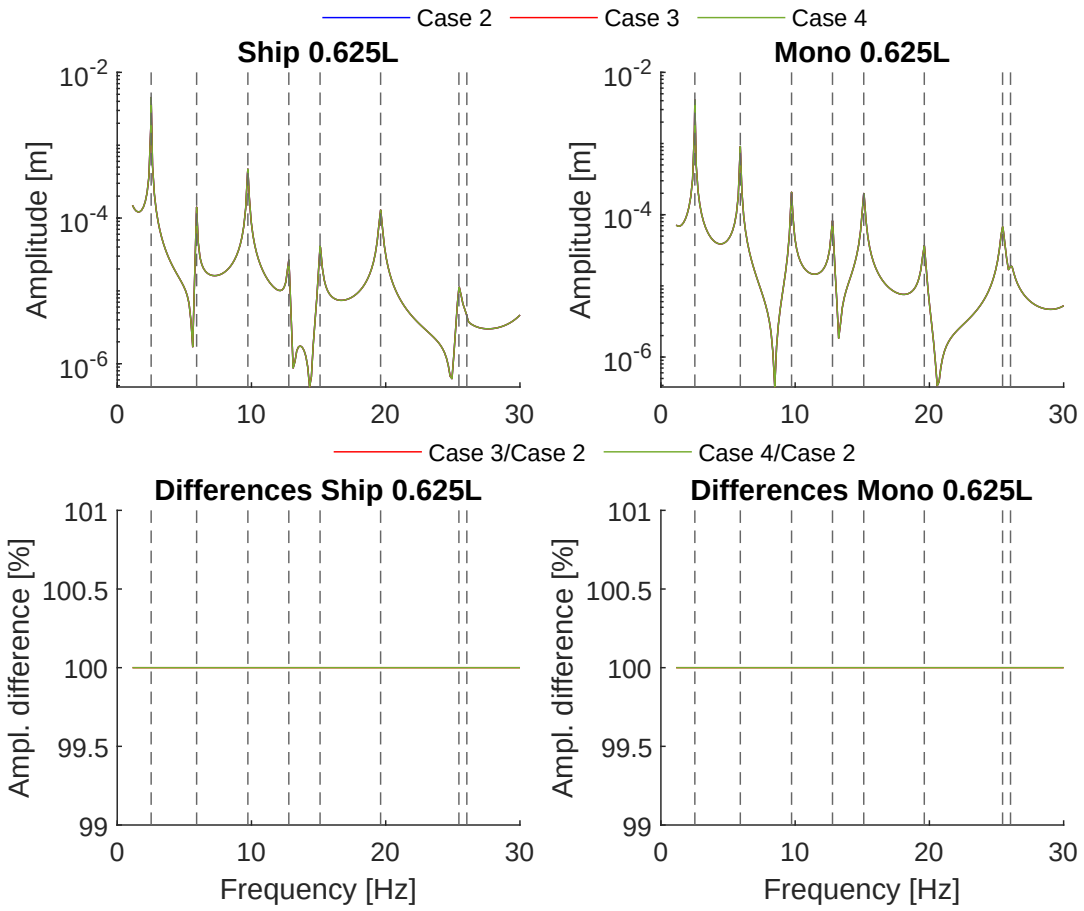

Figure A.9: Ship & Mono 0,625L case 2 responses compared to case 3 & 4, with the vertical lines '- -' respresenting the natural frequency locations

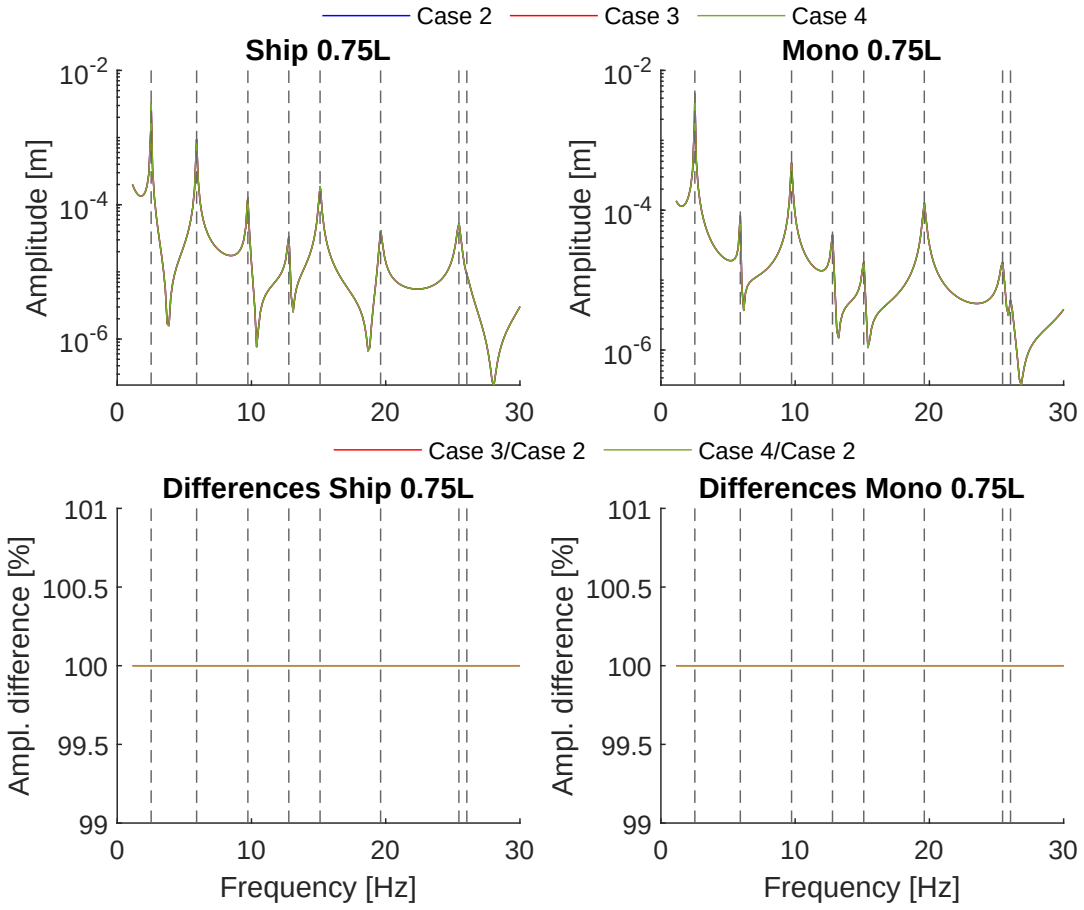

Figure A.10: Ship & Mono 0,75L case 2 responses compared to case 3 & 4, with the vertical lines '- -' respresenting the natural frequency locations

A.3. Ship & monopile (1x) responses factor, lashing stiffness influence

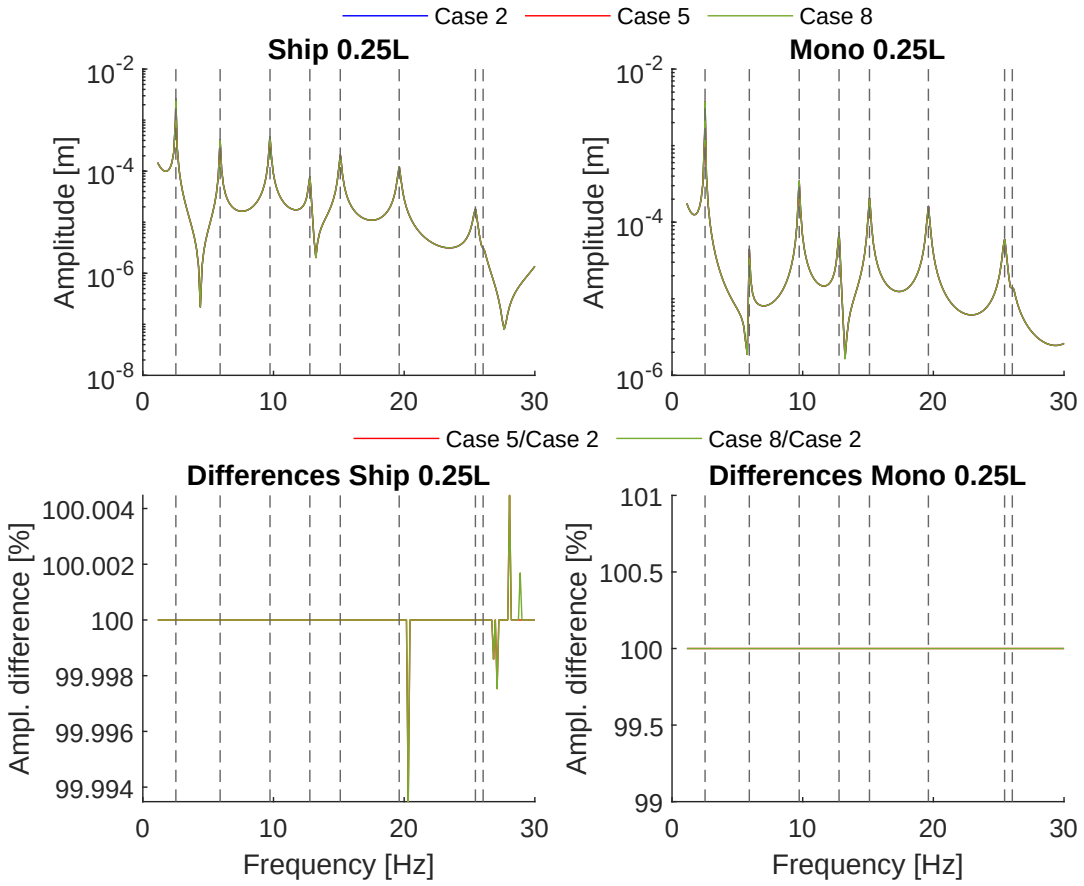

Figure A.11: Ship & Mono 0,25L case 2 responses compared to case 5 & 8, with the vertical lines '- -' respresenting the natural frequency locations

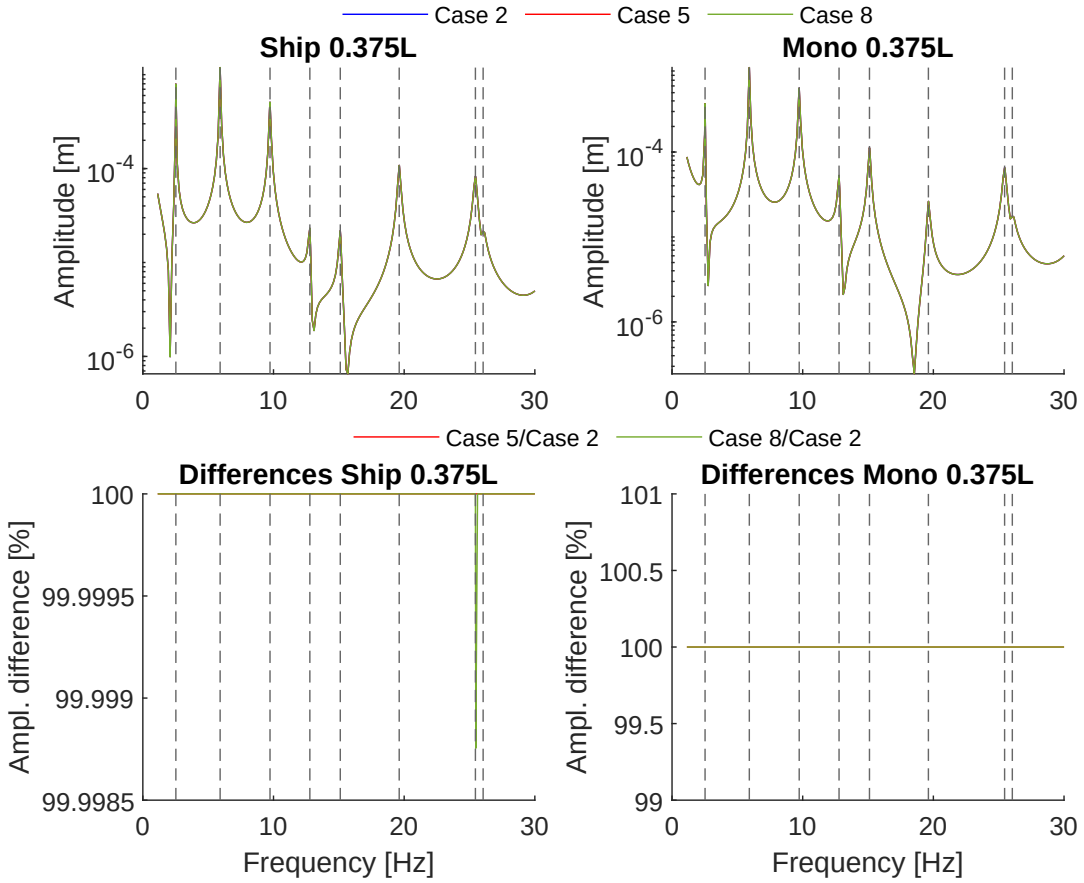

Figure A.12: Ship & Mono 0,375L case 2 responses compared to case 5 & 8, with the vertical lines '- -' respresenting the natural frequency locations

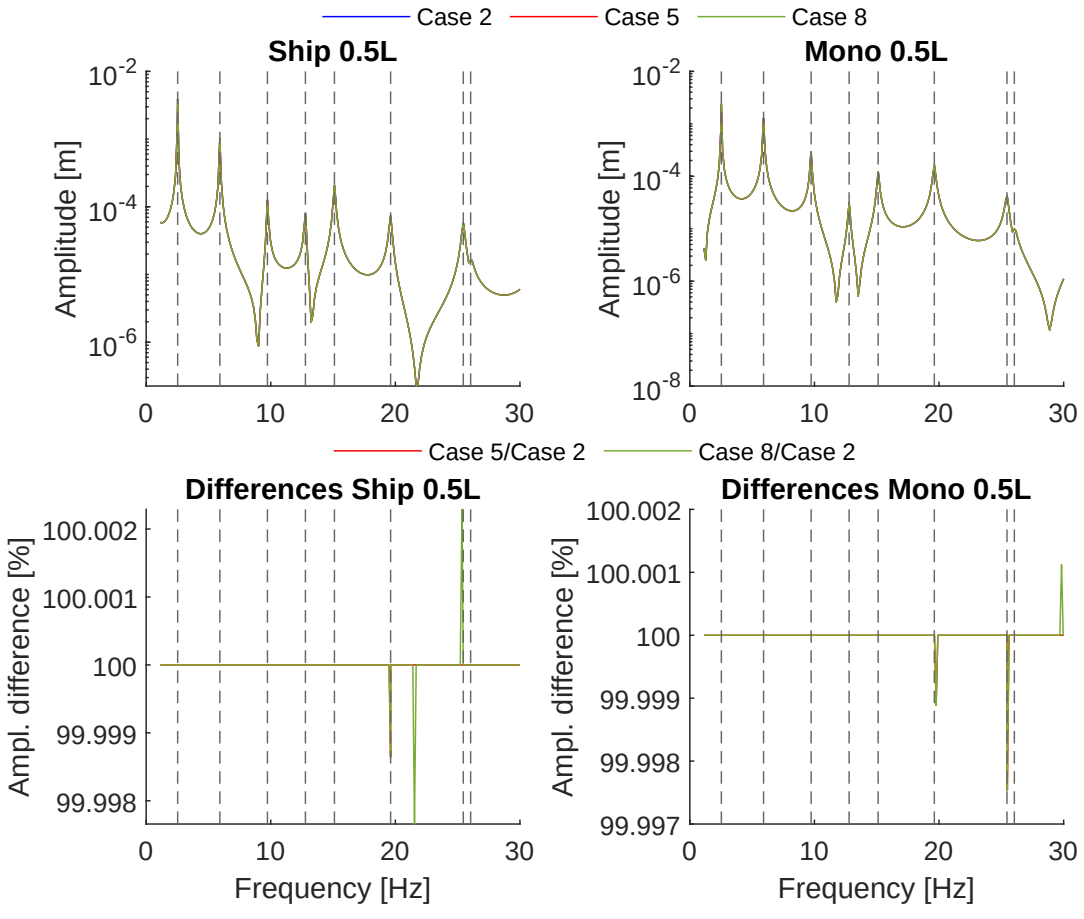

Figure A.13: Ship & Mono 0,5L case 2 responses compared to case 5 & 8, with the vertical lines '- -' respresenting the natural frequency locations

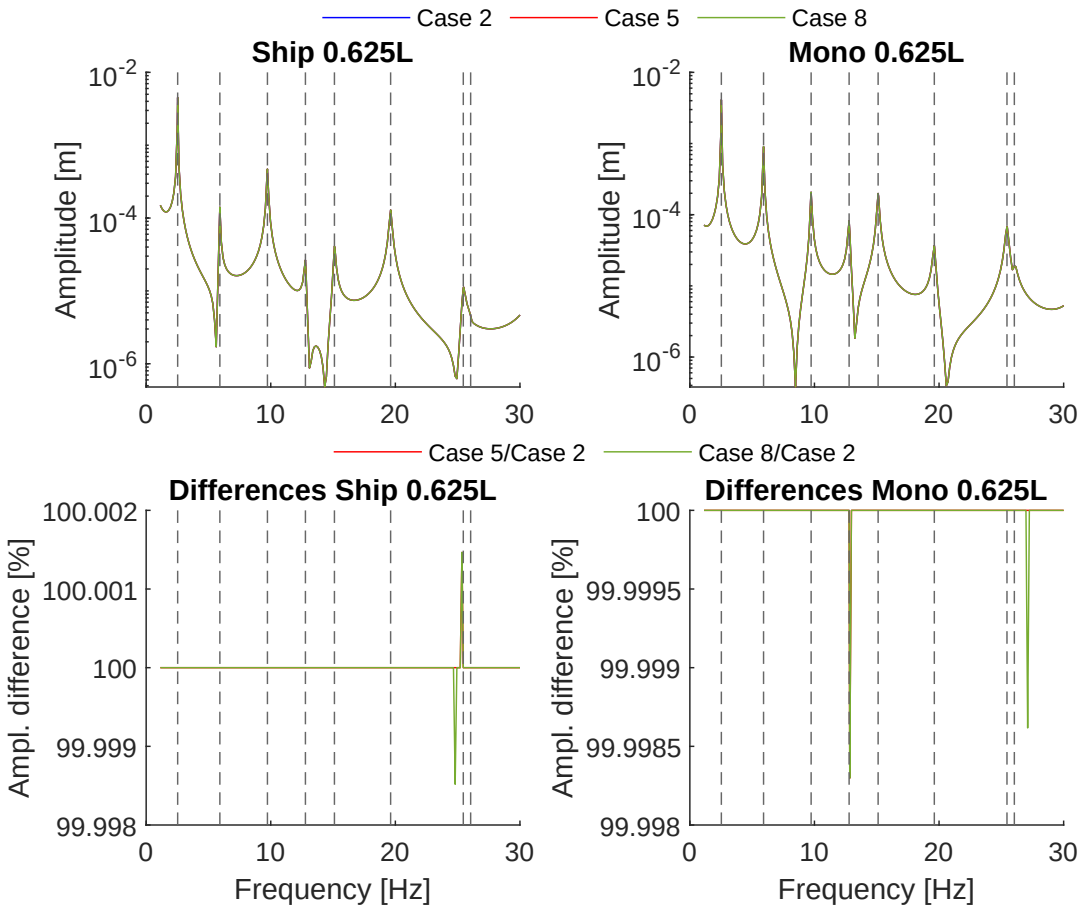

Figure A.14: Ship & Mono 0,625L case 2 responses compared to case 5 & 8, with the vertical lines '- -' respresenting the natural frequency locations

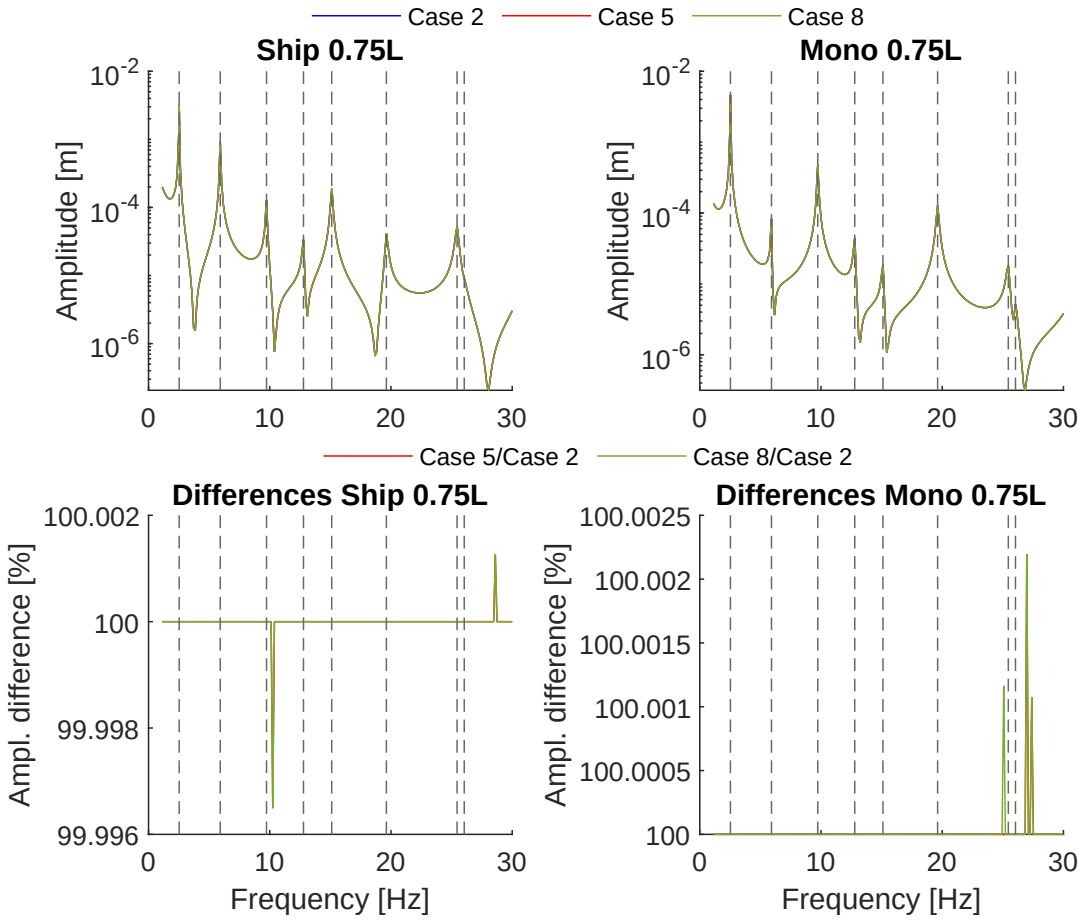

Figure A.15: Ship & Mono 0,75L case 2 responses compared to case 5 & 8, with the vertical lines '- -' respresenting the natural frequency locations

A.4. Ship & monopile (3x) responses factor, friction contact influence

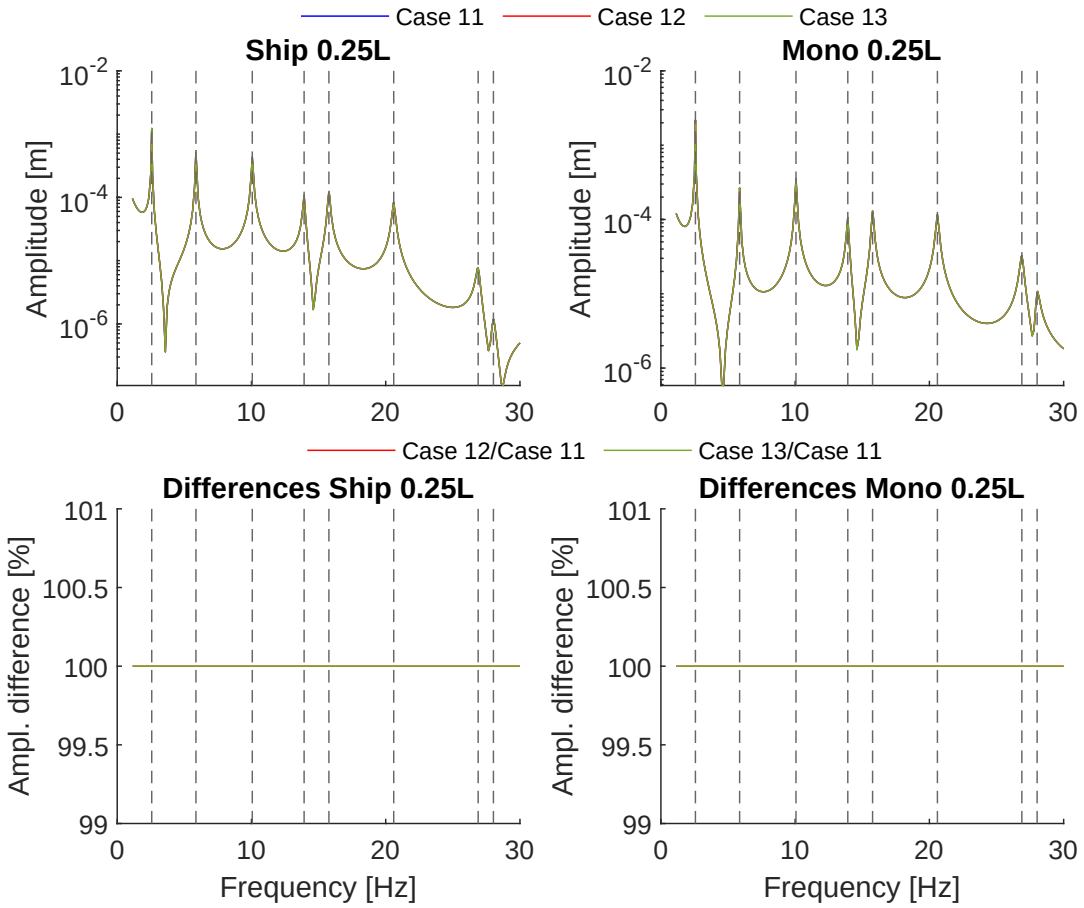

Figure A.16: Ship & Mono 0,25L case 11 responses compared to case 12 & 13, with the vertical lines '- -' respresenting the natural frequency locations

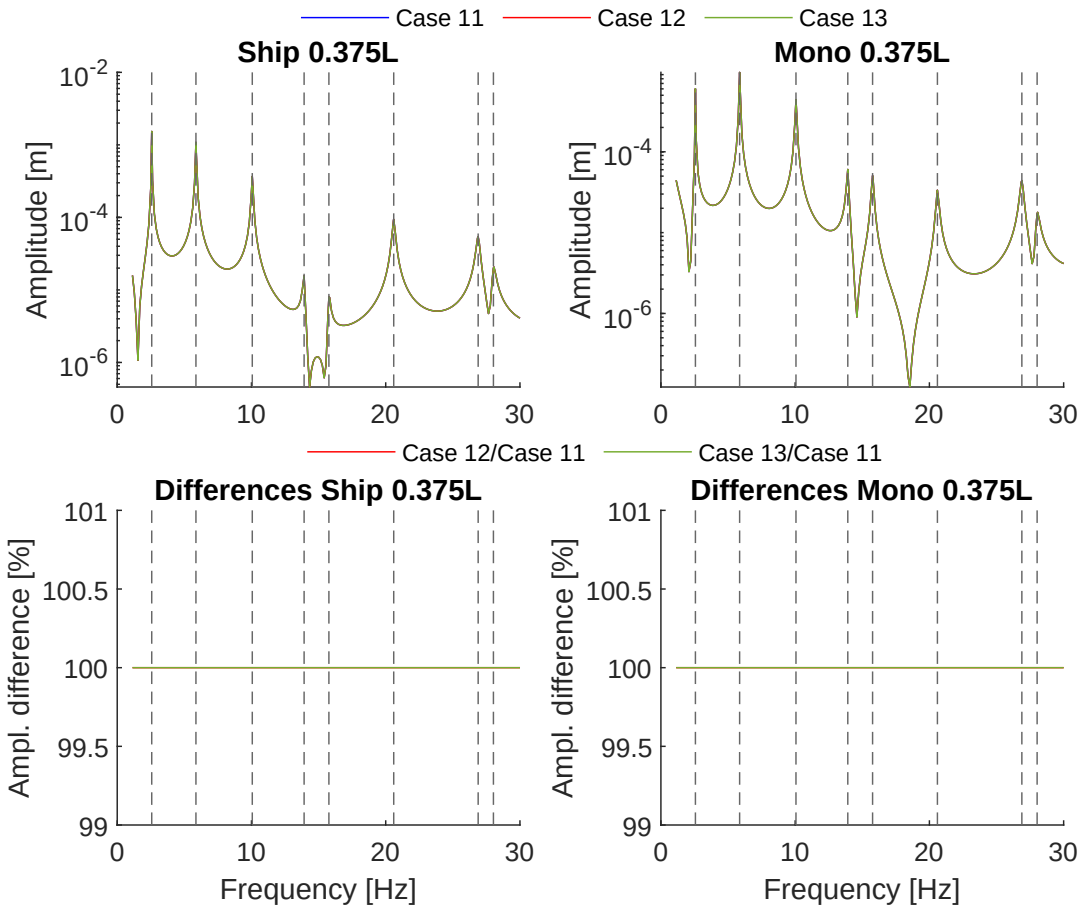

Figure A.17: Ship & Mono 0,375L case 11 responses compared to case 12 & 13, with the vertical lines '- -' respresenting the natural frequency locations

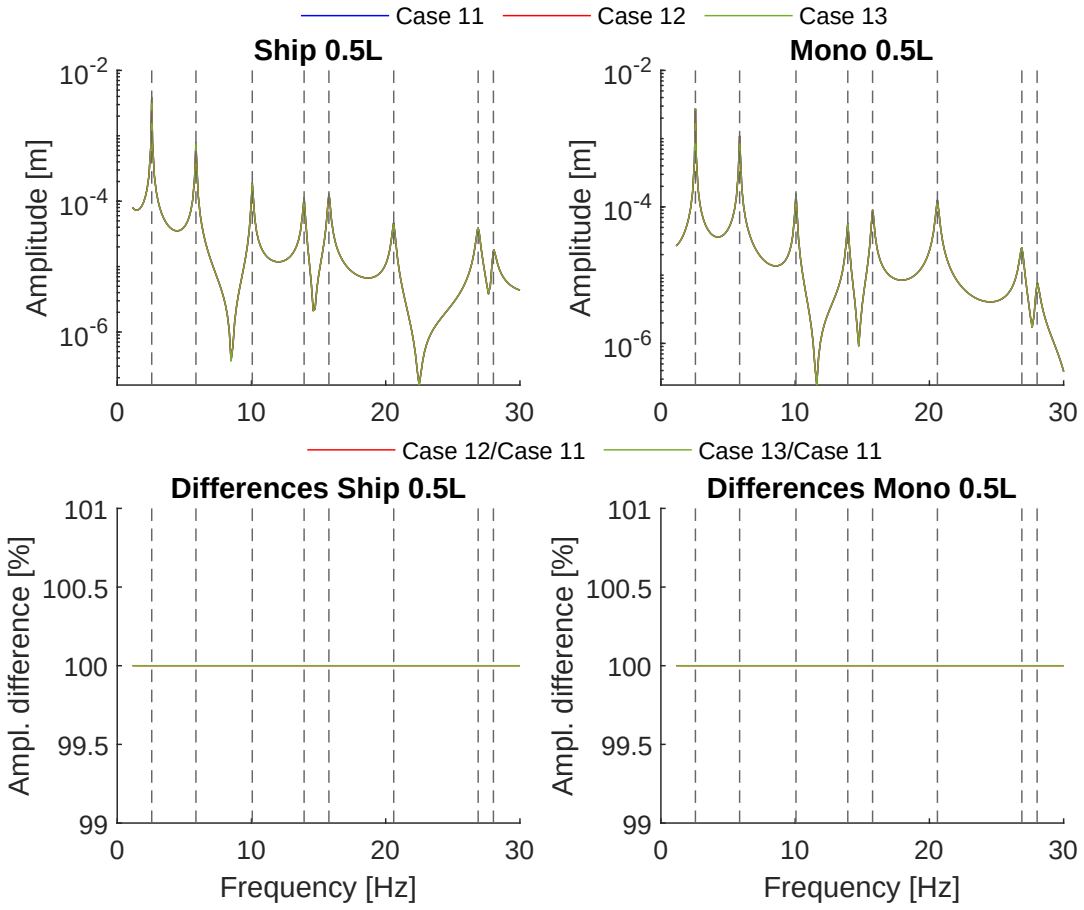

Figure A.18: Ship & Mono 0,5L case 11 responses compared to case 12 & 13, with the vertical lines '- -' respresenting the natural frequency locations

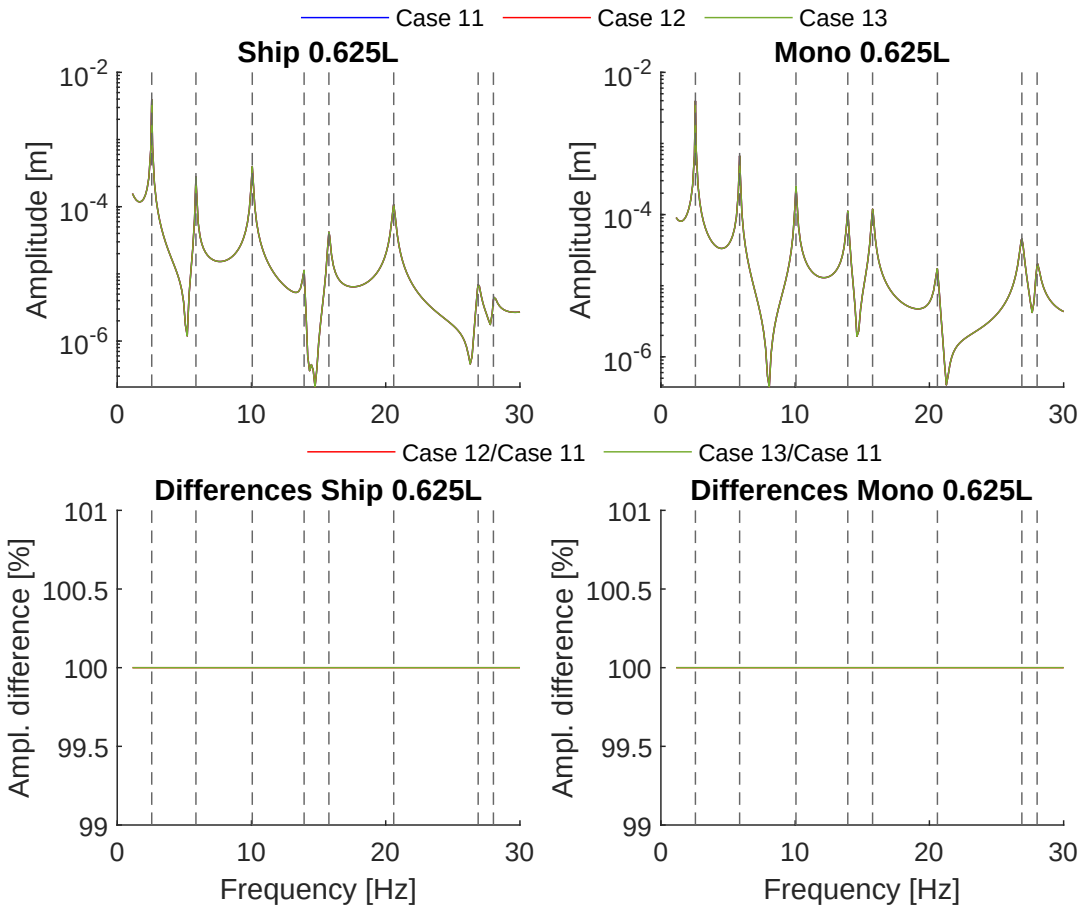

Figure A.19: Ship & Mono 0,625L case 11 responses compared to case 12 & 13, with the vertical lines '- -' respresenting the natural frequency locations

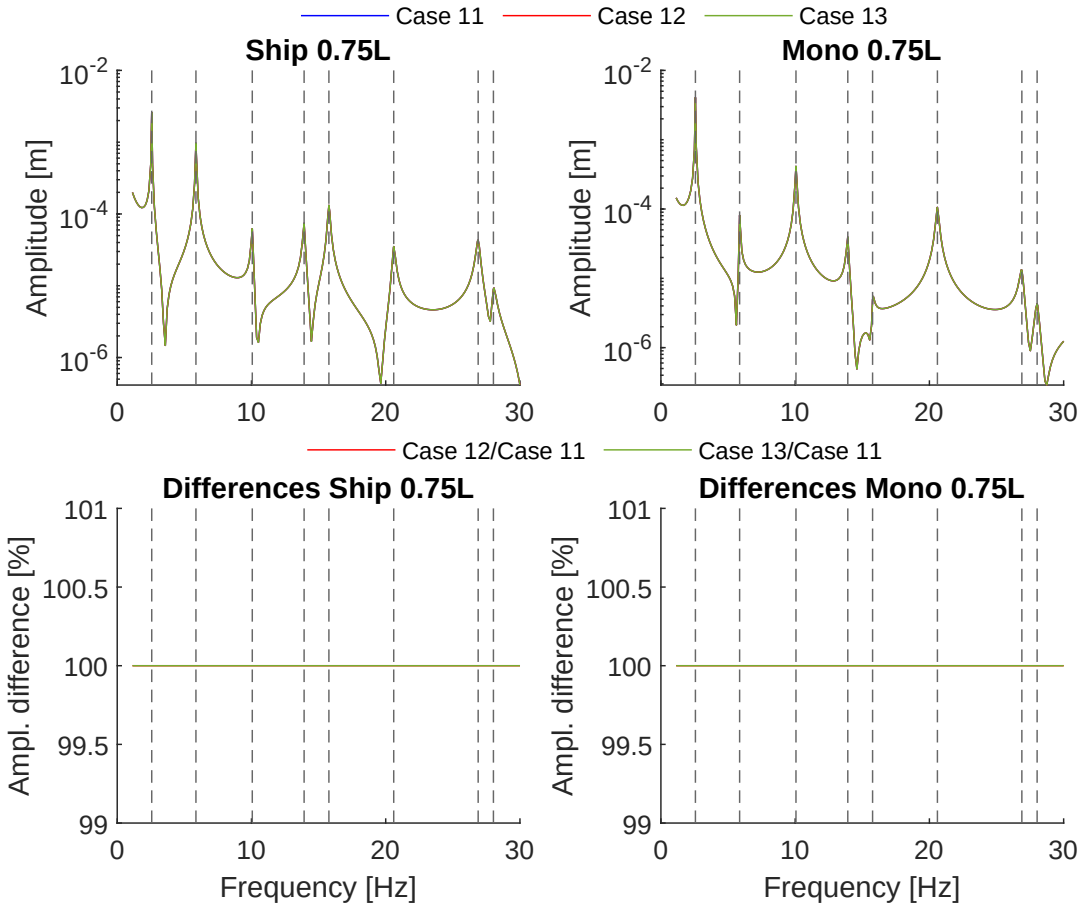

Figure A.20: Ship & Mono 0,75L case 11 responses compared to case 12 & 13, with the vertical lines '- -' respresenting the natural frequency locations

A.5. Ship & monopile (3x) responses factor, lashing stiffness influence

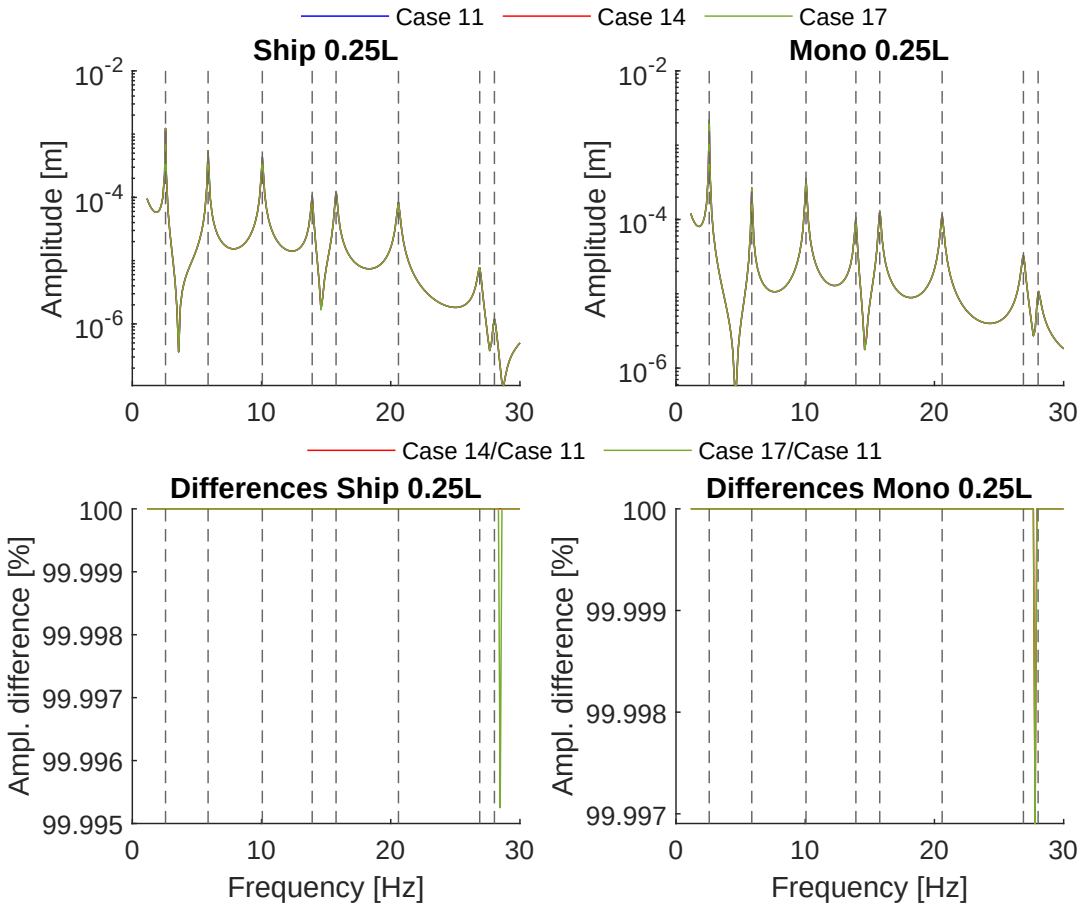

Figure A.21: Ship & Mono 0,25L case 11 responses compared to case 14 & 17, with the vertical lines '- -' respresenting the natural frequency locations

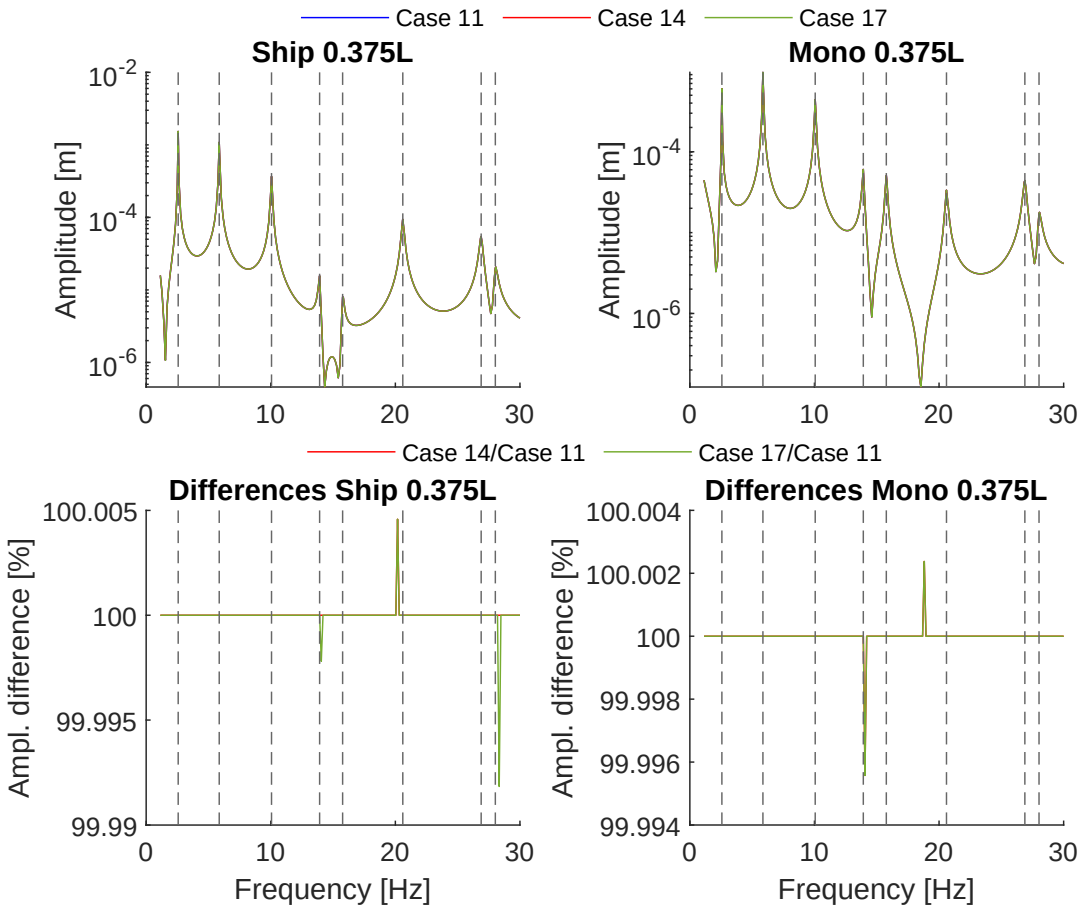

Figure A.22: Ship & Mono 0,375L case 11 responses compared to case 14 & 17, with the vertical lines '- -' respresenting the natural frequency locations

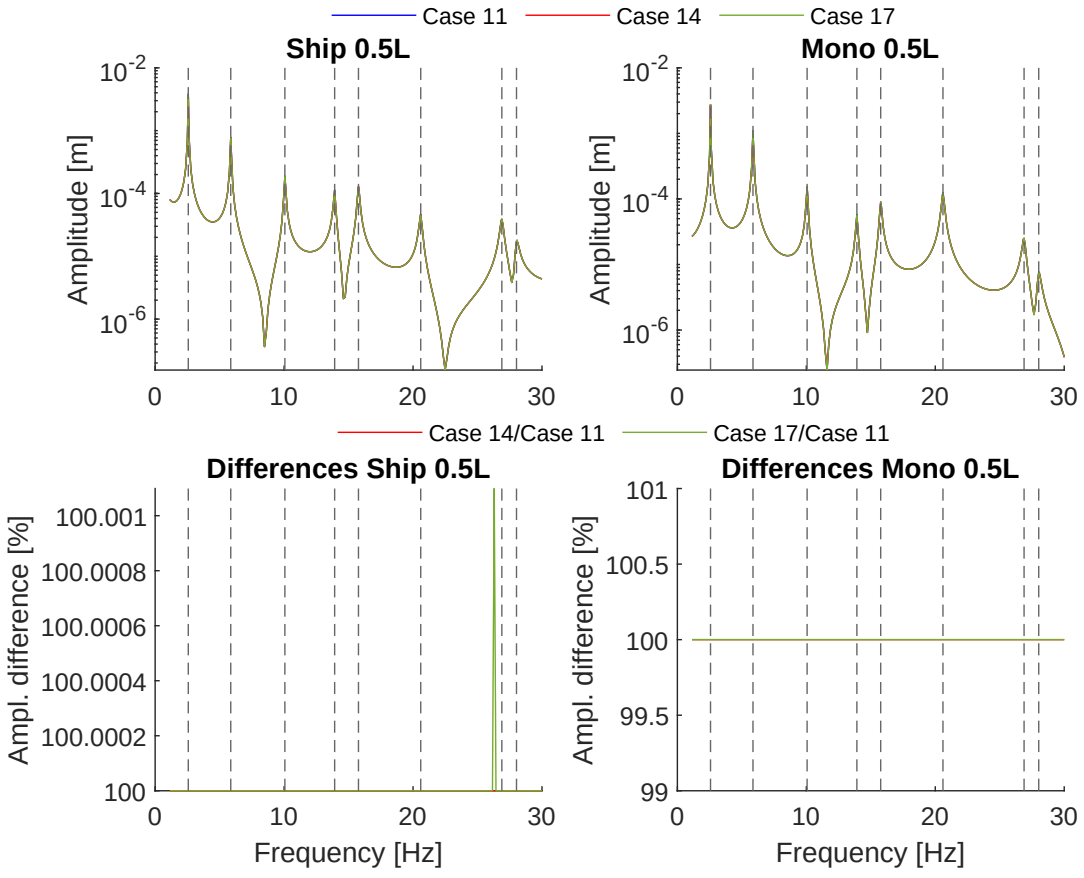

Figure A.23: Ship & Mono 0,5L case 11 responses compared to case 14 & 17, with the vertical lines '- -' respresenting the natural frequency locations

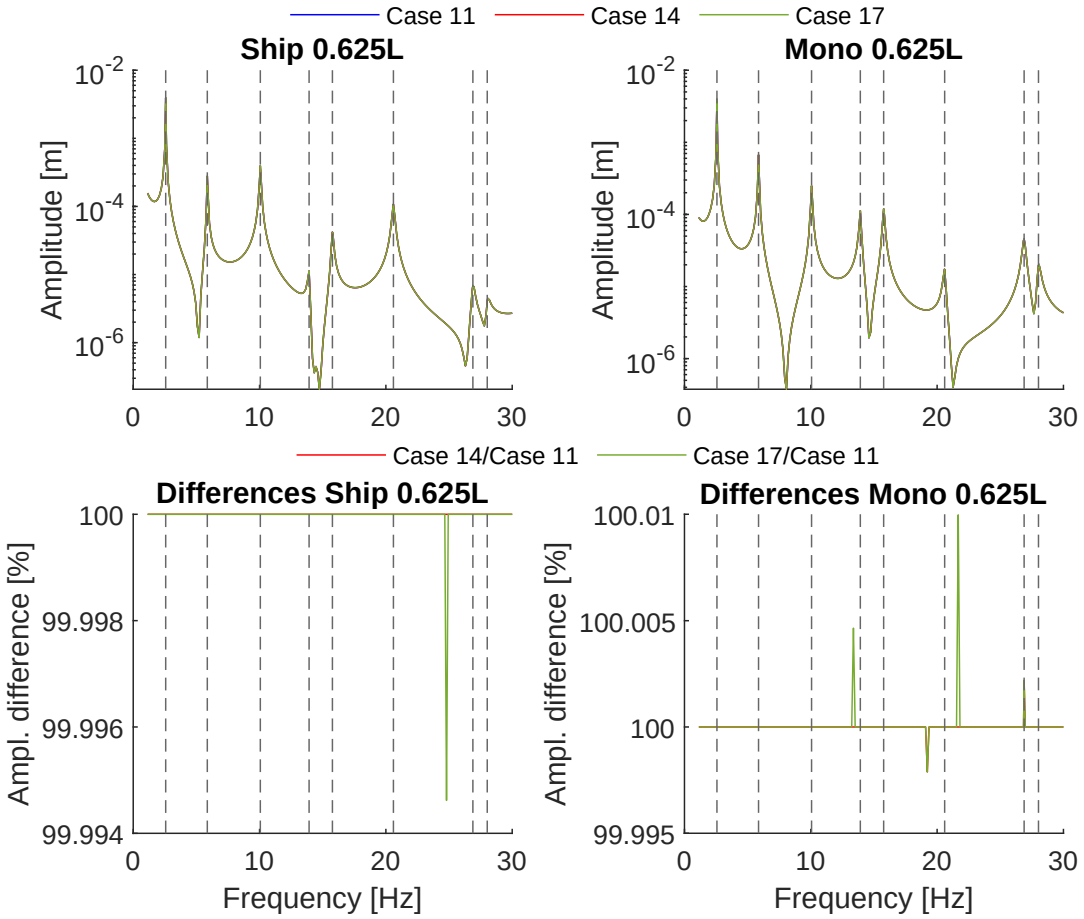

Figure A.24: Ship & Mono 0,625L case 11 responses compared to case 14 & 17, with the vertical lines '- -' respresenting the natural frequency locations

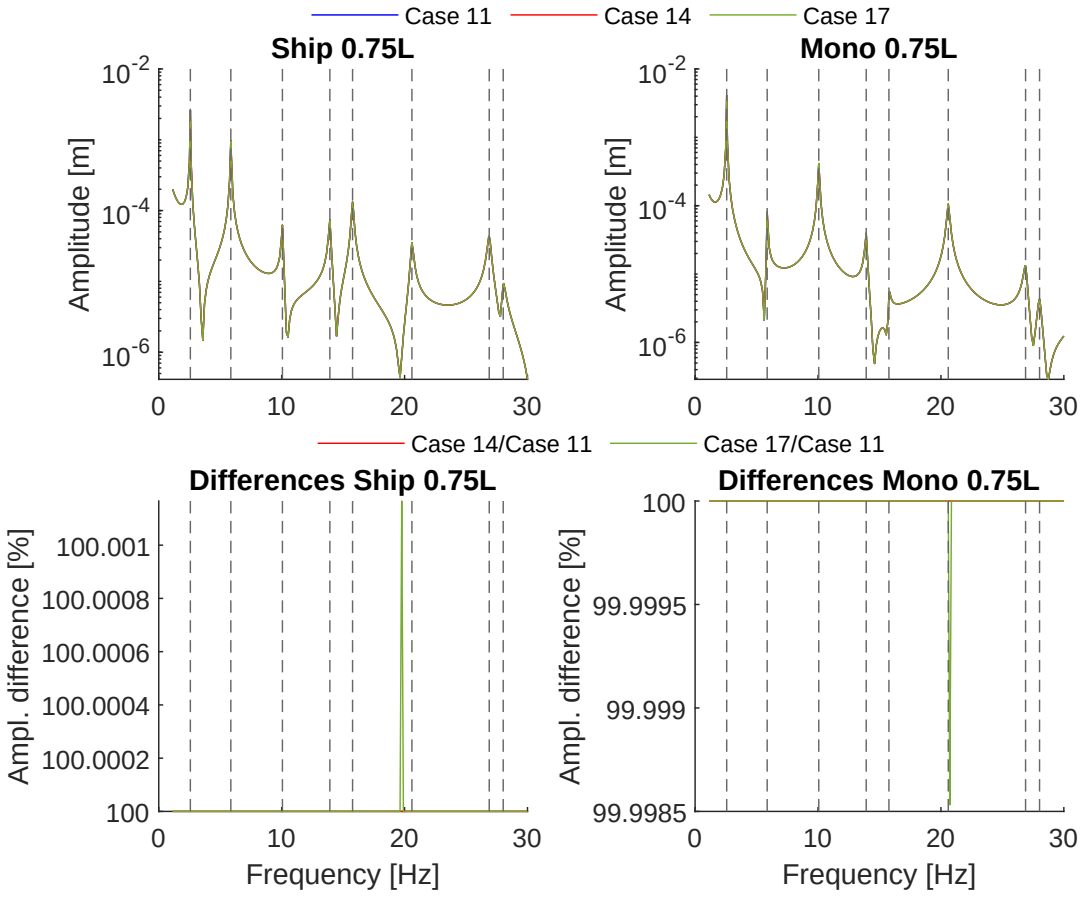

Figure A.25: Ship & Mono 0,75L case 11 responses compared to case 14 & 17, with the vertical lines '- -' respresenting the natural frequency locations

A.6. Ship responses, monopile influences

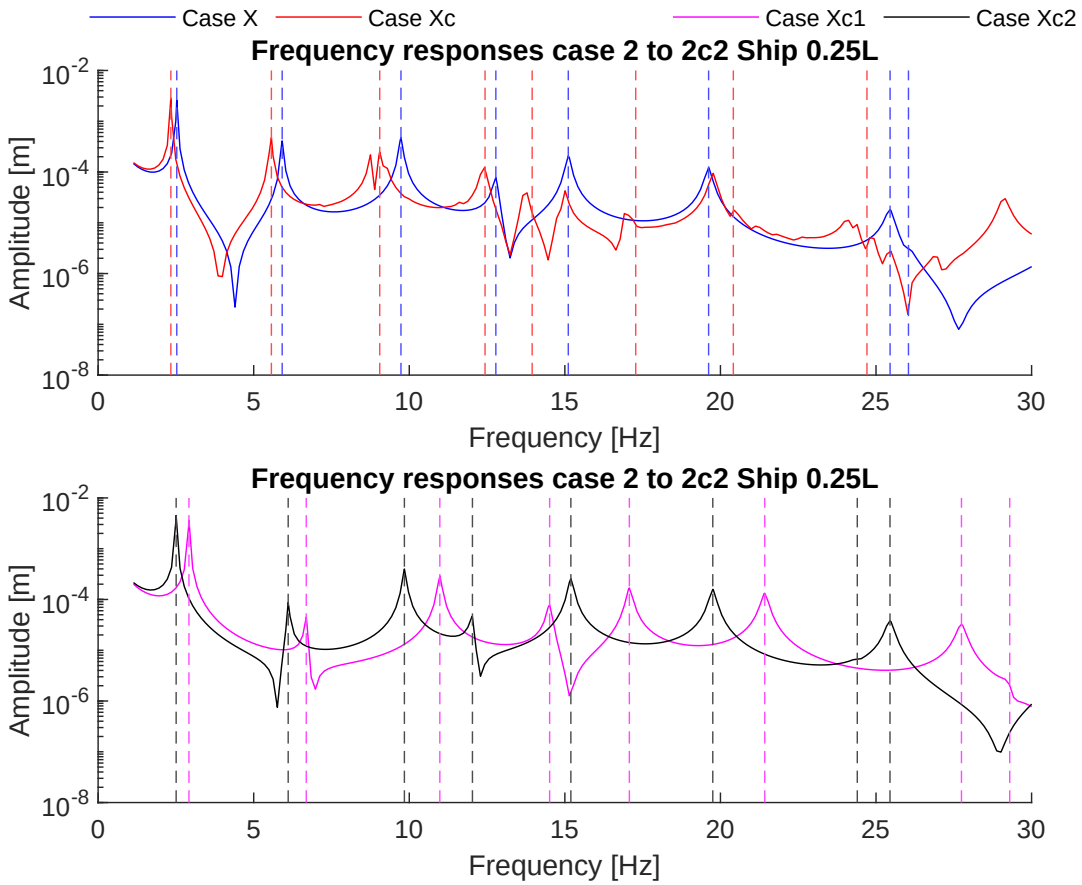

Figure A.26: Ship 0,25L responses due to monopile (1x) parameter tweaks, with the vertical lines '- -' respresenting the natural frequency locations

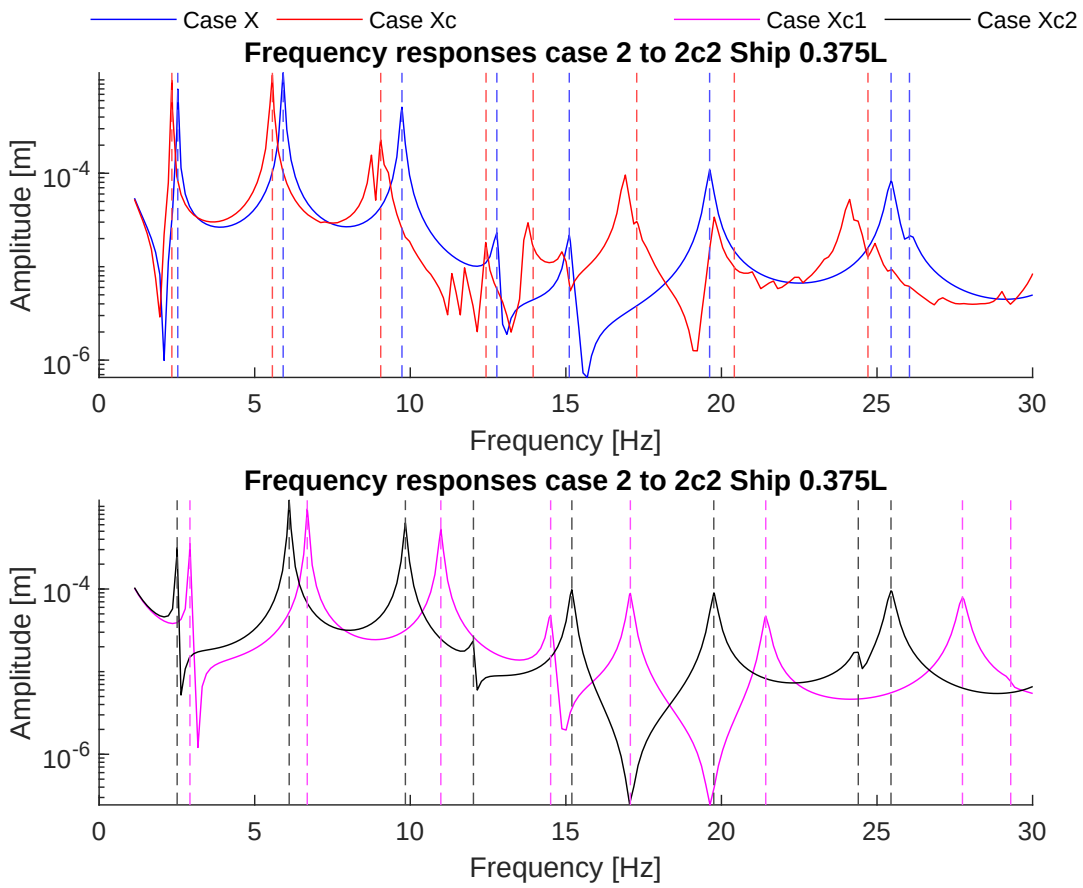

Figure A.27: Ship 0,375L responses due to monopile (1x) parameter tweaks, with the vertical lines '- -' respresenting the natural frequency locations

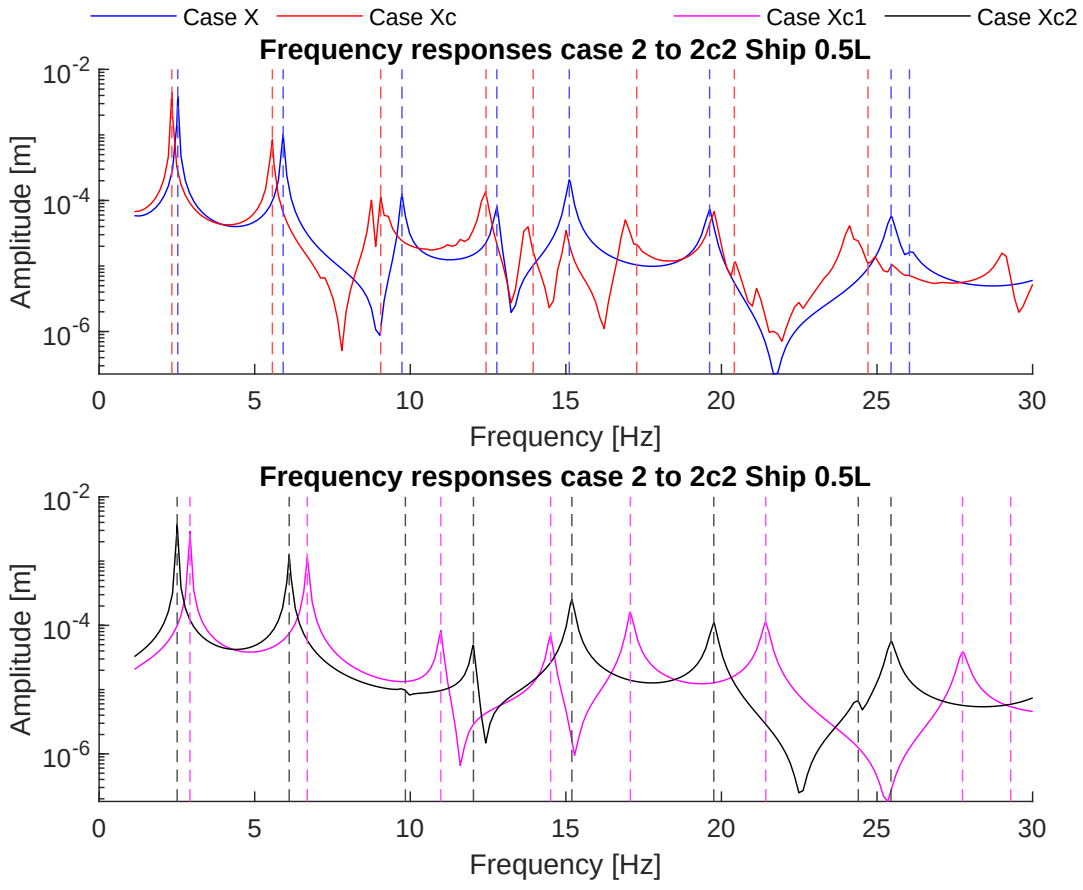

Figure A.28: Ship 0,5L responses due to monopile (1x) parameter tweaks, with the vertical lines '- -' respresenting the natural frequency locations

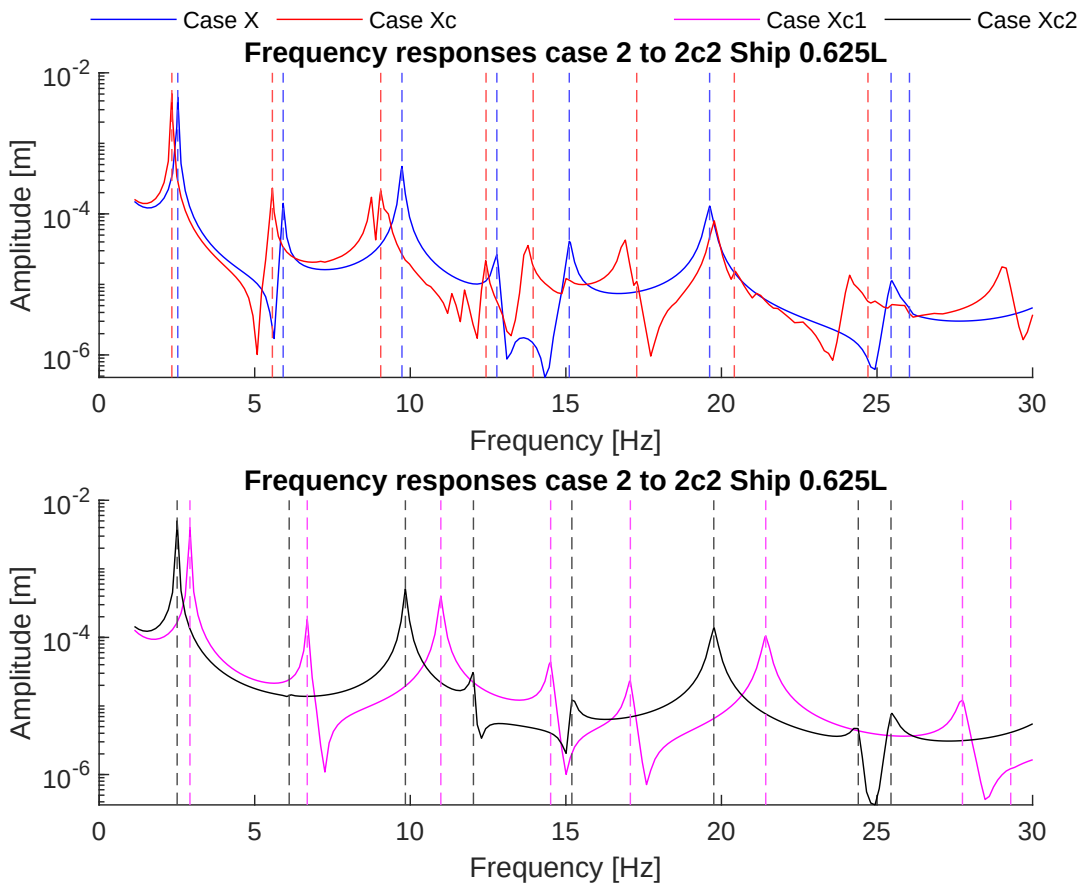

Figure A.29: Ship 0,625L responses due to monopile (1x) parameter tweaks, with the vertical lines '- -' respresenting the natural frequency locations

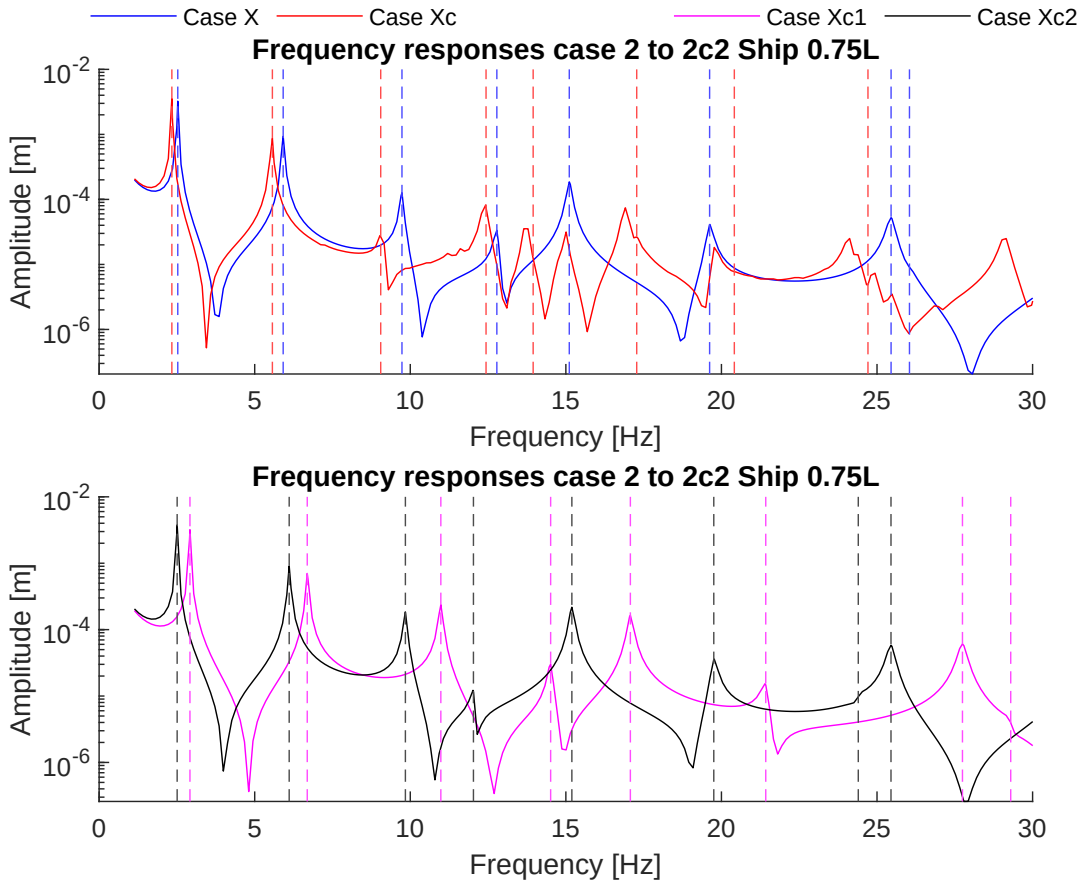

Figure A.30: Ship 0,75L responses due to monopile (1x) parameter tweaks, with the vertical lines '- -' respresenting the natural frequency locations

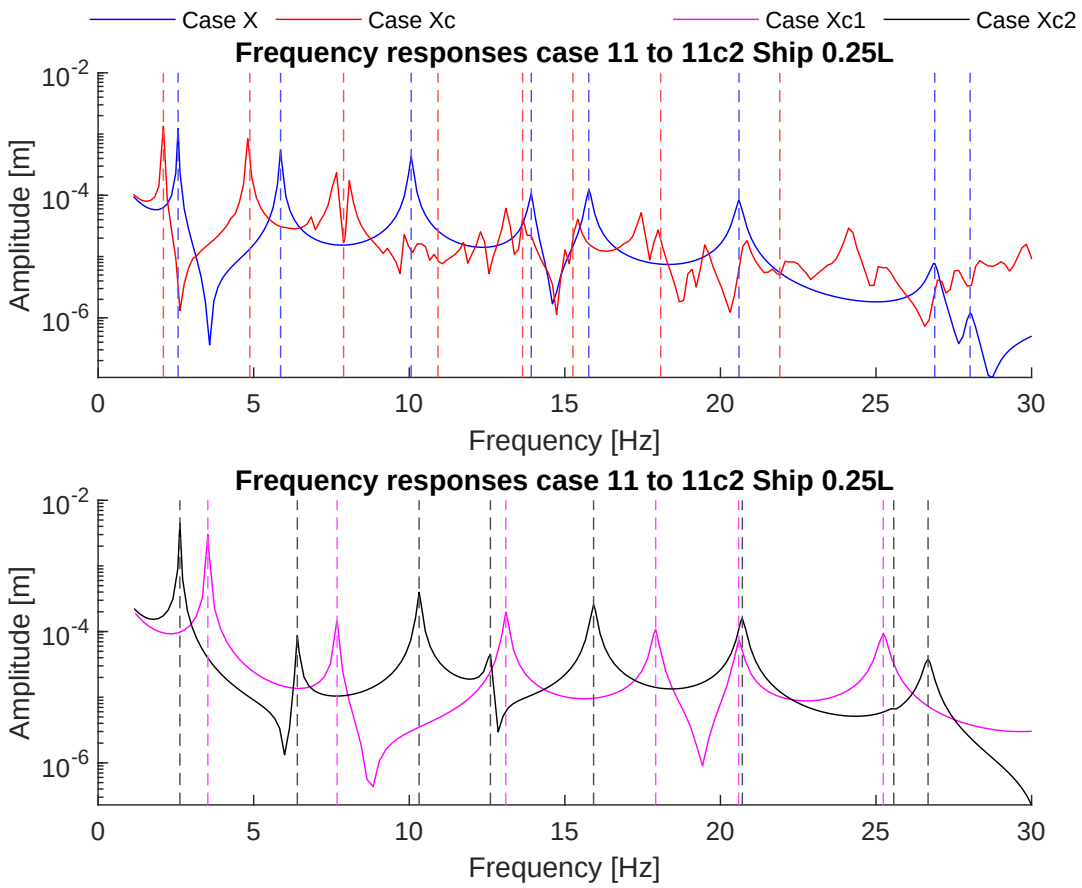

Figure A.31: Ship 0,25L responses due to monopile (3x) parameter tweaks, with the vertical lines '- -' respresenting the natural frequency locations

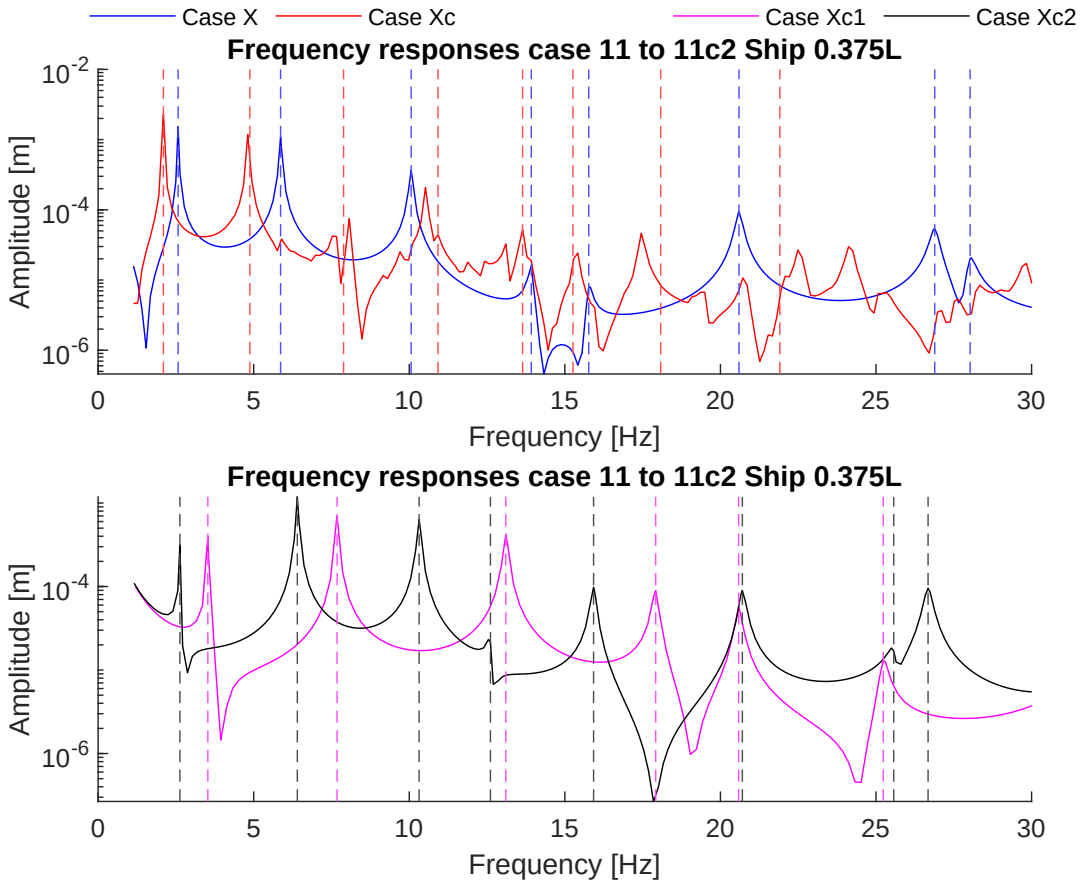

Figure A.32: Ship 0,375L responses due to monopile (3x) parameter tweaks, with the vertical lines '- -' respresenting the natural frequency locations

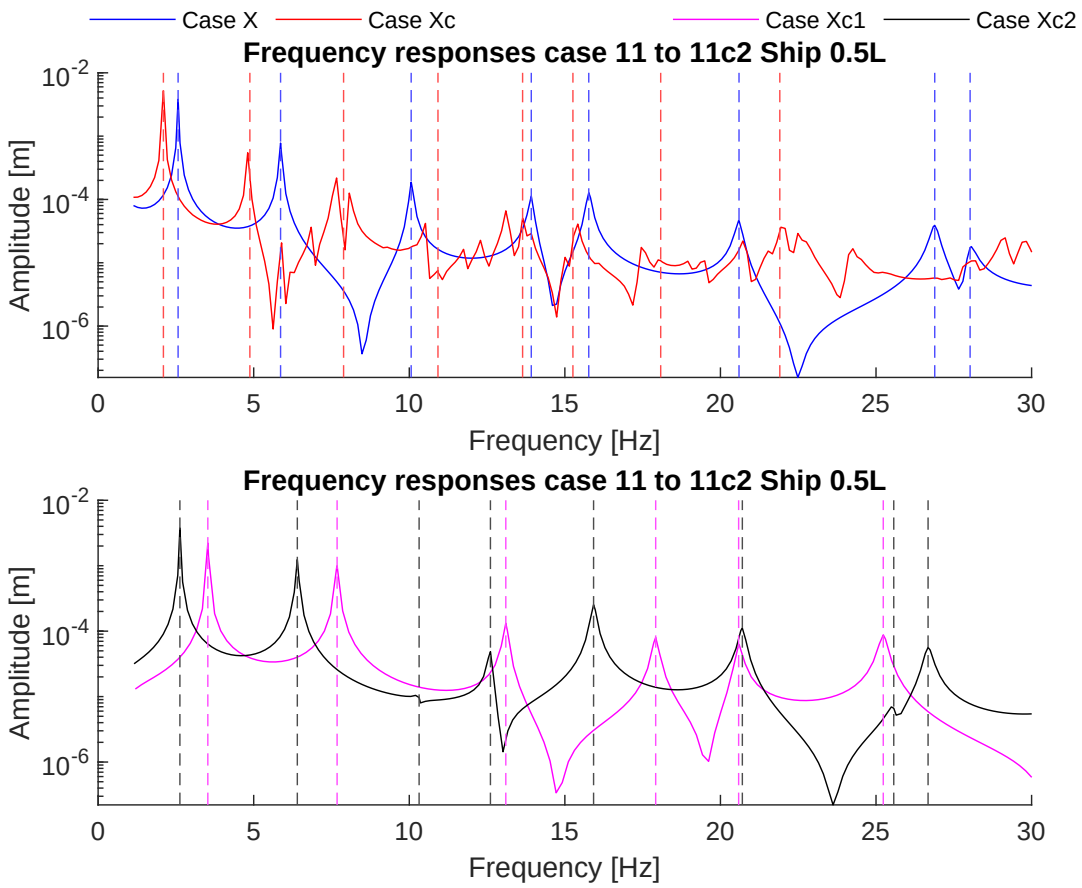

Figure A.33: Ship 0,5L responses due to monopile (3x) parameter tweaks, with the vertical lines '- -' respresenting the natural frequency locations

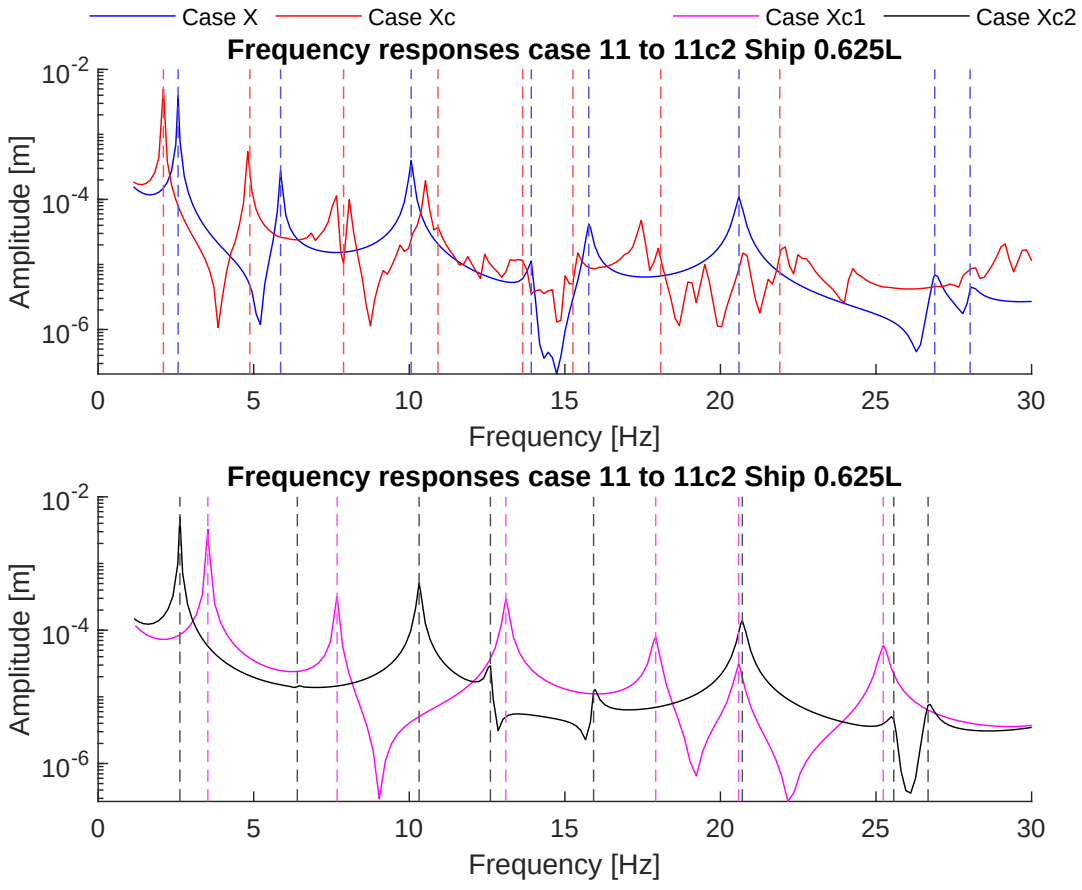

Figure A.34: Ship 0,625L responses due to monopile (3x) parameter tweaks, with the vertical lines '- -' respresenting the natural frequency locations

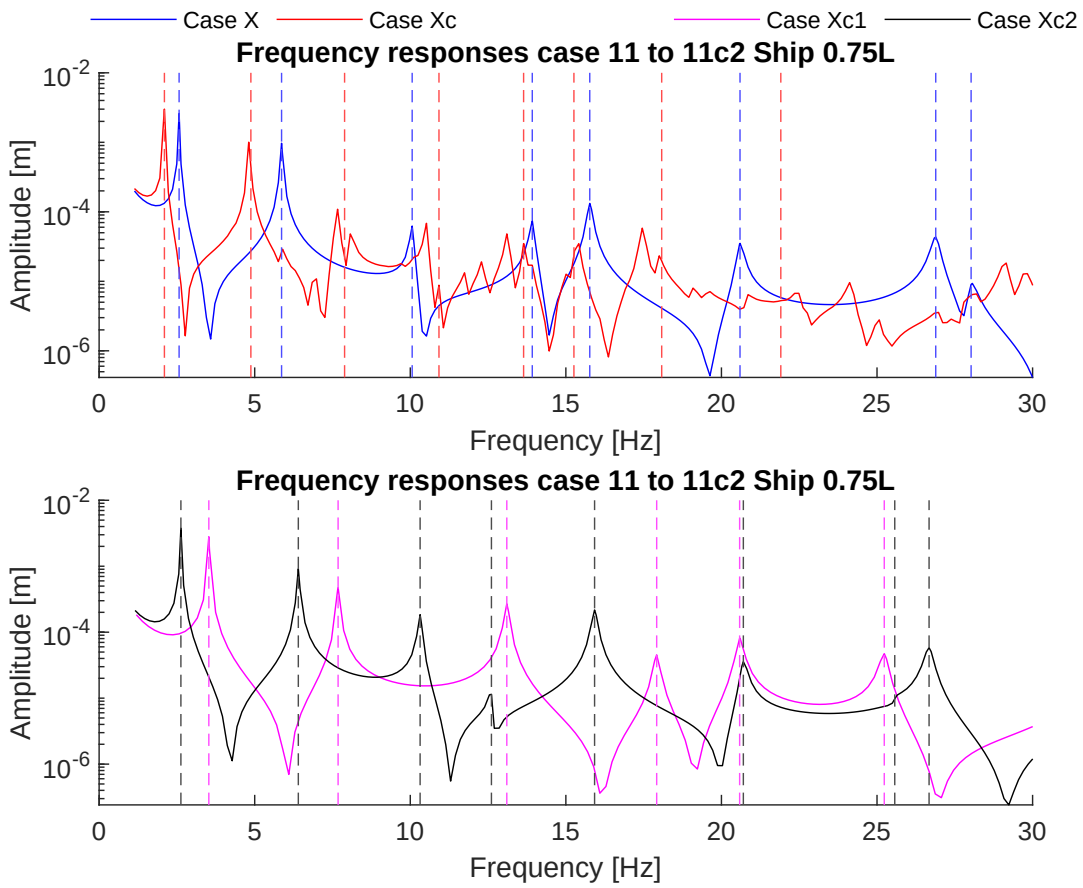

Figure A.35: Ship 0,75L responses due to monopile (3x) parameter tweaks, with the vertical lines '- -' respresenting the natural frequency locations

A.7. Absolute bending moments, ship

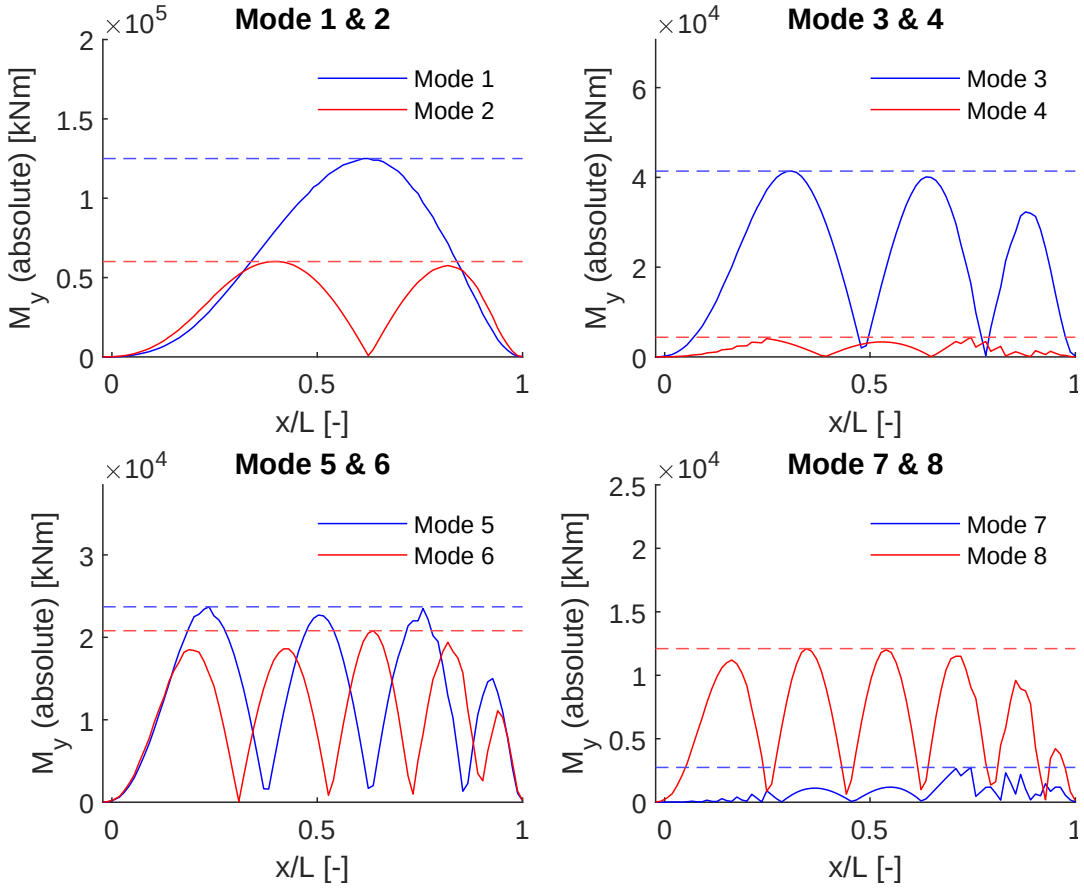

Figure A.36: Case 1 absolute longitudinal bending moments for modes 1 to 8, with the horizontal lines '- -' respresenting the absolute maximums

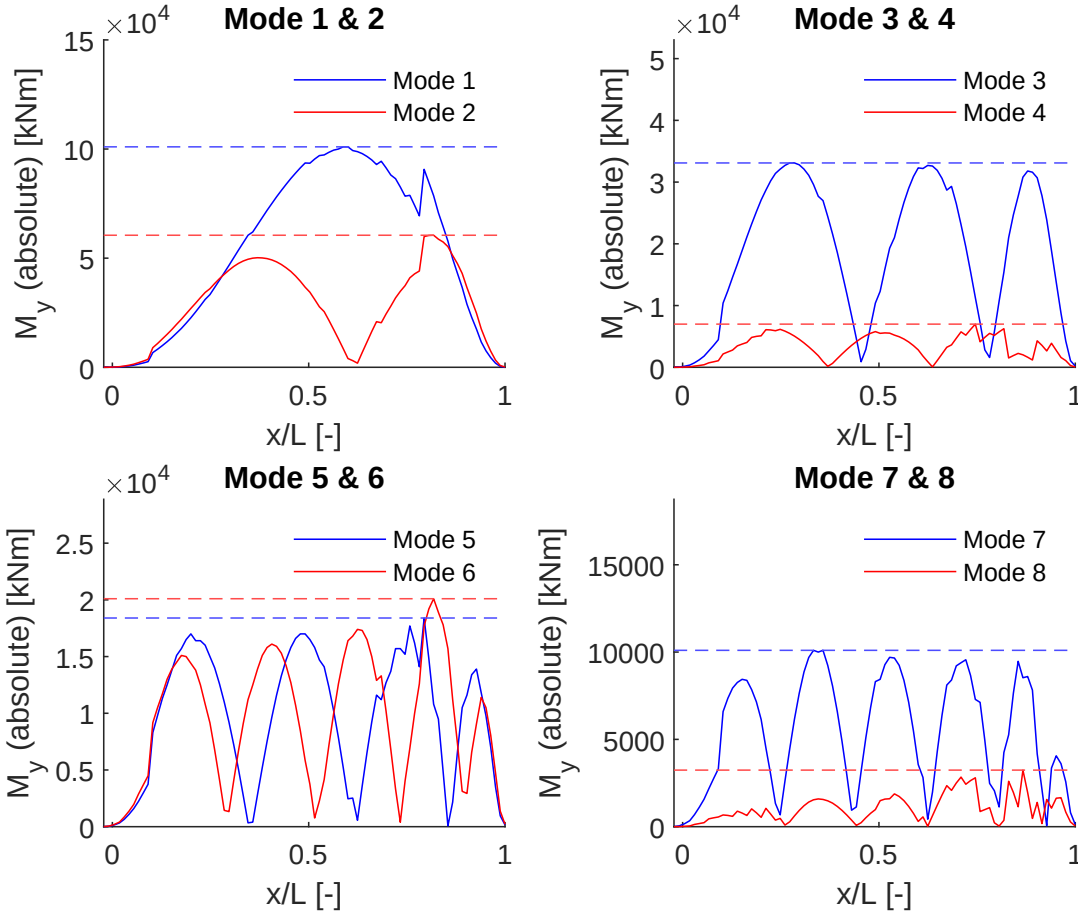

Figure A.37: Case 2 absolute longitudinal bending moments for modes 1 to 8, with the horizontal lines '- -' respresenting the absolute maximums

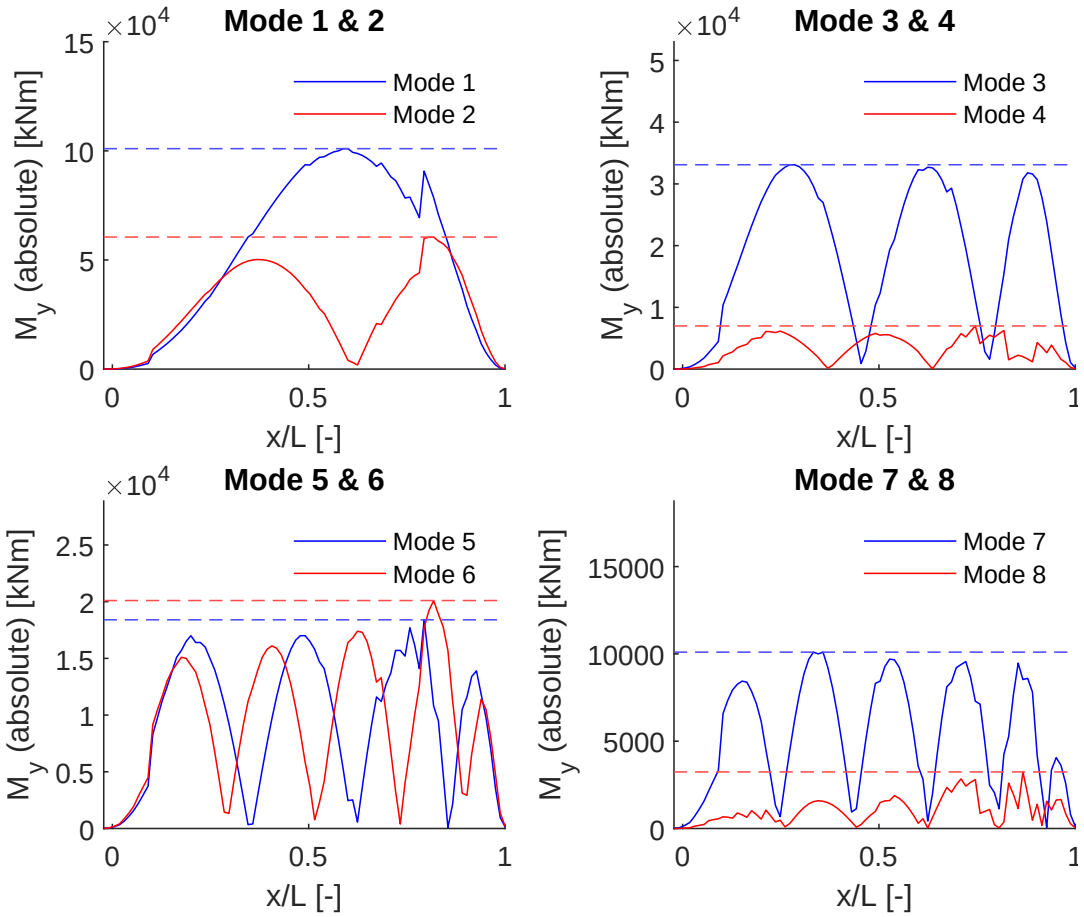

Figure A.38: Case 3 absolute longitudinal bending moments for modes 1 to 8, with the horizontal lines '- -' respresenting the absolute maximums

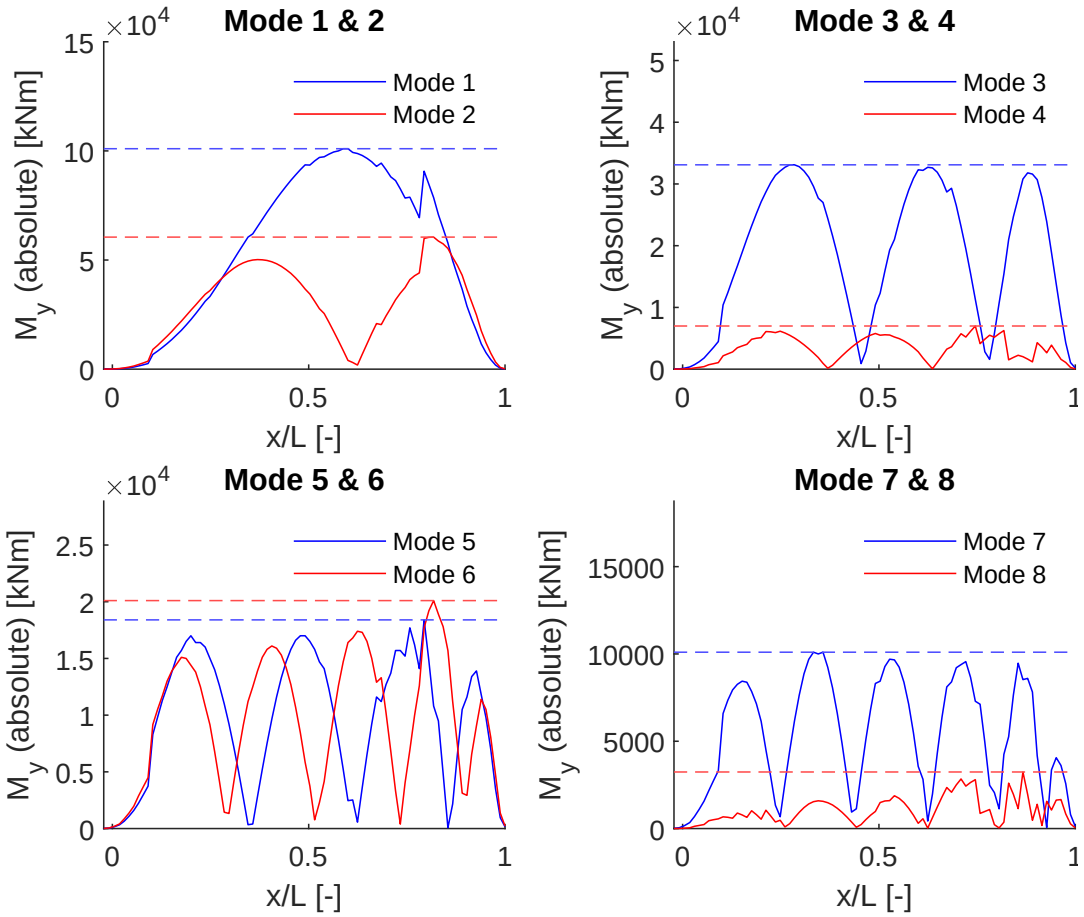

Figure A.39: Case 4 absolute longitudinal bending moments for modes 1 to 8, with the horizontal lines '- -' respresenting the absolute maximums

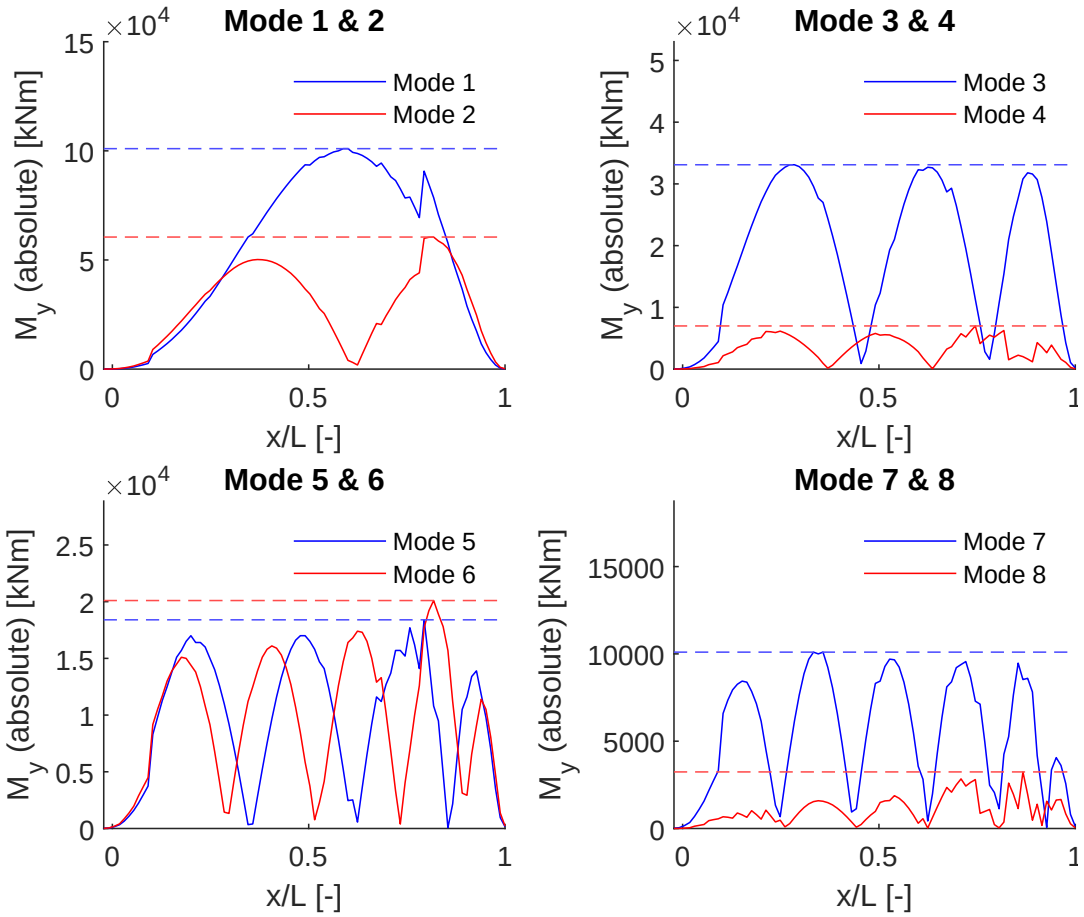

Figure A.40: Case 5 absolute longitudinal bending moments for modes 1 to 8, with the horizontal lines '- -' respresenting the absolute maximums

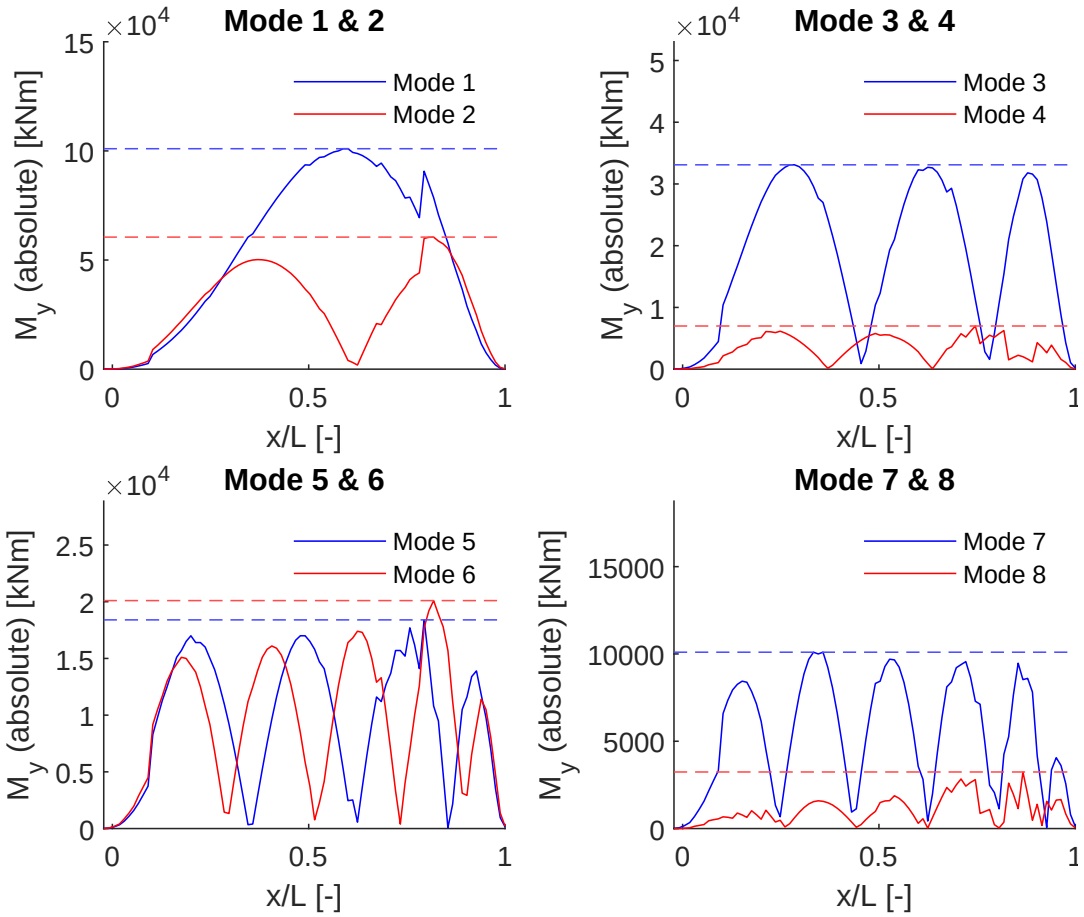

Figure A.41: Case 6 absolute longitudinal bending moments for modes 1 to 8, with the horizontal lines '- -' respresenting the absolute maximums

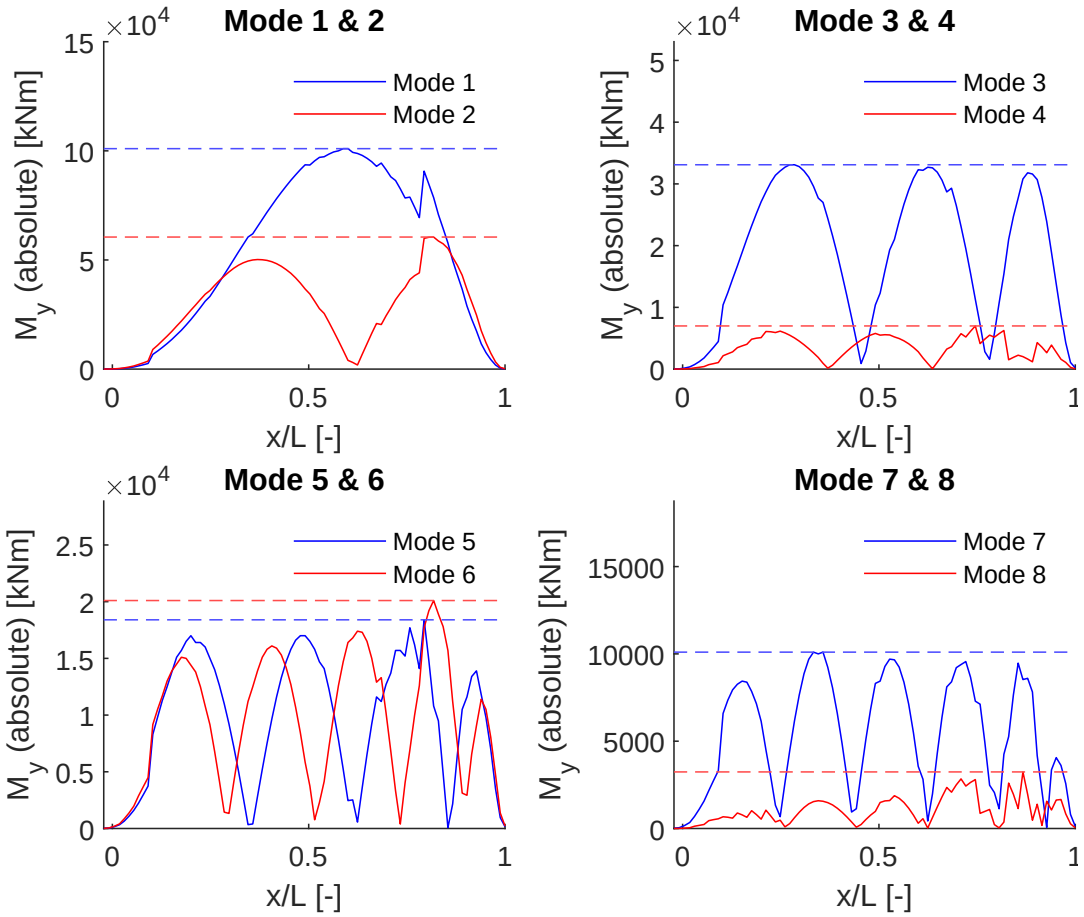

Figure A.42: Case 7 absolute longitudinal bending moments for modes 1 to 8, with the horizontal lines '- -' respresenting the absolute maximums

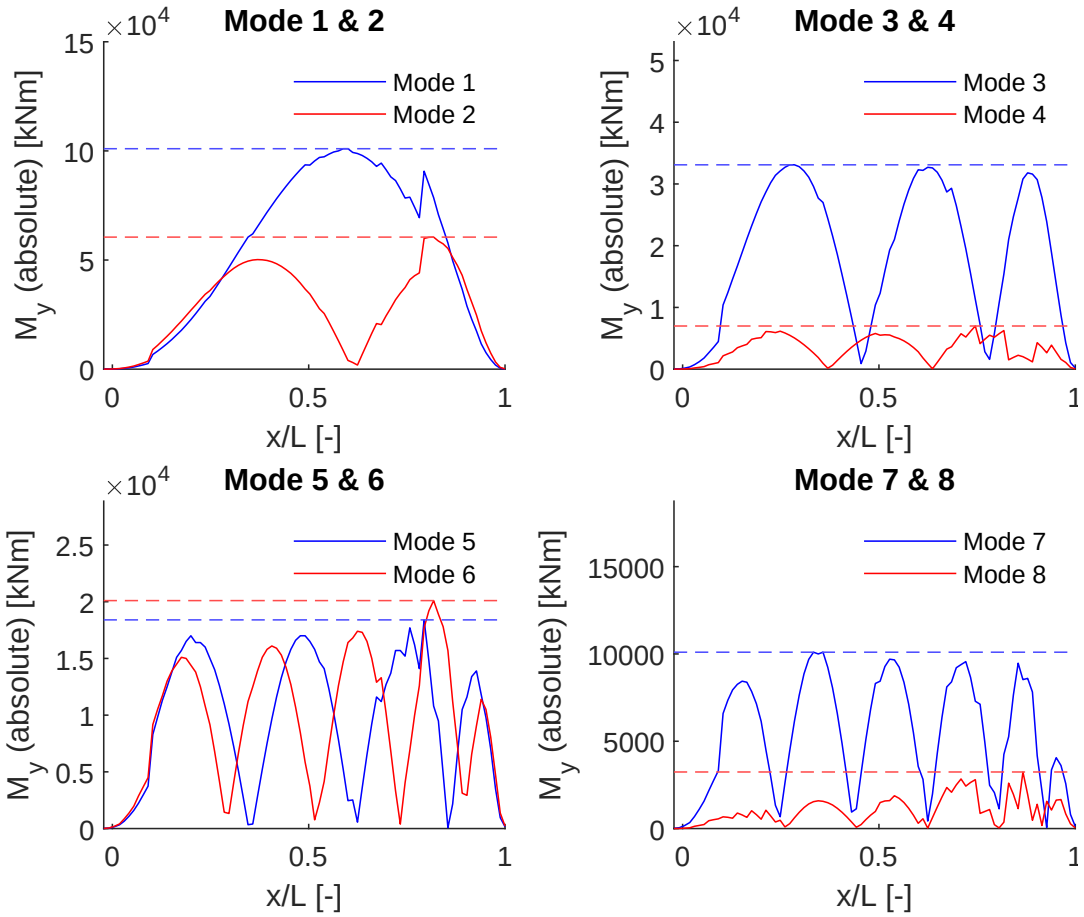

Figure A.43: Case 8 absolute longitudinal bending moments for modes 1 to 8, with the horizontal lines '- -' respresenting the absolute maximums

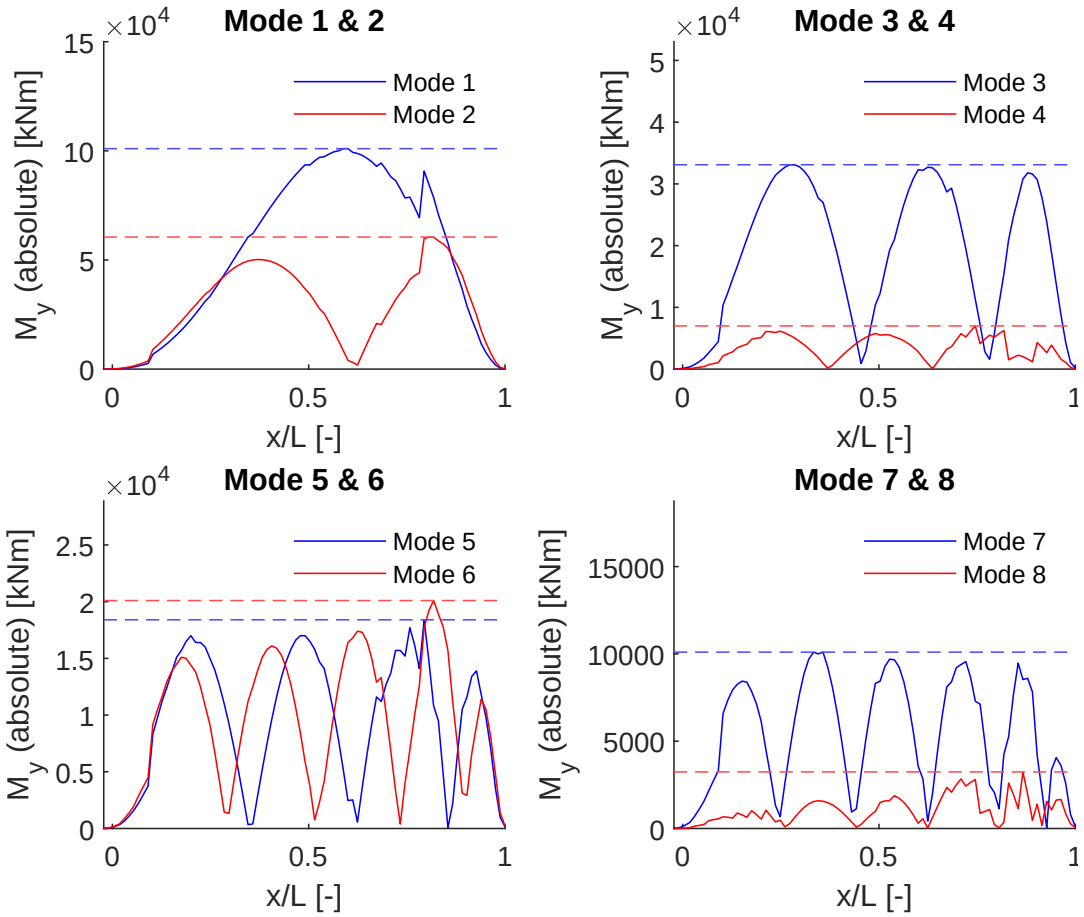

Figure A.44: Case 9 absolute longitudinal bending moments for modes 1 to 8, with the horizontal lines '- -' respresenting the absolute maximums

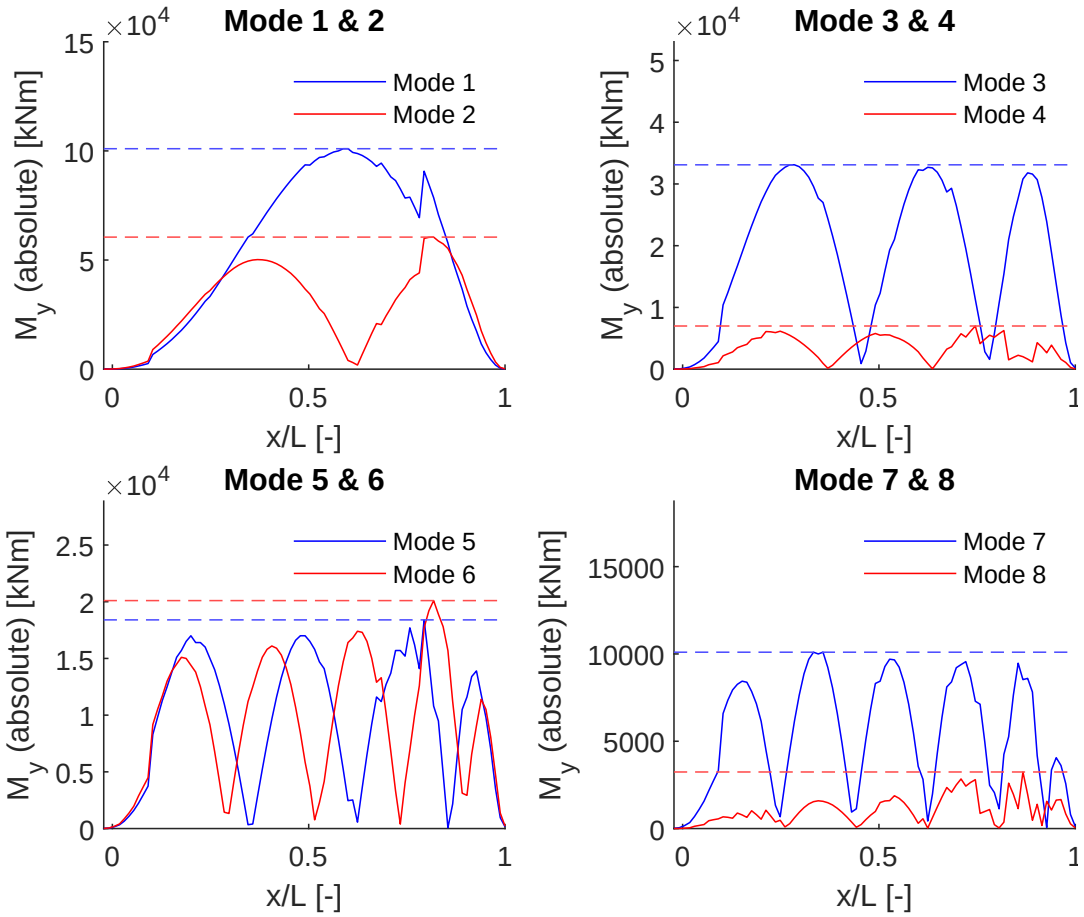

Figure A.45: Case 10 absolute longitudinal bending moments for modes 1 to 8, with the horizontal lines '- -' respresenting the absolute maximums

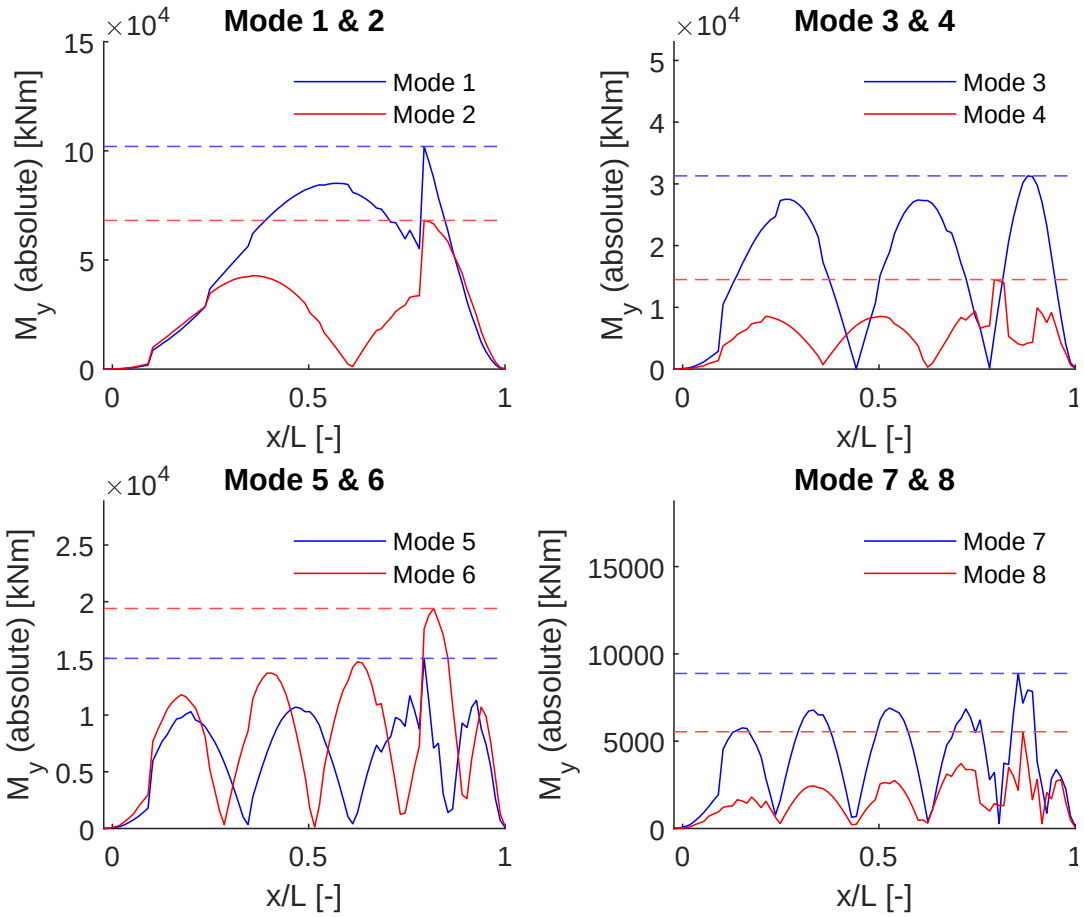

Figure A.46: Case 11 absolute longitudinal bending moments for modes 1 to 8, with the horizontal lines '- -' respresenting the absolute maximums

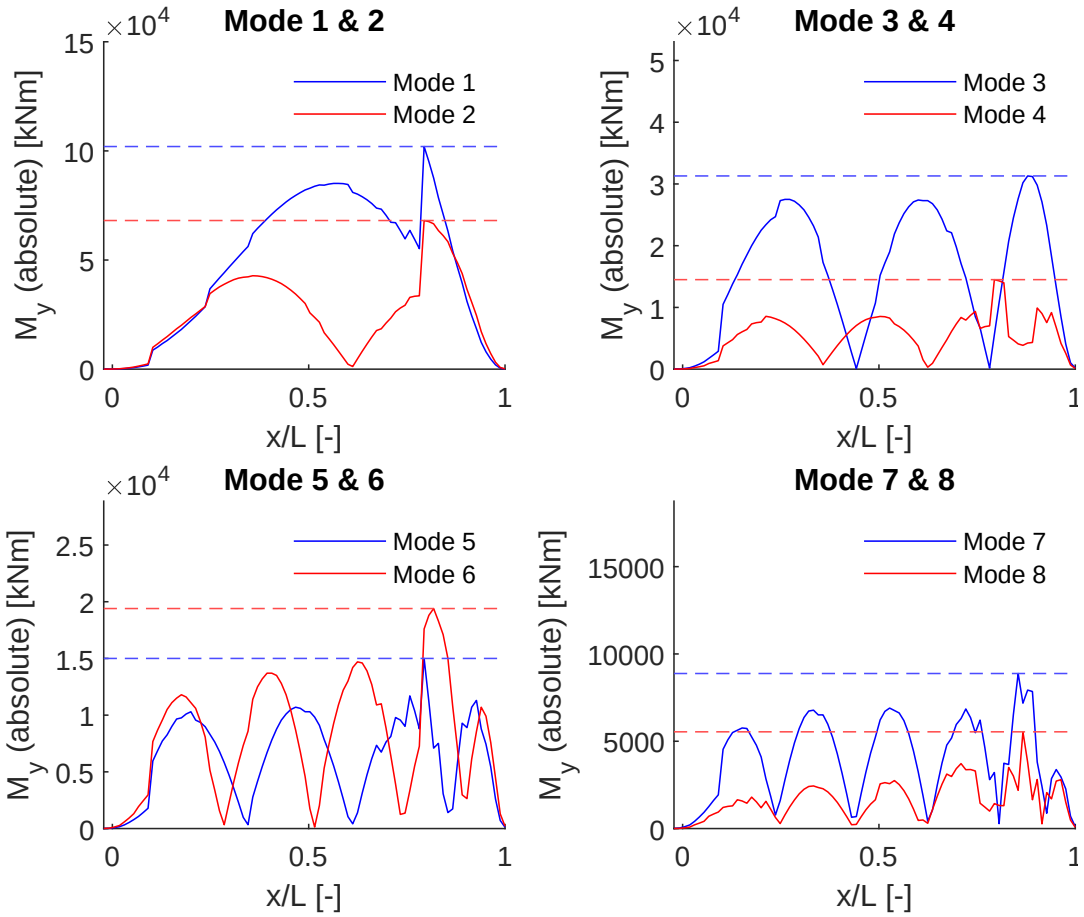

Figure A.47: Case 12 absolute longitudinal bending moments for modes 1 to 8, with the horizontal lines '- -' respresenting the absolute maximums

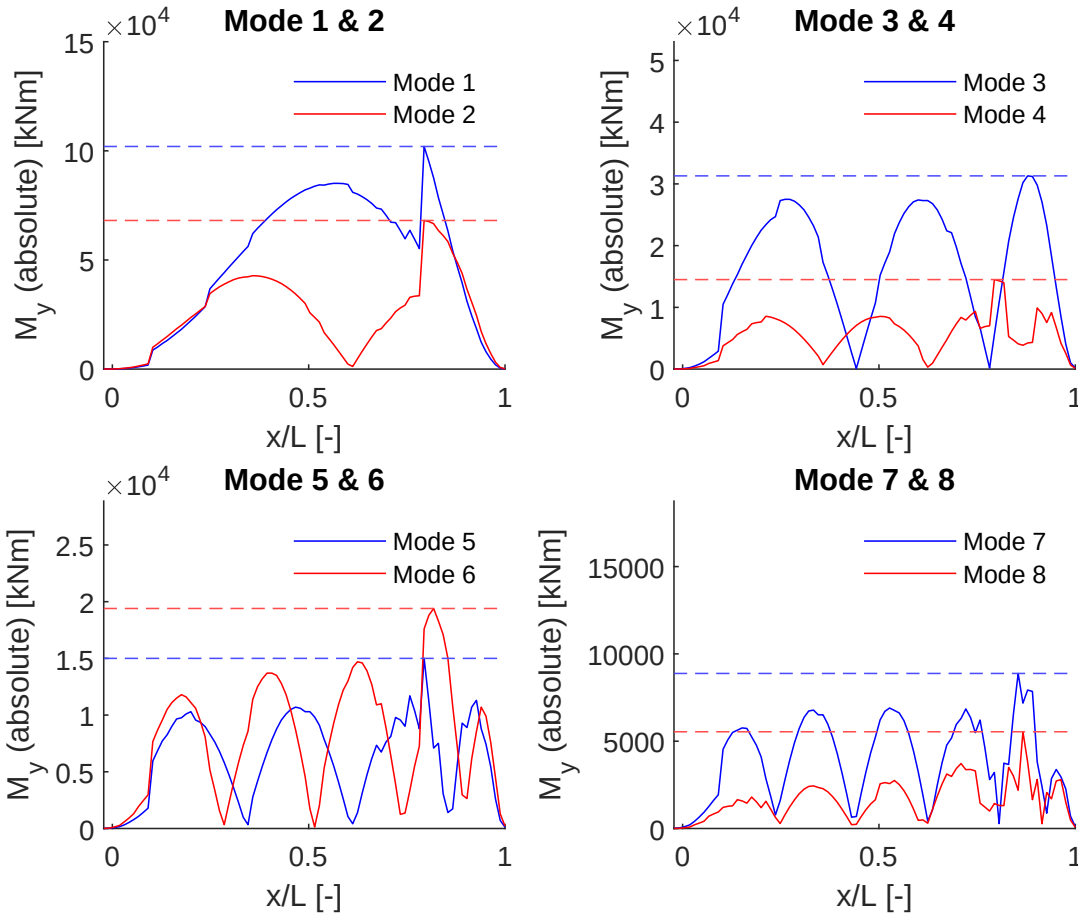

Figure A.48: Case 13 absolute longitudinal bending moments for modes 1 to 8, with the horizontal lines '- -' respresenting the absolute maximums

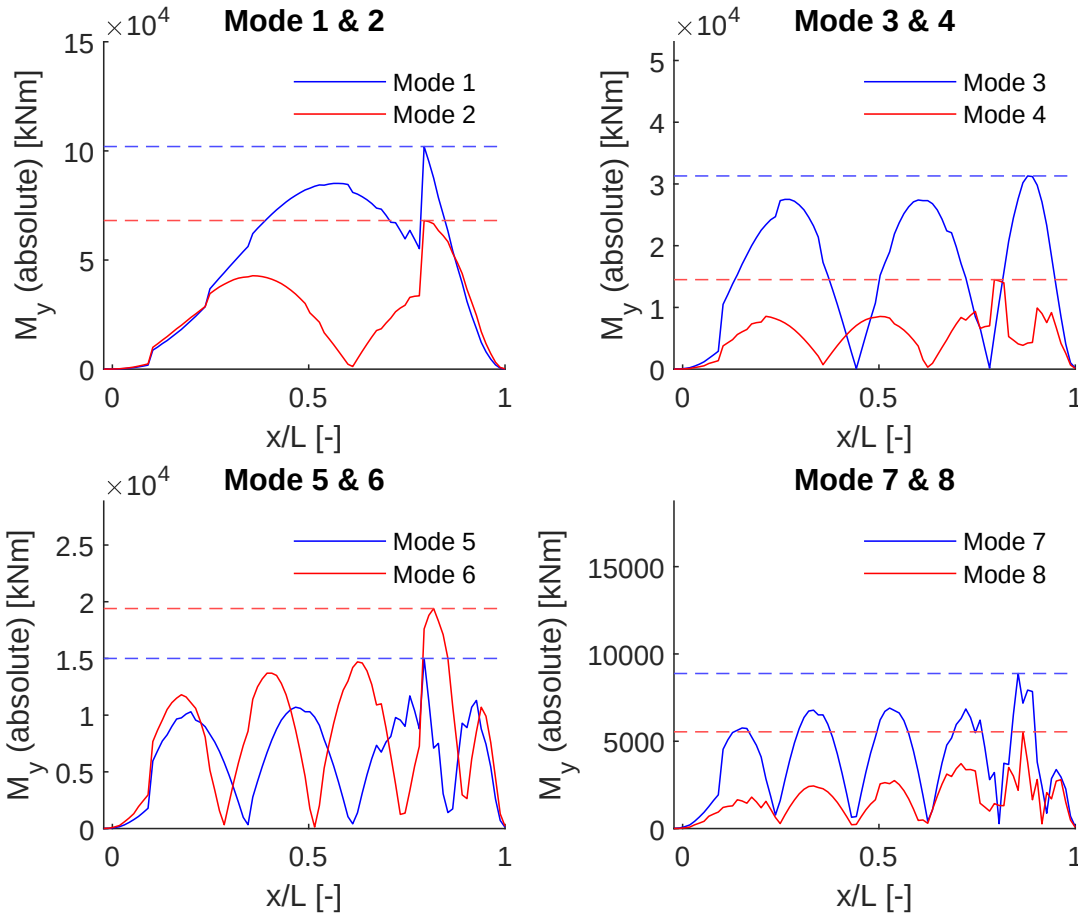

Figure A.49: Case 14 absolute longitudinal bending moments for modes 1 to 8, with the horizontal lines '- -' respresenting the absolute maximums

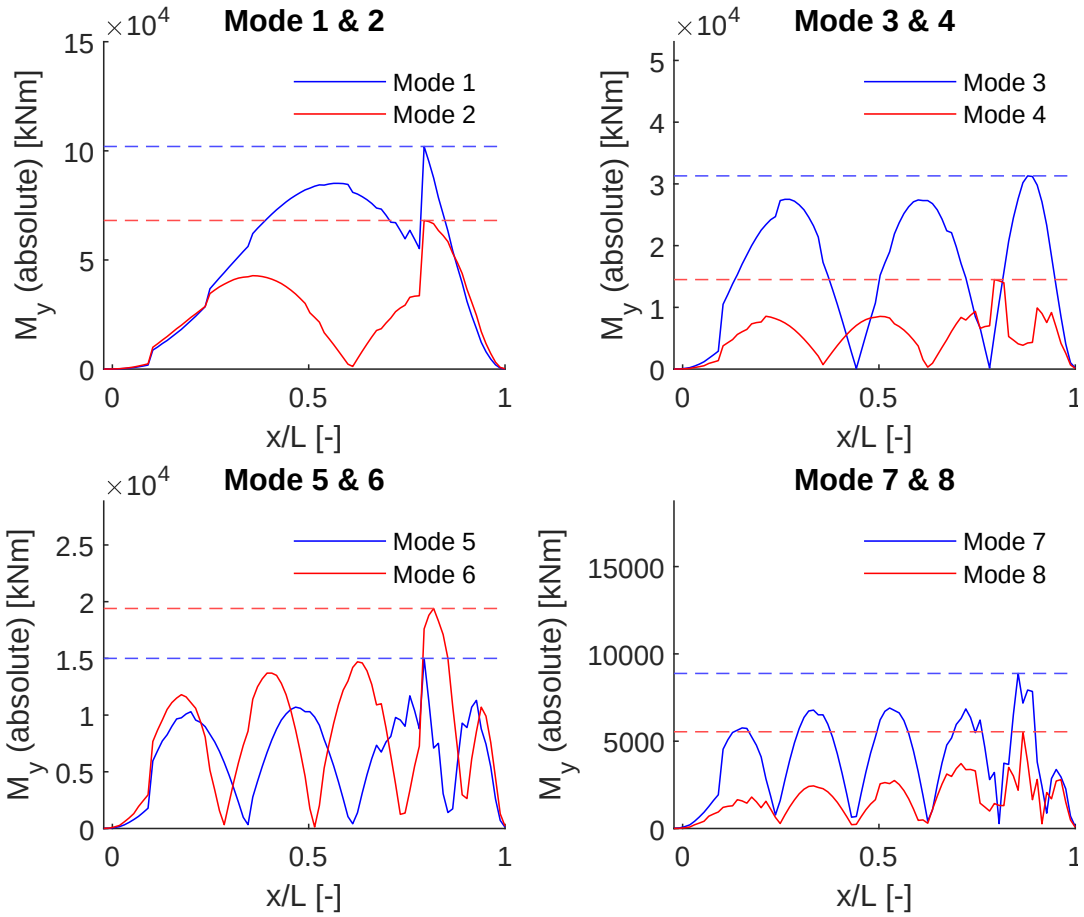

Figure A.50: Case 15 absolute longitudinal bending moments for modes 1 to 8, with the horizontal lines '- -' respresenting the absolute maximums

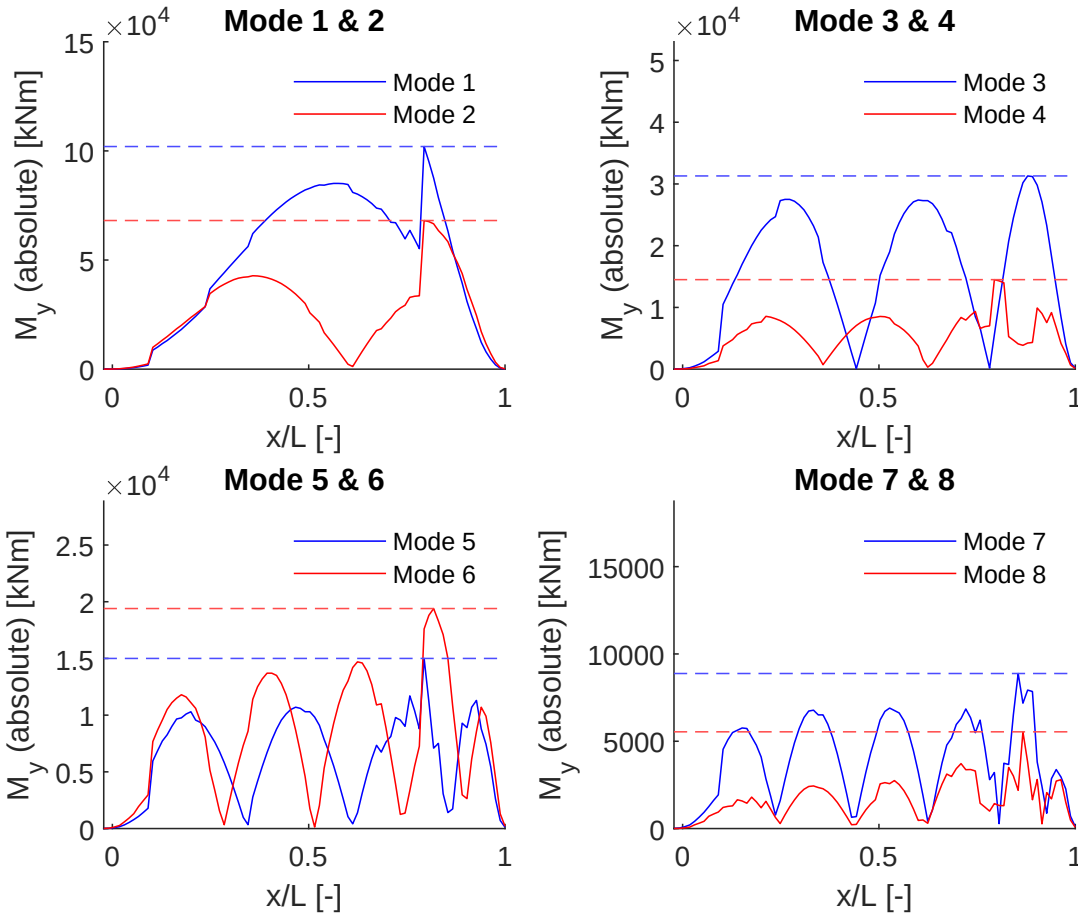

Figure A.51: Case 16 absolute longitudinal bending moments for modes 1 to 8, with the horizontal lines '- -' respresenting the absolute maximums

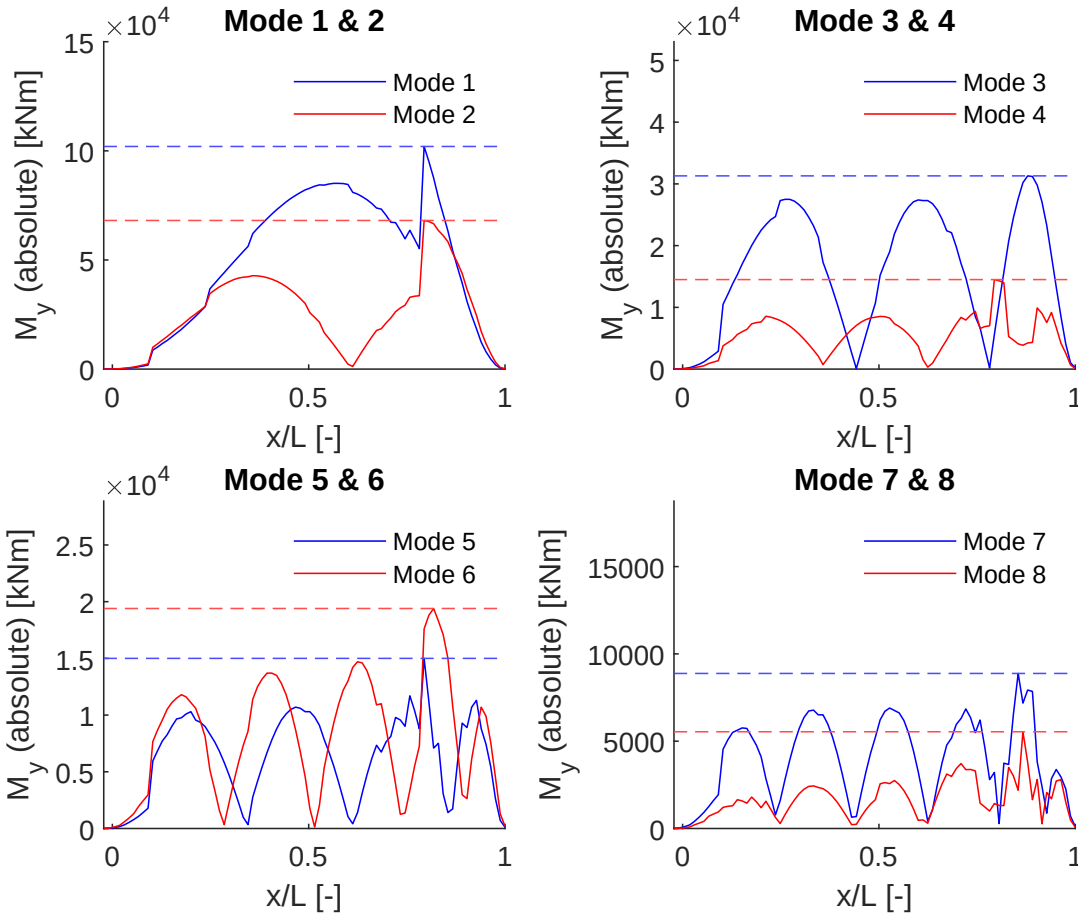

Figure A.52: Case 17 absolute longitudinal bending moments for modes 1 to 8, with the horizontal lines '- -' respresenting the absolute maximums

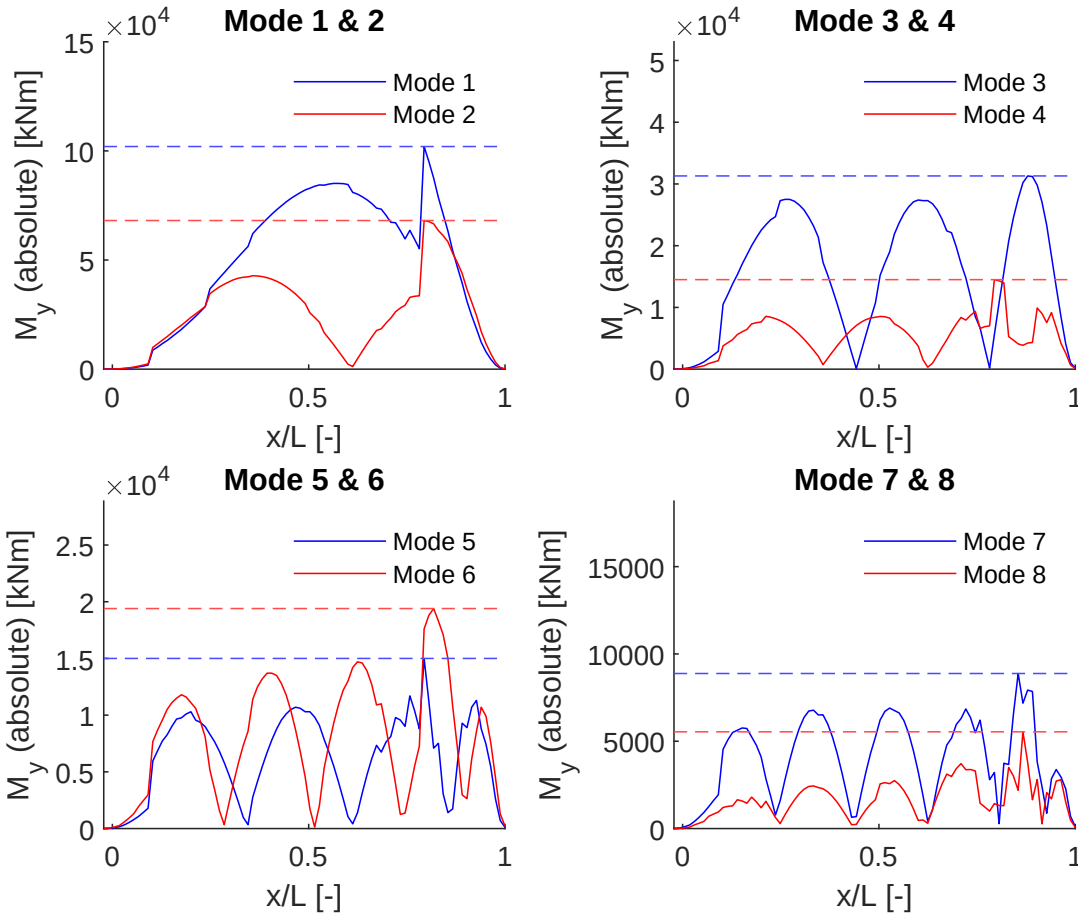

Figure A.53: Case 18 absolute longitudinal bending moments for modes 1 to 8, with the horizontal lines '- -' respresenting the absolute maximums

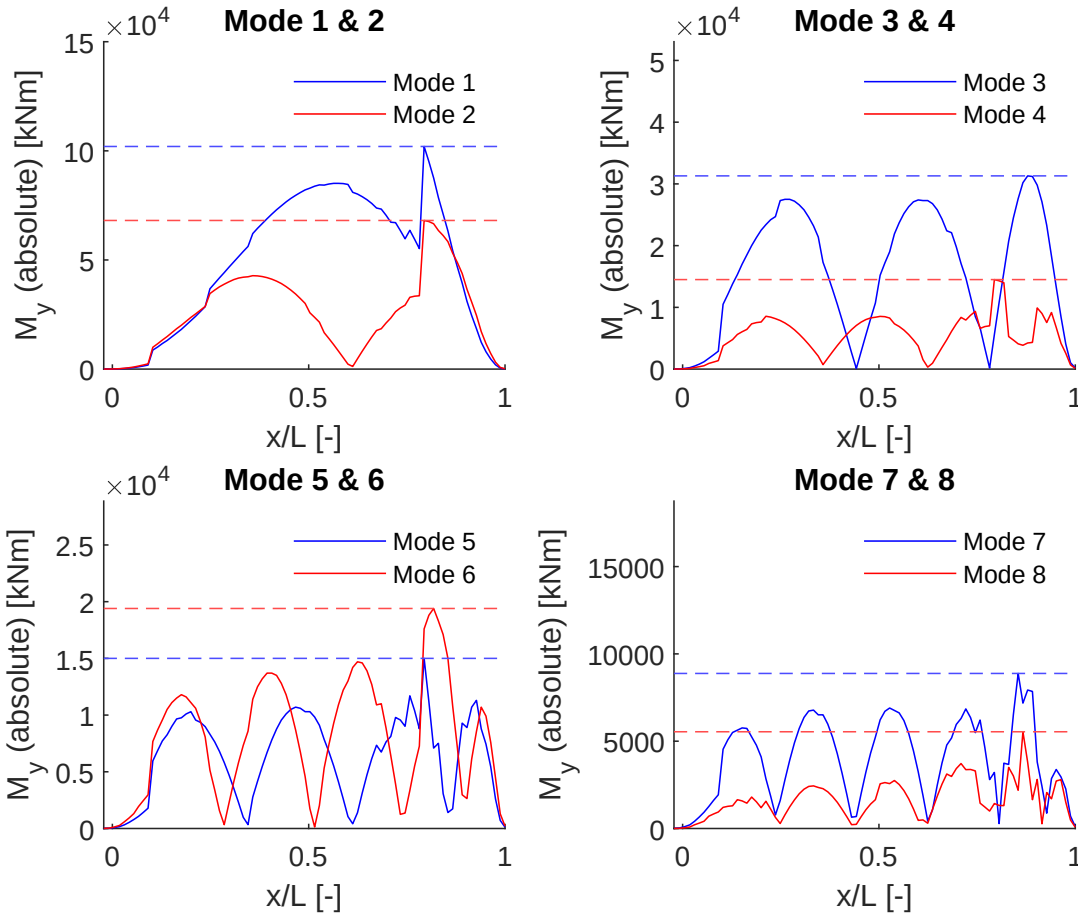

Figure A.54: Case 19 absolute longitudinal bending moments for modes 1 to 8, with the horizontal lines '- -' respresenting the absolute maximums

B

Appendix: Non-linear modelling data

B.1. Ship response base deformations (case 2 & 11)

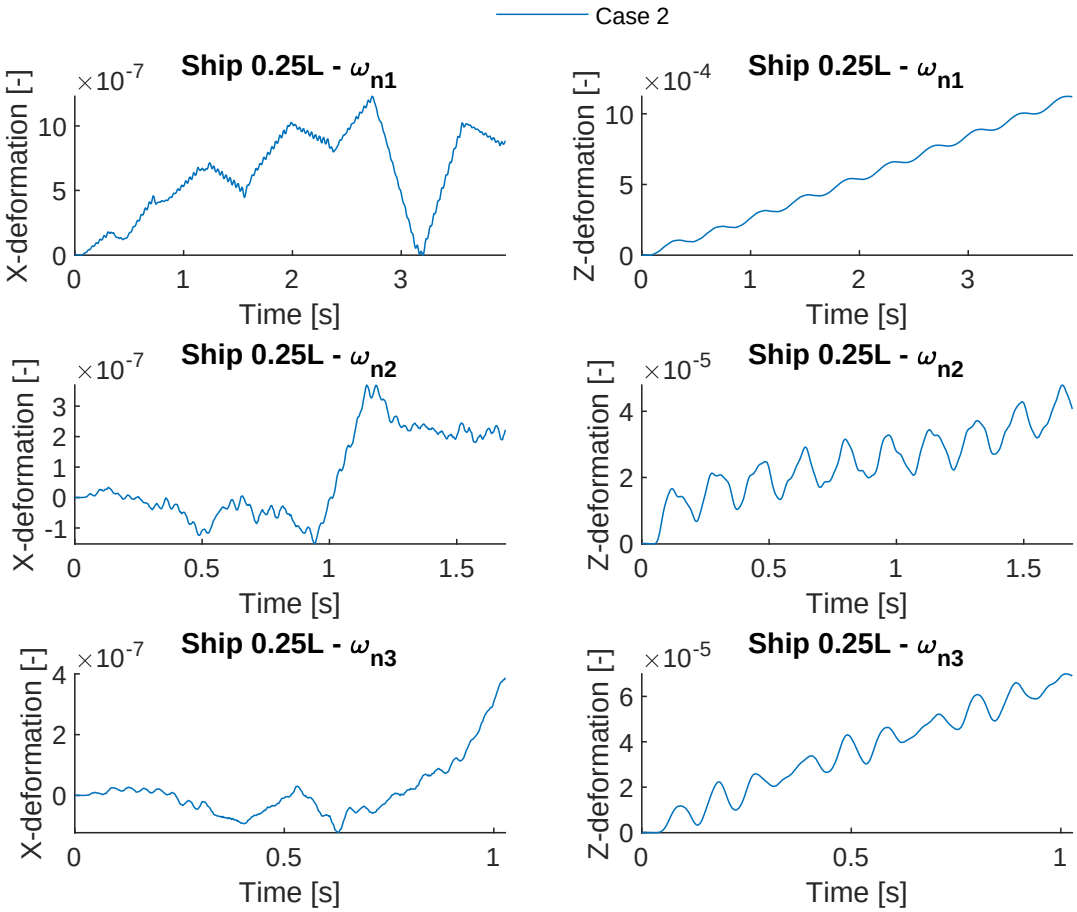

Figure B.1: Deformations case 2 - Ship 0.25L X- & Z-direction

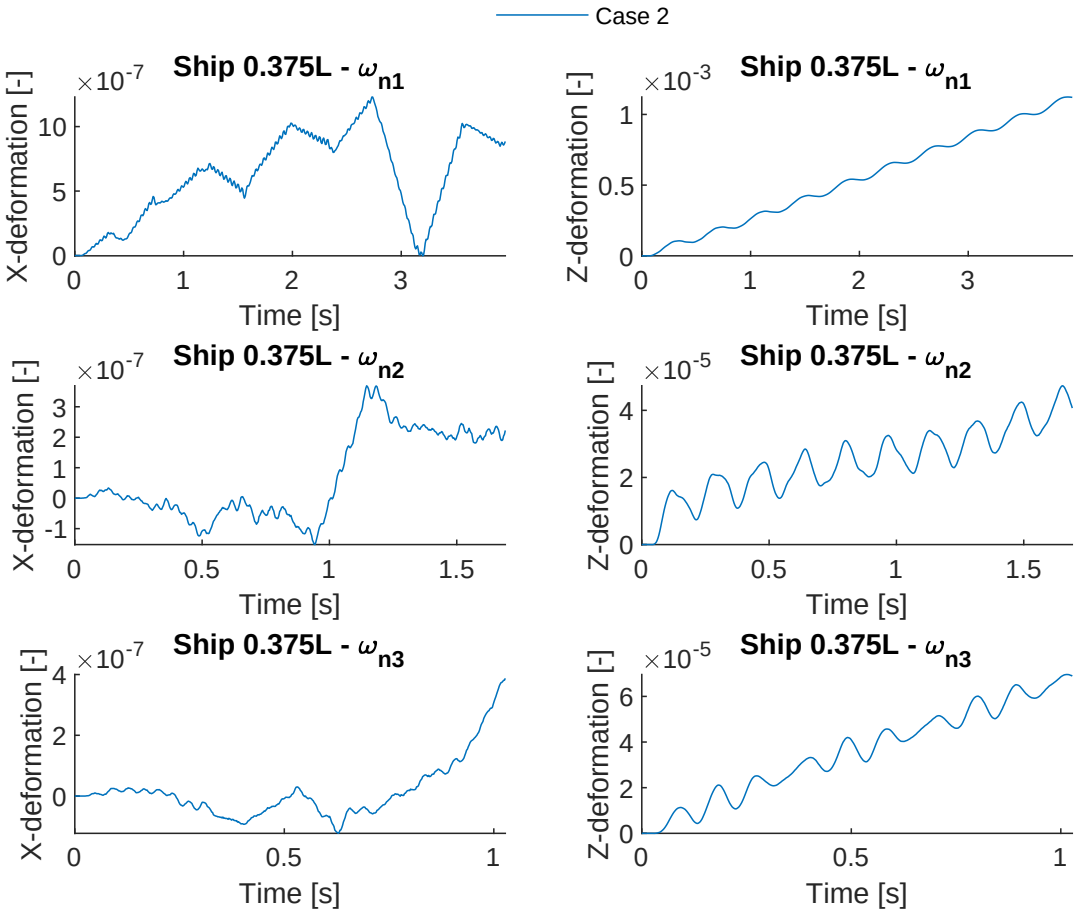

Figure B.2: Deformations case 2 - Ship 0.375L X- & Z-direction

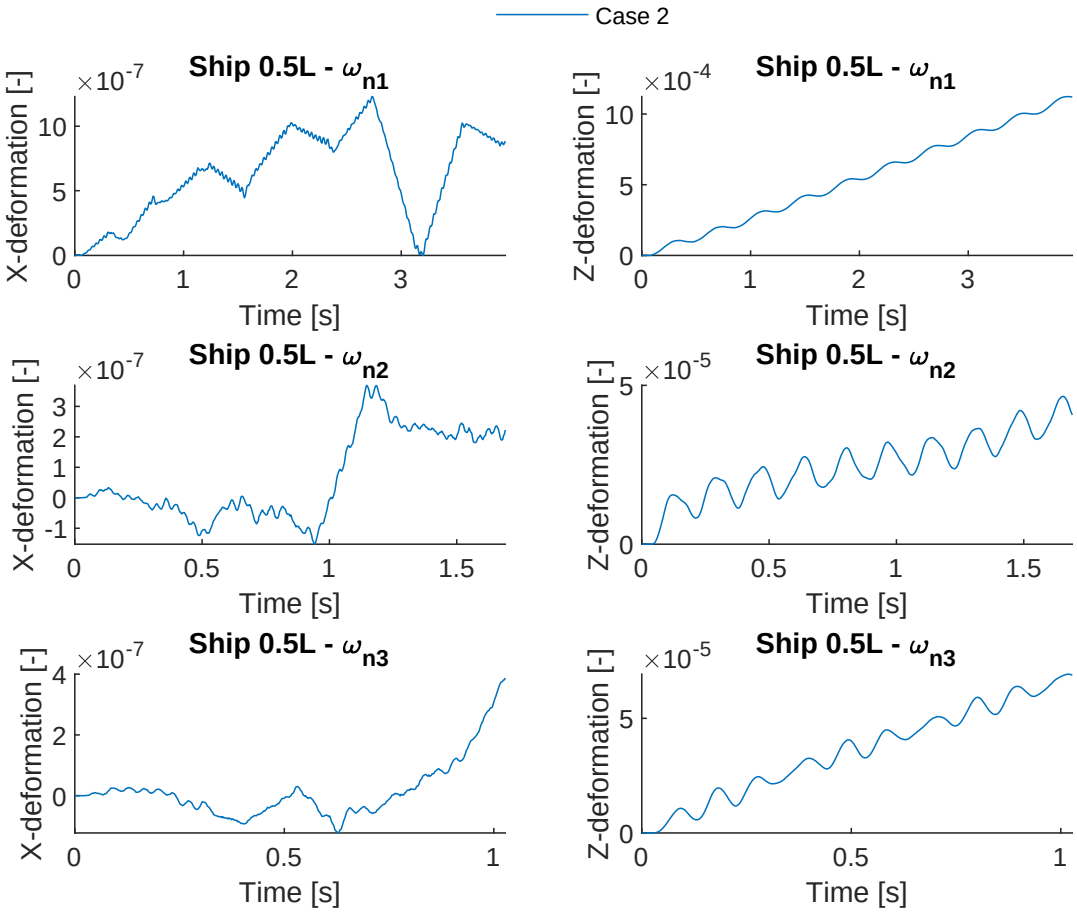

Figure B.3: Deformations case 2 - Ship 0.5L X- & Z-direction

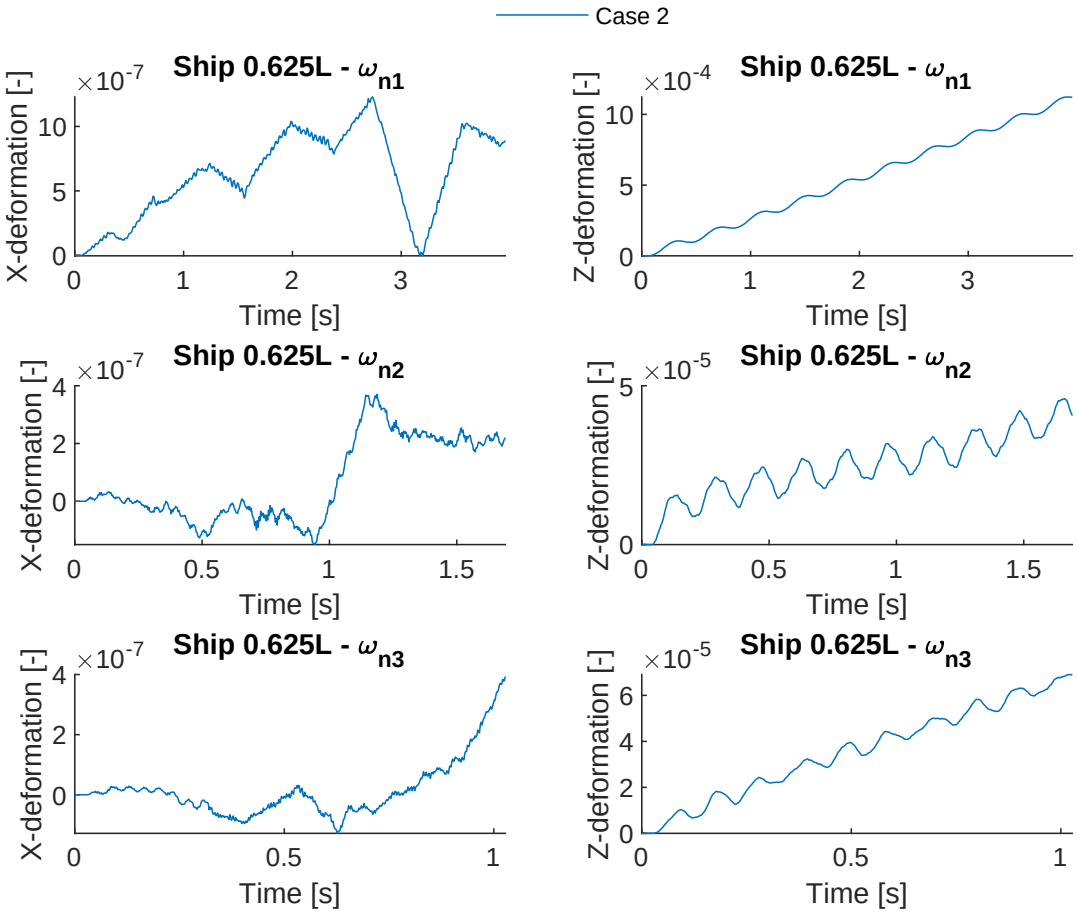

Figure B.4: Deformations case 2 - Ship 0.375L X- & Z-direction

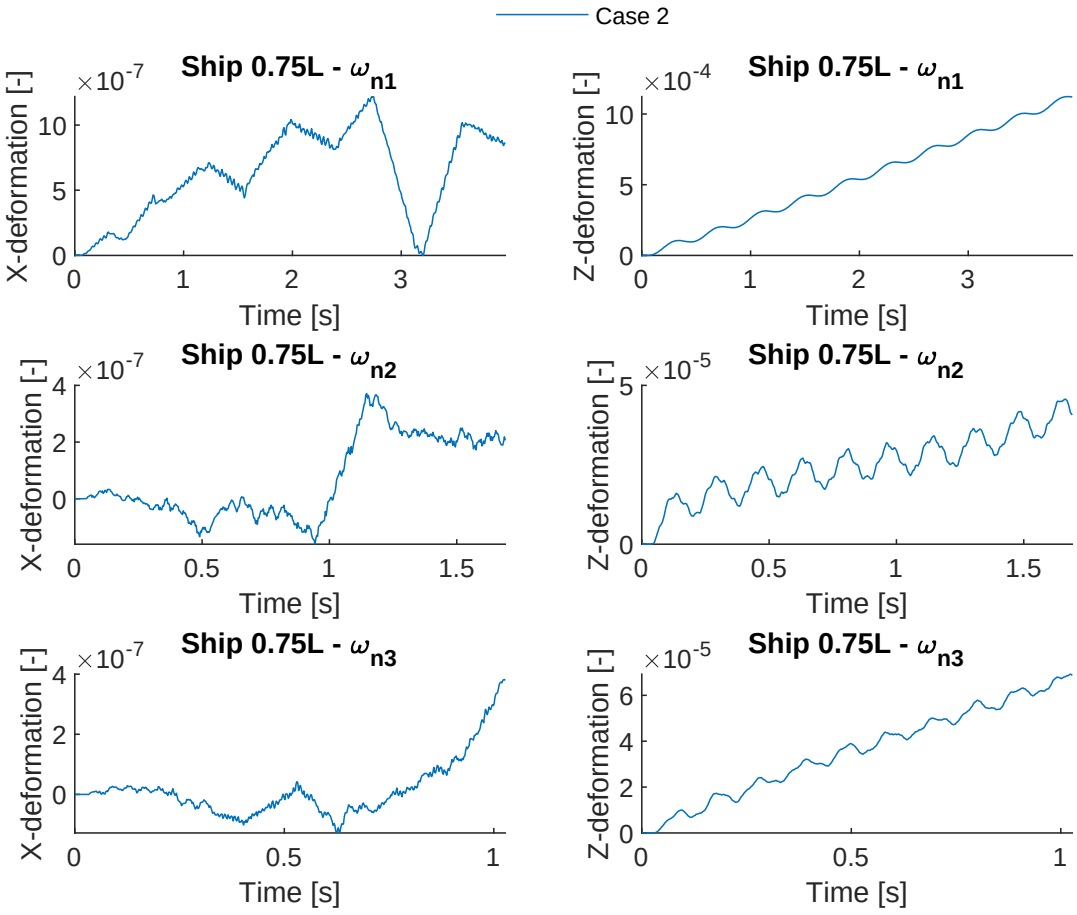

Figure B.5: Deformations case 2 - Ship 0.5L X- & Z-direction

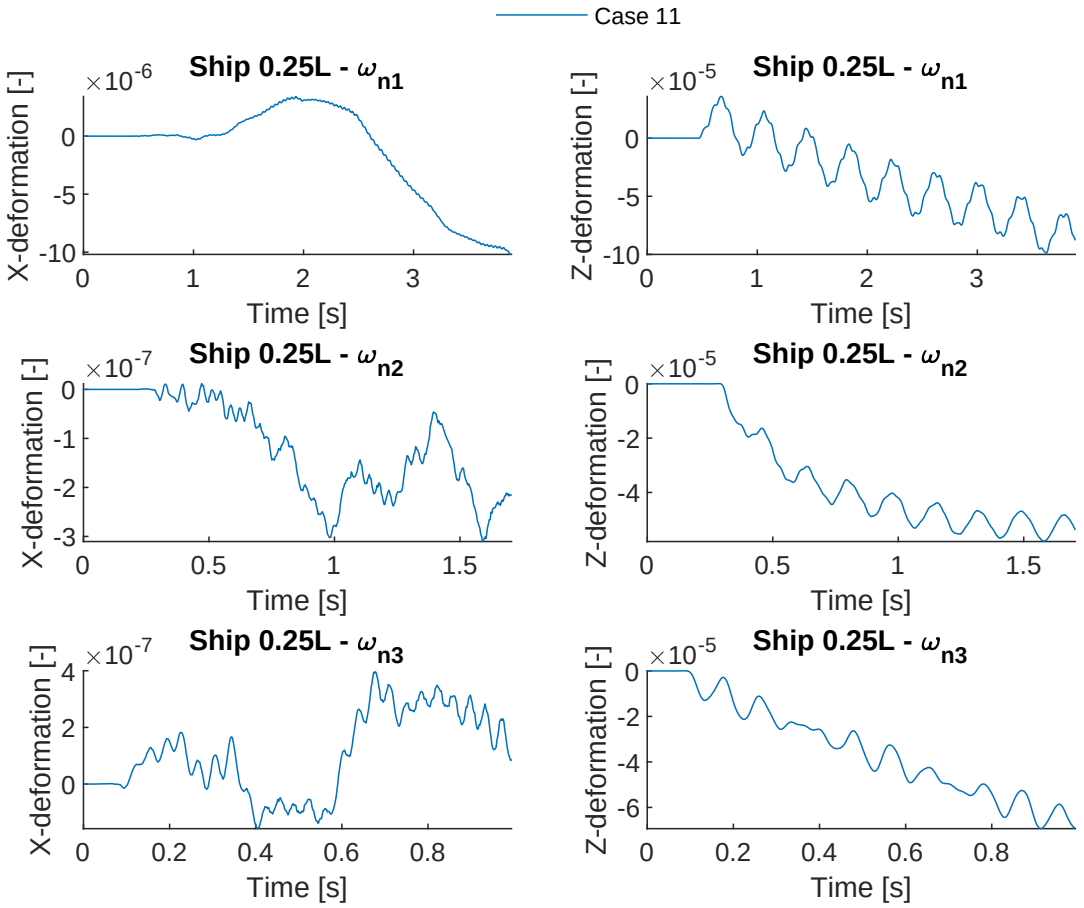

Figure B.6: Deformations case 11 - Ship 0.25L X- & Z-direction

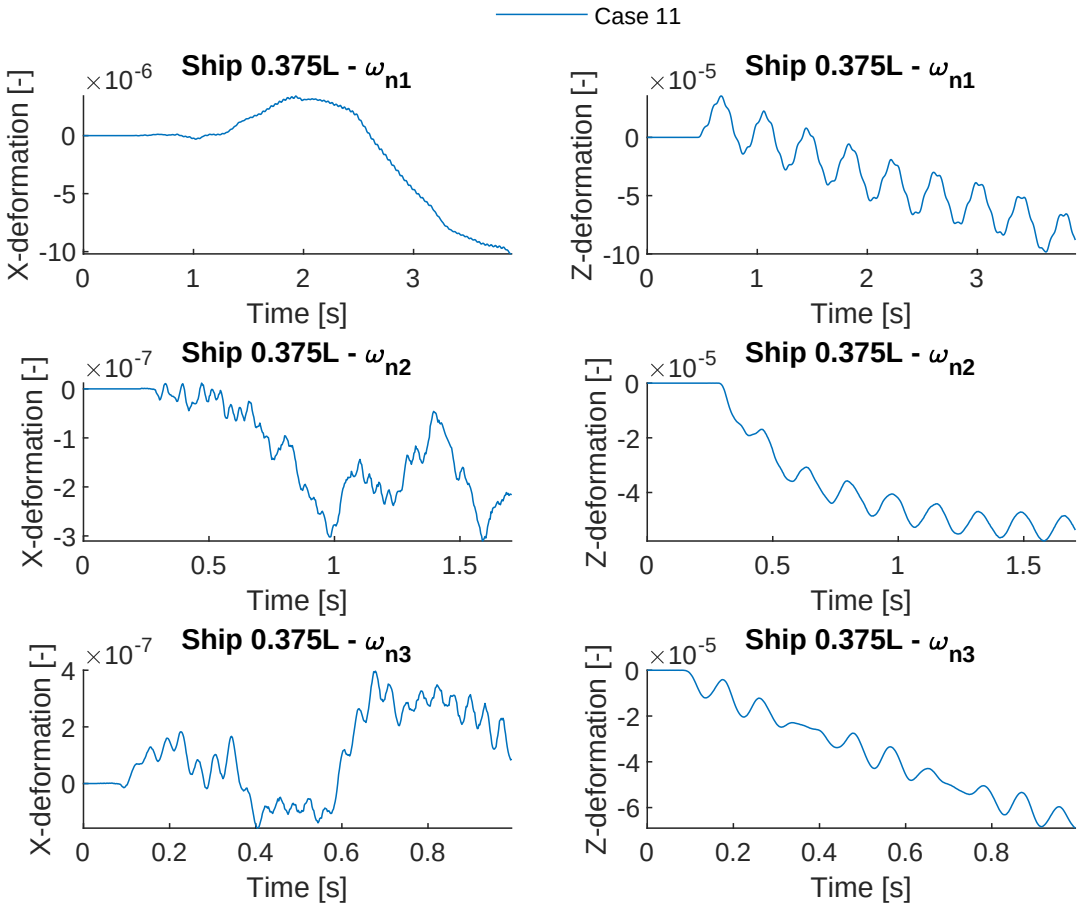

Figure B.7: Deformations case 11 - Ship 0.375L X- & Z-direction

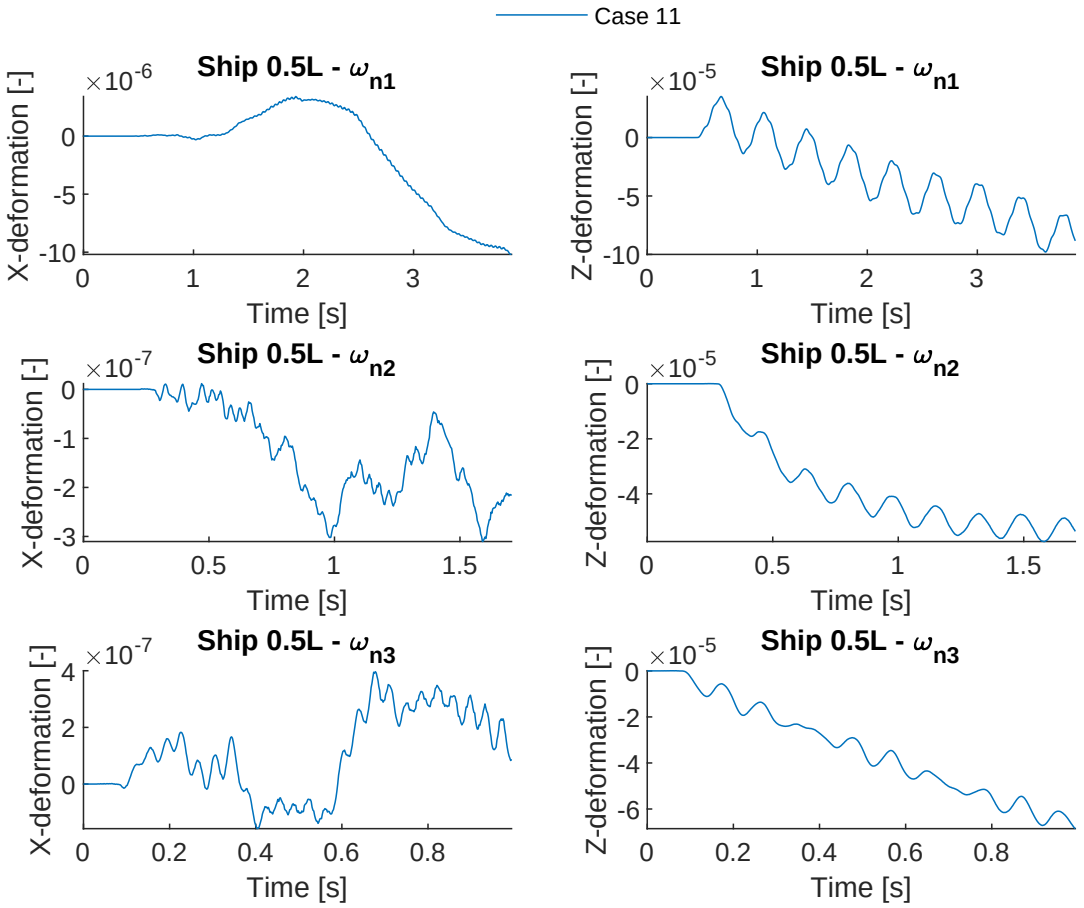

Figure B.8: Deformations case 11 - Ship 0.5L X- & Z-direction

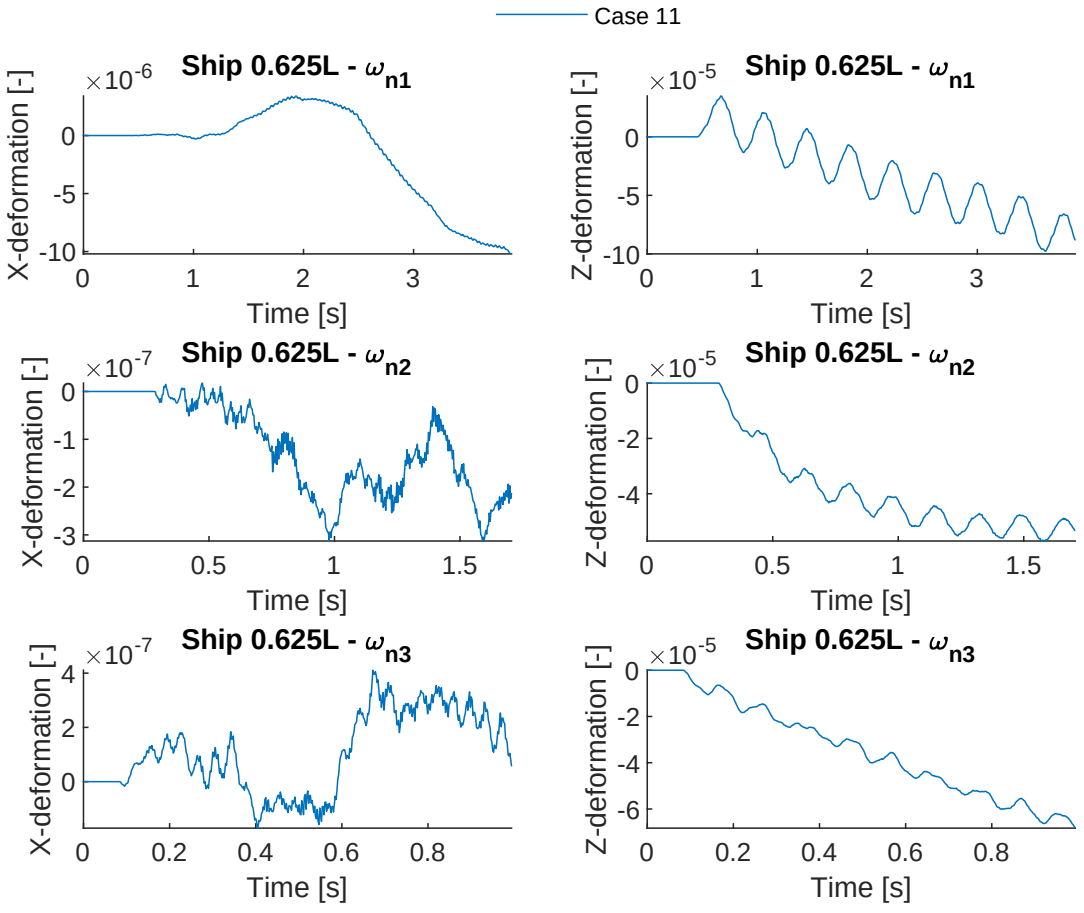

Figure B.9: Deformations case 11 - Ship 0.375L X- & Z-direction

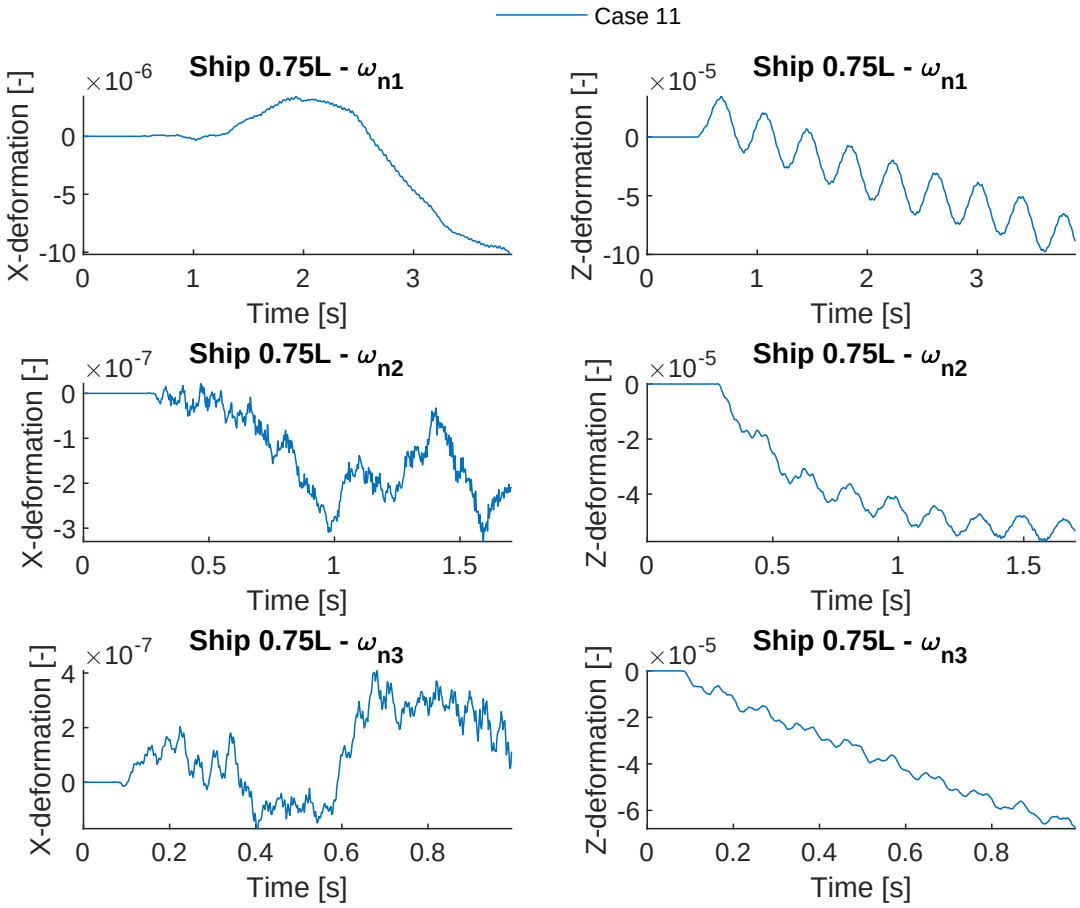

Figure B.10: Deformations case 11 - Ship 0.5L X- & Z-direction

B.2. Ship response differences due to lashing stiffness adjustments

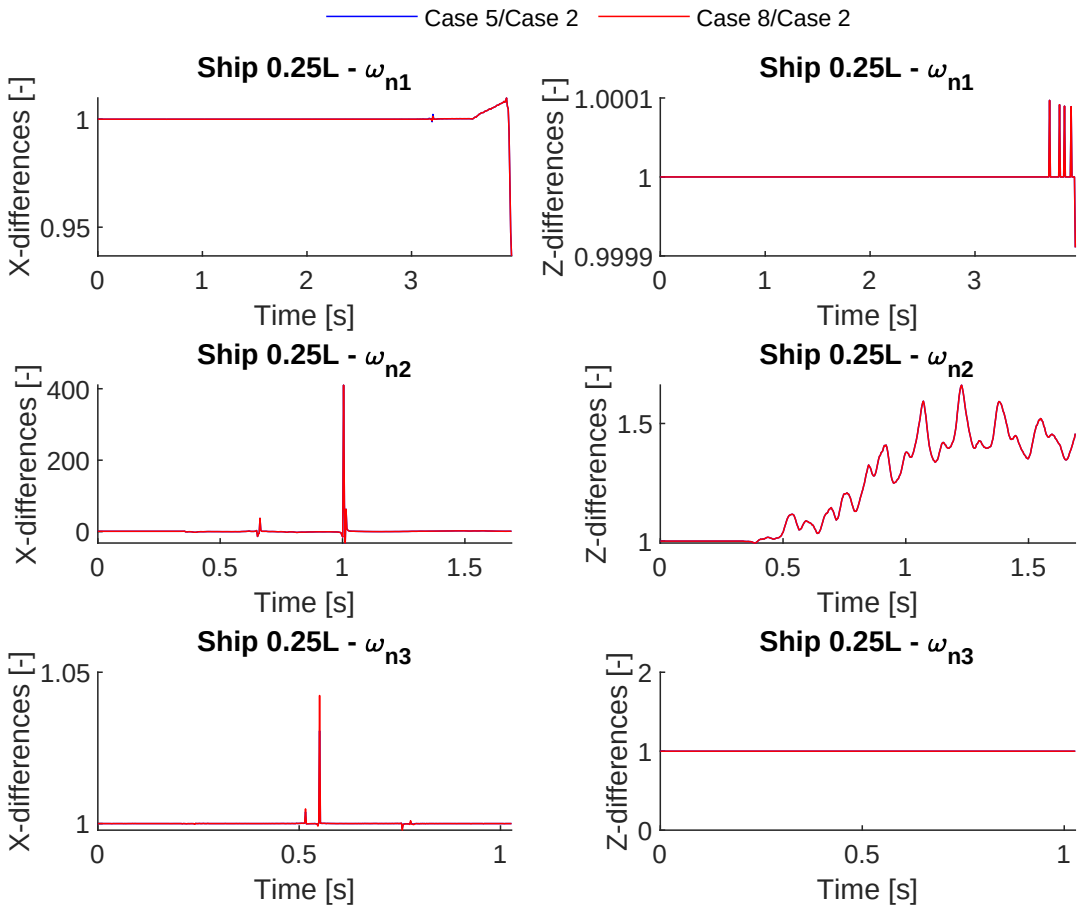

Figure B.11: Differences between cases 2,5 & 8 - Ship 0.25L X- & Z-direction

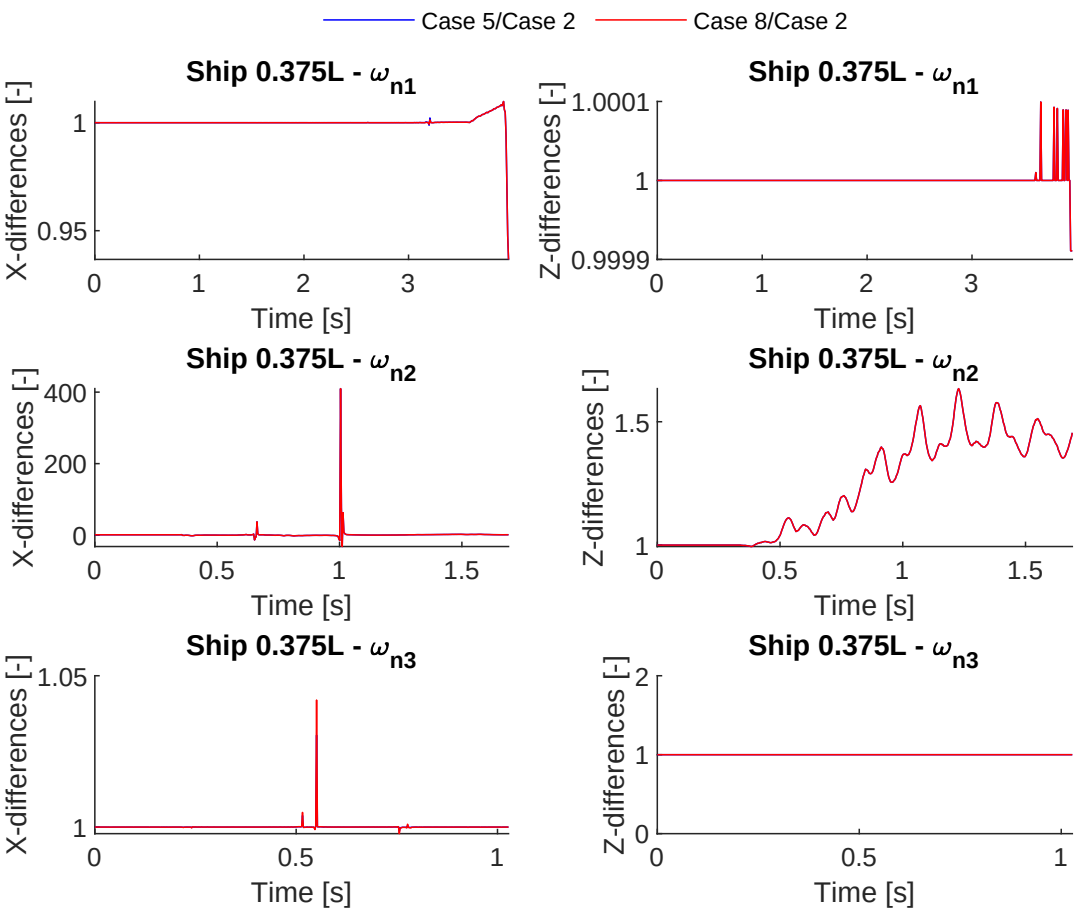

Figure B.12: Differences between cases 2,5 & 8 - Ship 0.375L X- & Z-direction

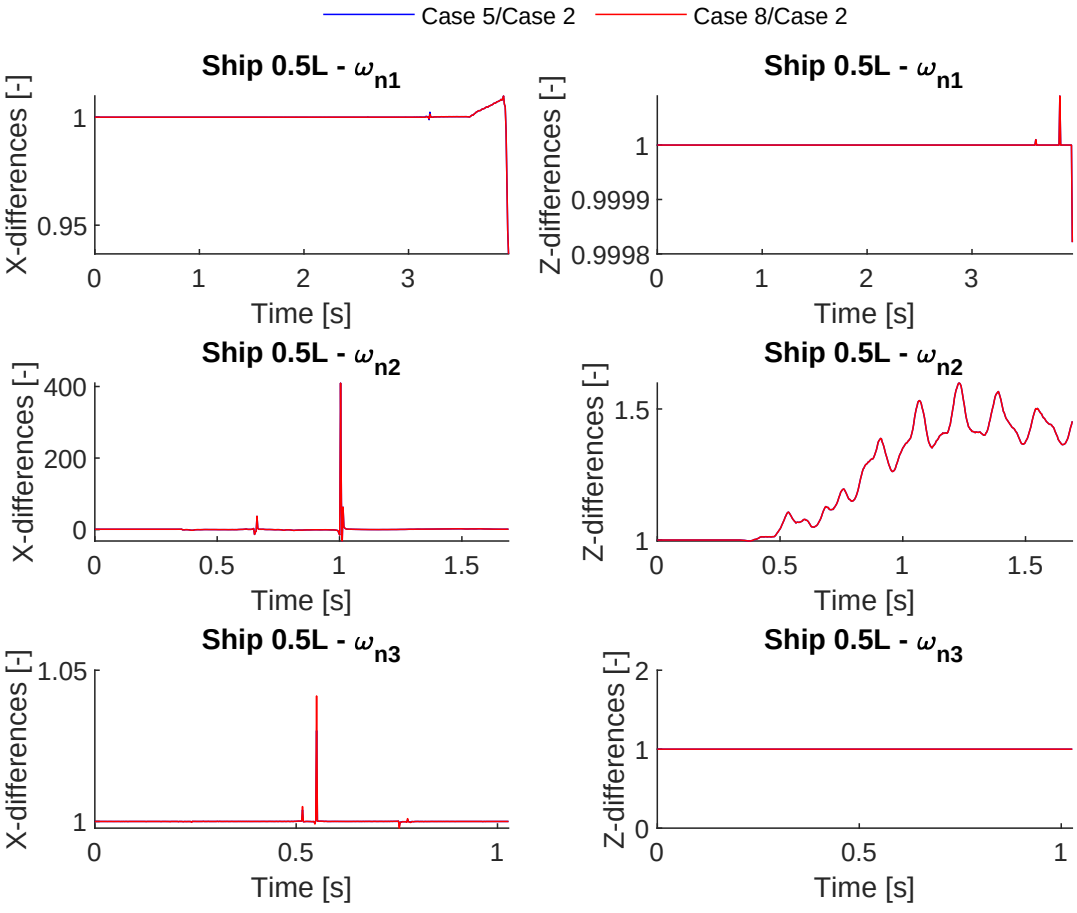

Figure B.13: Differences between cases 2,5 & 8 - Ship 0.5L X- & Z-direction

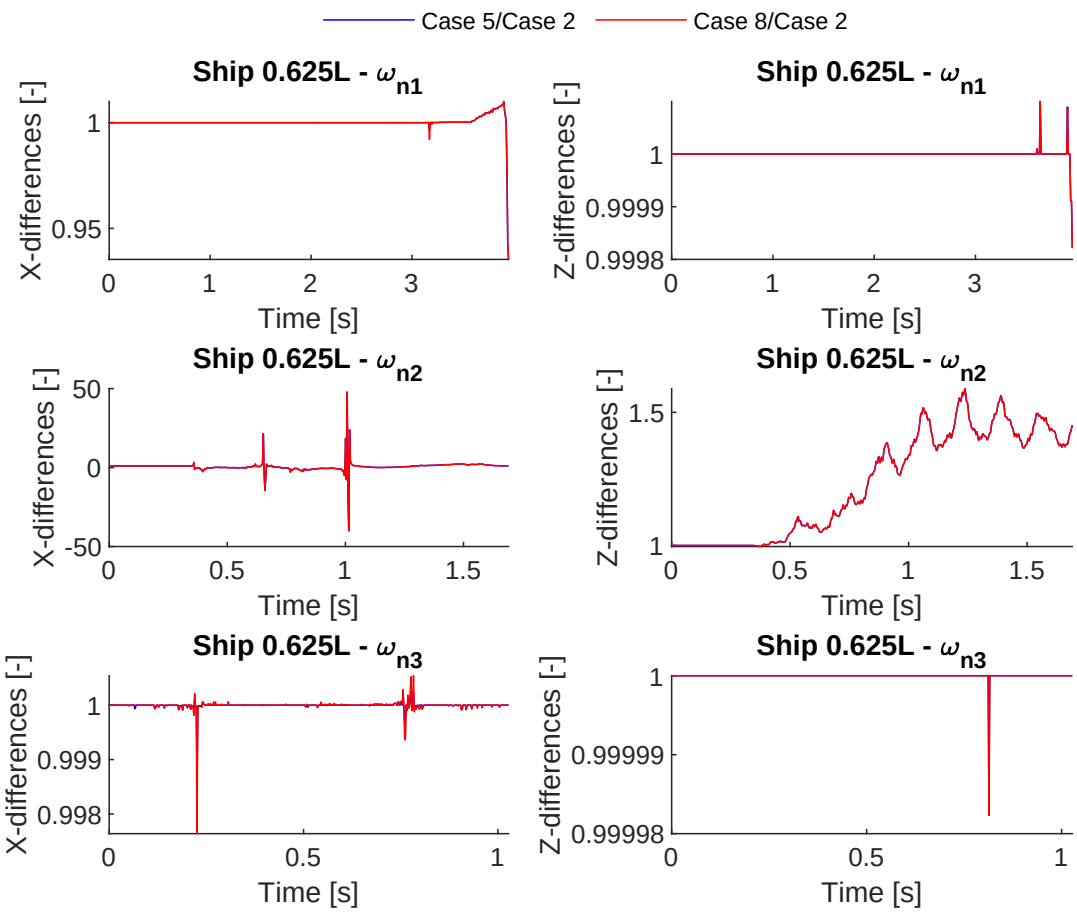

Figure B.14: Differences between cases 2,5 & 8 - Ship 0.625L X- & Z-direction

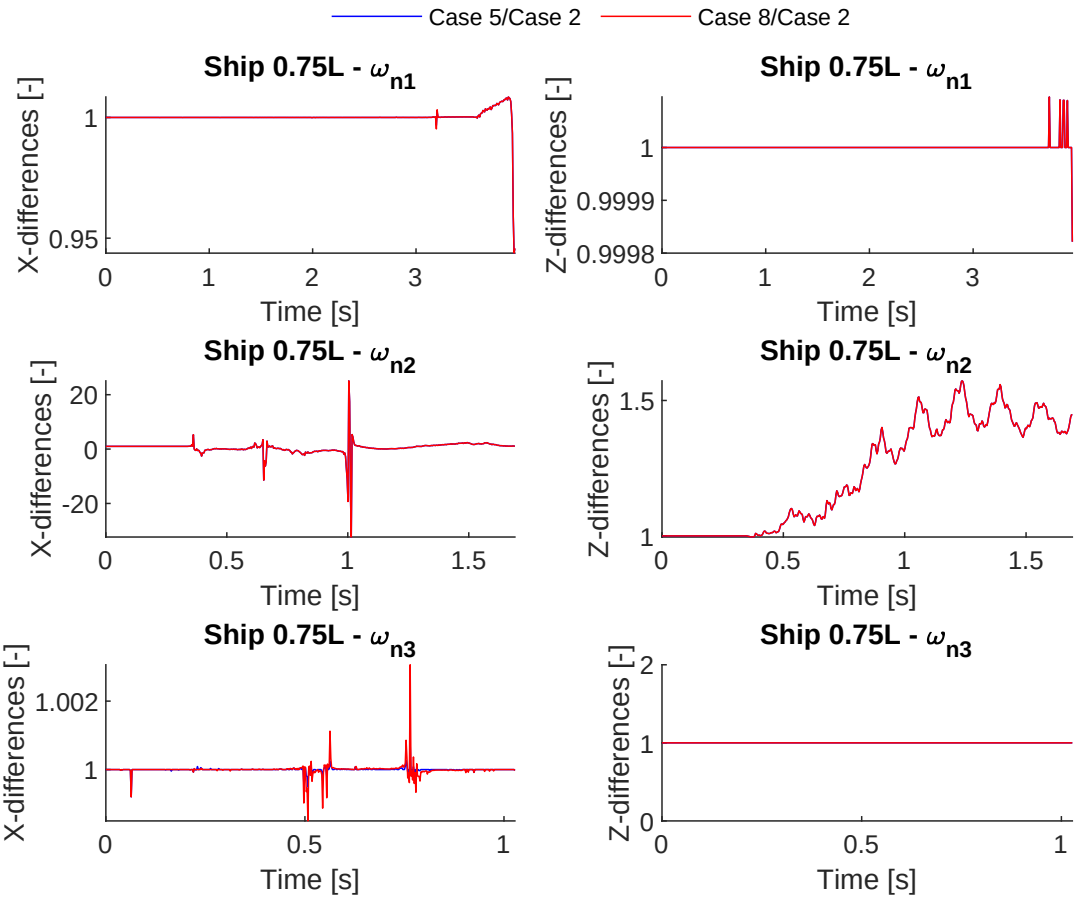

Figure B.15: Differences between cases 2,5 & 8 - Ship 0.75L X- & Z-direction

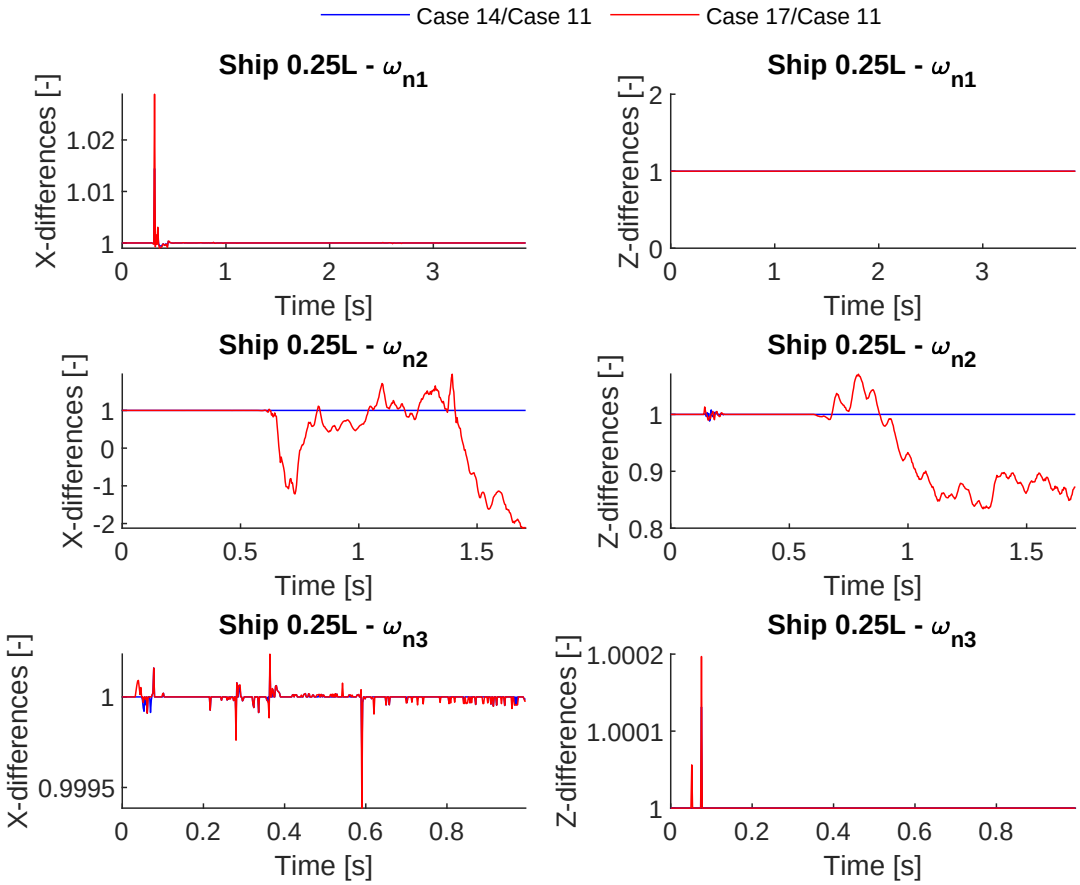

Figure B.16: Differences between cases 11,14 & 17 - Ship 0.25L X- & Z-direction

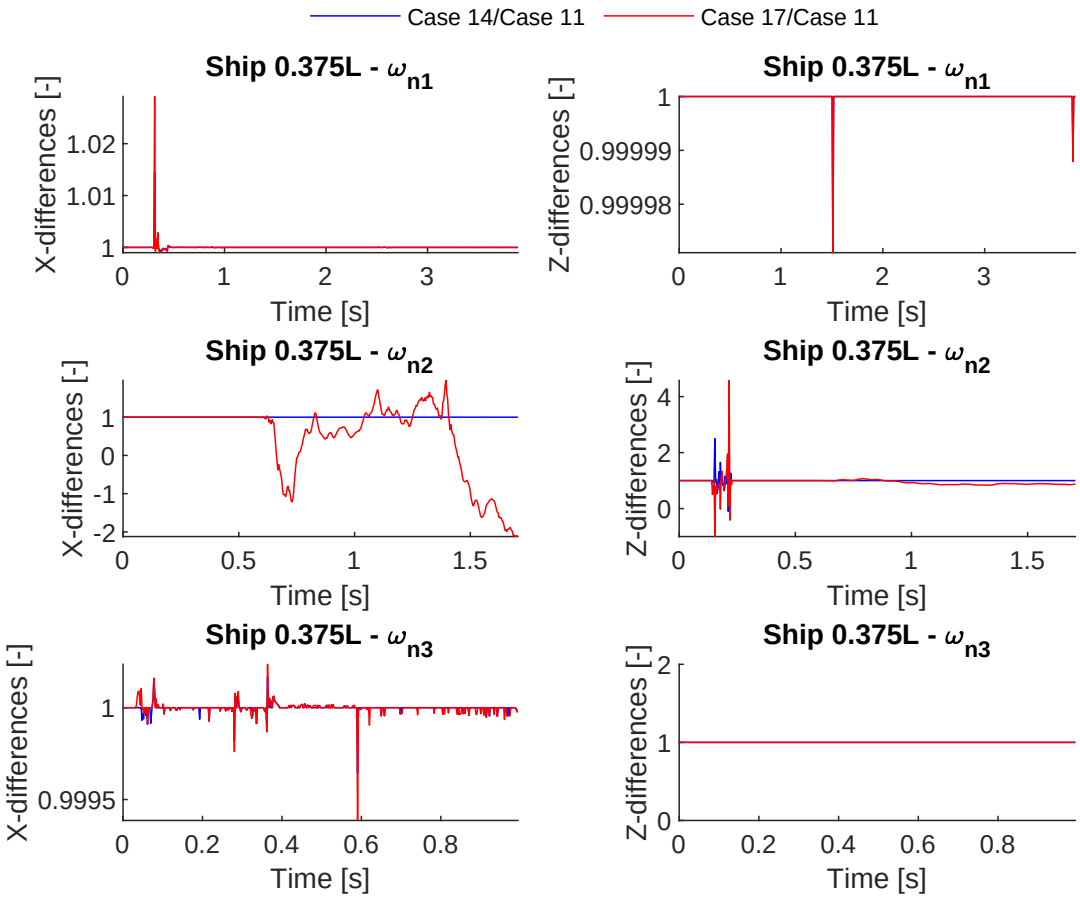

Figure B.17: Differences between cases 11,14 & 17 - Ship 0.375L X- & Z-direction

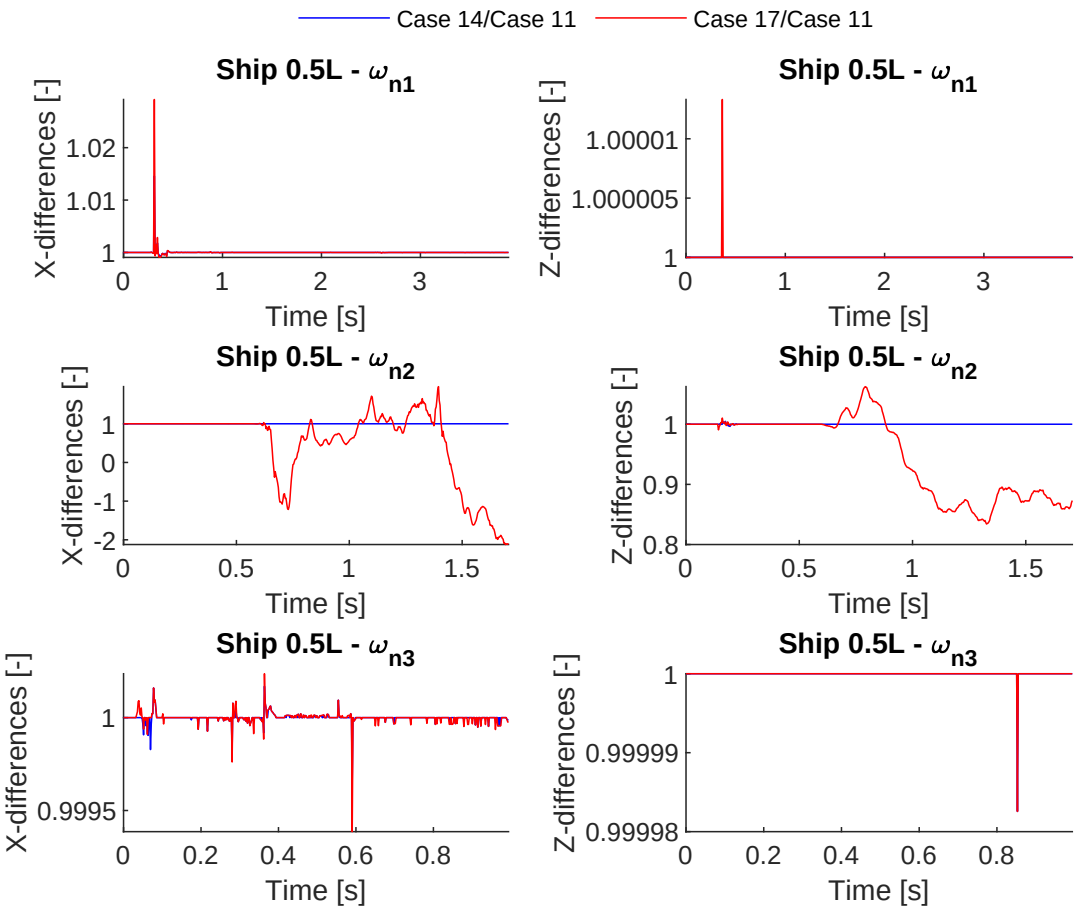

Figure B.18: Differences between cases 11,14 & 17 - Ship 0.5L X- & Z-direction

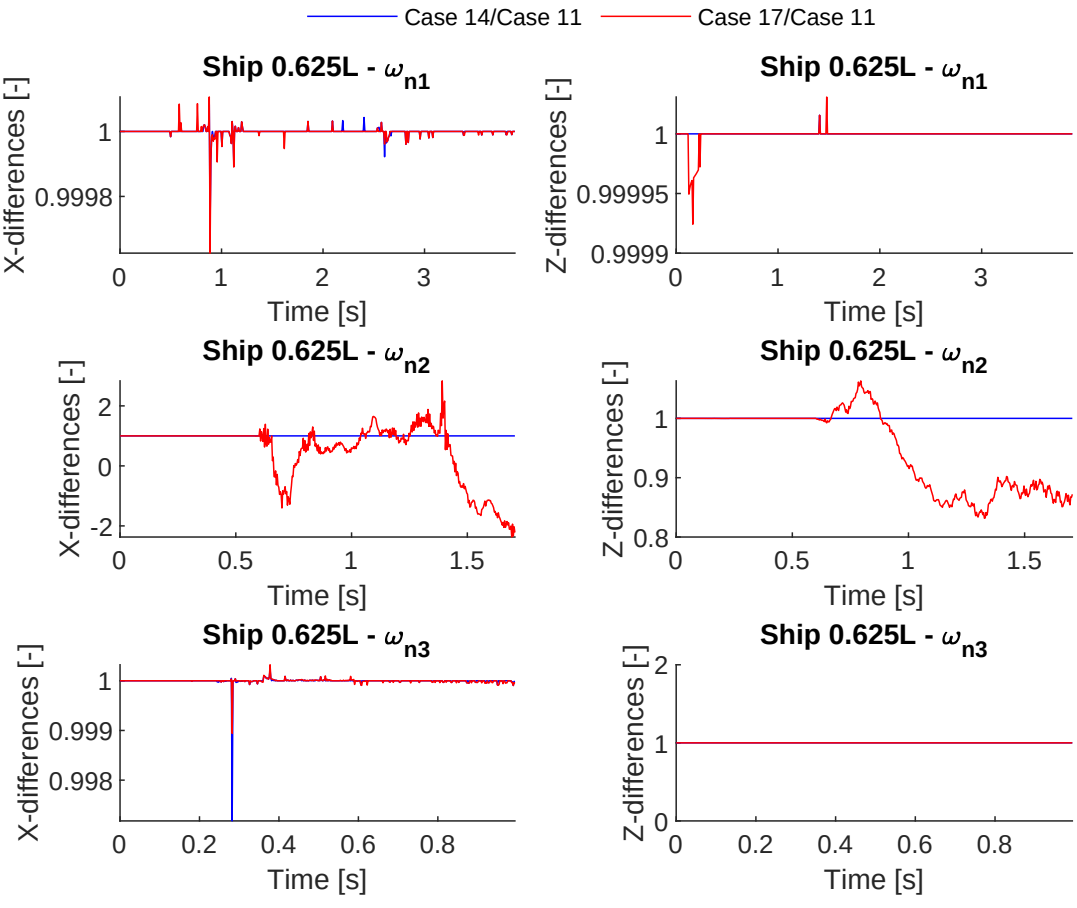

Figure B.19: Differences between cases 11,14 & 17 - Ship 0.625L X- & Z-direction

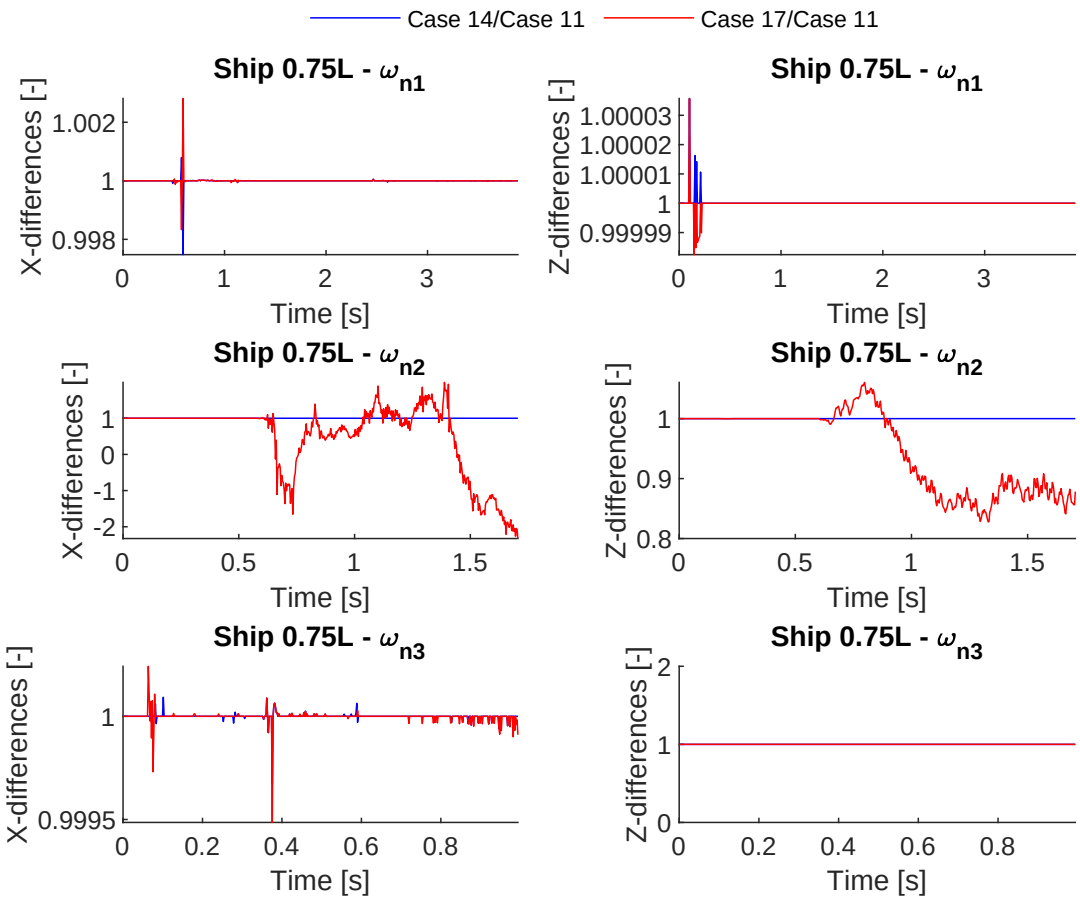

Figure B.20: Differences between cases 11,14 & 17 - Ship 0.75L X- & Z-direction

B.3. Monopile response base deformations (case 2 & 11)

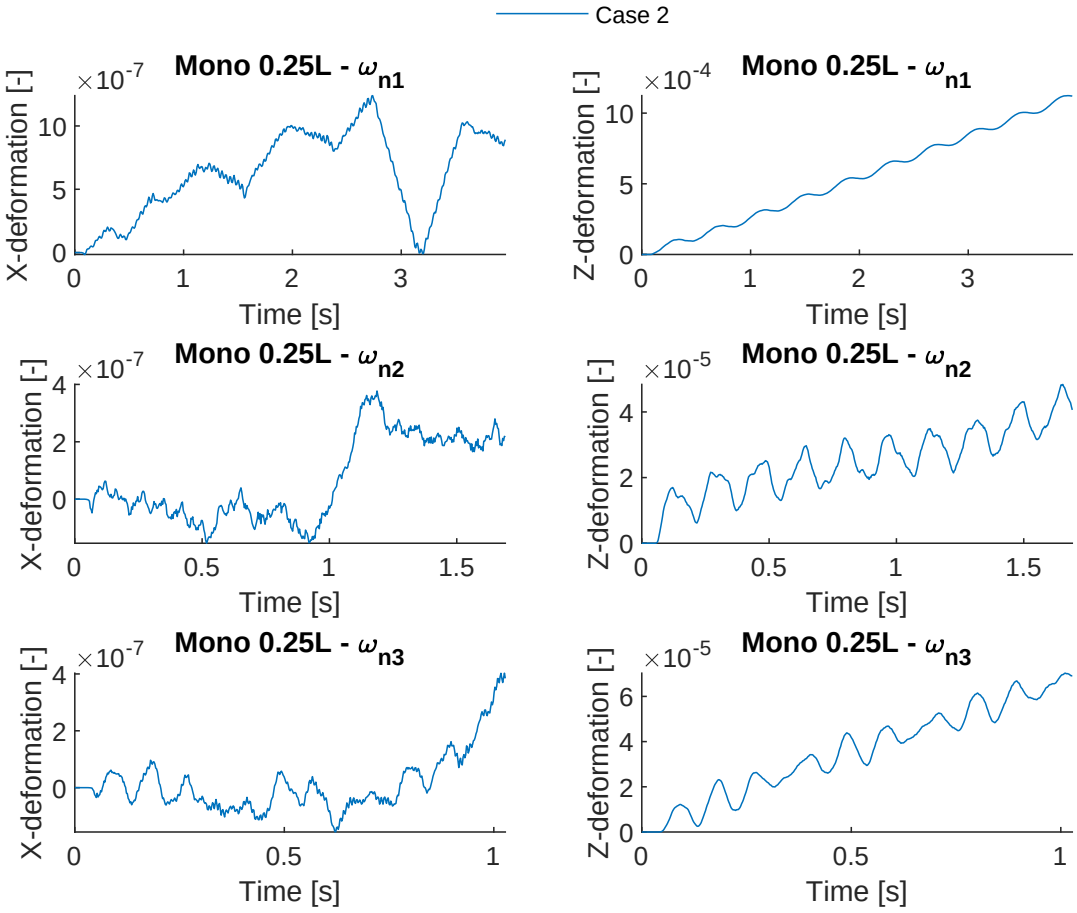

Figure B.21: Deformations case 2 - Monopile 0.25L X- & Z-direction

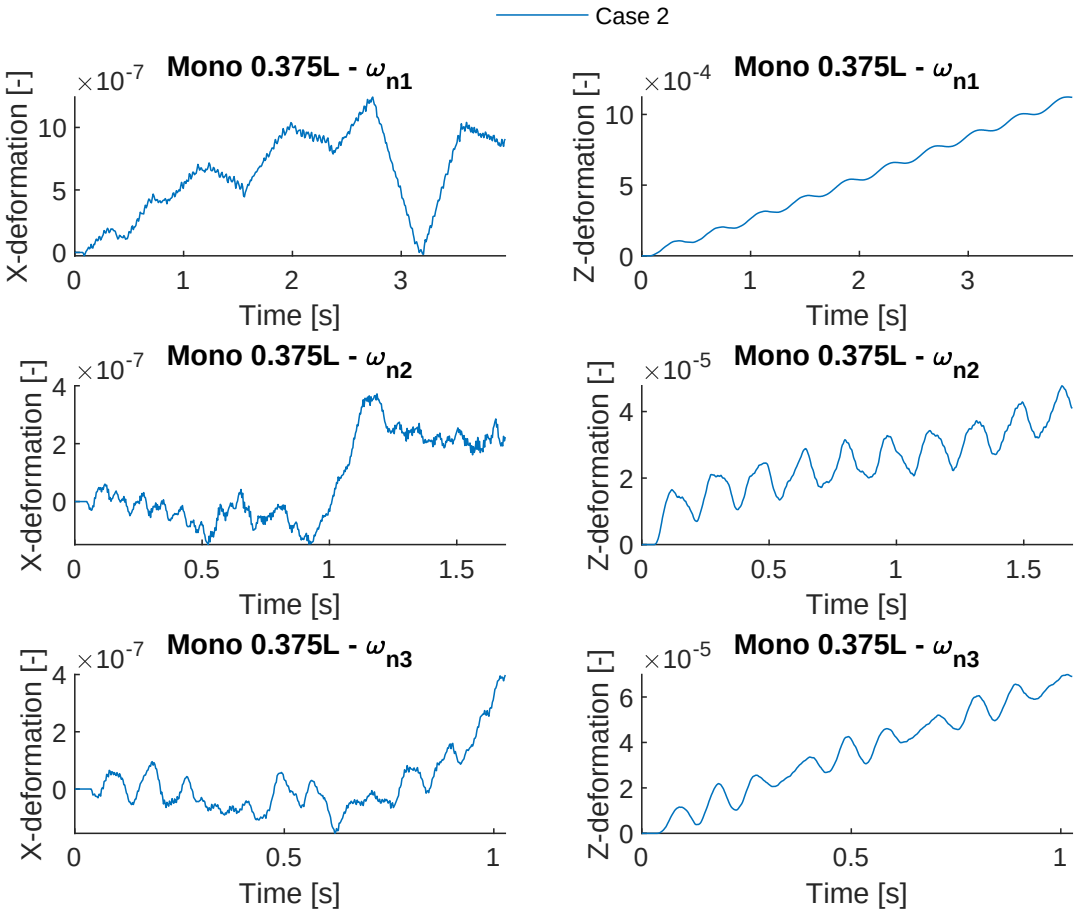

Figure B.22: Deformations case 2 - Monopile 0.375L X- & Z-direction

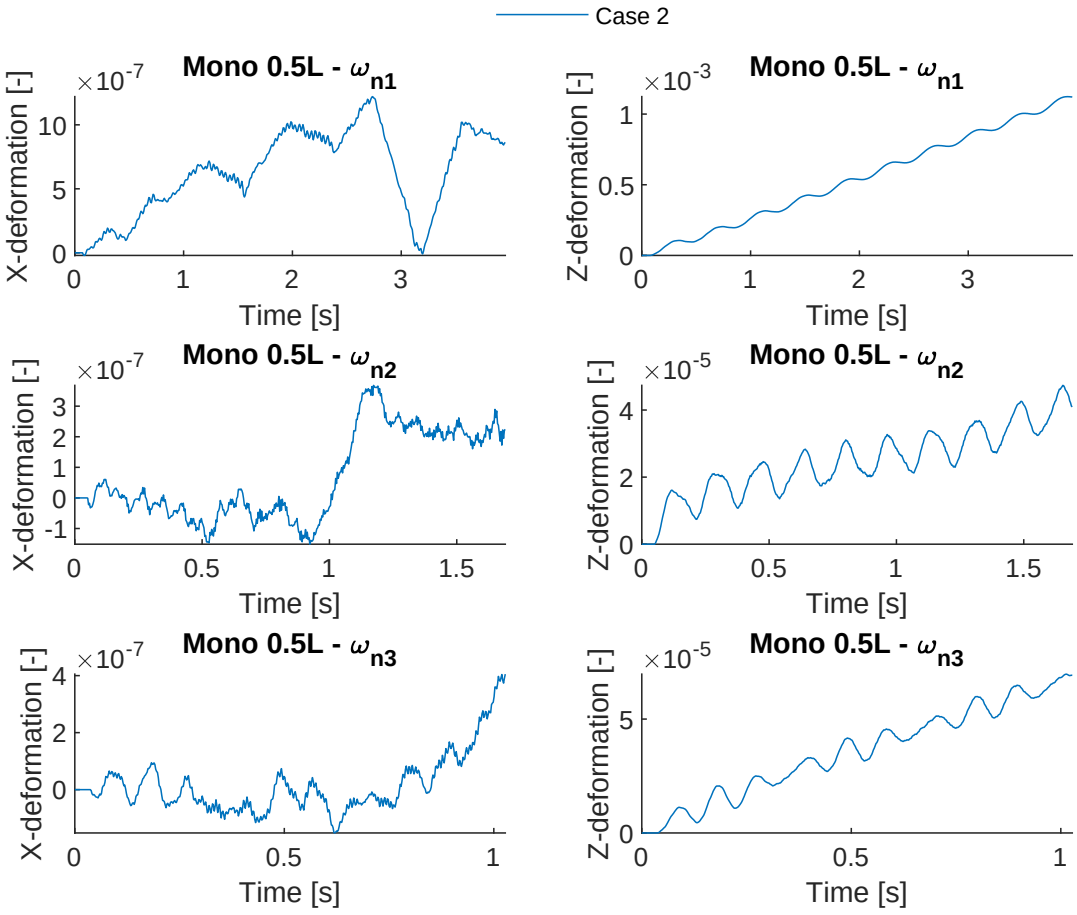

Figure B.23: Deformations case 2 - Monopile 0.5L X- & Z-direction

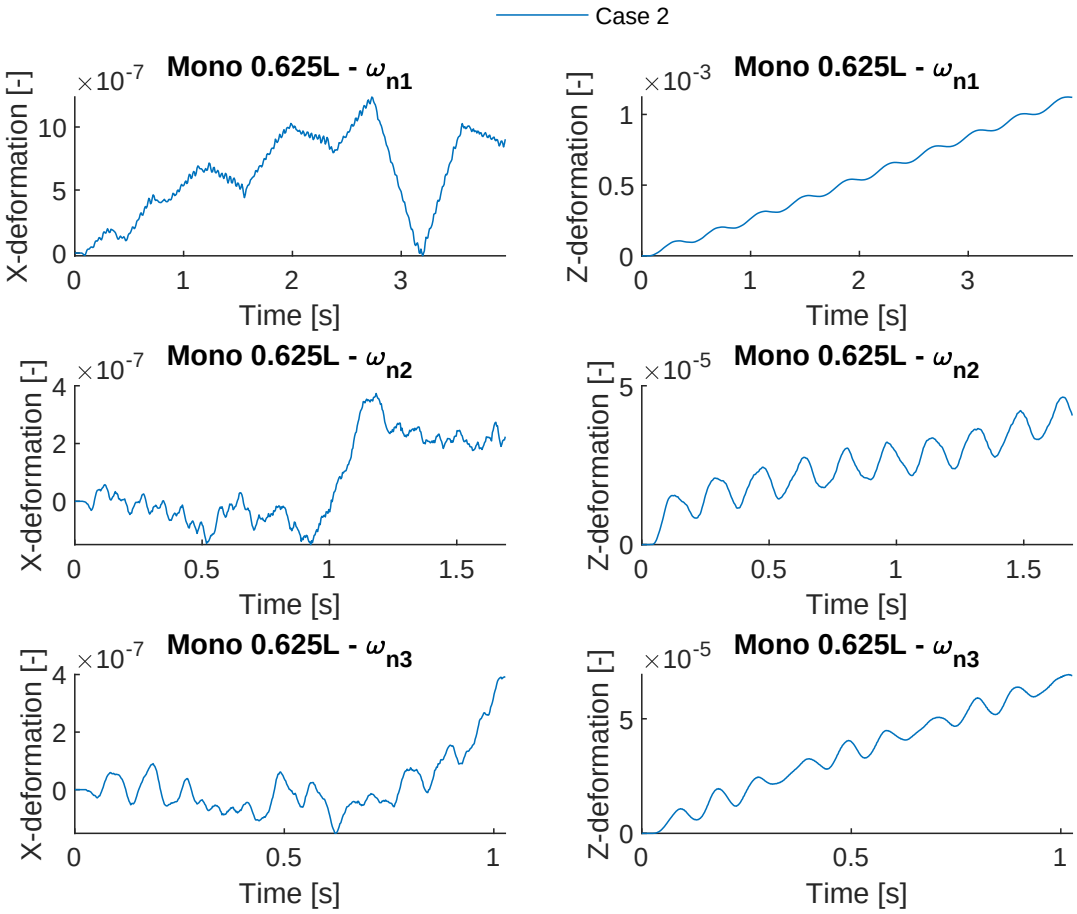

Figure B.24: Deformations case 2 - Monopile 0.375L X- & Z-direction

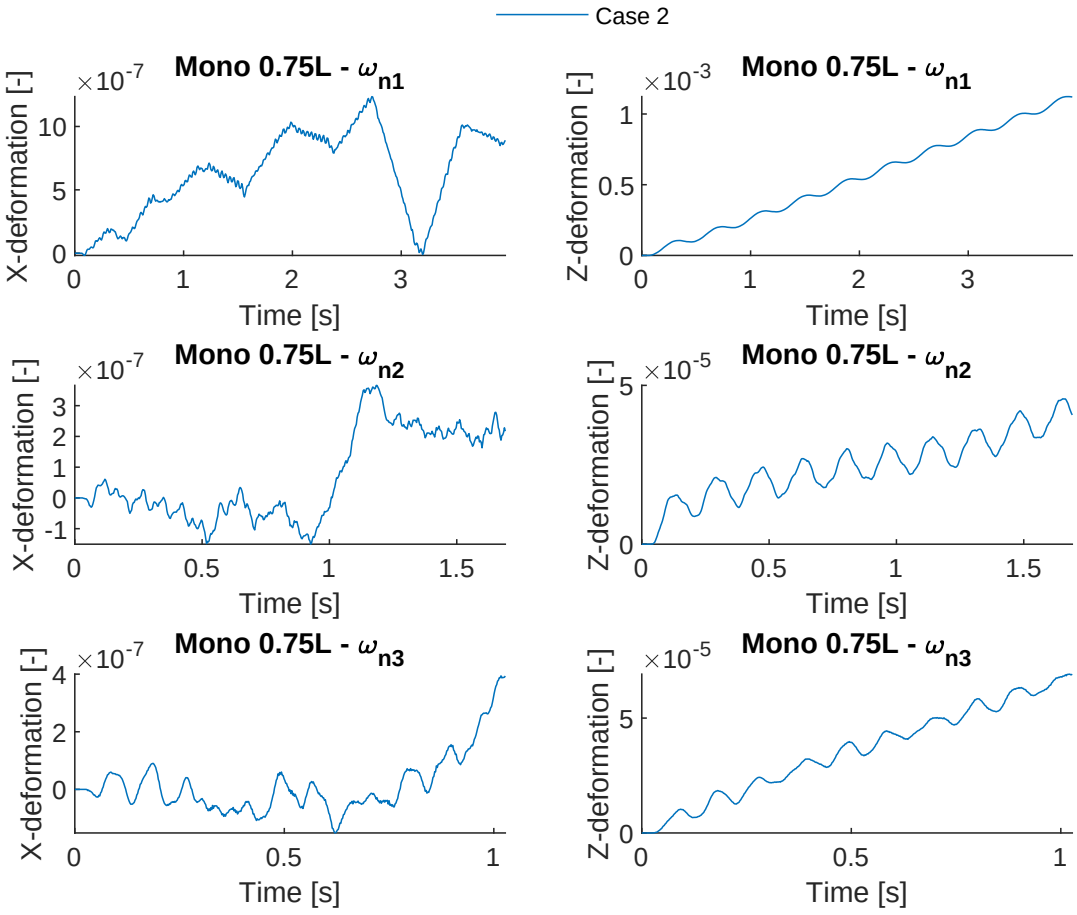

Figure B.25: Deformations case 2 - Monopile 0.5L X- & Z-direction

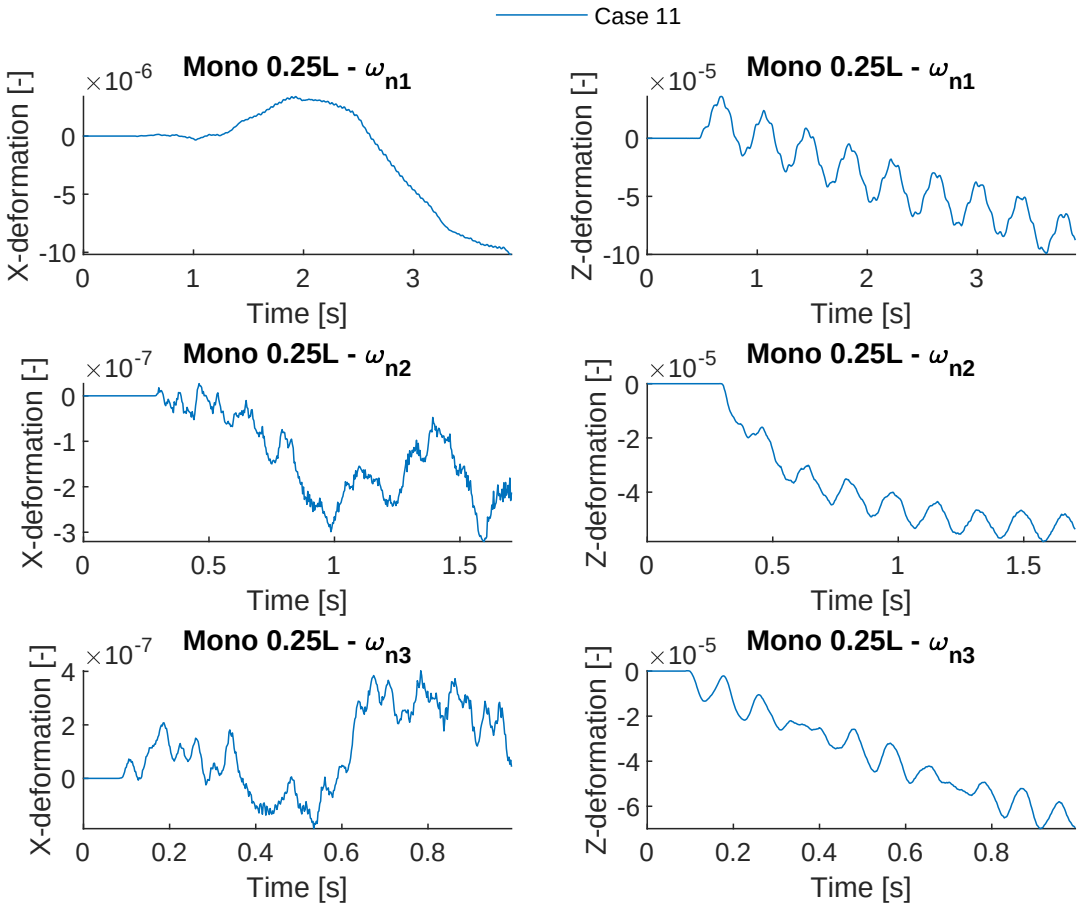

Figure B.26: Deformations case 11 - Monopile 0.25L X- & Z-direction

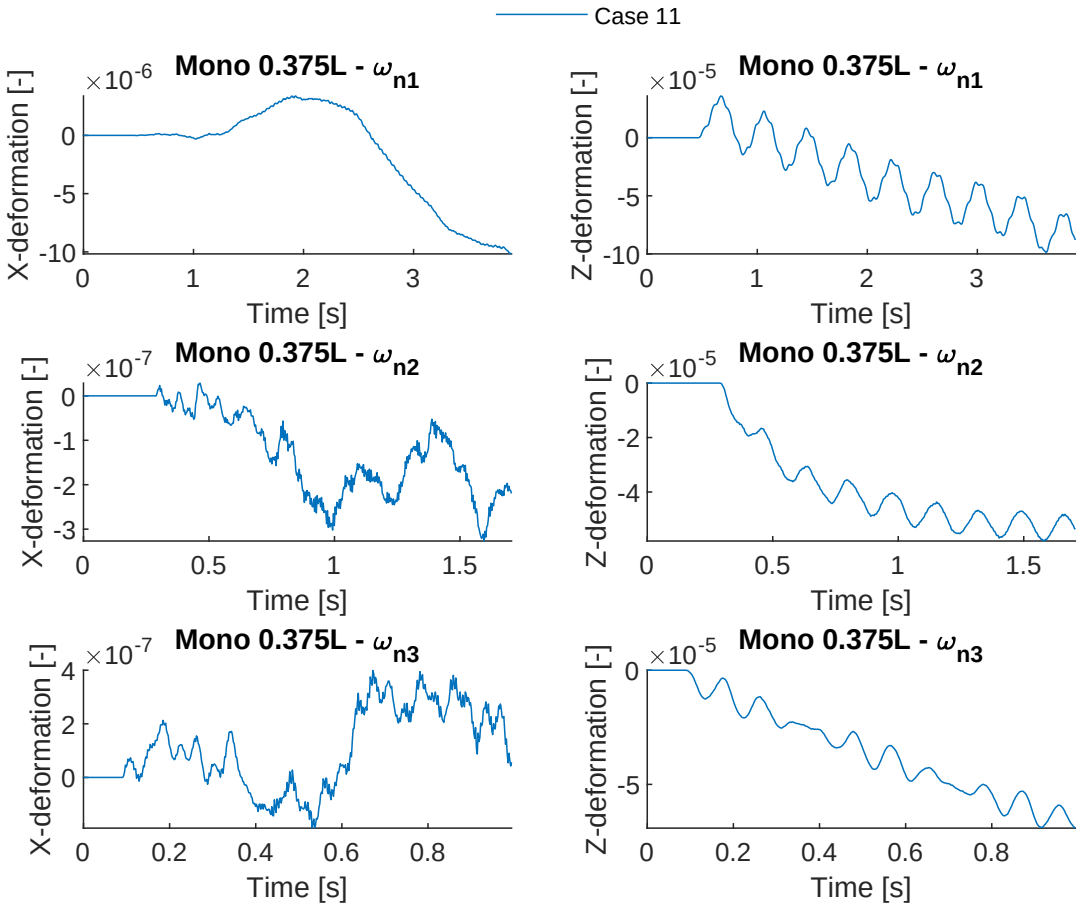

Figure B.27: Deformations case 11 - Monopile 0.375L X- & Z-direction

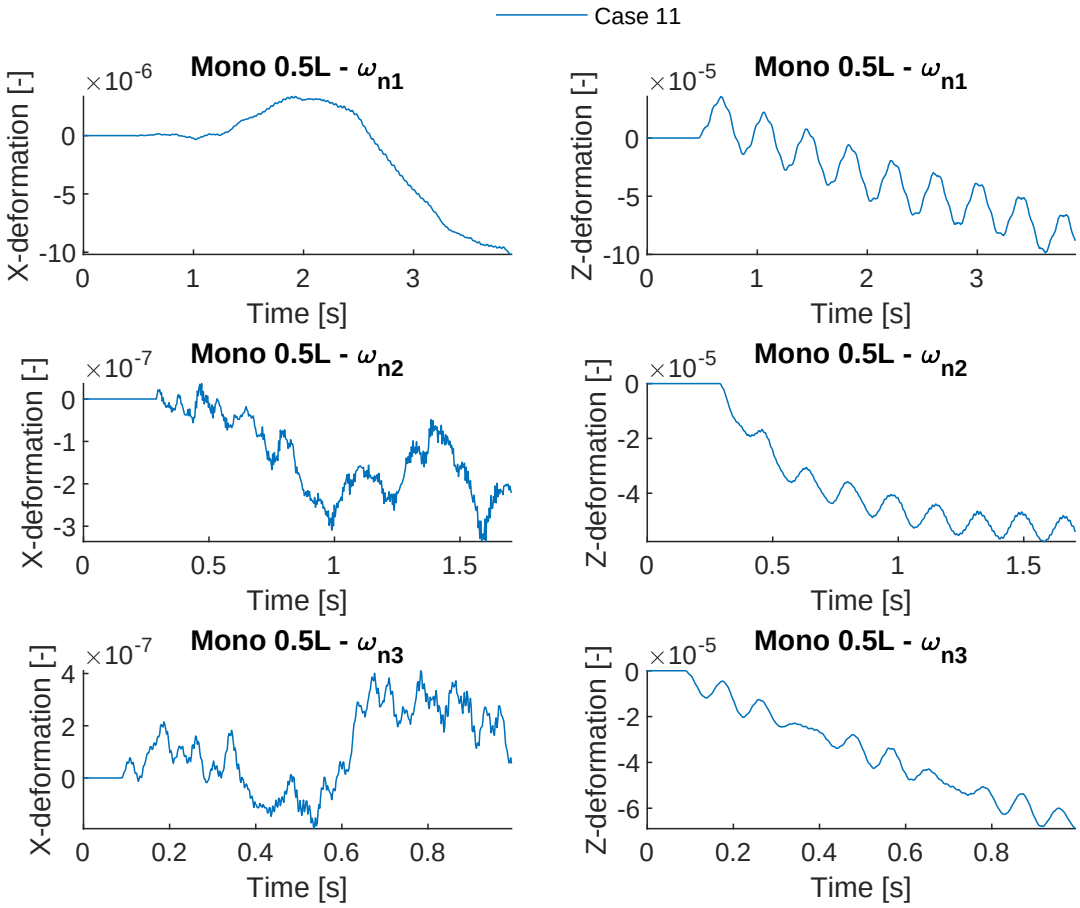

Figure B.28: Deformations case 11 - Monopile 0.5L X- & Z-direction

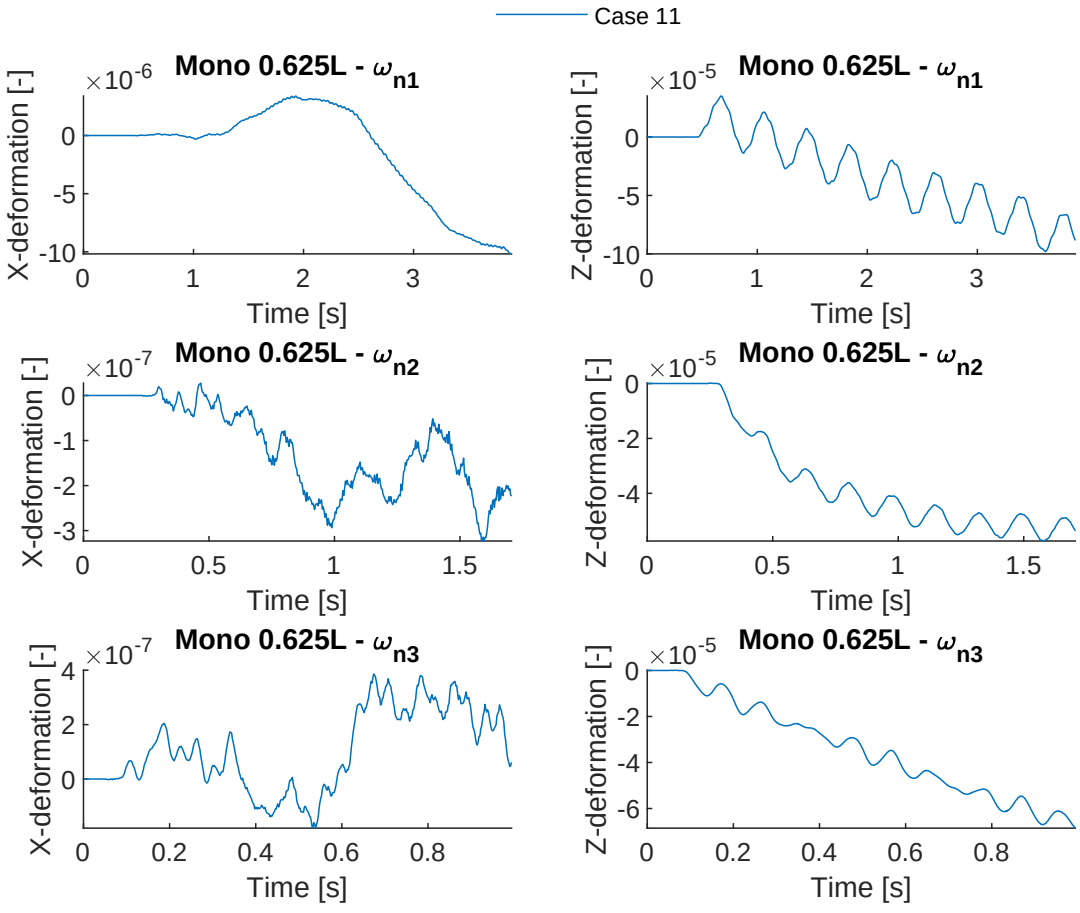

Figure B.29: Deformations case 11 - Monopile 0.375L X- & Z-direction

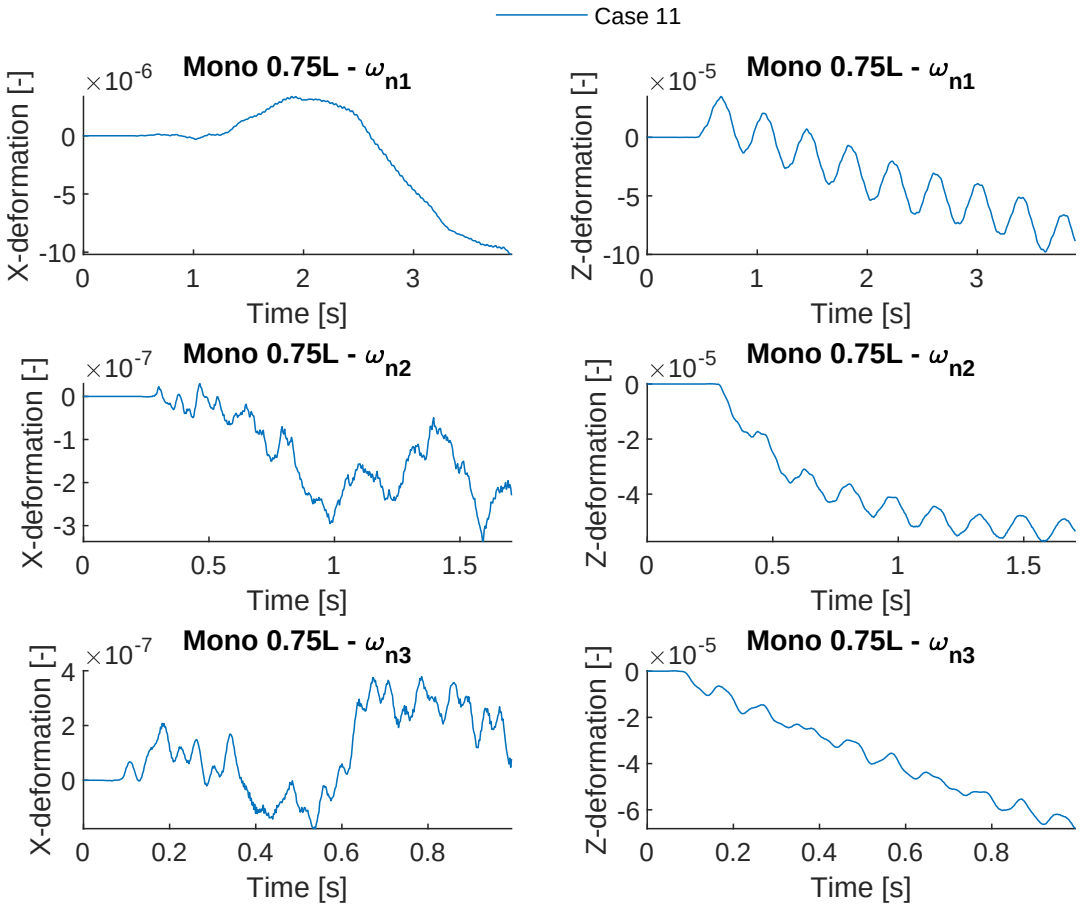

Figure B.30: Deformations case 11 - Monopile 0.5L X- & Z-direction

B.4. Monopile response differences due to lashing stiffness adjustments

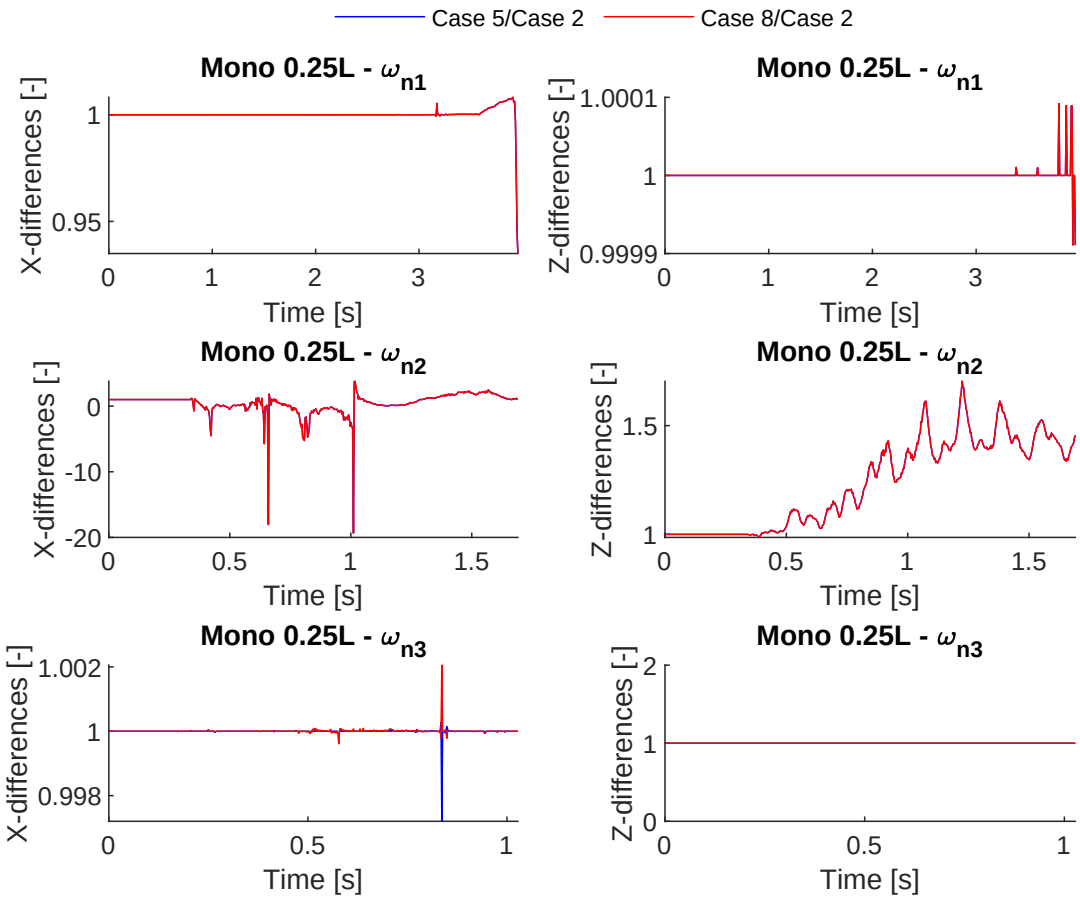

Figure B.31: Differences between cases 2,5 & 8 - Monopile 0.25L X- & Z-direction

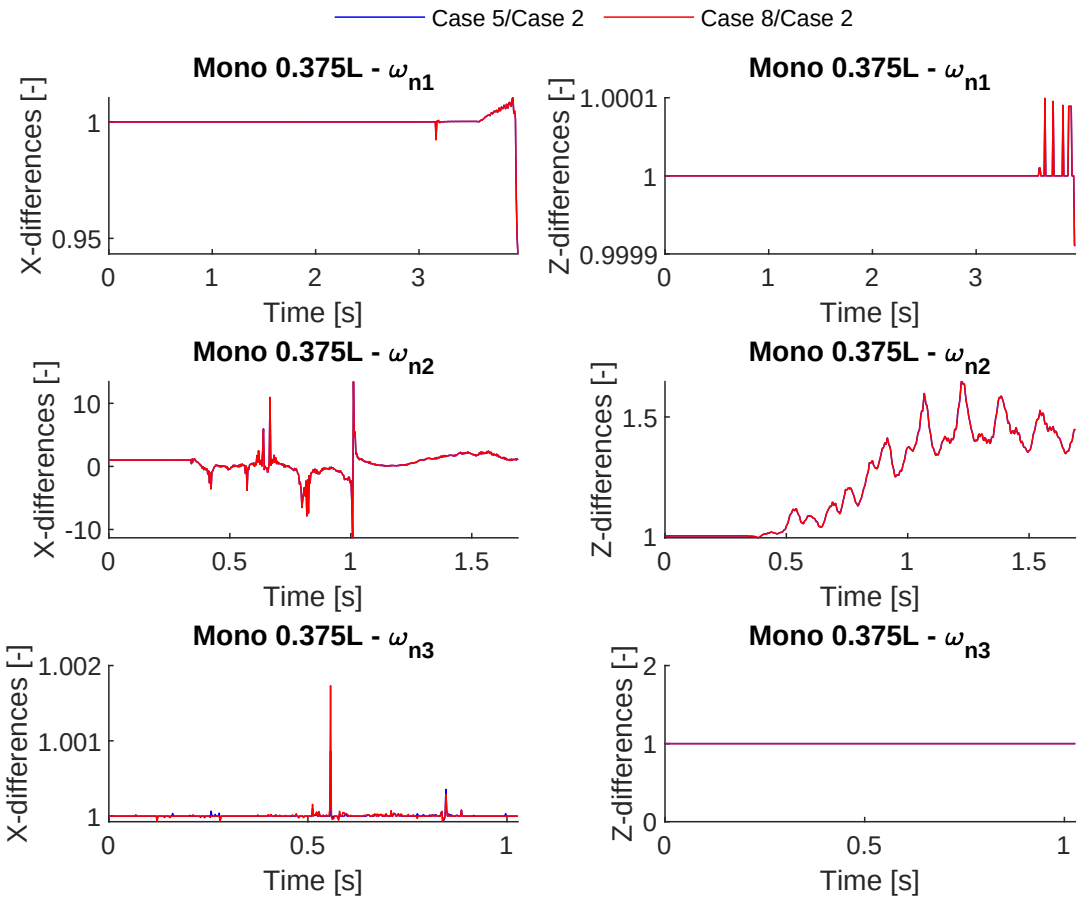

Figure B.32: Differences between cases 2,5 & 8 - Monopile 0.375L X- & Z-direction

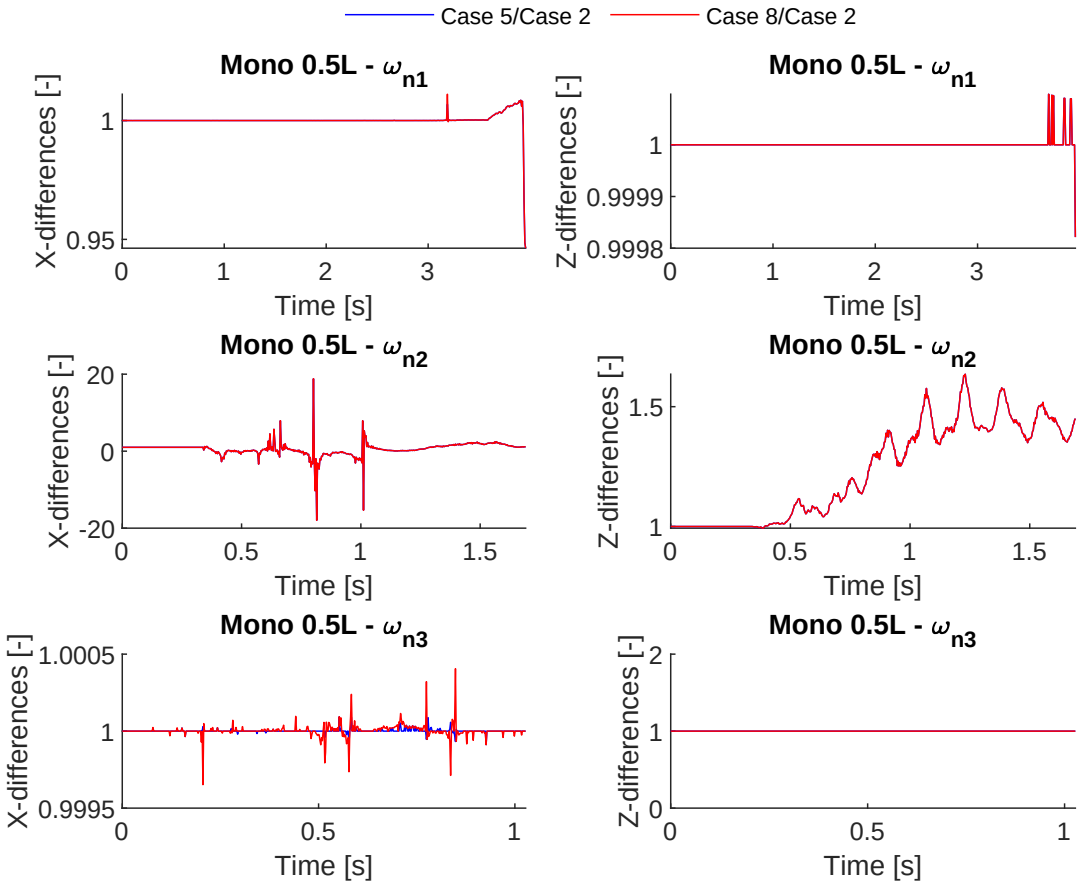

Figure B.33: Differences between cases 2,5 & 8 - Monopile 0.5L X- & Z-direction

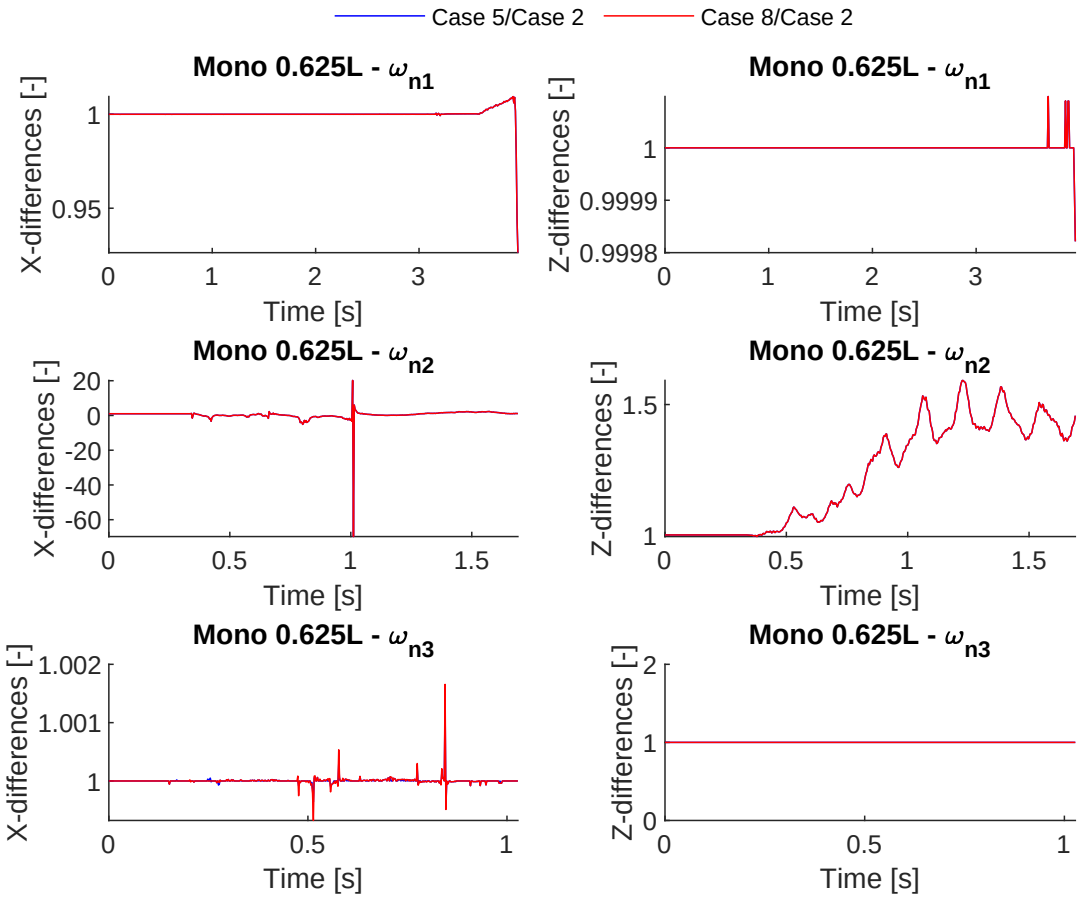

Figure B.34: Differences between cases 2,5 & 8 - Monopile 0.625L X- & Z-direction

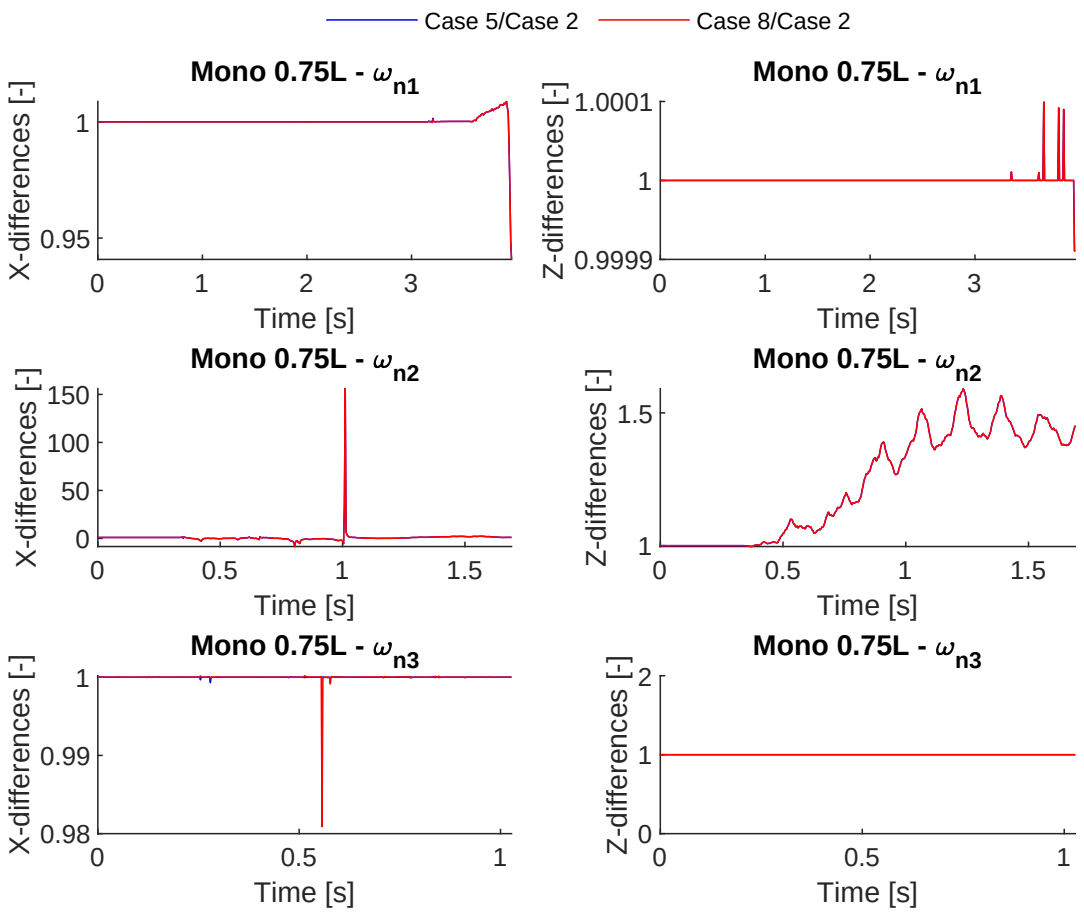

Figure B.35: Differences between cases 2,5 & 8 - Monopile 0.75L X- & Z-direction

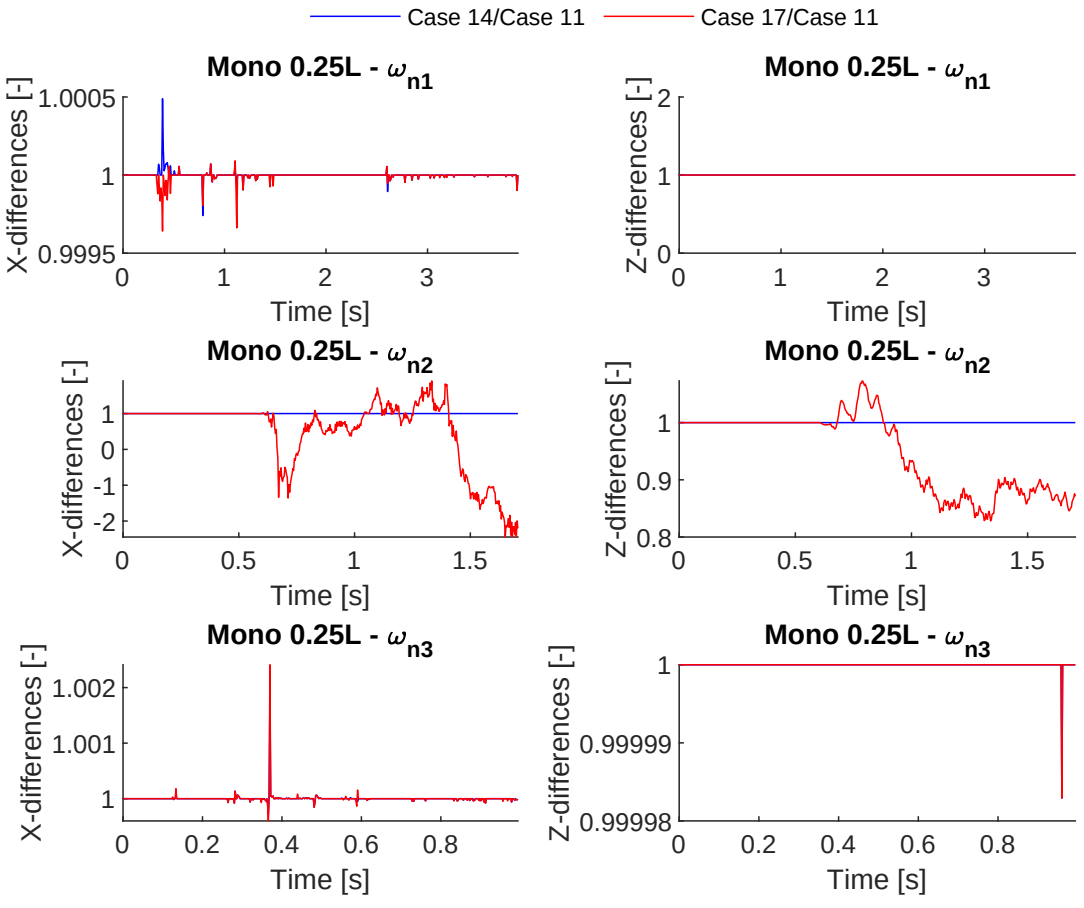

Figure B.36: Differences between cases 11,14 & 17 - Monopile 0.25L X- & Z-direction

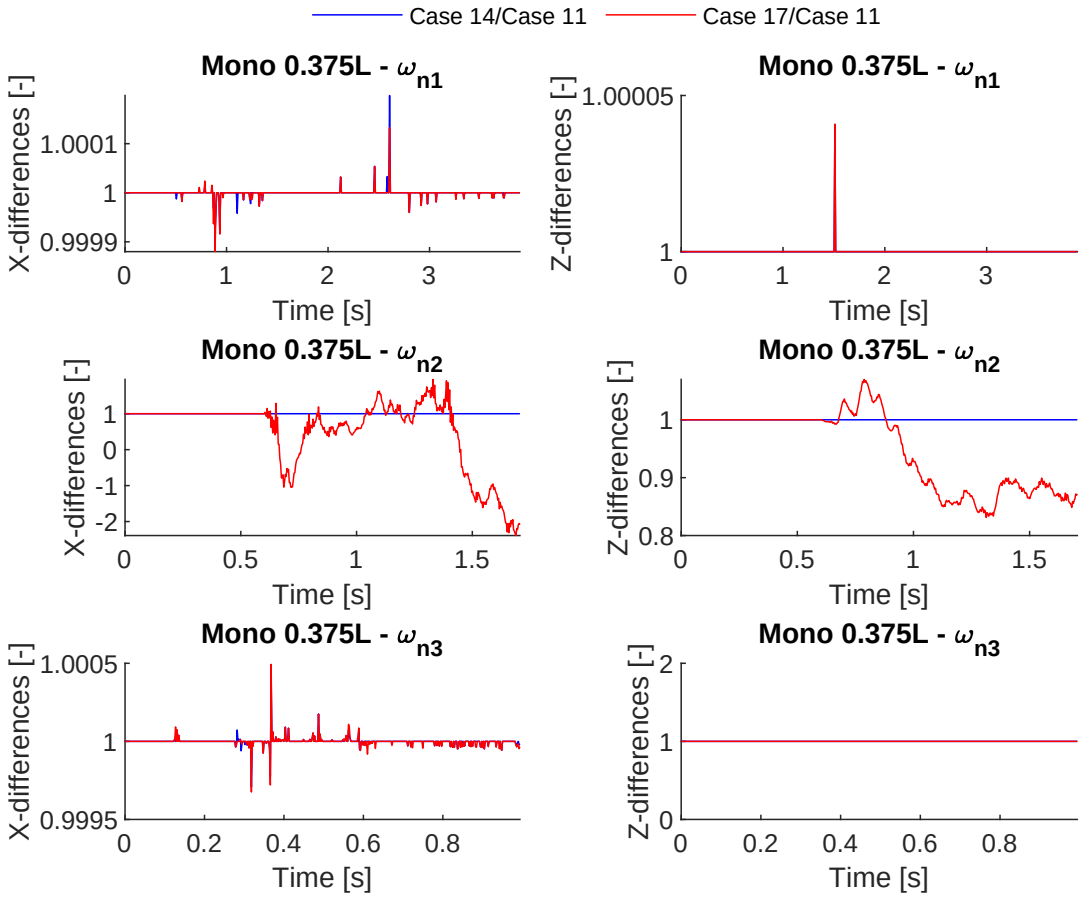

Figure B.37: Differences between cases 11,14 & 17 - Monopile 0.375L X- & Z-direction

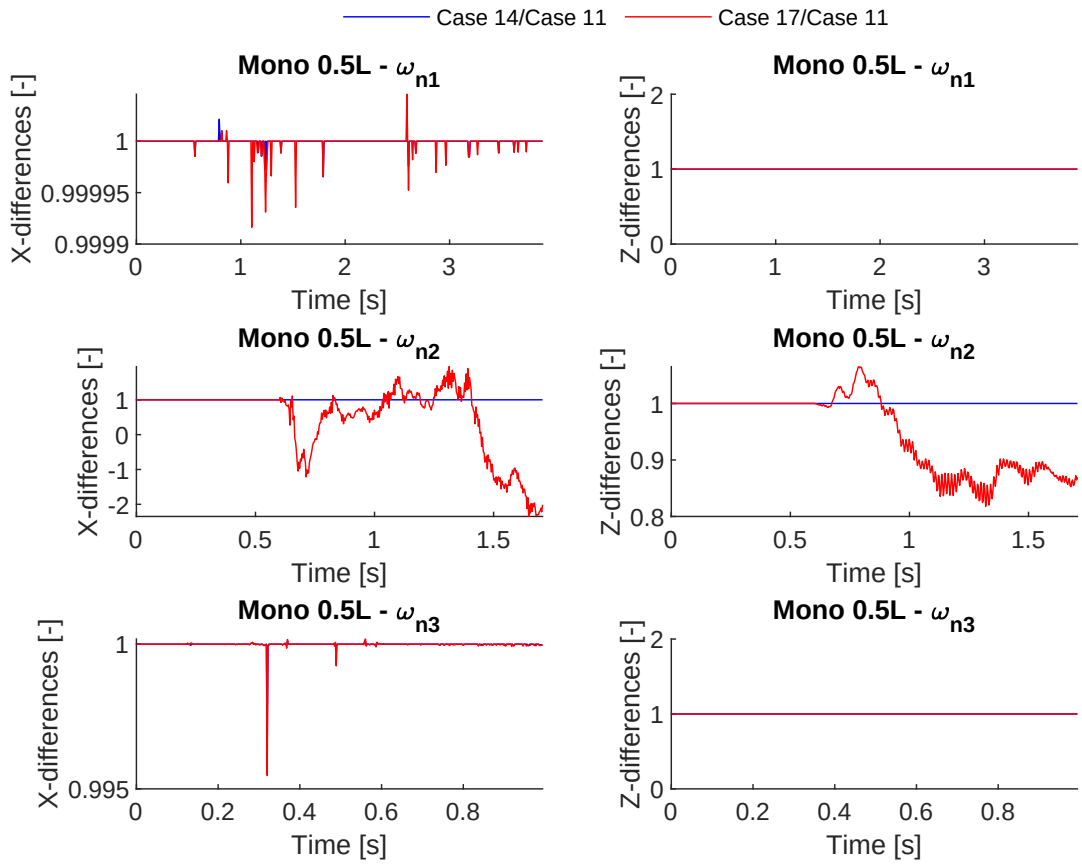

Figure B.38: Differences between cases 11,14 & 17 - Monopile 0.5L X- & Z-direction

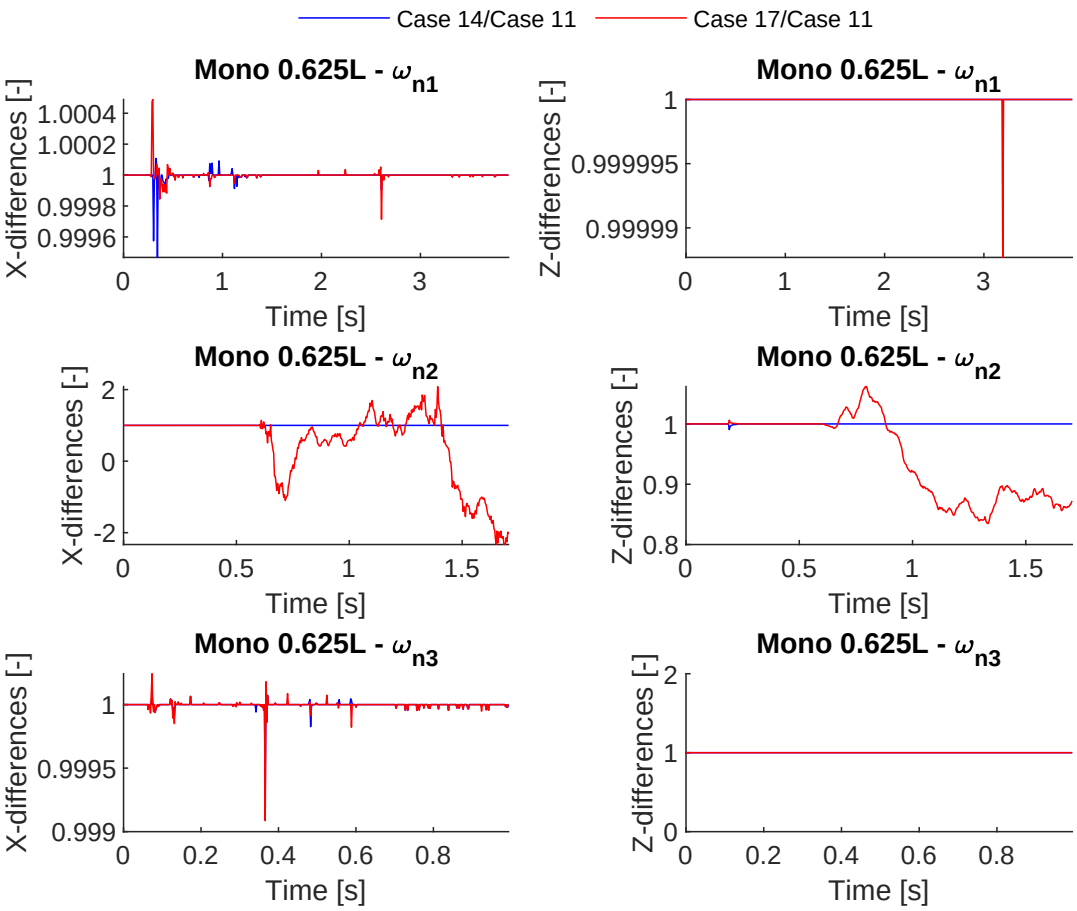

Figure B.39: Differences between cases 11,14 & 17 - Monopile 0.625L X- & Z-direction

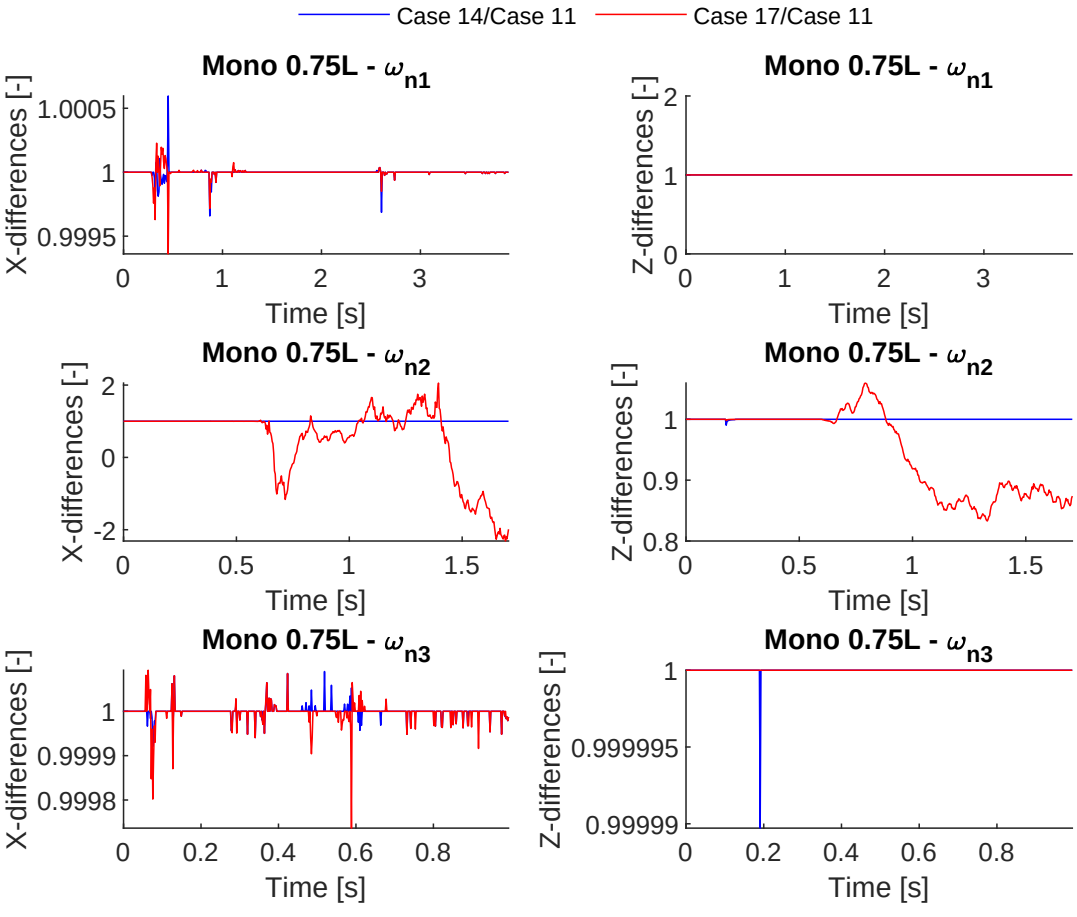

Figure B.40: Differences between cases 11,14 & 17 - Monopile 0.75L X- & Z-direction